Motion of Individual Domain Walls in a Nickel-Iron Ferrite

By J. K. GALT

Samples have been cut from single crystals of the nickel-iron ferrite $(NiO)_{0.75}$ $(FeO)_{0.25}Fe_2O_3$ in such a way that they contain one and only one movable ferromagnetic domain wall. The viscous damping coefficient for this wall, which is a measure of the losses associated with domain wall motion in this material, has been measured as a function of temperature. This damping shows a very large increase as the temperature goes down to the region of $77°K$. The value of this damping is correlated with the Landau-Lifshitz equation for the rotational motion of magnetization by means of previously available theoretical analysis. In addition, it is suggested that the sharp increase in damping at low temperatures is due to a relaxation associated with a rearrangement of the valence electrons on the divalent and trivalent iron ions in the ferrite. A tentative phenomenological theory of the losses based on this mechanism is presented.

INTRODUCTION

The mechanism which contributes most to the permeability of high-permeability magnetic materials is the motion of ferromagnetic domain walls. These walls are thin lamellae in which the direction of the spontaneous magnetization of the material changes from one domain to another. As a result, this mechanism contributes a major part of the energy losses which accompany rapid changes in the direction of the

magnetization in such materials. In the ferromagnetic metals, it is well known that these losses ordinarily arise largely from the eddy currents which are induced by the motion of the domain walls. In the ferrites, however, the conductivity is so low that the contribution of eddy currents to the losses is never overwhelming and is often negligible; the losses must therefore in large part arise from other sources not yet understood. It is the purpose of this paper to present some recent studies of these losses and to discuss their relevance to the losses in ferrites generally.

In any ordinary sample of a ferromagnetic material, a study of domain wall motion and the associated energy losses is complicated by the fact that the domain pattern is very complex. Any attempt to provide a theoretical explanation of data taken on such samples must involve an averaging process over many domain walls of varying area, crystal orientation, etc. This makes it extremely difficult to describe the behavior of such patterns uniquely and quantitatively, although some progress has been made.[1,2] A method of avoiding this difficulty has been developed by Williams, Bozorth, Shockley, Kittel[3] and Stewart[3a] in working on silicon iron. This method consists in cutting a polygonal ring from a single crystal in such a way that each leg of the ring lies along one of the easy directions of magnetization in the crystal. In silicon iron this leads to a rectangular ring with each leg along a [100] crystal direction. In the ferrite which we use this technique to study here, the easy directions are [111] directions, and we use a diamond shaped sample as shown by the solid lines in Fig. 1. Each leg is along a [111] direction, and the major face is a (110) plane. If the sample is good enough, the domain pattern is that indicated by the dotted lines in Fig. 1. This pattern consists of four stationary walls, one at each corner, and one movable wall which goes all the way around the sample. The magnetization thus travels around the sample in two paths, one clockwise and the other counter-clockwise, and the position of the movable wall therefore determines the net circumferential magnetization. In such samples we study quantitatively and in some detail the motion of an individual movable wall.

Williams, Shockley and Kittel[3] studied the motion of the movable wall on one of the rectangles cut from a single crystal of silicon iron. They found the motion to be viscously damped, as Sixtus and Tonks[4] had in earlier experiments with more complicated domain walls. Because of the simplicity of their domain pattern, Williams, Shockley and Kittel were able to calculate the eddy current losses in their experiments, and to show that they accounted for most of the observed damp-

ing as expected. There was an additional contribution, however, which Kittel suggested was due to mechanisms of the sort which give rise to the width of ferromagnetic resonance lines.[5] These mechanisms of course are the controlling ones in the ferrites, where eddy current losses are small. The motion of a domain wall damped by such effects and unaffected by eddy currents was first discussed in a classic paper by Landau and Lifshitz.[6]

The experiments reported in the present paper consist of measurements of the velocity of a movable wall as a function of applied magnetic field in a sample like that shown in Fig. 1. The measurements are made by observing the voltage induced in a secondary winding on such a sample when a known field is applied by means of a pulse of current in a primary winding. The composition of the ferrites used in these studies is given by the approximate chemical formula $(NiO)_{0.75}(FeO)_{0.25}$-Fe_2O_3. Data have been taken as a function of temperature on several samples. The large, perfect crystals of the ferrites which are essential to the success of these experiments have been obtained through Dr.
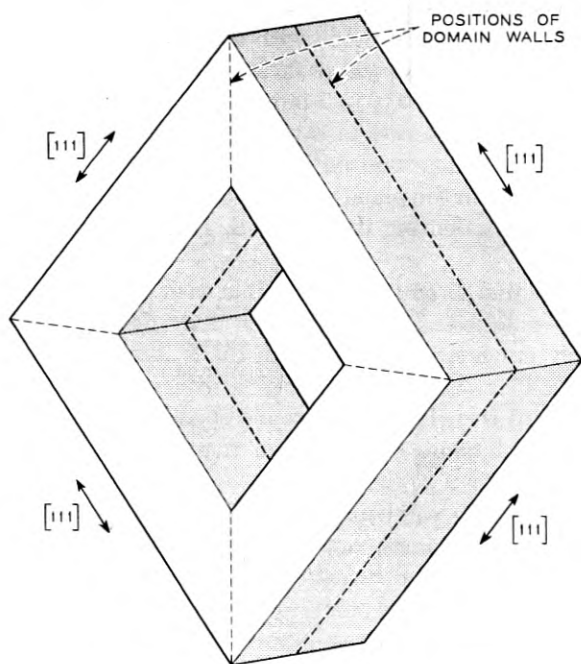

Fig. 1 — Sample of ferrite used in this study.

G. W. Clark from the Linde Air Products Company. Similar studies have been performed previously at room temperature on Fe_3O_4 [7] by the author, and in a preliminary way on $(NiO)_{0.91} (FeO)_{0.09} Fe_2O_3$ [8] by the author in collaboration with J. A. Andrus and H. G. Hopper.

THE EXPERIMENTS

Preparation of Samples

The key to the success of experiments of this sort is of course obtaining the domain pattern shown in Fig. 1, so that we have only one movable wall in the sample. The achievement of this pattern, and the observation of it when achieved, depend in turn on success in producing a perfect or almost perfect sample. It therefore seems worth while to describe the process which has finally emerged as a satisfactory way of producing these samples.

The rough crystal is first oriented by means of X-rays (Laue and X-ray goniometer techniques) to an accuracy of a few minutes while it is mounted in such a position that afterwards we can grind a flat on it which is coincident with the (110) plane. This flat is ground simply with a belt grinder. A cut is then made with a diamond saw parallel to this flat, so that we have a disc whose faces are (110) crystal planes. This disc is usually made about $2\frac{1}{2}$ to 3 mm thick. The second face is ground accurately parallel to the first in a paralleling block. A flat coincident with the (100) plane is ground on the edge of this disc for later use in orienting the sample in the plane of the disc. This flat is also ground with a belt grinder after orienting the disc with Laue and X-ray goniometer techniques.

The disc is ground as smooth as possible with $303\frac{1}{2}$ emery, and then very carefully polished. The polishing is done first on a lap surfaced with No. 0000 french emery paper, with Linde A abrasive loose on top of the emery paper. After this the lap is surfaced with a sheet of very smooth paper and then Linde B abrasive is used. The polishing process takes four to eight hours per disc, and removes all pits visible under $50\times$ magnification, except those inherent in the crystal. Only on such a smooth surface can the very small holes which sometimes occur in these crystals be seen. Sometimes, however, the polishing process conceals fine cracks. It also cannot reveal variations in chemical composition which sometimes occur from point to point in the crystals. Such composition variations are presumably variations in the concentration of divalent iron from point to point in the crystal. In order to reveal these latter imperfections, the disc is etched for three hours by boiling it in

50 per cent H_2SO_4 under a reflux condenser. An asbestos pad is placed between the flame and the bottom of the flask containing the H_2SO_4 in order to prevent sharp temperature fluctuations in the bath. The rate of the etching attack, and the quality of the surface it leaves are sharply dependent upon temperature. It should be mentioned that if this etch is used on the discs *before* polishing, the surface remains rough or may even be made rougher, so that it is impossible to detect the imperfections in the disc. The etch must start on a smooth surface.

Once the disc is cut, polished, and etched, if it is found to be sufficiently free of imperfections, a sample is cut from it in such a way as to avoid those which there are, as they are revealed by the polishing and etching processes. First the diamond-shaped hole is cut by means of a jig whose rotational position with respect to the disc is determined from the (100) flat on the edge of the disc. This jig is a piece of steel which is driven in vibration vertically with a magnetostrictive drive.[9] The surface of the disc is covered with a slurry of carborundum or diamond dust, and this abrasive is made to cut a hole in the disc as the vibrating jig is slowly lowered. With the hole cut in the proper orientation, the outer parts of the disc are ground down to form the legs of the sample. Another jig of the proper shape is used to hold the sample in position during this process.

A hysteresis loop is taken as soon as the sample is cut. A relatively good loop taken on our best sample is shown in Fig. 2. All such loops on these samples are taken on the Cioffi recording fluxmeter.[10] This loop is obviously not yet in the form which we finally need. In order to square the hysteresis loop, we anneal the sample for approximately an hour at 600°C in a magnetic field of 10 to 20 oersteds. The field is produced by running a current through a few turns of glass insulated wire wound on the sample. After such a heat treatment the hysteresis loop of this sample assumed the form shown in Fig. 3.

Once the sample is prepared, the next problem is to observe the domain pattern and find if any important deviations from the pattern shown in Fig. 1 occur. The heat-treatment we give them corrodes the polished surfaces of the sample, and of course the faces exposed when the sample is cut from the disc have not yet been polished. Consequently both the major (110) faces of the sample and the outer faces of the legs are polished, and the sample is then etched in the same way as before. Usually a hysteresis loop is again taken at this point as a check. If the sample is good, it is not significantly different from the loop taken immediately after heat-treatment. The sample is brought to a demagnetized condition at this point so that the movable wall will be near the center of the sample where it can be observed. This completes the process of
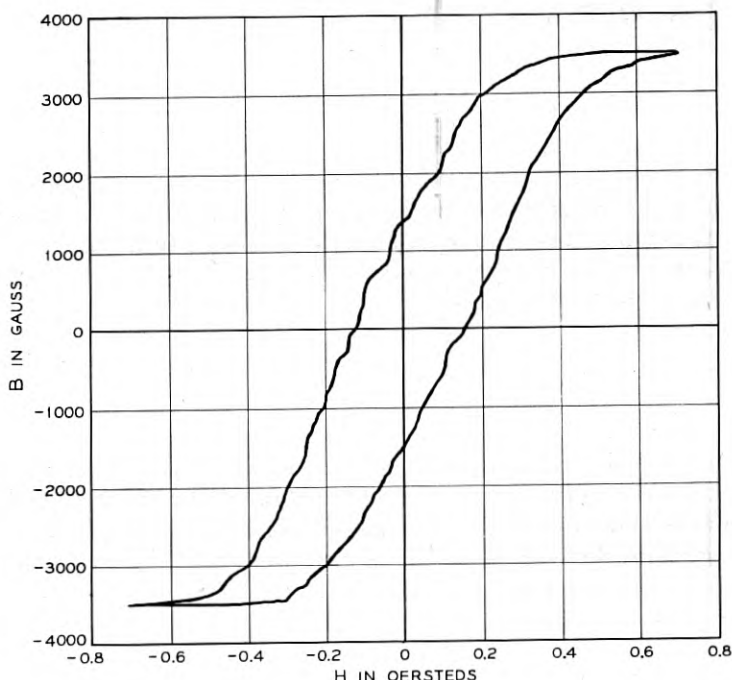
Fig. 2 — Hysteresis loop taken on sample before heat treatment in a magnetic field.

preparing the samples for observing their domain pattern and for performing our experiments on them.

Four samples have been prepared in this way for our studies on $(NiO)_{0.75}$ $(FeO)_{0.25}$ Fe_2O_3 .

Domain Pattern Observations

The method used to observe the domain walls on these surfaces is the same as that used by Williams and his collaborators.[3] We will therefore not describe it in detail. It consists essentially of observing through a microscope the pattern formed by a magnetic colloid on the surface.

The observation of domain patterns, even on these carefully prepared samples, is difficult. There is still some pitting on the surfaces. Also, many of the surfaces become rounded in the process of polishing. This produces surface spikes of the sort discussed by Williams, Bozorth and Shockley.[3] The result is that on many surfaces the domain pattern of the sample as a whole has to be discerned in a substantial amount

of extraneous structure such as surface spikes and pits. It is therefore impossible to show in one picture the whole pattern as diagrammed in Fig. 1. However, more detailed pictures of parts of the pattern do show that it is there. The essential features of the pattern on our best sample are shown in Figs. 4 and 5. Fig. 4 shows the stationary wall at one corner, and Fig. 5 shows a section of the movable wall on one leg. Differentiation of the domain walls in Figs. 4 and 5 from the many scratches is not very difficult after one has some experience in such observations.

The variation in wall position along the leg shown in Fig. 5 is due to the effects of strains and other imperfections, present even in this carefully prepared sample, in determining the position of the wall at rest.
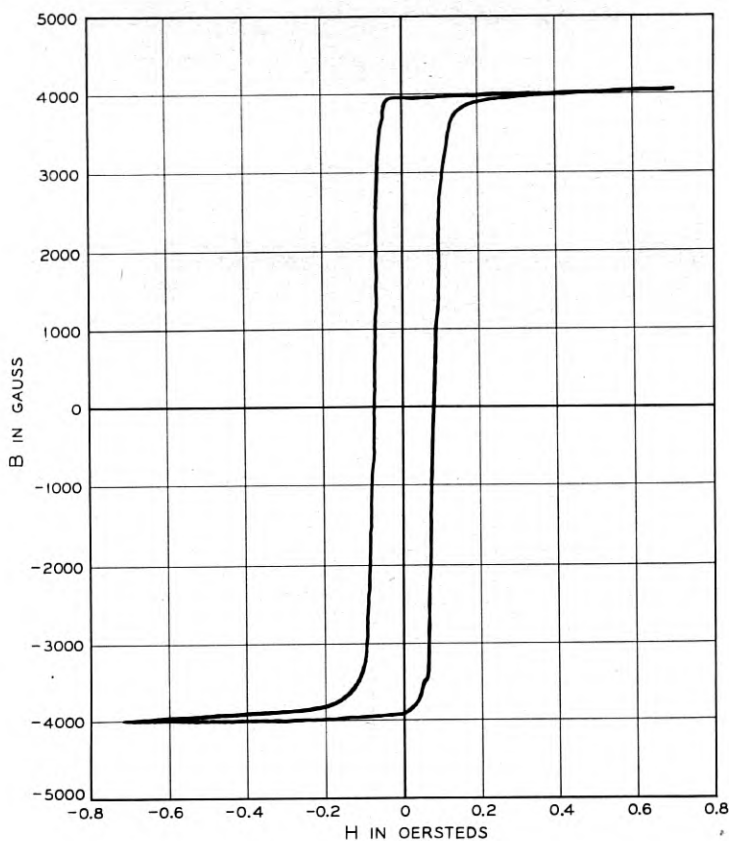

Fig. 3 — Hysteresis loop taken on same sample as loop in Fig. 2 after annealing for one hour at 580°C in a magnetic field of approximately 20 oersteds.
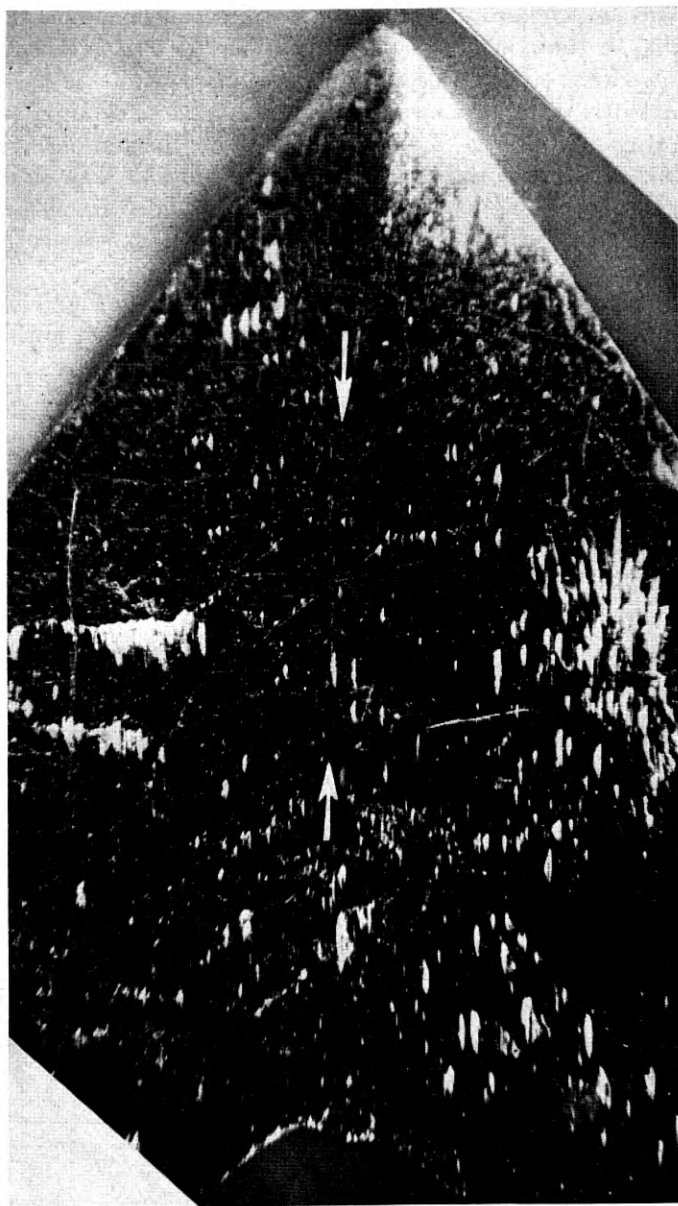
Fig. 4 — Picture of domain pattern at one corner of sample. The stationary wall is indicated by arrows.

Fig. 5 — Picture of a section of the movable wall along one leg of sample. The line has been slightly emphasized by retouching after the picture was taken. The edge of the leg can be seen at the bottom of the figure.

It is unlikely that the wall is so distorted from a plane when in rapid motion, however, since then the driving force and the viscous damping resistance to motion are both much larger than the effects of these imperfections. The imperfections, of course, are primarily effective in determining the coercive force, as read from the hysteresis loop.

The domain pattern as traced out on each of four samples is discussed below:

Sample 1. Although they had spikes associated with them, the stationary walls expected at the corners could be seen, at least in part. In addition, at one of the acute angle corners there was some rather extensive domain wall structure. This structure had one form when the sample was magnetized in one direction, another when it was magnetized in the other. It was due to the presence of a small void at this corner whose magnetic energy was reduced by having domains of reversed magnetization around it. The existence of this void was established from structure which appeared in the spots on an X-ray Laue photograph taken at this point. The process of magnetization in this sample consisted in (a) the growth of the wall from the nucleus around this void until it existed all around the ring, and (b) the motion of this wall to the other side of the sample, where it again shrank to a configuration

which minimized the magnetic energy of the void. As a result of this state of affairs, the wall was not in equilibrium in the middle of the sample, but always shrank around the void so as to magnetize the sample in one direction or the other. It was impossible therefore to demagnetize the sample so that the wall was at the center of the legs and then have the wall stay there to be observed. The wall could be brought to the center, however, and held there using the technique mentioned by Williams and Shockley[3] (see Fig. 8 in their paper). The legs of the sample were so small that it was difficult to do this, but the wall was found on three legs of the sample at different times in this way. The wall curved a good deal in traveling along the legs. This sample was etched repeatedly so that data could be obtained as a fuction of sample dimensions. The variations observed led to a viscous domain wall damping independent of dimensions if it was assumed that the domain wall was perpendicular to the major (110) face. Therefore it was to this (11$\bar{2}$) plane that the wall was brought for observation.

Sample 2. Stationary walls at the corners were rather patchy but visible. The movable wall was traced along the outside faces of two legs, which indicates that it lay in the (110) plane. The wall curved a good deal. There were also other walls which enclosed patches of surface. It is suspected that these patches were the bases of spike domains extending into the sample from strain patterns on the surface. The sample was therefore etched again. Unfortunately, the bath apparently became locally overheated, and this etch took off rather more material than expected. It also left a matte surface on which domain walls could not be observed. The data taken on this sample, however, check those on other samples if we assume a pattern in which the movable wall is in the (110) plane, as our observations lead us to suspect.

Sample 3. The stationary walls at the corners were seen, but only with difficulty. They were patchy. There was a good deal of structure all along the legs on the major (110) face of this sample, but no wall which ran around the sample could be seen on this face.

On the outside of two of the legs, which are (11$\bar{2}$) faces, pitting and extraneous walls were so bad that the main wall could not be discerned. On a third, the wall could be traced most of the way. On the fourth, however, there were two walls, one of which could be traced along the whole leg, the other of which went only three-fourths of the way along the leg. Both walls on this leg showed a good deal of curvature. It therefore appears that the movable wall lies in the (110) plane, but that there is *another wall* big enough so that it may move and affect our data. This picture of a domain pattern with two movable walls was confirmed by checking the data obtained on this sample with those from others.

Sample 4. The stationary walls at the corners, although patchy, were seen. There was some extraneous domain wall structure on the major (110) faces, but nothing which looked at all like the main wall.

On the outside (11$\bar{2}$) faces of the legs, however, the wall was traced almost all the way around. Only short sections were impossible to trace. The wall curved as usual, and there was some extraneous domain wall structure on these faces, but substantially the whole of the ideal pattern shown in Fig. 1 was seen on this sample. The hysteresis loops shown in Figs. 2 and 3 and the domain pattern pictures shown in Figs. 4 and 5 were taken on this sample.

Not only was the domain pattern on sample 4 the best and most complete, but the data taken on this sample was much the most reproducible. We shall therefore report the data taken on this sample in detail, and simply refer to the results on other samples as a check and to indicate the sort of variations which occurred from sample to sample.

Measurements

Our procedure in making the measurements is as follows. The sample is wound with a primary and a secondary winding. A square pulse of positive voltage is applied to the primary winding in series with a resistor which is large enough to keep the pulse rise time short. The rise time must be short compared to the time required for the field produced by the pulse to reverse the magnetization of the sample. On the other hand, since the pulse is applied for the purpose of reversing the magnetization of the sample, the length of the pulse must be at least comparable with the time required for the reversal to occur; if possible, it should be longer than this. The reversal time, of course, is the time required for the mobile domain wall to move from one side of the sample to the other under the field produced by the applied pulse. A second pulse, of negative voltage, is applied to the primary during each cycle of the pulser in order to bring the wall back to its original position so that the phenomenon may be observed repetitively.

By synchronizing an oscilloscope sweep with the pulser, the signal induced in the secondary winding is observed while the applied pulse is on the primary. Since this signal is proportional to the velocity of the wall, it is constant to a first approximation during the application of a constant field. Irregularities in the crystal may cause the velocity of the wall to vary somewhat as it moves across the sample, however, and this will cause the signal to vary too. In this case, the observer reads the average value. Fig. 6 shows an example of the signal induced in the secondary winding as seen on an oscilloscope. Sample 4 was used to obtain this picture.
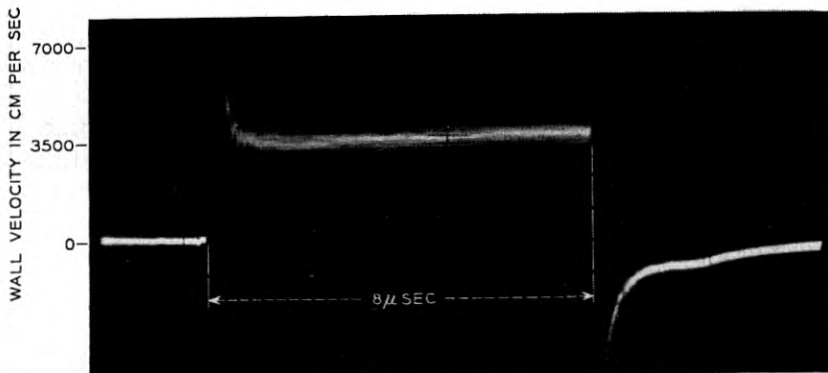
Fig. 6 — Oscilloscope trace of the induced voltage in the secondary winding while a square current pulse 8μ sec long was applied to the primary. The voltage spike at the beginning is not completely understood, but is thought to be connected with the fact that the domain wall spikes associated with imperfections do not pull back on the domain wall until it has moved a little distance. In this sample, once this initial peak is over, the wall velocity comes to its steady state value and is not much disturbed by imperfections, so that the observer need do no averaging. In this case, the wall was moving with a velocity of 3500 cm/sec. At this velocity, the wall was unable to reverse the magnetization in 8μ sec, so the signal ends as the magnetic field goes to zero at the end of the pulse. After the pressure on the wall due to the magnetic field stops, the domain wall spikes associated with imperfections pull the wall back slightly, giving rise to the voltage spike in the opposite direction.

The applied field due to the primary pulse is deduced from the current in the primary winding (measured by observing the voltage across the series resistor) using the solenoid formula $H = 4\pi NI$. To obtain the relation between wall velocity and induced voltage per secondary turn we have:

$$\text{Volts/turn} = (d\Phi/dt) \times 10^{-8} = 8\pi M_s(\Delta z/\Delta t)w_{\text{wall}} \times 10^{-8}, \quad (1)$$

where $(\Delta z/\Delta t)$ is equal to the domain wall velocity v, and w_{wall} is the width of the wall between the boundaries of the sample in the direction perpendicular to the direction of magnetization. It is in deriving (1), of course, that we use our detailed knowledge of the domain pattern in the sample.

We are thus able to obtain a value of the domain wall velocity v for each value of the applied field H. These data are the results of the experiment.

The value of M_s used in (1) is the measured value (322.5 cgs units/cc) at room temperature. The values used at other temperatures have been deduced on the assumption that M_s varies the same way with temperature in this material as it does in magnetite as measured by Weiss and

Forrer.[11] We have extrapolated their data to get the variation up to our highest temperatures.

In general, a plot of the data turns out to have the form shown in Fig. 7. This is the data taken on Sample 4 at 201°K. The wall does not move until the field exceeds the coercive force required to get it past various imperfections in the crystal. Its motion in fields higher than this is viscously damped. The wall velocity, v, therefore follows the relation:

$$v = G(H - H_c), \qquad (2)$$

where H_c is the coercive field and G is the slope of the line drawn through the data. The value of G is high if the losses are low, and vice versa, of course.

RESULTS

Data on Sample 4 of the sort shown in Fig. 7 have been taken at various temperatures. We show in Fig. 8 a plot of $v/(H - H_c)$ as a function of temperature for this sample. Clearly, the outstanding feature of the data is a tremendous increase in the viscous damping of the domain wall at low temperatures.

Since the other samples were not as satisfactory, for reasons given above, we do not reproduce the data on them explicitly. Similar data have been taken on Samples 1 and 2, however, and they show the same behavior within their accuracy except that the very sharp decrease in $v/(H - H_c)$ seemed to occur at a somewhat higher temperature. This difference may be due to slight variations in composition among the
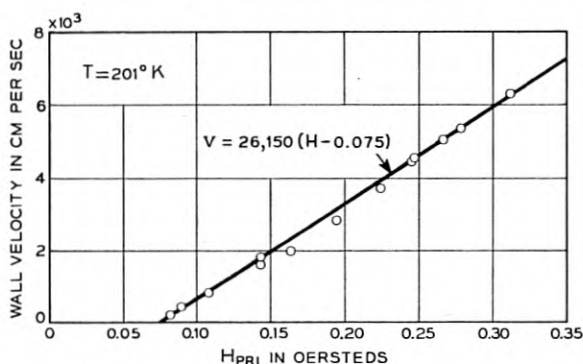

Fig. 7 — Typical plot of actual data for domain wall velocity as a function of applied field.

samples (Chemical analysis indicated that Sample 1 was

$$(NiO)_{0.77}(FeO)_{0.23}Fe_2O_3 ,$$

as distinct from

$$(NiO)_{0.75}(FeO)_{0.25}Fe_2O_3$$

for Sample 4) but it is possible that other more subtle differences such as the arrangement of the divalent nickel and iron ions are involved. Voltages induced in the secondary winding on Sample 3 for various applied fields were much higher than for the other samples at room temperature. This confirms the presence of more than one wall as indicated by the domain pattern. Therefore no further data were taken on this sample.

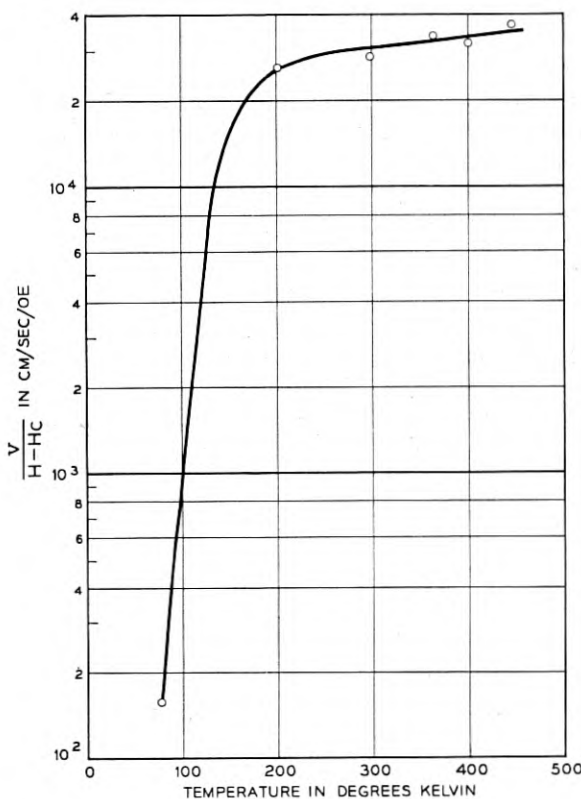Each sample, after it had been cooled to the temperature of liquid

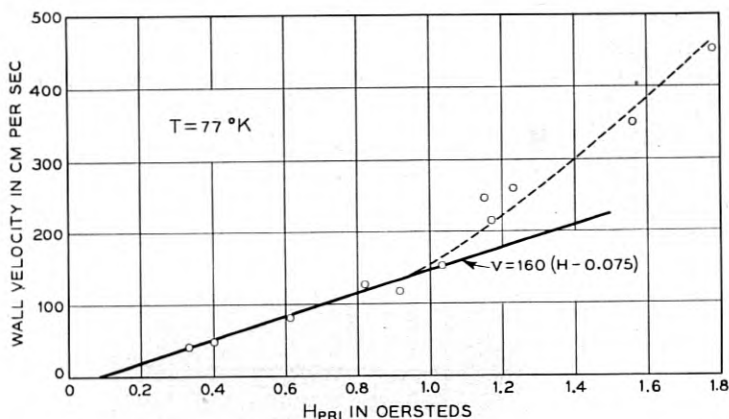Fig. 8 — Plot of $v/(H - H_c)$ for Sample 4 as a function of temperature.

Fig. 9 — Plot of wall velocity as a function of applied field at 77°K. Note that at the higher fields the velocity is no longer a linear function of the applied field.

air once, gave the same value of $v/(H - H_c)$ as before. Samples 1 and 2, however, were cooled several times, and after the later runs they no longer did this. In both cases the value of $v/(H - H_c)$ as deduced from the ideal domain pattern and (1) was lower by about one-half; we interpret this to mean that the domain pattern in these samples was changed by the repeated thermal shock. Direct confirmation of this interpretation by observation was not possible, however, for reasons indicated above in connection with domain pattern observations on these samples.

In view of the fact that only one point is plotted beyond the knee of the curve in Fig. 8, it should be emphasized that continuous qualitative observations made while the sample was cooling showed that the change was continuous and monotonic. On Sample 1, furthermore, the data at 201°K was somewhat down from the knee of the curve $[v/(H - H_c) = 18000$ cm/sec/oe] because of the fact that the knee occurred at higher temperature as mentioned above.

Another feature of the data is indicated by Figs. 9 and 10. Data discussed thus far have been taken at the lowest convenient velocities in order to minimize the possibility of wall distortion. However, when data were taken at higher fields, a non-linearity of the sort shown in Fig. 9 appeared. The average velocity increases more rapidly at the higher fields than our viscous damping coefficient would lead us to expect. This effect was observed at all temperatures, but as comparison of Figs. 7 and 9 will show, it set in at lower velocities at low temperatures where the enlarged viscous damping appeared. Simultaneously with the appearance of this non-linearity in the apparent average velocity of the

wall, the voltage induced in the secondary winding during the pulse of constant applied field is seen from the oscilloscope trace to distort with time. Fig. 10 shows a series of traces observed at room temperature on Sample 4 which show this distortion increasing from (a) to (d) as the applied field is increased. At the highest fields the trace forms a peak which is almost triangular in shape.

We shall discuss the theoretical implications of these data in the next two sections.
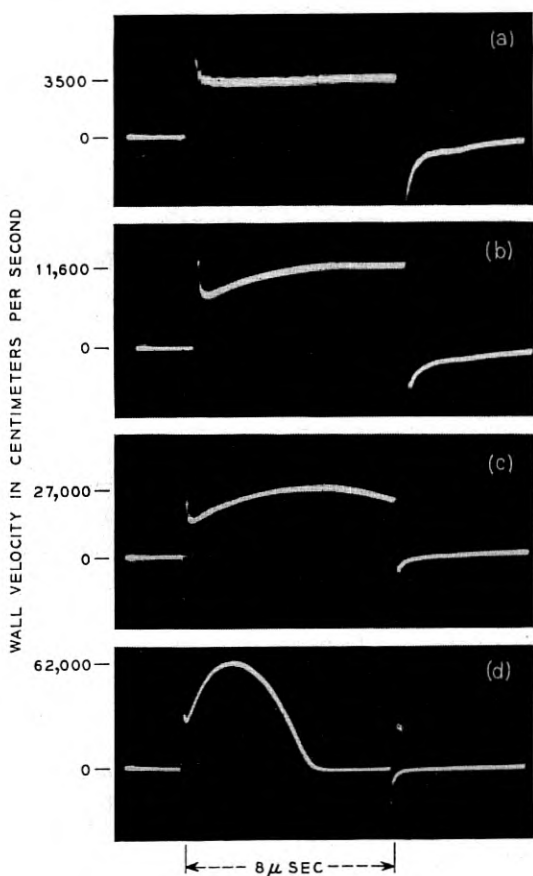

Fig. 10 — A series of oscilloscope traces showing the deviation of the wall velocity from a constant with time at the higher applied magnetic fields and therefore at the higher velocities. These pictures were taken at room temperature, but similar phenomena occur at all other temperatures in the range of applied fields where the nonlinearity in velocity shown in Fig. 9 becomes apparent. The velocities, as shown, increase from a to d.

THEORY

A theoretical analysis of the experimental results given in the last section divides itself rather naturally into three parts. First we characterize the data in terms of an equation of motion for unit area of domain wall. This means we determine the constants of motion (viscous resistance and coercive force in our case) of unit area of wall. Secondly, we show the relation between the viscous resistance of unit area of domain wall, and the constants which characterize the ferromagnetic material in general (saturation magnetization, crystal anisotropy, etc.). This is essentially an application of the recent work of Becker[12] and Kittel.[13] Lastly, we calculate the magnitude of the damping from a relaxation mechanism which accounts for the low temperature effect shown in Fig. 8 at least qualitatively.

Consider unit area of a 180° domain wall between two regions of saturated material. Such a system has an equation of motion for small amplitudes of the applied magnetic field H which may be written:

$$m\ddot{z} + \beta\dot{z} + \alpha z = 2M_s H, \tag{3}$$

where z is the displacement of the domain wall along its normal, m is its mass per unit area, β is a parameter measuring viscous resistance, and α is a stiffness parameter which has meaning only for small fields such as those used in initial permeability measurements. When fields larger than the coercive force are applied, as in our experiments, the term containing α disappears and the field effective in moving the wall is less than the applied field by an amount equal to the coercive force; this is shown by the data given previously in the section on results. This reformulation of (3) is quite reasonable when one remembers the spikes which pull back on the wall, in the experiments of Williams and Shockley, for small wall motions and snap off entirely if the wall moves a large distance. Furthermore, since the velocity of the domain wall rises to its steady value in a negligible time in these experiments (Fig. 6) the initial term in (3) is also negligible. As these remarks indicate, under the conditions of the experiment in wall velocity, (2) takes the form:

$$\beta\dot{z} = 2M_s(H_{app} - H_c). \tag{4}$$

This relation obviously fits the data given previously.

The second step in the theoretical analysis starts from an equation of motion for the magnetization $\vec{M}$ in a small volume which was first used by Landau and Lifshitz,[6] and takes advantage of more recent work of Becker[12] and Kittel.[13] If we consider a volume small enough so that the

magnetization in it is everywhere uniform even if we are inside the domain wall, our equation of motion is:

$$\frac{d\vec{M}}{dt} = \gamma[\vec{M} \times \vec{H}] - \lambda/M^2[\vec{M} \times (\vec{M} \times \vec{H})]. \tag{5}$$

Here γ is the gyromagnetic ratio ($ge/2$ mc), and λ is a parameter, assumed to be characteristic of a given ferromagnetic material, which is determined by the magnitude of the damping effects in the motion of $\vec{M}$. The magnitude of the last term on the right in (5) is thus determined by the amount of the damping losses.

The rate of dissipation of energy in the small volume is $\vec{H} \cdot (d\vec{M}/dt)$, where $\vec{M}$ is the magnetic moment of the volume, and $\vec{H}$ is the total magnetic field in the volume. The value of $\vec{H}$ requires some discussion. Outside the wall $\vec{H} = \vec{H}_0$ where $\vec{H}_0$ is the applied field, which is parallel to the wall. When the wall is moving, however, there is an additional field $\vec{H}_e$ inside it. This field, which is normal to the wall, is a demagnetizing field which arises from the tendency of $\vec{M}$ in the moving wall to have a component normal to the wall. This field has just such a value that the magnetization in the moving wall precesses about it with the Larmor frequency. Its value is:

$$\vec{H}_e = -(\vec{v}/\gamma)(\partial\theta/\partial z), \tag{6}$$

as Becker[12] has shown. Here $\vec{v}$ is the velocity of the wall, z is a distance coordinate normal to the wall, and θ is the rotational angle of the magnetization as we pass through the wall along z. Inside the wall, $\vec{H}_e$ is much larger than $\vec{H}_0$, but in any case $\vec{H} = \vec{H}_e + \vec{H}_0$. From (5) we find:

$$\vec{H} \cdot d\vec{M}/dt \cong \lambda H_e^2, \tag{7}$$

as Kittel[13] first showed. In the theory of the domain wall it is shown that $\partial\theta/\partial z$ in the wall is equal to the square root of the ratio of the increase in anisotropy energy as the magnetization turns away from the easy direction of magnetization, to the exchange energy constant. That is[14]:

$$\frac{\partial\theta}{\partial z} = ([g(\theta) - g(\theta_0)]/A)^{1/2}. \tag{8}$$

The exchange energy constant A is defined by the following expression for the exchange energy per unit volume due to gradients in the direction

of magnetization:

Exchange energy/unit vol $= A[(\nabla\alpha_1)^2 + (\nabla\alpha_2)^2 + (\nabla\alpha_3)^2]$, (9)

where α_1, α_2, and α_3 are the direction cosines of the magnetization. $g(\theta)$ is the anisotropy energy:

$$g(\theta) = K_1 (\alpha_1^2\alpha_2^2 + \alpha_2^2\alpha_3^2 + \alpha_3^2\alpha_1^2),$$ (10)

expressed in terms of θ, and $g(\theta_0)$ is the anisotropy energy along the direction of easy magnetization. Note that $[g(\theta) - g(\theta_0)]$ is always positive. K_1 is the first order anisotropy constant.

If we use (6) and (8) in (7), and integrate over z along a cylinder of unit cross-section normal to the wall to get the rate of energy dissipation for unit area of moving wall, we have:

$$\int_{-\infty}^{\infty} \vec{H} \cdot \frac{d\vec{M}}{dt}\, dz = (\lambda v^2/\gamma^2 A^{1/2}) \int_{\theta_1}^{\theta_2} [g(\theta) - g(\theta_0)]^{1/2}\, d\theta = 2H_0 M_s v, \quad (11)$$

where θ_1 and θ_2 are the angular positions of $\vec{M}$ on the two sides of the wall. $\theta_2 - \theta_1 = \pi$, of course, since we are considering a 180° domain wall. In order to obtain (11), we have used (8) to transform from integration over z to integration over θ as well as to evaluate (7). We set our result equal to $2M_s H$ (pressure on the wall) times v since this is the rate at which the wall, considered phenomenologically, does work. We may now write:

$$v = \frac{2M_s\gamma^2 A^{1/2}}{\lambda \int_{\theta_1}^{\theta_2} [g(\theta) - g(\theta_0)]^{1/2}\, d\theta} H_0.$$ (12)

This is the desired relation between wall velocity and applied field which is to be compared with (4). In this way we find:

$$\beta = (\lambda/\gamma^2 A^{1/2}) \int_{\theta_1}^{\theta_2} [g(\theta) - g(\theta_0)]^{1/2}\, d\theta.$$ (13)

We have thus shown the relation between the wall parameter β and the parameter λ which measures in general the losses associated with motions of the magnetization.

The third part of our theoretical analysis is concerned with a calculation of the damping parameter λ, or rather the relation between v and H itself, from an explicit physical mechanism. Such a calculation has not been made in the past since the appropriate mechanism on which to base it has remained obscure. Verwey and his co-workers[15] have explained the well known transition at about 115°K in Fe_3O_4 as

an order-disorder transition in the arrangement of the divalent and trivalent iron ions. M. Fine of Bell Telephone Laboratories has found a remnant of this transition in crystals of the same composition as those studied in the present research, by means of ultrasonic measurements of elastic constants.[16] We propose that the mechanism which causes the sharp rise in the damping of domain wall motion at low temperatures is a relaxation associated with this transition. Wijn and van der Heide[17] have explained in this way observations of theirs of losses associated with initial permeability at low frequencies in certain other polycrystalline ferrites. The time associated with this relaxation should be short because this rearrangement of ions involves only the motion of electrons from one site to another.[18] It should be of the order of the relaxation time associated with the electrical conductivity of Fe_3O_4. Snoek[19] has suggested some time ago that losses in the ferrites were due to an after-effect (relaxation) which, because of the short time constant involved, must be associated with electron migrations.

It is extremely useful to compare our data with a theory of the damping based on the above relaxation mechanism no matter what assumptions we make in detail about what it is that relaxes. We shall see that we are led quite generally to the result that $v/H \sim 1/\tau$ where τ is the relaxation time for the process. However, in order to perform this calculation explicitly we must make more detailed assumptions about exactly what quantity relaxes with the relaxation time τ. Changes in the direction of the magnetization cause changes in stress in the sample because of magnetostriction. One possible assumption is that the resulting strain would lag behind this stress and mechanical energy would be dissipated in the crystal. This mechanism, however, cannot act in our case. The magnetization in the two domains on each side of the wall points in opposite directions, but causes the same strain in both, and they have such a large stiffness that the thin region occupied by the domain wall assumes this same strain even though the direction of the magnetization is different there. Thus regardless of the stresses produced in the wall, the strains remain the same, inside and outside the wall, whether it is moving or not; under these conditions no work is done on the lattice, and no energy can be lost in this way by the moving wall. A calculation has been made by the author on the assumption that it is the magnetization itself which relaxes with relaxation time τ. This assumption leads to the result that wall velocity is *not* linearly dependent upon $(H - H_c)$; it is therefore not correct, since the data shows such a linear dependence. A similar result is to be expected if we assume that the dielectric polarization relaxes.

What seems at present likely to be the approximate nature of the mechanism, and what we will assume is the nature of the mechanism for the purposes of an illustrative calculation is as follows. As the domain wall passes a point in space, and the direction of $\overrightarrow{M}$ changes, the electrons on the divalent and trivalent iron ions tend to rearrange themselves so as to minimize the magnetocrystalline anistropy energy.[20] If $\overrightarrow{M}$ changes slowly this anistropy energy is near the minimum possible value (the *reversible* value) at all times, and the process is almost isothermal. As a result of the fact that the process deviates irreversibly from equilibrium, however, net work is done in bringing about the change. If, on the other hand, the direction of $\overrightarrow{M}$ changes so suddenly that the electrons have no time to rearrange, the process is adiabatic, and the magnetocrystalline anistropy energy varies more widely with the angular position of $\overrightarrow{M}$.

Since our data is taken at low velocities and extrapolated to zero velocity, it seems most appropriate for us to make a calculation of the losses on the assumption that as we increase the velocity of the wall we are deviating from the isothermal condition. Let us define as a thermodynamical system the part of the magnetic lattice which lies in a small volume fixed in space. This volume is a sheet of unit cross-section in which the magnetization is uniform and which is part of the cylinder of unit cross-section normal to the wall mentioned in connection with (11). From the first law of thermodynamics, as the wall passes the small volume, we have:

$$dw = dU - dQ = dg, \tag{14}$$

where dQ is heat added to the system, dU is a change in internal energy, dw is work done on the system, and g is the anisotropy energy associated with our rearranging electrons. Note that g, is a term in the free energy of the magnetic lattice. The free energy includes other terms in addition to g, and indeed there is in general another term in the magnetocrystalline anisotropy energy; we will not consider any of these, however, since they also integrate to zero as the domain wall passes our small volume. Similarly, there are many contributions to dw, but we will concern ourselves only with the term which does net work on our system, the pressure on the wall times its velocity. If we now consider changes in our system with time we have from (14):

$$\frac{dw}{dt} = \frac{dg}{dt}. \tag{15}$$

The rate of doing work on unit area of the wall moving along our

cylinder, which is the integral of dw/dt over the cylinder, is $2M_s H_0 v$ as in (11). The rate of dissipation of energy in this section of the wall is somewhat more difficult to calculate. It is the sum of contributions from all the small volumes along the cylinder. In order to calculate the contribution from the small volume we are considering, we first note that if the process is reversible,

$$dg = \frac{dg}{d\theta} \, d\theta, \tag{16}$$

where θ is the angle of rotation of $\overrightarrow{M}$. Physically, the factor $dg/d\theta$ represents a torque on the magnetization. We will assume that (16) holds even when the domain wall passes our system at a finite velocity and we have departed slightly from isothermal equilibrium. The field H_e defined in (6) transmits this torque to make the magnetization rotate through the angle θ, but we will not go further into the details of this process.

As the domain wall goes by, $dg/d\theta$, which we will abbreviate as g', changes. If the process were reversible, g' would be zero at all times and the torque on the magnetization would always have its equilibrium value. Actually, as we deviate more and more from the reversible process by moving the wall faster, the electrons are no longer able to rearrange fast enough, and g' deviates from zero while continually relaxing toward it. We must form our analysis in such a way that a maximum is established for g', since even if the magnetization moves infinitely rapidly, g' does not become infinite. Since the electrons minimize their free energy, it must be positive, and we write $g = g_{1\infty} - g_1$ so that $g' = g'_{1\infty} - g'_1$, where g'_1 relaxes toward $g'_{1\infty}$. Note that the torque relaxes *downward* from a value, $g'_{1\infty}$, associated with the adiabatic anisotropy energy (fast motions of the magnetization) to a value zero, associated with the isothermal anisotropy energy (slow motions of the magnetization). We may now write:

$$\frac{dg'_1}{dt} = \frac{g'_{1\infty} - g'_1}{\tau}. \tag{17}$$

Physically, this relation assumes that the torque on the magnetization relaxes in the same way if $g'_{1\infty}$ is a continuous function of time as it would if $g'_{1\infty}$ and g'_1 differed but $g'_{1\infty}$ was constant. Here τ is the relaxation time associated with the rearrangement of divalent and trivalent iron ions. If we write (17) in the form:

$$\frac{dg'_1}{dt} + \frac{g'_1}{\tau} = \frac{g'_{1\infty}}{\tau}, \tag{18}$$

we see at once that the solution for g_1' as a function of t as the domain wall passes the position of our small volume is:

$$g_1'(t) = \frac{1}{\tau} e^{-t/\tau} \int g_{1\infty}'(t) e^{t/\tau} \, dt. \tag{19}$$

We have ignored the solution of the homogeneous equation, as it contains a factor $e^{-t/\tau}$.

In order to evaluate (15) for our small volume, we need a more explicit value for g_1'. From the Fourier transformation we may write:

$$g_{1\infty}'(t) = \int_{-\infty}^{\infty} G_{1\infty}'(\omega) e^{i\omega t} \, d\omega. \tag{20}$$

Consequently:

$$g_1'(t) = \frac{1}{\tau} e^{-t/\tau} \iint_{-\infty}^{\infty} G_{1\infty}'(\omega) e^{(1/\tau + i\omega)t} \, d\omega \, dt. \tag{21}$$

This can be integrated over t. If we do this, then bring the factor $e^{t/\tau}$ out from under the integral sign, we find:

$$g_1'(t) = \int_{-\infty}^{\infty} \frac{G_{1\infty}'(\omega)}{1 + i\omega\tau} e^{i\omega t} \, d\omega. \tag{22}$$

Now the frequencies for which we get a contribution to the integral in (22) have an upper bound determined by the velocity and the thickness of the domain wall, of course. The faster the domain wall moves, the higher the upper bound on the frequency. We have been careful to make our measurements near zero wall velocity, and the data clearly extrapolates linearly to zero. This was done in order to minimize the possibility of wall distortion, but it also is consistent with our assumption of almost isothermal conditions. We are therefore justified in assuming that $\omega\tau \ll 1$ for all the frequencies in $G_{1\infty}'(\omega)$, and we can expand the factor $1/(1 + i\omega\tau)$ in (22). We obtain:

$$g_1'(t) = \int_{-\infty}^{\infty} [1 - (i\omega\tau) + (i\omega\tau)^2 + \cdots] G_{1\infty}'(\omega) e^{i\omega t} \, d\omega, \tag{23}$$

and if we form the derivatives of (20) and compare them with the terms in (23), we see that:

$$g_1'(t) = g_{1\infty}'(t) - \tau \frac{dg_{1\infty}'(t)}{dt} + \tau^2 \frac{d^2 g_{1\infty}'(t)}{dt^2} + \cdots \tag{24}$$

Since the value of τ is very much less than one, the series in (24) converges quite rapidly at low domain wall velocities, and we only keep the first two terms.

Until now, we have been concerned with a small volume of the magnetic lattice fixed in space. As in deriving (11), if we wish to calculate the rate of loss of energy for unit area of the domain wall moving with constant velocity, we must integrate dg_1/dt over a cylinder of unit cross-section normal to the wall. $g'_{1\infty}$ is now a function of $(t - z/v)$ where v is the velocity of the domain wall, and z is a coordinate normal to the wall. If we form this integral, and use (16) and (24), we find:

$$\int_{-\infty}^{\infty} \frac{dg_1}{dt}\, dz = \int_{-\infty}^{\infty} \left[g'_{1\infty}(t - z/v) - \tau \frac{dg'_{1\infty}}{dt}(t - z/v) \right] \frac{d\theta(t - z/v)}{dt}\, dz \quad (25)$$

We note that:

$$\begin{aligned}
\frac{dg'_{1\infty}(t - z/v)}{dt} &= -v\, \frac{dg'_{1\infty}(t - z/v)}{dz}\,, \\
\frac{d\theta(t - z/v)}{dt} &= -v\, \frac{d\theta(t - z/v)}{dz}\,.
\end{aligned} \quad (26)$$

For the first term in (25) we find, using (26):

$$\int_{-\infty}^{\infty} g'_{1\infty}(t - z/v)\, \frac{d\theta(t - z/v)}{dt}\, dz = -v \int_{\theta_1}^{\theta_2} g'_{1\infty}(t - z/v)\, d\theta = 0, \quad (27)$$

since $g_{1\infty}$ is the same on both sides of the domain wall. Now if we use (26) in the second term of (25), and remember the result in (27), we have:

$$\int_{-\infty}^{\infty} \frac{dg_1}{dt}\, dz = -\tau v^2 \int_{-\infty}^{\infty} \frac{dg'_{1\infty}(t - z/v)}{dz}\, \frac{d\theta(t - z/v)}{dz}\, dz. \quad (28)$$

We may, without loss of generality, evaluate the intergral in (28) at $t = 0$. It is therefore the integral of a function of z over z. In order to evaluate it, we wish to express $g'_{1\infty}$ as a function of θ. We have:

$$\int_{-\infty}^{\infty} \frac{dg_1}{dt}\, dz = -\tau v^2 \int_{-\infty}^{\infty} \frac{dg'_{1\infty}}{d\theta} \left(\frac{d\theta}{dz} \right)^2 dz, \quad (29)$$

$$= -\tau v^2 \int_{\theta_1}^{\theta_2} \frac{d^2 g_{1\infty}}{d\theta^2} \frac{d\theta}{dz}\, d\theta, \quad (30)$$

where we have replaced $g'_{1\infty}$ by $dg_{1\infty}/d\theta$. We note now, from the relation between g and g_1, that $dg_1/dt = -dg/dt$. We therefore set the right hand

side of (30) with reversed sign equal to:

$$\int_{-\infty}^{\infty} \frac{dw}{dt}\, dz = 2M_s H_0 v,$$

as mentioned after (15) to get the relation between the velocity of the domain wall and the applied field. As we shall see later, the right hand side of (30) is positive if we use a g_{1_∞} associated with a positive contribution to the anisotropy energy. We find:

$$v = \frac{1}{\tau}\, \frac{2M_s}{\displaystyle\int_{\theta_1}^{\theta_2} \frac{d^2 g_{1_\infty}}{d\theta^2} \frac{d\theta}{dz}\, d\theta}\, H_0 . \tag{31}$$

The derivatives of θ with respect to z in (29), (30), and (31) are to be evaluated by means of (8) and (10). In using these equations, of course, we are assuming that the wall is moving slowly enough so that its shape remains that of the wall at rest.

Equation (31) shows that $v \sim H/\tau$ as we mentioned earlier. Inspection of Fig. 8 shows that this relationship explains very satisfactorily the sharp drop in $v/(H - H_c)$ at low temperatures if we remember that τ depends on temperature as follows:

$$\tau = \tau_\infty\, e^{\epsilon/kT}, \tag{32}$$

where ϵ is an activation energy.

Finally, the right hand side of (30) may be set equal to:

$$\int_{-\infty}^{\infty} (\vec{H} \cdot d\vec{M}/dt)\, dz,$$

as calculated from the Landau-Lifshitz equation, see (11), to obtain a value for λ. We find:

$$\lambda = \tau\, \frac{\gamma^2 A^{1/2} \displaystyle\int_{\theta_1}^{\theta_2} \frac{d^2 g_{1_\infty}}{d\theta^2} \frac{d\theta}{dz}\, d\theta}{\displaystyle\int_{\theta_1}^{\theta_2} [g(\theta) - g(\theta_0)]^{1/2}\, d\theta} . \tag{33}$$

DISCUSSION

It is clear that (4) fits our experimental data at each temperature. By fitting our data to this expression we obtain values for β, the parameter characteristic of the material which measures the damping of the wall. Values of β obtained in this way are given in Table I. A more

correct value of M_s for Fe_3O_4 at room temperature (475 c.g.s. units) has been used in calculating the β given in Table I than has been used in previous calculations.

In Table I we give in addition to values of β, values of λ at room temperature obtained from (13). The value for Fe_3O_4 is calculated from the new value of β and also corrected for the error mentioned in Reference 14. Values given in References 7 and 8 are somewhat in error. The values of β and λ given for Fe_3O_4 in Table I are the remainders after the contribution due to eddy currents has been subtracted out by means of the low field calculation of Williams, Shockley, and Kittel,[3] [see their Equation (11)].

TABLE I — ROOM TEMPERATURE DATA ON Fe_3O_4 AND
$(NiO)_{0.75} (FeO)_{0.25} Fe_2O_3$

	(c.g.s. units)		
	β (corrected for eddy currents)	λ domain wall	λ ferromagnetic resonance
Fe_3O_4............................	0.44	5.5×10^8	9×10^8
$(NiO)_{0.75} (FeO)_{0.25} Fe_2O_3$........	0.023	4.6×10^7	10×10^7

TABLE II — DATA FOR $(NiO)_{0.75} (FeO)_{0.25} Fe_2O_3$*

$T(°K)$	M_s (c.g.s. units)	K_1 (ergs/cc)	$v/(H - H_c)$ (cm/sec/oe)	λ domain wall (c.g.s. units)
77	341	-8.1×10^4	158	6.3×10^9
201	335	-5.4×10^4	26150	4.4×10^7
300	322.5	-3.8×10^4	28500	4.6×10^7
363	309	-3.1×10^4	32500–35300	$4.0–4.3 \times 10^7$
400	298	-2.8×10^4	31750	4.5×10^7
445	281	-2.4×10^4	36850	3.9×10^7

* The value of M_s at $300°K$ is measured from the hysteresis loop of Fig. 3. Other values were obtained by assuming that M_s varied with T in the same way as observed by Weiss and Forrer[11] in Fe_3O_4.

The evaluation of λ from (13) is done as follows. Since the wall is in a (110) plane, we find from (10):

$$g(\theta) - g(\theta_0) = \frac{|K_1|}{4} (2/\sqrt{3} - \sqrt{3} \sin^2 \theta)^2, \qquad (34)$$

where θ is the angle between $\overrightarrow{M}$ and the [100] direction which lies in the plane of the domain wall. θ is $\cos^{-1}(1/\sqrt{3})$ on one side of the wall, and

$\pi + \cos^{-1} 1(/\sqrt{3})$ on the other. Then,

$$\int_{\cos^{-1}(1/\sqrt{3})}^{\pi+\cos^{-1}(1/\sqrt{3})} [g(\theta) - g(\theta_0)]^{1/2} d\theta = 0.92 \sqrt{|K_1|} . \qquad (35)$$

In performing this integration, care must be taken to use the positive value of the square root over the whole interval. It should be noted that in using (8) and (10) to evaluate (13) we are assuming that the wall is moving slowly enough so that its shape is the same as that of the wall at rest. A is best evaluated from a fundamental relation derived by Herring and Kittel[21] between A and the Bloch constant:

$$A = [S_0/\Omega]^{1/3}[k/13.3C^{2/3}], \qquad (36)$$

where k is Boltzmann's constant, C is Bloch's constant as used in the relation $M_s = M_0(1 - CT^{3/2})$, S_0 is the atomic spin, and Ω is the atomic volume. (S_0/Ω) is equal to the saturation magnetization at 0°K divided by twice the Bohr magneton.

For Fe_3O_4, we find $C = 4 \times 10^{-6}$ by fitting the Bloch $T^{3/2}$ law to the saturation magnetization measurements of Weiss and Forrer.[11] From (36), assuming M_s at 0°K is 505 c.g.s. units, we then find $A = 1.24 \times 10^{-6}$. Furthermore, $K_1 = -1.1 \times 10^5$ as given by Bickford,[22] and

$$\gamma = (1.76 \times 10^7)g/2 = 1.865 \times 10^7,$$

where we have used Bickford's[22] value (2.12) of g.[23] Now from (13) we find

$$\lambda = 5.5 \times 10^8$$

in Fe_3O_4 at room temperature.

For $(NiO)_{0.75}(FeO)_{0.25}Fe_2O_3$, we assume that M_s, while different from that for Fe_3O_4, varies in the same way with temperature so that $C = 4 \times 10^{-6}$. From our measurement of M_s at room temperature (322.5 c.g.s. units) and this assumption about the variation of M_s with T, we find that M_s at 0°K is 342 c.g.s. units. This leads by (36) to $A = 1.09 \times 10^{-6}$. Ferromagnetic resonance experiments[24] done by W. A. Yager and F. R. Merritt in collaboration with the author on spherical single crystals of the same ferrite material as that used in the present research give a g value of 2.14 at all the temperatures mentioned in Table II except 77°K, where $g = 2.19$. These values are used in determining the value of $\gamma[= 1.76 \times 10^7\ g/2]$ in (13). The anisotropy values in Table II are also taken from the results of these ferromagnetic resonance experi-

ments. The K_1 at room temperature is -3.8×10^4. The room temperature value of λ domain wall given in Table I and the values at various temperatures given in Table II are obtained from (13) using these data.

An independent value of λ may be obtained from the ferromagnetic resonance line width. The relation between the observed line width $2\Delta H$ and λ has been given elsewhere.[25] Sample shape enters this relation, but not in a critical way, and we therefore ignore it except as it affects the value of the dc magnetic field at resonance, H_{res}. The relation is:

$$\lambda = \Delta H \gamma M_s / H_{res} . \tag{37}$$

From Bickford's[22] data on line width and (37) we find $\lambda = 9 \times 10^8$ for Fe_3O_4 at room temperature. From the ferromagnetic resonance data reported elsewhere[24] on $(NiO)_{0.75}(FeO)_{0.25}Fe_2O_3$, the material used in the present research, we find $\lambda \cong 10 \times 10^7$ at room temperature. Table I compares the room temperature values of λ obtained in the two ways on the two materials.

The differences between the domain wall experiments and the ferromagnetic resonance experiments lead to quite different behavior of λ in the two cases at low temperatures. These differences can be understood in terms of the frequency dependence of λ as given by an extension of the relaxation theory given in the third part of the theoretical discussion. A discussion of these relationships must await the detailed report on the ferromagnetic resonance results which is now in preparation, where such an extension will be given. As Table I shows, the room temperature values obtained in the two ways are of the same order of magnitude.

Let us now turn to a discussion of the relation between (31) and (33) and the data shown in Fig. 8. Qualitatively, of course, the $1/\tau$ factor in v/H_0 which (31) reveals, taken together with (32) explains most satisfactorily the sharp increase in viscous damping of the domain wall at low temperatures. Furthermore, it seems quite possible, although the author has not investigated it, that the higher order terms in (24) account for the nonlinearities in Figs. 9 and 10.

It should be mentioned that an increase in relaxation time at low temperatures which is consistent with (32) has been deduced by Bloembergen and Wang[26] and Healy[27] from ferromagnetic resonance data taken by them.

Quantitatively, we have inadequate data for a satisfactory comparison between Fig. 8 and (31), and the assumptions of the theory should perhaps be investigated further before any such comparison is taken

seriously. Nevertheless, plausible assumptions can be made which make an instructive comparison possible. g_{1_∞} in (31) is equal to the difference in the variation of the anisotropy energy when measured adiabatically and when measured isothermally. At this stage of our knowledge, many assumptions which still retain the symmetry of the crystal are possible concerning the form of $g_{1_\infty}(\theta)$. For our present purposes we will assume that it is given to within a constant by (34), but we must introduce a minus sign to take account of the fact that the rearranging electrons must have a *positive* anisotropy energy associated with them. Since we differentiate before substituting in (31), we do not need to subtract out the constant. The amplitude of g_{1_∞} is not given by $|K_1|$ of course; we will call this amplitude $|K_r|$. When we introduce the minus sign into (34), and calculate the integral in (31), we find:

$$v = \frac{1}{\tau} \frac{4.0 M_s}{|K_r| \sqrt{\dfrac{|K_1|}{A}}} H_0 . \tag{38}$$

This relation points up the fact that the mechanism we are discussing here is characterized by two parameters, an amplitude factor $|K_r|$ and a time τ. Our experiment tells us nothing about $|K_r|$, so we will arbitrarily assume it is about $\frac{1}{2}$ of $|K_1|$ at room temperature, or 20000 ergs/cc. $|K_r|$ can be measured by comparing values of $|K_1|$ determined isothermally, say by measuring the torque on a disc, and values of $|K_1|$ determined adiabatically, say by ferromagnetic resonance experiments, but this has not been done as yet. To determine τ at 77°K, assume that the maximum frequency of rotation of dipoles in the wall is such that $\omega\tau \cong 0.1$ when the non-linearity shown in Fig. 9 first occurs (at $v = 150$ cm/sec). We calculate the thickness of the wall to be 4×10^{-5} cm from standard formulae (see Kittel's review article, Reference 14) and find $\tau \cong 0.5 \times 10^{-8}$. These values of τ and $|K_r|$, together with $|K_1|$ from Table II at 77°K and A as calculated above, give $v/H_0 \cong 40$ when inserted into (38). This is to be compared with a measured $v/(H - H_c)$ of 160 at 77°K. In view of the preliminary nature of (31), and the arbitrariness of some of our assumptions, this check is quite satisfactory. It would be naive to expect the theoretical result to be closer than an order of magnitude to the experimental one. Inspection of Fig. 8 suggests that the mechanism which gives the sharp increase in damping at 77°K is submerged at room temperature in the effects of other mechanisms, perhaps other electronic rearrangements, perhaps exchange effects of the sort recently suggested in metals by Rado.[28] Equation (39) confirms this expectation when we use $\tau \cong 10^{-12}$, as determined either

from ferromagnetic resonance data[24] or from the conductivity of Fe_3O_4. The above method of calculating τ from domain wall data is less satisfactory at room temperature.

The idea of associating losses in ferrites such as this one with changes of order in the divalent and trivalent iron ions explains the fact that the damping observed in domain walls at room temperature in Fe_3O_4,[7] where none of the divalent iron is replaced by nickel, is larger than that observed in $(NiO)_{0.75}(FeO)_{0.25}Fe_2O_3$. Finally, as Wijn and van der Heide[17] have pointed out, and as (31) and (33) show more analytically, this mechanism is a very satisfactory explanation of the sharp change in domain wall relaxation frequency observed by Galt, Matthias, and Remeika.[29]

REFERENCES

1. Rado, Wright and Emerson, Phys. Rev., **80**, p. 273, 1950. Rado, Wright, Emerson and Terris, Phys. Rev., **88**, p. 909, 1952. G. T. Rado, Revs. Mod. Phys., **25**, p. 81, 1953. Welch, Nicks, Fairweather and Roberts, Phys. Rev., **77**, p. 403, 1950.
2. D. Polder and J. Smit, Revs. Mod. Phys., **25**, p. 89, 1953. J. J. Went and H. P. J. Wijn, Phys. Rev., **82**, p. 269, 1951. Wijn, Gevers and van der Burgt, Revs. Mod. Phys., **25**, p. 91, 1953. H. P. J. Wijn and H. van der Heide, Revs. Mod. Phys., **25**, p. 98, 1953. H. P. J. Wijn, Thesis, Leiden, 1953. Separaat 2092, N. V. Philips Gloeilampenfabrieken, Eindhoven, Holland.
3. H. J. Williams, Phys. Rev., **52**, p. 747, 1937. H. J. Williams and W. Shockley, Phys. Rev., **75**, p. 178, 1949. Williams, Bozorth and Shockley, Phys. Rev.,

75, p. 155, 1949. Williams, Shockley and Kittel, Phys. Rev., **80,** p. 1090, 1950. H. J. Williams, Bell Labs. Record **30,** p. 385, 1952.

3a. K. H. Stewart, Proc. Phys. Soc., **63A,** p. 761, 1950 and J. Phys. et Radium, **12,** p. 325, 1951.

4. K. J. Sixtus and L. Tonks, Phys. Rev., **42,** p. 419, 1932.

5. W. A. Yager and R. M. Bozorth, Phys. Rev., **72,** p. 80, 1947.

6. L. Landau and E. Lifshitz, Physik. Z. Sowjetunion, **8,** p. 153, 1935.

7. J. K. Galt, Phys. Rev., **85,** p. 664, 1952.

8. Galt, Andrus and Hopper, Revs. Mod. Phys., **25,** p. 93, 1953.

9. W. L. Bond, Phys. Rev., **78,** p. 646, 1950, Abstract I 10.

10. P. P. Cioffi, Phys. Rev., **67,** p. 200, 1945 and Rev. Sci. Instr., **21,** p. 624, 1950.

11. P. Weiss and R. Forrer, Ann. Phys., Series 10, **12,** p. 279, 1929. After the present work was completed, the author became aware of the extensive measurements of Pauthenet (Ann. Phys., Series 12, **7,** p. 710, 1952) on M_s in nickel ferrite and magnetite, among other materials. Interpolation between Pauthenet's values for these two materials suggests that the value of M_s we have used for $(NiO)_{0.75} (FeO)_{0.25} Fe_2O_3$ is about 6% too high at 445°K and 3% too low at 77°K, with intermediate errors between these temperatures and room temperature. Since, however, the accuracy of our data is not significantly better than this, and since our conclusions would be unaffected by any such changes, no correction has been made to our data.

12. R. Becker, J. Phys. et Radium, **12,** p. 332, 1951.

13. C. Kittel, Phys. Rev., **80,** p. 918, 1950; J. Phys. et Radium, **12,** p. 291, 1951.

14. C. Kittel, Revs. Mod. Phys., **21,** p. 541, 1949. See Equation 3.3.9. Since a wall perpendicular to the [100] direction in a crystal with a positive anisotropy energy constant is discussed in this reference, $g(\theta_0) = 0$ and is left out. The author is grateful to A. M. Clogston for pointing out the need for it in the present research. It was ignored in References 7 and 8 with the result that the values given for λ in those references were somewhat in error. Correct values are given in Table I.

15. E. J. W. Verwey and J. H. de Boer, Rec. Trav. Chim., **55,** p. 531, 1936. E. J. W. Verwey and P. W. Haaymann, Physica, **8,** p. 979, 1941. Verwey, Haaymann and Romeijn, J. Chem. Phys., **15,** p. 181, 1947.

16. M. E. Fine and N. T. Kenny, paper to be published.

17. H. P. J. Wijn and H. W. van der Heide, Revs. Mod. Phys., **25,** p. 99, 1953. H. P. J. Wijn, Thesis, Leiden, 1953. Separaat 2092, N. V. Philips Gloeilampenfabrieken, Eindhoven, Holland.

18. The author wishes to acknowledge a conversation with B. T. Matthias in which this mechanism was independently suggested in connection with the present research.

19. J. L. Snoek, New Developments in Ferromagnetic Materials, Elsevier, 1947.

20. It should be mentioned that Néel (J. Phys. et Radium **12,** p. 339, 1951; **13,** p. 249, 1952) has suggested that the after-effect losses discussed by Snoek[19] in connection with the diffusion of carbon and oxygen in iron arise from an anisotropy relaxation. Néel's analysis, however, leads him to predict zero loss for large motions of a 180° domain wall, which is contrary to our experimental results. We suggest that he is led to an erroneous result because he allows the anisotropy energy itself to follow a relaxation of the form of Equation (18), whereas kinetic losses of this sort are due to the relaxation of one of two conjugate thermodynamical variables whose *product* is an energy. In our case these variables are the torque on the magnetization due to anisotropy, and the angle of rotation of the magnetization. It is this torque which satisfies the relaxation equation.

21. C. Herring and C. Kittel, Phys. Rev., **81,** p. 869, 1951. See Equation 5.

22. L. R. Bickford, Jr., Phys. Rev., **78,** p. 449, 1950.

23. C. Kittel, Phys. Rev., **76,** p. 743, 1949.

24. Galt, Yager and Merritt, Phys. Rev., **93,** p. 1119, 1954. A more detailed description of this work is in preparation.
25. Yager, Galt, Merritt and Wood, Phys. Rev., **80,** p. 744, 1950. See Equation (A-6). The λ of the present paper is equal to $\gamma \alpha M_s$ in the notation of this reference.
26. N. Bloembergen and S. Wang, Phys. Rev., **93,** p. 72, 1954.
27. D. W. Healy, Jr., Phys. Rev., **86,** p. 1009, 1952.
28. G. T. Rado and J. R. Weertman, Phys. Rev., **94,** p. 1386, 1954.
29. Galt, Matthias and Remeika, Phys. Rev., **79,** p. 391, 1950.

Negative Impedance Telephone Repeaters

By J. L. MERRILL, JR., A. F. ROSE, and J. O. SMETHURST

In the exchange telephone plant, speech is transmitted largely at voice frequencies over a single pair of wires that carries conversation in both directions. Until recently, adequate transmission was assured through a suitable choice of coil loading and conductor size. The need for voice frequency amplifiers had long been recognized, but wide use of the conventional hybrid type of repeater with separate amplifiers for conversation in the two directions had not been economic. In 1948, however, a new type of repeater was introduced that used the same source of gain for transmission in both directions, and did not require costly filters. This repeater is known as the E1 repeater. It operates as a negative impedance in the line.

This paper describes the wide field of usefulness of two new types of negative impedance repeaters, the E2 and E3. Sufficient theory is given to show the advantages of using two types of negative impedance in a line, the series type and the shunt type, and how, by the addition of the shunt type to the series type, it is possible to insert gain without serious reactions on line impedance. The new equipment is described and maintenance features, together with methods of testing this relatively new type of repeater, are discussed.

APPLICATION IN THE BELL SYSTEM

INTRODUCTION

The application of the telephone repeater, the development of which made countrywide telephone service practicable, had been confined largely to toll plant from the year 1915 when the transcontinental line was first established, until a few years ago. About 1948 the negative impedance repeater[1] was developed and placed in production. This repeater operates on the principle of inserting negative resistance (and, if desired, negative inductance or capacitance) in series with the line, thus reducing the overall impedance and increasing the current in the line. This results in transmission gain in the same sense as that resulting from a repeater of the conventional type. This principle and the package

THE BELL SYSTEM TECHNICAL JOURNAL, SEPTEMBER 1954

nature of the assembly resulted in a telephone repeater so low in cost and so simple in application and installation that it has found extensive use primarily in the local telephone plant.

In the period from 1948 to the present time, over 50,000 series-type negative impedance repeaters were manufactured and incorporated in the Bell System telephone plant. These repeaters have been used largely on intraexchange trunks and on trunks extending from the exchange areas to near-by smaller towns. Such installations have been very effective in improving the transmission on short haul calls and in many cases have also reduced trunk costs by permitting the use of smaller and cheaper conductors. They are usually operated at gains that reduce the nonrepeatered trunk loss by more than half.

Negative impedance repeaters are especially suited to exchange trunk use, not only because of their simplicity and ease of maintenance, but also because unlike earlier types of repeaters, they preserve the dc continuity of the circuits on which they are installed. This latter feature means that they do not interfere appreciably with the signaling methods ordinarily used on such trunks. Also, they have the added advantage that, in the event of tube failure, the circuit still functions but with its loss substantially raised until the defective tube has been replaced.

APPLICATION OF SERIES-TYPE NEGATIVE IMPEDANCE REPEATERS

In a multioffice exchange area, trunks can generally be grouped in three classes. Largest in number are those known as interoffice trunks which extend directly from one local operating center to another local center in the same exchange operating area. In some cases direct trunks between two centers can not be justified and each office has trunks to a central location known as a tandem center where a through connection is made when required. This second class of trunks is known as "tandem" trunks. Frequently trunks of this type are provided to supplement the direct trunks and thus give the added advantage of alternate routing. A third type of trunk extends between the local office and the toll office and therefore always forms part of a toll connection to the local office. These are known as toll connecting trunks. In single office areas the toll connecting trunks to neighboring small towns are known as "tributary" trunks.

In some large multioffice exchange areas there are also trunks between the toll office and tandem centers which may be some distance from the toll office and through which local offices reach the toll office for long distance calls. These trunks are also called tandem trunks but are more

in the nature of intertoll links and are required to operate at very low loss similar to an intertoll circuit.[2]

The most extensive use of negative impedance repeaters has been in connection with the interoffice trunks. In this role they have been extremely useful and have contributed greatly to transmission improvement in the last few years. It would also be desirable to utilize this new and effective tool in reducing the losses of toll connecting and tandem trunks. There have been many cases of this type where improvement has been effected, but a very wide use has been prevented by their effect on return loss.

The insertion of a series negative impedance in an otherwise uniform loaded circuit introduces an impedance discontinuity which means that a substantial amount of energy is returned to the sending end of the circuit as "echo." As the introduction of negative impedance is the method of obtaining gain from the series repeater it follows that the magnitude of the impedance discontinuity and therefore the "echo," is proportional to the gain of the repeater. The effect of echo on ease of conversation depends both on its magnitude and on the amount of delay[3] before the echo reaches the talker's ear. When the delay is small as in the case of an interoffice trunk a large amount can be tolerated, but in the case of a toll connecting trunk which becomes a part of a toll connection the delay may be large and only a small amount of echo can be permitted. This limits the amount of gain from a series repeater when it is used in toll connecting trunks.

As a result of this feature of the series negative impedance repeater, most cases requiring substantial gains in toll connecting or tributary trunks usually had to be handled by the older and more expensive hybrid-coil type repeater. With this latter repeater, it is practicable to introduce gain without serious reflection effects if proper attention is given to network design and to uniformity of construction of the line itself. However, the cost of the more complicated repeater was relatively high so that the new development described herein was undertaken to meet the indicated need, i.e., a repeater embodying the same desirable features of simplicity of design but still approaching in performance that of the hybrid-coil repeater in its effect on return loss.

The new repeater (E23) consists essentially of the earlier series repeater with the addition of a shunt negative impedance element. This combination has approximately as small an effect on return loss as the hybrid-coil repeater and will give about the same gain when used under similar line conditions. As a result, the field of use of the negative impedance type repeater will be greatly extended, especially in the toll

connecting plant where, from a practical standpoint, certain features of the hybrid-coil repeater are not needed. For example, more than 10 db gain is rarely required, and unequal gains in opposite directions would not ordinarily be useful. Besides, methods of signaling requiring a 4-wire split of the repeater are not utilized on exchange area trunks.

In addition to its important new characteristics, the series-shunt combination retains the desirable features of the earlier series repeater, i.e., it preserves dc continuity, it is simple in design and it is easy to install and maintain. If properly engineered and installed on circuits of reasonably uniform impedance, the new repeaters can be operated in tandem, do not have serious reactions on return loss, and are capable of reducing the losses of the trunks to about the same values as hybrid-type repeaters.

SCOPE OF APPLICATION OF THE NEW REPEATER

With the reduction of the return loss reaction of the earlier form of negative impedance repeater, the extent of application of the new E23 repeater becomes largely a matter of economics. In the telephone trunk plant, there are generally three gauges of conductors available for trunk use, namely, 19, 22 and 24. The larger gauges, utilizing more copper and requiring more conduit space, naturally cost more than the smaller
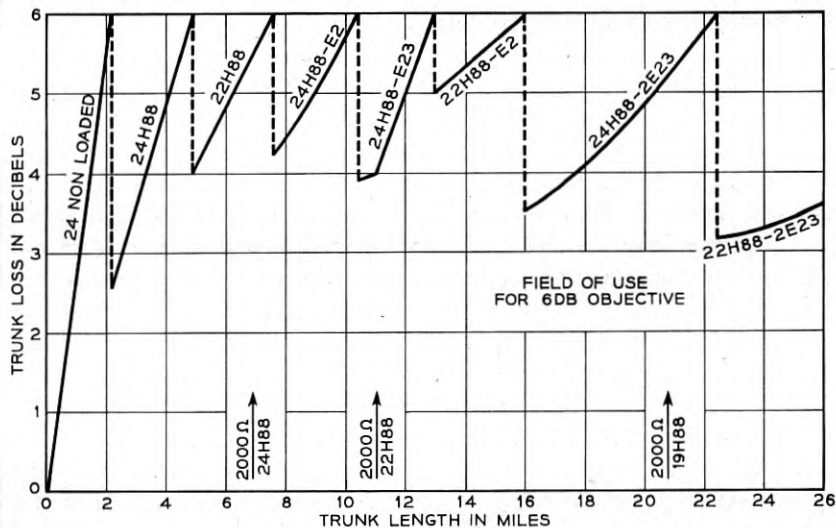
Fig. 1 — Illustrative field of use; interoffice trunks.
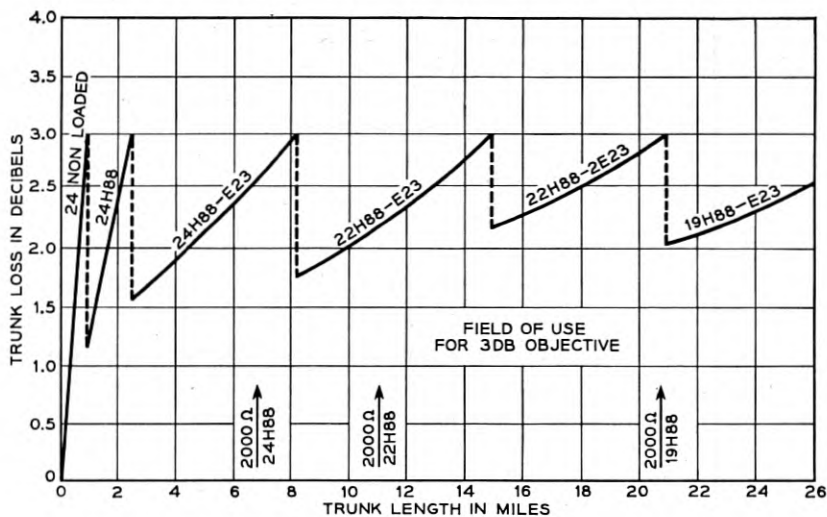
Fig. 2 — Illustrative field of use; toll connecting or tandem trunks.

gauge. In general, it is the practice to select the smallest gauge which will give the required transmission loss. For short distances, the differential in cost between trunks of different gauges is not large but as trunk length increases it will be found that a smaller gauge trunk with a repeater will cost less than one of larger gauge without a repeater. For example, at 10 miles a 22-gauge circuit with a repeater will cost substantially less than a 19-gauge circuit with no repeater. Also, as transmission objectives are improved, there may be cases where a smaller gauge trunk with two repeaters will be cheaper than a larger gauge with one repeater. Furthermore, in cases where the costs are about equal or even where the larger gauge is slightly cheaper, it will be found that lower losses can be obtained with repeatered circuits and the engineering choice would accordingly favor the smaller gauge.

Construction costs differ considerably depending on local conditions; hence the differential cost between the various gauges of conductors will differ correspondingly. However, for illustrative purposes Figs. 1 and 2 have been prepared which utilize average Bell System costs for both outside plant and telephone repeaters. In the case of the E23 repeaters, the experience so far has been somewhat limited so there is a greater degree of uncertainty as to the actual costs than for the older type repeater or the outside plant construction.

Fig. 1 shows the field of use for various conductor gauges when used in interoffice trunks where an over-all transmission objective of 6 db for

the trunks has been assumed. In considering this chart it will be seen that non-loaded 24-gauge conductors can be utilized for the shorter distances up to about two miles. The next step is to apply loading, which is indicated in the chart by the symbol H88 meaning 88 millihenry coils at 6,000 foot spacing. After reaching the limit of about 7 miles without repeaters on 22-gauge, the differential between 22- and 24-gauge is more than enough to pay for a repeater, the simple series repeater (E2) being used for distances up to 10 miles and then the improved E23 re-. peater extending the use of 24-gauge to about 14 miles. Beyond this point the most economical combination is indicated.

The general effect of the introduction of the negative impedance repeater is to shift the average gauge distribution so that more small gauge cable can be economically utilized, accompanied in most cases by improved transmission. It will be noted from the figure that no 19-gauge cable will need to be added in the future to care for interoffice trunks up to distances as great as 25 miles between offices. Of course, in cases where 19-gauge is already available in plant it can be used to advantage despite the fact that for new construction a smaller gauge with the negative impedance repeaters would be cheaper.

It has also been assumed in making up Fig. 1 that supervision or pulsing requirements will not limit the use of the smaller gauges. In a specific case where some of the older type central offices are involved, signaling may have an important bearing and substantially distort the economic ranges indicated on the chart.

Fig. 2 illustrates the field of use of toll connecting or tandem trunks. As a toll connecting trunk forms part of a multilink connection, and since there are always at least two (and often more) trunks in series on connections involving these trunks, the Bell System companies find it economical to plan for a maximum loss of 3 db for this type of trunk. Likewise for the tandem trunks, where two in series may be used in place of an interoffice trunk, 3 db is considered a reasonable objective.

It will be noted again by referring to this chart that 19-gauge has very little future field of use and in all cases the new "series-shunt" repeater will be utilized rather than the earlier series type because of return loss considerations and also because of the greater gain required to reduce the trunk losses to the desired values. In the tandem and toll connecting case, signaling may again be a distorting factor though not to so great an extent as in the direct interoffice trunk case. To this extent, however, the curves are theoretical, as they have been made up without regard to this limitation which may apply in a few practical cases.

SPECIFIC APPLICATIONS

Many installations of the new repeaters have been engineered for completion in 1954. In all cases economic studies were made and results of these studies broadly confirmed the indications of the two charts discussed above. To bring out more clearly the effectiveness of the E23 repeater, it may be worth while to consider a few specific cases involving installations of the new repeaters being made this year.

The first case shown on Fig. 3 is in the area of the Pacific Telephone and Telegraph Company. The figure shows the two alternatives that were considered for providing additional tandem trunks between San Francisco proper and the East Bay Area, needed this year because of an extension of customer toll dialing arrangements.

The engineering study for this project was somewhat more complicated than would ordinarily be the case because two possible routes of unequal length and with slightly different amounts of submarine cable were involved. The present route which touches Yerba Buena Island is subject to some hazard from dragging ship anchors but the circuit relief would have been cheaper here than on the other route shown, were it not for the new repeaters. The second route is considerably less hazardous and, in addition, is sufficiently removed from the present one to provide increased reliability under disaster conditions. Without the repeaters, however, the second route would have been somewhat impracticable, since it does not allow easy installation and access to required loading points between the two shore lines. However, with two of the new repeaters on each pair of conductors, nonloaded 22-gauge cable gives substantially the same effective transmission loss as loaded 19-gauge conductors on the shorter route and over a future period will involve less annual cost per circuit. Furthermore, the use of 22-gauge cable permits more than twice as many pairs to be included in the same size sheath in the expensive submarine section.

The initial installation of the new type repeaters on this cable will total about 1,300, divided between the Main Office in San Francisco and the Main Office on the East Bay side. Individual repeater gains are 5 to 7 db at 1,000 cycles but the repeater gain characteristic is shaped to offset the increasing cable losses at the higher frequencies so that the over-all circuit has relatively uniform transmission in the voice range.

The second case is one where the need for the repeaters results from the complex toll switching system at Chicago, Illinois. Here it has been found desirable, because of the great volume of toll traffic, to have several toll offices scattered throughout the city and suburbs. In general, toll calls coming into these offices from other cities are completed over toll
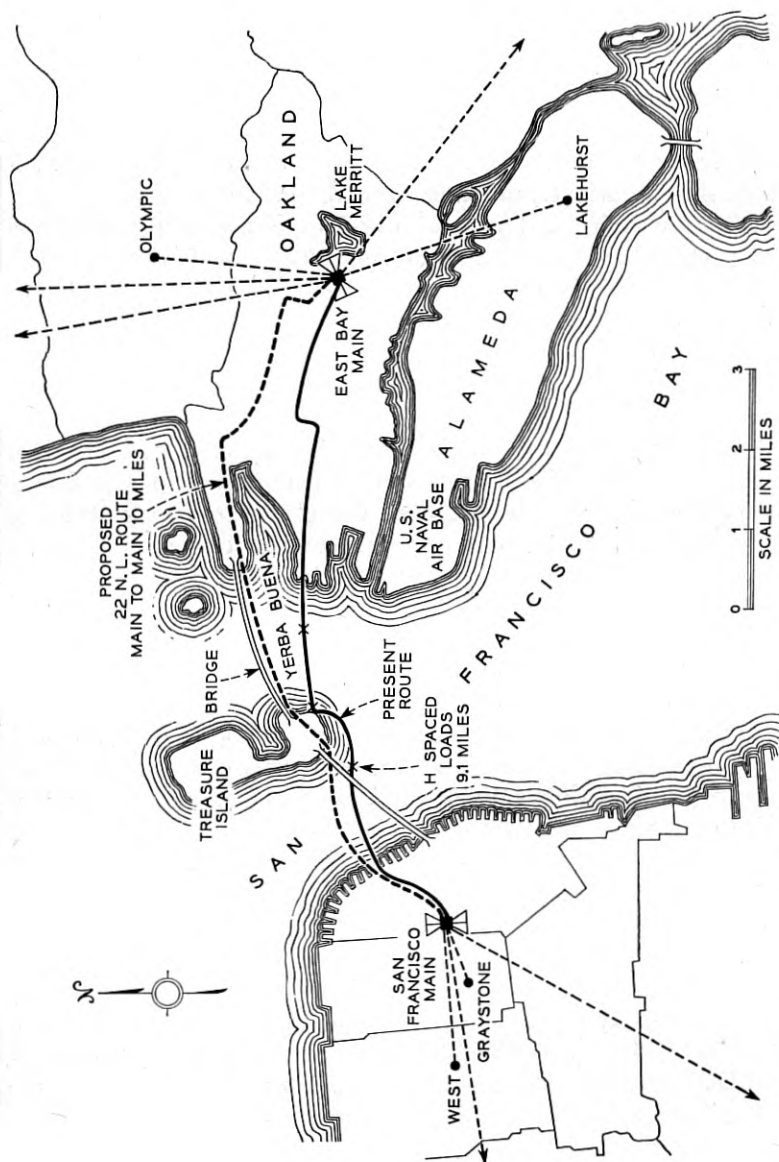
Fig. 3 — Typical E23 repeater application, San Franciso — East Bay tandem trunks.

connecting trunks direct to the called subscribers' central offices. It is not economical, however, to provide enough such trunks to handle peak loads. When all of these direct trunks are busy, an incoming toll call is switched to the subscriber's central office via a tandem office serving his general area. Since the losses of trunks between the tandem and local offices are of the same order as those of the direct trunks from toll to local offices, it would be desirable to operate the trunks between the toll and tandem offices at losses close to 0 db if this were practicable. In this way the same transmission objectives would be met on both routings and no contrast in transmission would be evident to the same subscribers on calls completed over the different routes at different times. Fig. 4 illustrates a specific case of 36 trunks between toll office No. 3
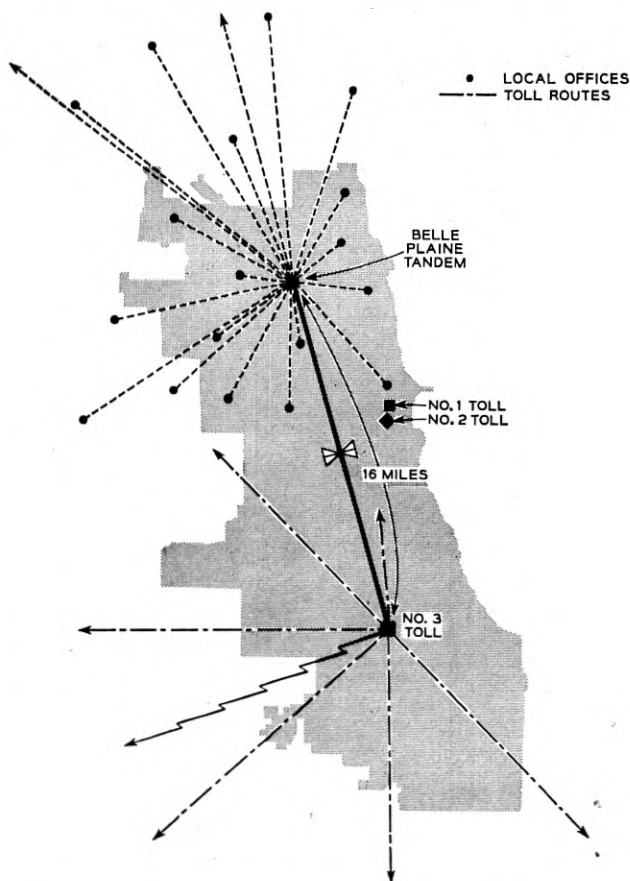
Fig. 4 — Typical E23 repeater application; Chicago toll tandem trunks.

and Belle Plaine tandem, a distance of about 16 miles. Without repeaters these trunks would have been operated at a loss of about 10 db but with the repeaters they are operated at about 2 db. The only alternative to using E repeaters in this specific case would have been to use the more expensive hybrid-type repeaters.

In some cases similar to this one, it was found practicable to temporize by installing the series repeater first and operating it at limited gain until the shunt element became available. Later, when the production of the shunt element was started, the additional units were added and full advantage of the new series-shunt design utilized in reducing the equivalent of the trunks to the lowest value permitted by echo return loss considerations.

The third example shown on Fig. 5 is in the city of Pittsburgh between Churchill tandem and the town of New Kensington, approximately 17 miles. Here the transmission on existing 19-gauge loaded cable without a repeater would have been about 8 db. The repeaters reduce this figure to between 2 and 3 db which should be satisfactory in this case. It should be noted, however, that 22-gauge with two repeaters would also provide a low enough equivalent, and should it become necessary to supplement the present cable at some future date, there will be an opportunity for further savings from the E23 repeaters.
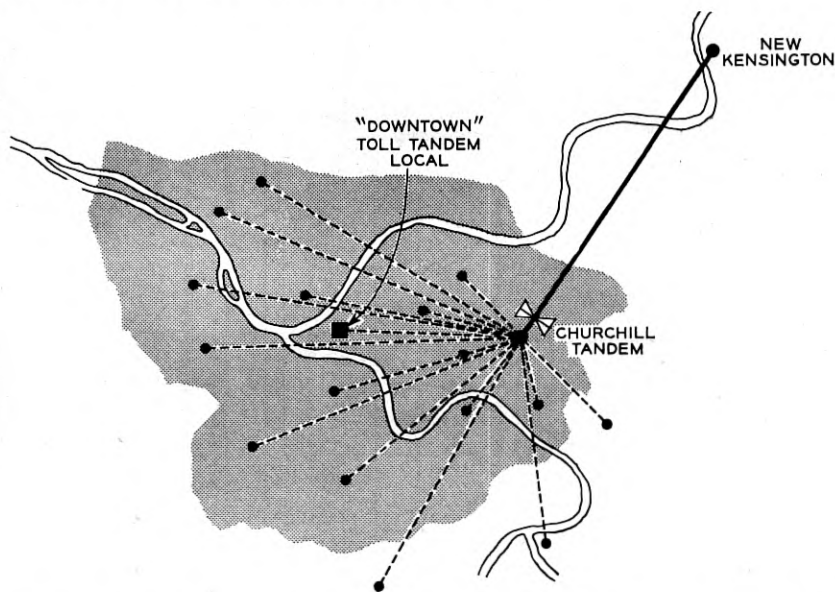
Fig. 5 — Typical E23 repeater application; Pittsburgh toll connecting trunks.

THEORY

NEGATIVE IMPEDANCE CONCEPT

Both the E2 and E3 repeater elements contain an amplifier having multiple feedback paths. The operation of an amplifier circuit of this type can be explained by classical feedback theory. However, experience with the E1 repeater over the past four years has shown the value of using a negative impedance concept in engineering such a device. Hence, in the explanation of operation given here, the repeater units will be treated simply as two-terminal networks which have negative impedance inputs over the frequency band of interest. The effect of introducing these impedances into telephone circuits can then be computed by the same simple network theory used to determine the effects of passive impedances.

THE E2 REPEATER UNIT

The E2 repeater is essentially a two-terminal network the impedance of which has a magnitude $|Z|$ and a negative phase angle that can vary with increasing frequency from minus 90 degrees, or less, through minus 180 degrees to at least minus 270 degrees. This type of negative impedance is shown in the diagram of Fig. 6(a). It has been known for many years as the series type because it could be produced by connecting the output of an amplifier back in series with its input. More recently it has come to be known as an open circuit stable, negative

(a)   (b)
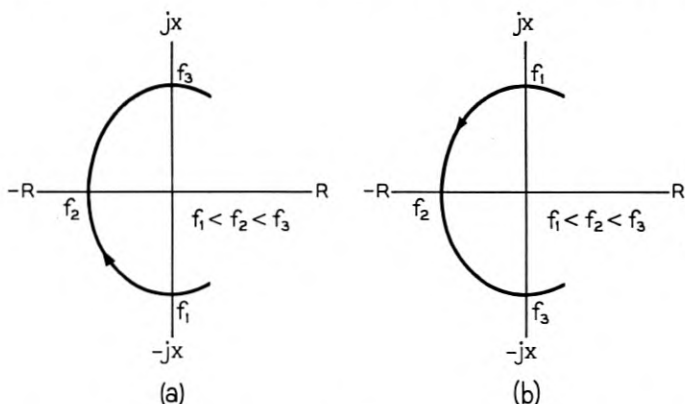
Fig. 6 — The two types of negative impedance: (a) Open Circuit Stable and (b) Short Circuit Stable.

impedance, because it will not oscillate when its two terminals are open circuited.

THE E3 REPEATER UNIT

The E3 repeater is essentially a two-terminal network the impedance of which has a magnitude $|Z|$ and a positive phase angle that can vary with increasing frequency from plus 90 degrees, or less, through plus 180 degrees to at least plus 270 degrees. This type of negative impedance is shown in Fig. 6(b). It has been known as the shunt type because it could be produced by connecting the output of an amplifier back in shunt with its input. In more recent years it has become known as the short circuit stable type because it will not oscillate when its two terminals are short circuited.

THE NEGATIVE IMPEDANCE CONVERTER

The amplifier circuits of both of these repeater units perform the same function: that of a negative impedance converter. The operation of such converters is illustrated in Fig. 7.

Fig. 7(a) shows the converter as a four-terminal network having a ratio of transformation k and a shift of phase through a negative angle of approximately 180 degrees over the operating band of frequencies. If, as shown, an impedance Z_N is connected to terminals 3 and 4 then the impedance seen at terminals 1 and 2 will be the impedance Z_N multiplied by the ratio k and shifted in phase through a negative angle of 180 degrees. This impedance will (over the frequency range of zero to infinity) fulfill the definition given for the impedance presented by the E2 repeater. Hence, Fig. 7(a) can represent the operation of the E2 repeater.
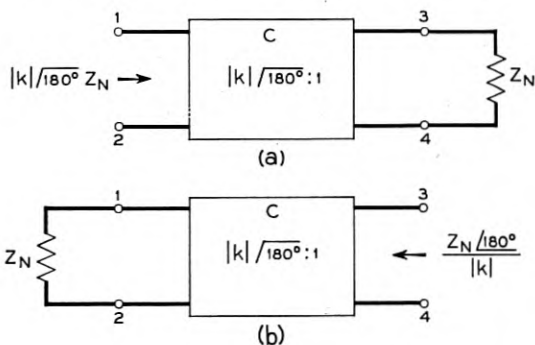
Fig. 7 — The Negative Impedance Converter: (a) E2, open circuit stable and (b) E3, short circuit stable.

Fig. 7(b) shows the same converter, but here the impedance Z_N is connected to terminals 1 and 2. The impedance seen at terminals 3 and 4 (at least over the frequency band of interest) will be Z_N divided by k and shifted in phase through a positive angle of approximately 180 degrees. This impedance will (if frequencies from zero to infinity are considered) fulfill the definition given above for the E3 repeater impedance. Thus Fig. 7(b) can represent the operation of the E3 repeater.

From Fig. 7, it is apparent that the same converter circuit could have been used for both the E2 and the E3 repeaters. For practical reasons it was not. However, the ratio k and the phase shift in both the converter of the E2 and that of the E3 were made approximately the same.

OPERATION IN TRANSMISSION LINES

Within limitations, the E2 repeater can be represented by a negative impedance, $-Z$, and the E3 repeater can be represented by a negative admittance, $-Y$. With a negative impedance and a negative admittance available, losses of transmission lines can be reduced in the manner illustrated in Fig. 8. The transmission line is represented by two networks as shown in Fig. 8(a). One of these (Network A) is in the form of a T network the series arms of which are represented by impedances Z; and the shunt arm, by an admittance Y. This network has a propagation constant $\alpha_1 + j\beta_1$. The attenuation α_1 represents the major portion of the line attenuation, and the phase shift β_1 is that just sufficient to make Network A realizable physically. This representation is necessary because Network A has image impedances each equal to the characteristic impedance (Z_0) of the line. If the characteristic impedance of the line were a pure resistance, then the phase shift through this network could be zero and β_1 could be zero. But the characteristic impedances of actual lines are not pure resistance; thus the phase shift β_1 must be included in Network A. The other network (Network B) is shown as a box. It has a propagation constant $\alpha_2 + j\beta_2$. Here β_2 represents the remaining phase shift in the transmission line and α_2 is an attenuation just sufficient to make Network B physically realizable in view of the image impedances which are both equal to Z_0, the characteristic impedance of the line. Fig. 8(b) shows the addition to this line of a repeater consisting of a T network made up of negative impedances $-Z$ in the series arms and a negative admittance $-Y$ in the shunt arm. The arm $-Z$ of the repeater adjacent to the line cancels Z of the line. The two admittances $-Y$ and Y cancel and the other series arms $-Z$ and Z also cancel. The result, as shown in Fig. 8(c), is that only the attenuation and phase shift of Network B remain.

In practice the amount of attenuation (α_1) which can be canceled by the repeater depends on the uniformity, the loss and the type of line. The permissible magnitude is computed by conventional methods which are beyond the scope of this paper.

Fig. 8 has shown how the combination of a series and a shunt repeater can annul a large part of the attenuation of a telephone line. Much may be accomplished also by a series negative impedance alone as illustrated in Fig. 9. In Fig. 9(a) a transmission line is again represented by two networks A and B. However, Network A now is shown as an L configuration having a series arm Z and a shunt admittance Y together with an ideal transformer of ratio $1:K$ where K exceeds unity. Network A of Fig. 9 is equivalent to Network A of Fig. 8, and Network B of Fig. 9 is the same as Network B of Fig. 8. In Fig. 9(b) the addition to this transmission line of a single $-Z$ such as the E2 repeater is shown. This negative impedance $-Z$ cancels the series impedance Z of Network A. The result is shown in Fig. 9(c).
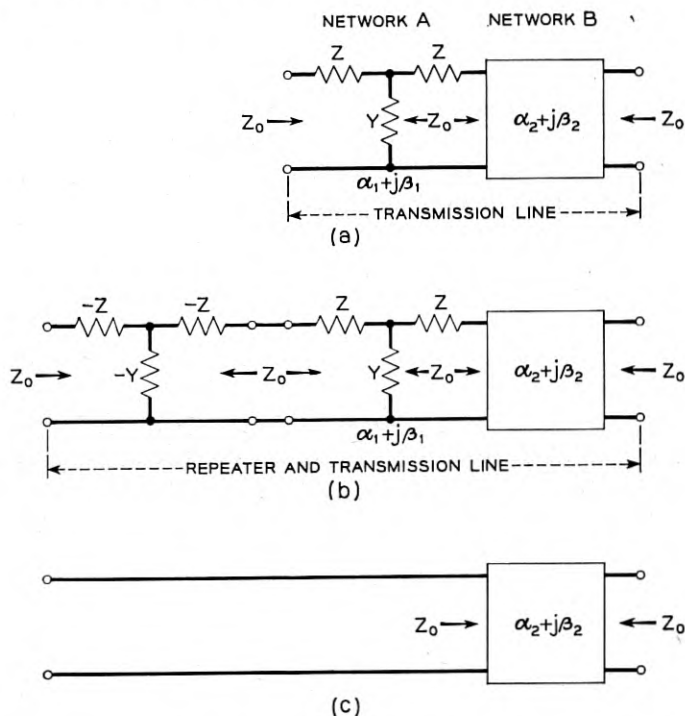
Fig. 8 — Operation of the "T" in a transmission line: (a) transmission line, (b) repeater and transmission line, and (c) result of addition of repeater.

Thus Fig. 9 shows that when a single $-Z$ is added in series with the conductors of a transmission line the attenuation is reduced, but the equivalent of a shunt conductance Y together with an impedance transformation is left. The impedance transformation $1:K$ could be corrected by means of a transformer if it were not for the shunt element Y. Thus an impedance irregularity is introduced, and this irregularity reflects power back toward the source. When the reflected power becomes a significant part of the total power passing through the line, transmission is unsatisfactory. Echo is excessive and therefore the use of the single series repeater is limited.

THE BRIDGED T STRUCTURE

The discussion of the T repeater, illustrated in Fig. 8, was based on the use of two series negative impedances and a shunt negative admittance. It is perfectly possible, and more economical, to obtain the same effect by using a single series impedance in a bridged T structure and this
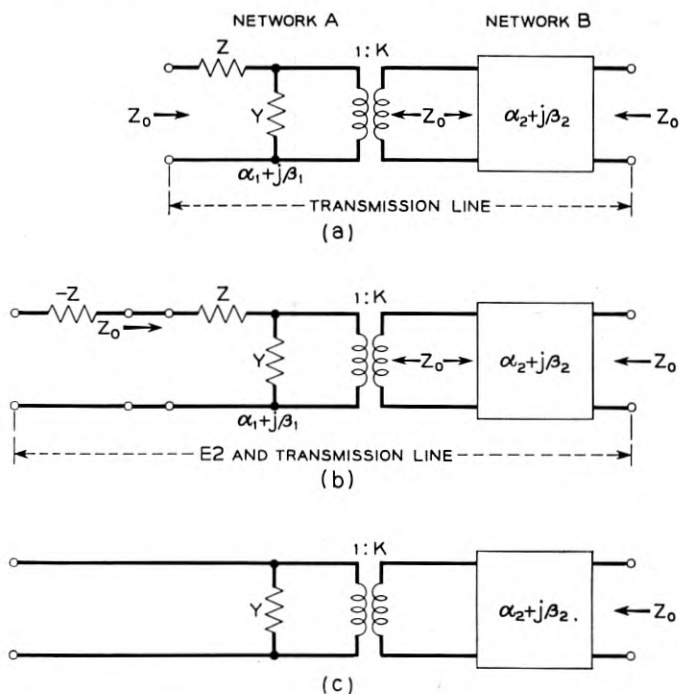
Fig. 9 — Operation of $-Z$ in a transmission line: (a) transmission line, (b) repeater and transmission line, and (c) result of adding repeater.

is, in fact, what is done with the E23 combination repeater. Fig. 10 shows how this is accomplished by using a center tapped line coil for the E2 repeater with the E3 connected as a shunt element to the midpoints of the coil. If the coil is considered to be ideal this arrangement is equivalent to the configuration shown in Fig. 11 in which the coil provides the basic bridge structure: the E2 repeater is the series arm; and the E3, the shunt arm. Incidentally this arrangement of E2 and E3 repeaters is similar to G. Crisson's twin 21-type repeater.[4]

For a bridged-T structure, the image impedance equals the square root of the product of the series and shunt arms and the attenuation (in db) is as indicated on Fig. 11.

If a network is to be inserted in an electrically long line without introducing an irregularity, its image impedance must match the characteristic impedance of the line. This would be the case for the bridged T network if Z_A were set equal to NZ_0 and Z_B were set equal to Z_0 divided by N. Then the square root of the product of Z_A and Z_B would be Z_0.

A network make up of negative impedances is designed to match a line in the same way and Fig. 12 is a representation of such a structure. Here, as a matter of convenience, the shunt arm is shown as an impedance
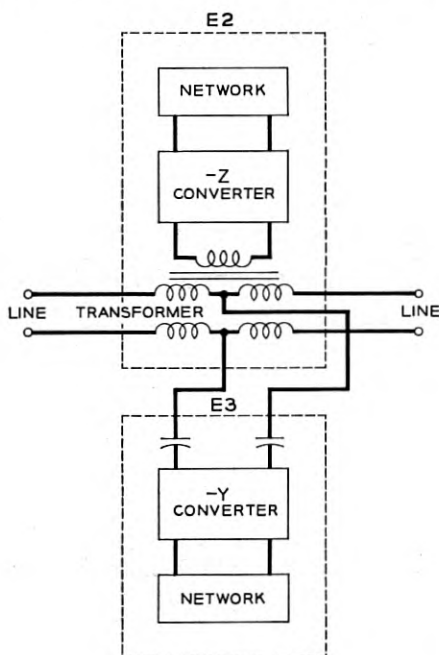
Fig. 10 — The bridged T repeater E23.

with a $+180°$ phase shift instead of an admittance as used previously. The letter N designates a numeric or proportionality constant. It will be observed that the product of the shunt and series impedances is a real or positive impedance and hence the image impedance is a positive impedance, Z_0. The gain is determined entirely by the value of N. Thus if the characteristic impedance of a transmission line is known, together with the gain that the line can support without risk of oscillation, then N is known and the repeater network can be adjusted to give the required gain.

The advantage of the bridged T as compared to a single series negative impedance such as the E2 can be demonstrated by comparing the relative transmission gains obtainable from the two arrangements. Fig. 13(b) shows the insertion loss of a single impedance Z_A connected in series with a transmission line having a characteristic impedance Z_0. If Z_A is a negative impedance such as that produced by the E2 repeater then the repeater gain becomes a function of N as shown in Fig. 13(c). If N equals 2 the gain is infinite and the system will oscillate. Thus N must always be less than 2 where Z_A is a negative impedance of the series or open circuit stable type. Practically, the impedance of the transmission line is not a constant Z_0 but varies with termination, line construction and temperature. Thus N should be decreased until the negative impedance is always less than the sum of the two line impedances in series with it taking into account all possible variations in these impedances.

The same limitations on N apply to the bridged T repeater of Fig. 12
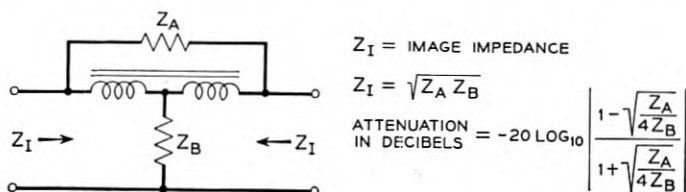
Fig. 11 — Schematic of the bridged T network.

$$Z_I = \text{IMAGE IMPEDANCE}$$
$$Z_I = \sqrt{Z_A Z_B}$$
$$\text{ATTENUATION IN DECIBELS} = -20 \log_{10} \left| \frac{1 - \sqrt{\frac{Z_A}{4Z_B}}}{1 + \sqrt{\frac{Z_A}{4Z_B}}} \right|$$
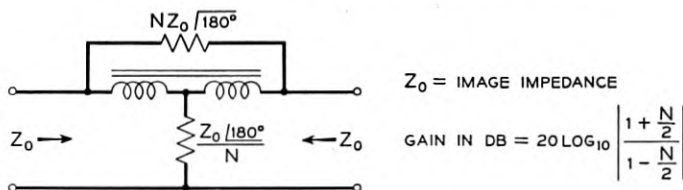
Fig. 12 — Schematic of the bridged T repeater.

$$Z_0 = \text{IMAGE IMPEDANCE}$$
$$\text{GAIN IN DB} = 20 \log_{10} \left| \frac{1 + \frac{N}{2}}{1 - \frac{N}{2}} \right|$$

as apply to the single series repeater. If N is 2 the gain is infinite and the circuit will sing. This similarity goes further. Assume that a single negative impedance Z_A equal to $NZ_0/\underline{180°}$ is inserted in series in an electrically long line and N is adjusted for stability. If this series element is removed and the bridged T of Fig. 12 is inserted in the same place and adjusted by changing N until the system is stable it will be found that N will have the same value in the bridged T structure as it had for the single series negative impedance.

Thus, if N is the same in the case of the bridged T as in the single series impedance, the gain advantage can be obtained by comparing formulas on Figs. 12 and 13 from which it can be seen that the gain advantage of the bridged T is equal in db to $20 \log_{10} [1 + (N/2)]$. If a single series repeater can be used in a line to give an insertion gain of 6 db ($N = 1$) then a bridged T can be used to provide $20 \log_{10} (1 + 0.5)$ or 3.5 db additional. Thus, in this case the series repeater gives 6 db gain as compared to $6 + 3.5$ or 9.5 db for the bridged T. These gains are theoretical; in actual lines with simply constructed repeaters the comparison may not be quite so favorable to the bridged T.

THE NEGATIVE IMPEDANCE CONVERTER

So far the discussion of the E2 and E3 repeaters has been in terms of a "black box" which translates a positive impedance into a negative
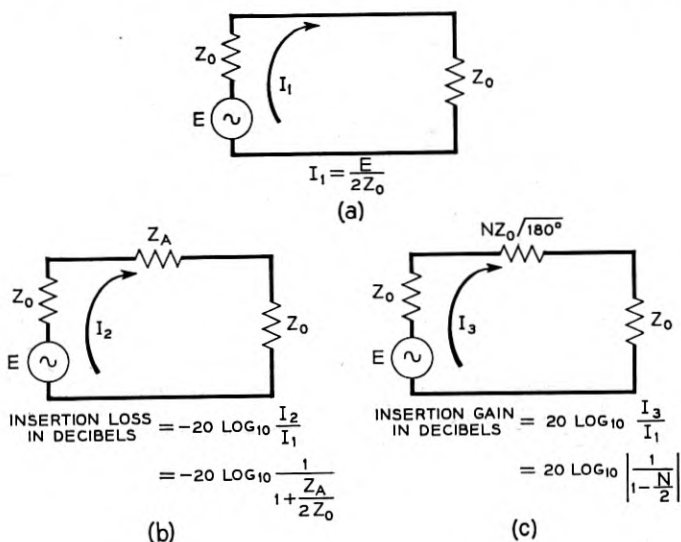
Fig. 13 — Insertion gain of the E2 repeater.

impedance through a multiplying and phase shift operation. It will be interesting to examine these boxes to see what factors determine their characteristics.

THE E2 CONVERTER

The E2 negative impedance converter is the same as the E1. As discussed elsewhere[5] it can be represented schematically as in Fig. 14(a) and also in terms of the equivalent circuit of Fig. 14(b) if the coils are assumed to be ideal. The converter performs much like a transformer. An impedance seen through it is not only transformed in magnitude by the ratio of $|1 - \mu\beta|$ to $|1 + \mu|$ it is also modified by the phase shift of this factor which over the operating band of frequencies approximates 180 degrees. The symbol μ stands for the voltage gain of the electron tube and β is the ratio of 1 to $1 + (1/j\omega CR)$. If both C and R are large β approaches unity in magnitude and the ratio of conversion approaches $1 - \mu$ to $1 + \mu$. If μ is large compared to unity then this conversion ratio approaches -1. This ratio of -1 is approximately realized in the E2 converter, and therefore the conversion ratio is not changed appreciably by small variations in μ.
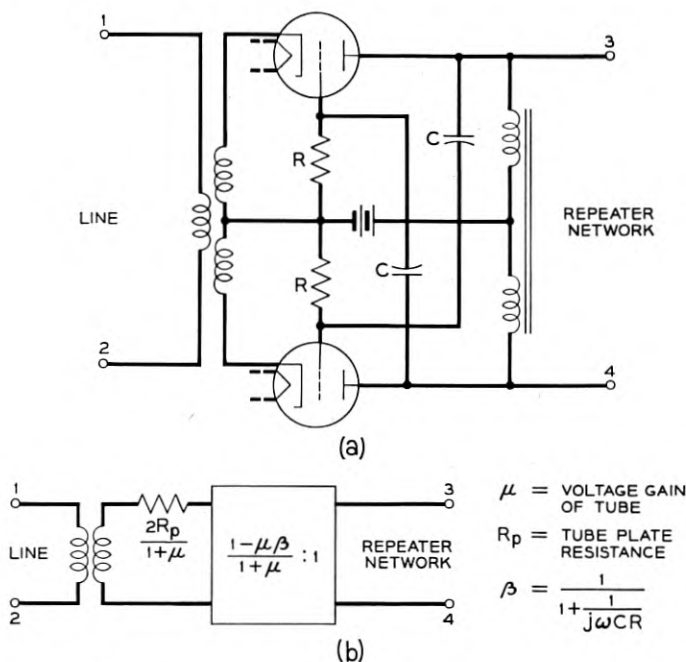
Fig. 14 — E2 Converter; (a) schematic and (b) equivalent circuit.

In addition to the transformation term there is also, as shown in Fig. 14(b), a series term, $2R_p$ divided by $1 + \mu$. Here R_p is the plate resistance of the tube, and μ is the voltage gain as mentioned before. The factor 2 results from the use of two tubes in push pull. If μ is large compared to unity then this series term becomes approximately $2R_p/\mu$. It is entirely dependent upon the characteristics of the electron tube. As the characteristics change from tube to tube with manufacturing variation or in the same tube over a period of time or with variation in battery supply potential, the term $2R_p/(1 + \mu)$ will change accordingly. Percentagewise this change may be large. This is the largest source of variation in the E2 converter. It can be minimized by operating the converter between impedances much larger in magnitude than $2R_p/(1 + \mu)$ so that variations in this term have relatively small effect. This has been done in the E2 repeater by stepping up the impedance of the transmission line by about 1:9 by means of the transformer shown in Fig. 14.

THE E3 CONVERTER

Theoretically, the same converter used for the E2 and shown in Fig. 14 could have been used for the E3. Instead of connecting the line to
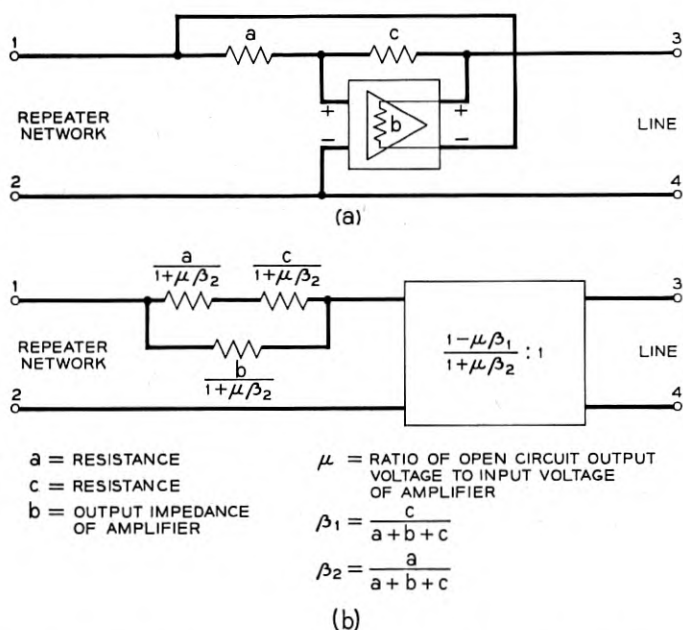
Fig. 15 — E3 Converter; (a) schematic and (b) equivalent circuit.

the converter through terminals 1 and 2, terminals 3 and 4 would be used. However, because the E3 must be designed for connection across a transmission line a coil or transformer input is not practical since the coil would shunt the line at low frequencies and introduce excessive loss to dial pulsing and 20 cps ringing. Without a coil to step up the impedance of the line, variations in $2R_p/(1 + \mu)$ with standard triodes are too large to be neglected. For this reason another converter circuit was designed for the E3 repeater.

This circuit is shown in schematic form in Fig. 15(a). It consists of two resistances, a and c, respectively, and an amplifier poled according to the plus and minus designation on Fig. 15(a). The output impedance of the amplifier has been designated as b. If the input impedance of this amplifier is high compared to other circuit impedances, Fig. 15(a) can also be represented by the equivalent circuit of Fig. 15(b). Here is a conversion factor similar to that in the E2 converter and also a series impedance. The factor μ is the ratio of the open circuit output voltage to the input voltage of the amplifier. In the E3 converter this voltage ratio μ is quite high because the amplifier is a two-stage arrangement. In the design of the E3 both β_1 and β_2 are approximately one half. Thus $\mu\beta_1$ and $\mu\beta_2$ are both large compared to unity so that the conversion ratio $(1 - \mu\beta_1)/(1 + \mu\beta_2)$ is approximately unity and relatively independent of variations in μ. Furthermore, because $\mu\beta_2$ is large compared to b, the series term in the converter circuit is relatively small and variations in this term have little effect on the operation of the converter.

CIRCUIT DESCRIPTION

THE E2 TELEPHONE REPEATER

The circuit function of the E2 telephone repeater can be divided into two parts: the electron tube (negative impedance) converter; and the adjustable two-terminal network associated with the converter.

In order to reduce the effect of variations in the electron tubes to negligible proportions, and at the same time to operate the tubes with load impedances that will permit optimum energy transfer from tube to connected circuit, the impedance of the telephone line is stepped up by means of the input transformer. To insure adequate balance for use in the telephone lines, the low voltage side of the transformer is divided into two equal, balanced windings. Each winding is center-tapped and connected in series with a line conductor. The circuit of the E2 repeater is shown in Fig. 16.

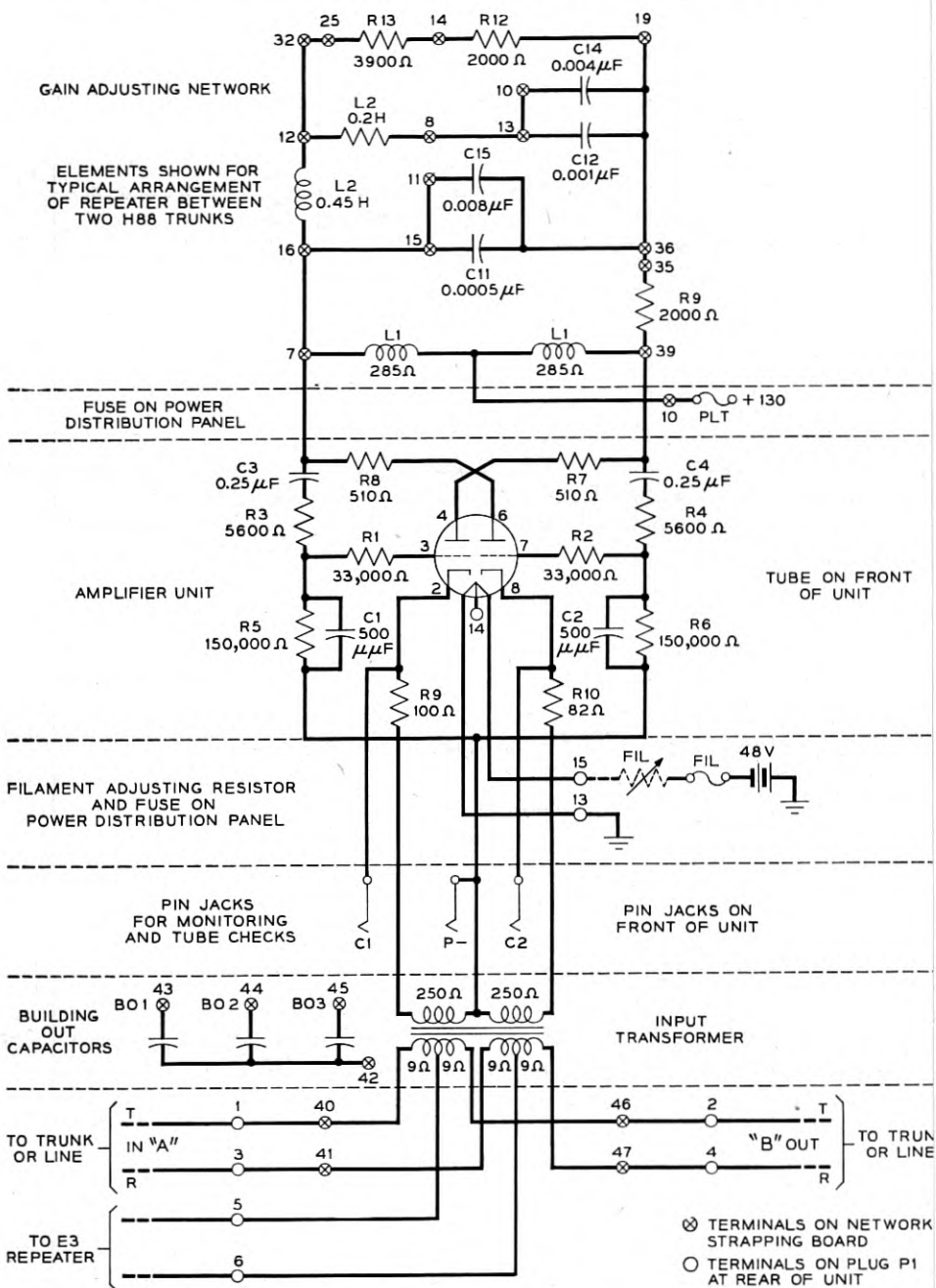In practice, it is advantageous to limit the conversion bandwidth so

Fig. 16 — Circuit of E2 repeater.

that the line and network impedances do not have to be controlled over an extended frequency band. The conversion gain is limited by reducing β to a small value at low frequencies by capacitors C_3 and C_4 of Fig. 16 in the plate-to-grid coupling network, and at high frequencies by the small capacitors C_1 and C_2 across the grid resistors R_5 and R_6 respectively.

The conversion ratio is affected by small losses inherent in the electron tube and transformer. These are balanced out by a fixed resistor $R9$ connected in series with the gain adjusting network to increase the amount of positive feedback.

The final negative series impedance presented to the line is equal to approximately $-0.1Z_N$ over the frequency band of 300 to 3,500 cycles. The impedance Z_N is determined by the configuration of the gain-adjusting network comprising several inductors, capacitors, and resistors. These components may be arranged in any form to obtain the desired negative impedance, which in turn, introduces the gain and frequency shaping characteristic desired for each type of line facility.

The E2 repeater employs a Western Electric 407A twin-triode electron tube of the 9-pin miniature type. The tube heater circuit can be operated from 24- or 48-volt office battery. The heater current is 100 milliamperes for 20-volt operation, 50 milliamperes for 40 volt operation and the plate current is 11 milliamperes.
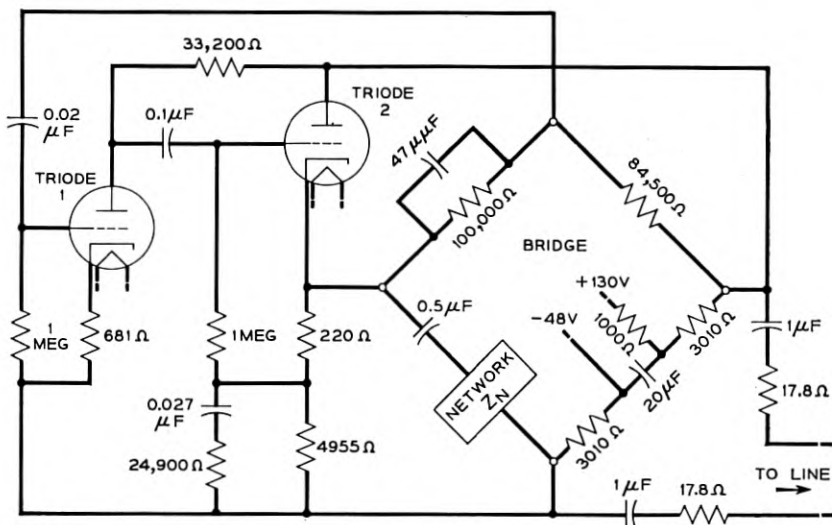
Fig. 17 — Schematic circuit of E3 repeater.
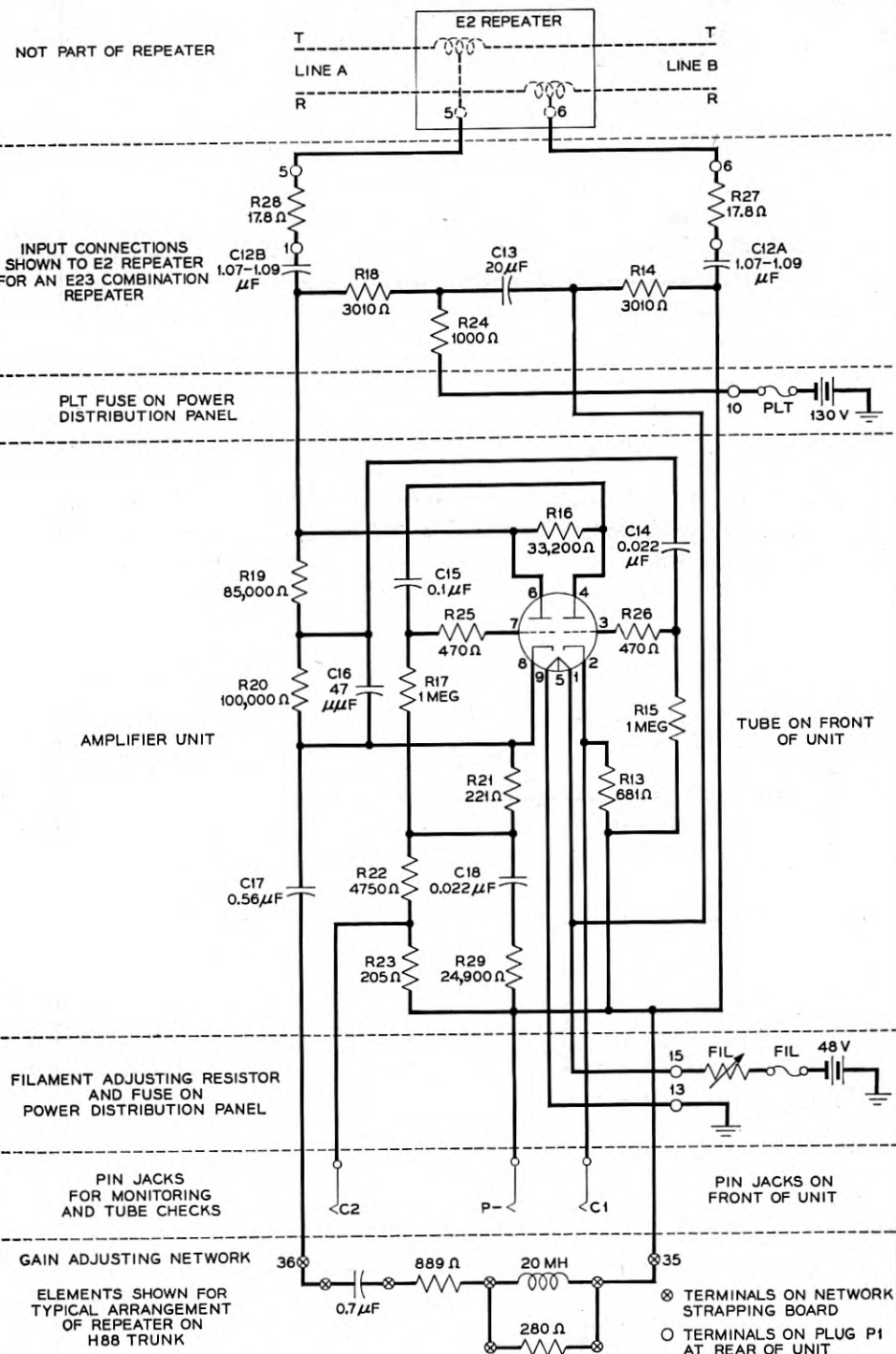
Fig. 18 — Circuit of E3 repeater.

1078

THE E3 TELEPHONE REPEATER

The E3 repeater is a two-terminal high impedance device designed to be bridged across the line in contrast with the E2 repeater which is a low impedance series connected device. Schematically shown in Fig. 17, its circuit is considerably different from that of the E2. The bridged telephone line and an adjustable network form two arms of a bridge connected to output and input circuits of a two-stage amplifier.

The bridge is so connected that a fairly large proportion of the amplifier output current flows into the telephone line and a fairly large proportion of the original line voltage is developed between the grid and cathode of the first tube since these circuits are connected to nonconjugate points of the bridge. The output and input terminals of the amplifier are connected to conjugate points of the bridge in such a manner than when the bridge circuit is balanced no feedback is effective at the input.

It has been shown, in the preceding Section, that the negative impedance generated by this form of converter is equal to the network impedance Z_N divided by a conversion factor. To obtain a practical design of the E3 repeater for the faithful conversion of the network impedances, with a minimum of spurious components, it is necessary to balance out, as nearly as possible, all converted circuit elements associated with the output bridge and connections to the line. Accordingly, the two line capacitors are balanced out by a network capacitor. The battery supply resistors, the resistor and capacitor of the plate-battery filter, and the plate-load resistor of the first-amplifier stage are all balanced out in the network by placing suitable values of resistors and capacitors in the cathode circuit of the second-amplifier stage. All of these elements combine to form an equivalent two-terminal network.

An ideal negative impedance device would convert any impedance in the network over a wide frequency band but it is advantageous to limit the negative impedance, in so far as practicable, to the frequency bandwidth required by the particular application. This is accomplished primarily in the network associated with the converter. The conversion bandwidth of the E3 repeater is restricted at the low frequencies by the design of the resistive-capacitive feedback coupling network, between the output bridge and the input grid, and at the high frequencies by the shunt capacitance connected across one resistive arm of the bridge circuit. The circuit is shown in Fig. 18.

The final negative impedance shunted across the line is equal to $-Z_N/0.94$, within ± 2.5 per cent, over the frequency range of 200 to 5,000 cycles. The magnitude and phase of the negative impedances are

controlled by the configuration of the gain-adjusting network, consisting of several inductors, capacitors, and resistors. These components may be arranged in a variety of ways to obtain the gain and frequency shaping characteristics desired for each type of line facility.

The E3 repeater employs a Western Electric 407A twin-triode electron tube of the 9-pin miniature type. The circuit is arranged so that the current for the heater of the tube can be obtained from 24- or 48-volt office battery. The heater power is 2 watts and the plate current is nominally 5 milliamperes.

Equipment

The objective of the equipment design of the E2 and E3 repeaters was to produce a repeater that would be simpler to manufacture, easier to engineer, install, and maintain, and make more efficient use of the mounting space, particularly on 23-inch bays, than the present E1 repeater. Because of the large demand, savings in manufacturing costs were realized by using a compact aluminum die-cast shell to house the repeater components. To facilitate manufacture, parallel thermoplastic strips were used for the mounting of "pigtail" type of components.[6] Further savings in shop costs were obtained by coordinating the designs of the E2 and E3 repeaters for maximum interchangeability of parts.

Engineering and installation effort has been reduced considerably by avoiding engineered options and by arranging the equipment so that the maximum portion of the assembly and wiring work is performed in the shop. Testing and maintenance routines are simplified by arranging the repeaters as plug-in units that can be removed from their bay positions and plugged into a portable test set located in a more convenient working space. In this way, the network strapping and any repair work which may be required on a repeater need not be performed while the repeater is in place, or is in a congested area. Maintenance and service interruptions are reduced to a minimum length of time by replacing a defective plug-in unit with a spare for immediate restoration of service, and the faulty repeater repaired at a more convenient time.

REPEATER UNITS

Both E2 and E3 repeater units use the same rectangular die-cast chassis, shown in Fig. 19. The front section of each unit carries the electron tube and test pin jacks which must be accessible for testing and routine maintenance. The gain-adjusting network strapping terminals are arranged, in three rows, along the left side of the repeater, and are accessible only after the unit is removed from its mounting shelf.
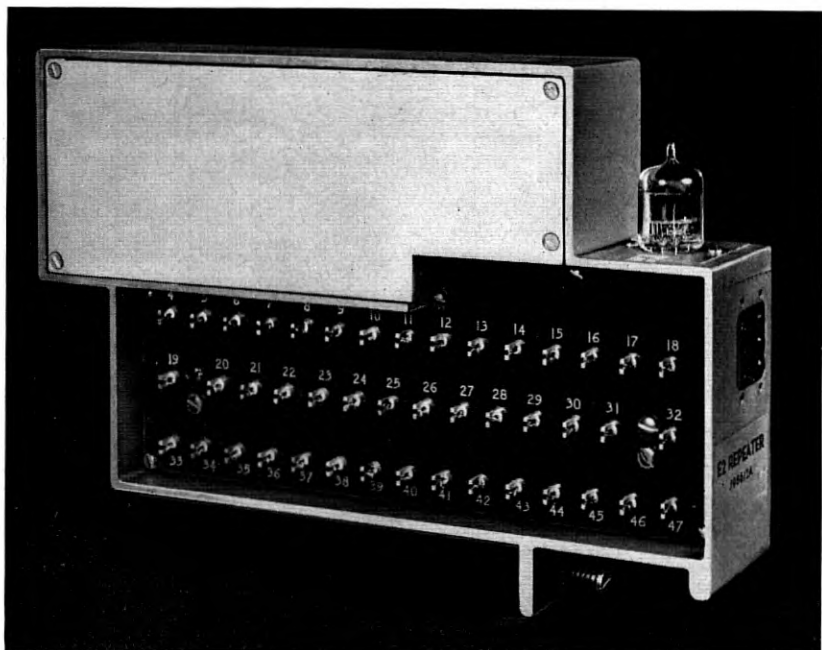
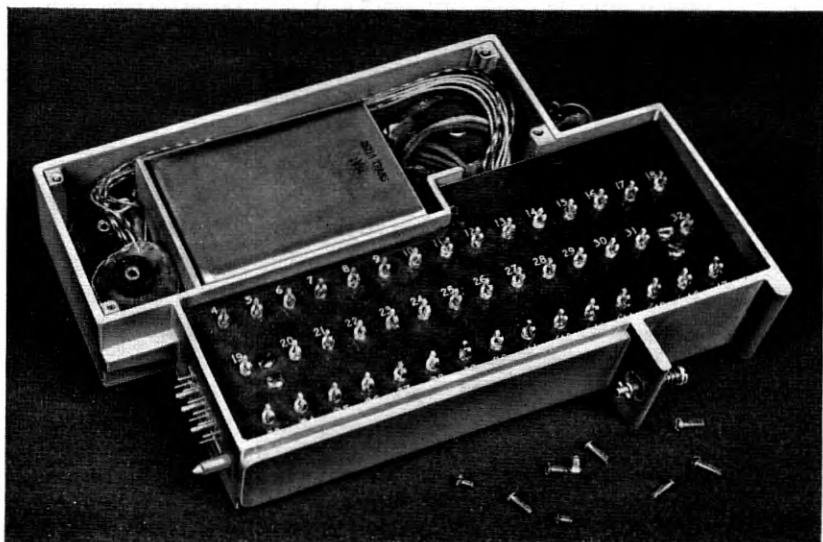Fig. 19 — Front and side view of E2 repeater.
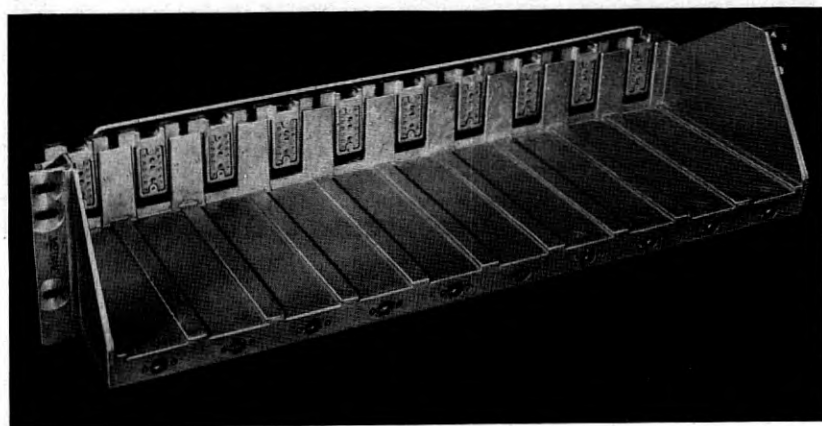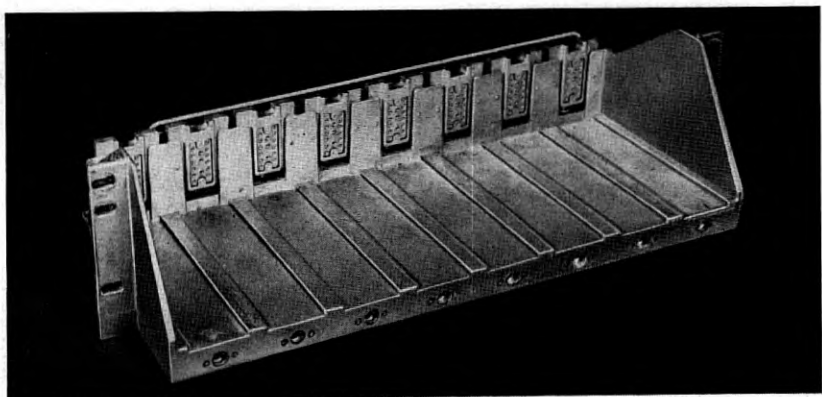

Fig. 20 — Assembly and wiring of E2 repeater.

Fig. 21 — Repeater mounting shelves. Upper for 19-inch bays, lower for 23-inch bays.

All external connections, to either type of repeater, are made through a male connector rigidly mounted into the repeater chassis, as shown in Fig. 20. The matching female socket is suspended in the mounting shelf, on a floating assembly, to relieve the strain on contacts and wiring when the repeaters are plugged into a shelf. Both connector units consist of molded rectangular phenolic blocks equipped with 15 gold plated contacts. Proper alignment between the male and female connectors is maintained by using a positioning key and guide pin on the repeater chassis, shown in Fig. 20, and a track on the mounting shelf. After a repeater is seated into its shelf position it is made secure by means of a screwdriver operated quick-acting fastener.

MOUNTING SHELF

An aluminum die-cast shelf, shown in Fig. 21, is used for mounting the repeaters on the relay rack bays. The shelf comes in two widths; one holding 8 repeaters is used for 19-inch bays and the second, containing 10 repeaters, is used on 23-inch bays. Grooves cut into the base of the shelf match a projection on the repeater to act as a track system for positioning the repeater into its connector socket. The shelf connector is mounted in a small die-cast block which, in turn, is fastened to the shelf by shoulder screws to provide a floating assembly. A tapered key, molded into the repeater casting, engages a slot in the connector block to secure the horizontal alignment, and a tapered pin, at the bottom of the repeater casting, raises the connector block for the vertical alignment.

Fifteen mounting shelves can be arranged on standard 11-foot 6-inch relay rack bays. The maximum complement of repeaters will be 120 for 19-inch bays and 150 for 23-inch bays.

POWER DISTRIBUTION PANELS

Fabricated power distribution panels which occupy $1\frac{3}{4}$-inches of mounting space are used for supplying plate and filament power to the repeater shelves. The primary unit, shown in Fig. 22, is required for furnishing power to the first three repeater shelves and one test-set power outlet. Four sets of plate and filament alarm-type fuses are provided, one set for each shelf and one set for the test power outlet. Four filament-adjusting rheostats are furnished and the panel is equipped with an alarm relay and lamp. Pin jacks are available on the front of the panel to measure the filament voltage.

A supplementary power distribution panel is available, equipped with plate and filament fuses, rheostats and pin jacks sufficient for six additional repeater mounting shelves. One primary and two supplementary power panels are required to fully equip an 11-foot, 6-inch bay with 15 repeater shelves. Both panels are completely wired in the shop to simplify installation. Fig. 23 shows a 19-inch relay bay mounting shelf complete with E2 and E3 repeaters and the two types of power distribution panels.

REPEATER TEST SET

A new test set has been developed, which will simplify the installation and maintenance of these devices. This test set has been designed
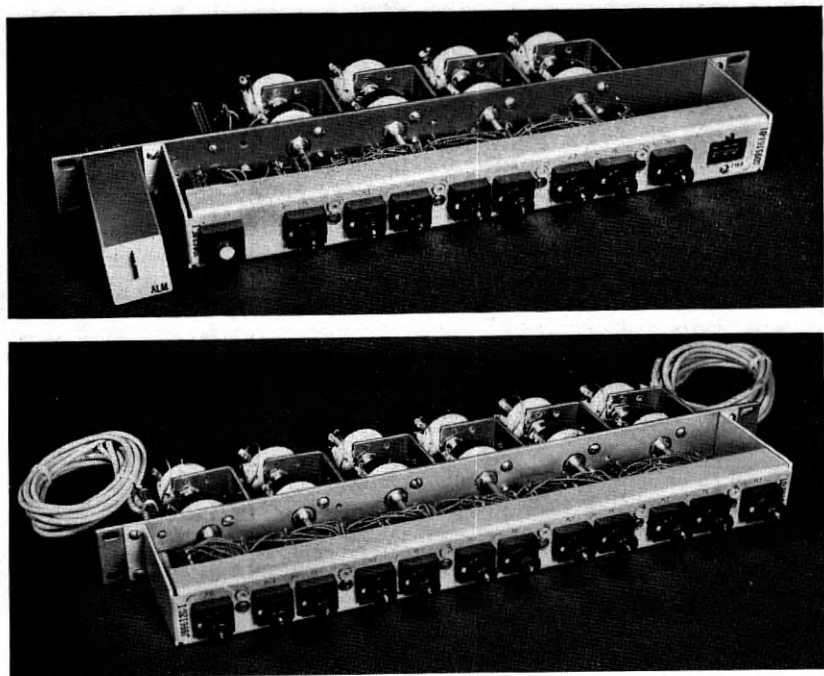
Fig. 22 — Power distribution panels. Upper is primary unit, lower is supplementary unit.
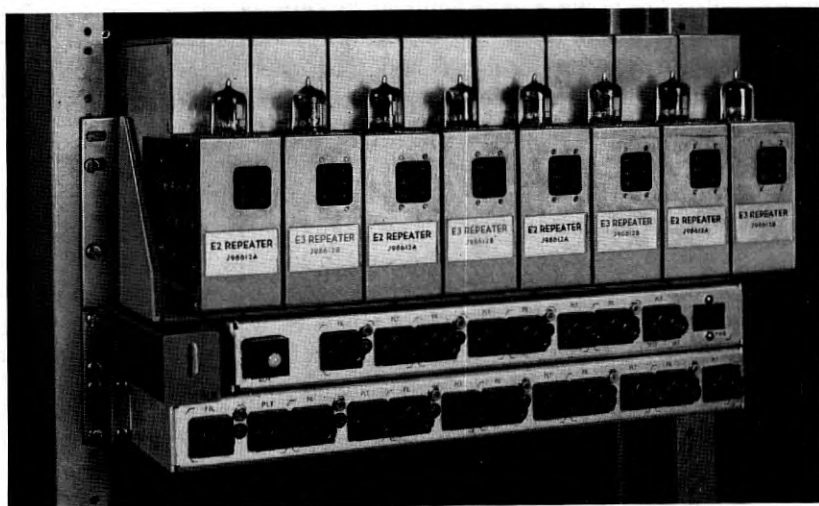

FIG. 23 — Shelf of E2 and E3 repeaters, with power distribution panels, for 19-inch bays.

not only to test the new E2 and E3 repeaters but also the older type of E1 repeater, which has been in use for several years. All test connections which are required to measure individual repeaters or combinations of E1 o.· E2 and E3 repeaters are made by the operation of a single rotary control function switch. Such a system will avoid the unintentional errors and time consuming operations which attend the setting-up of complicated patch cord connections.

The first five positions of the function switch are arranged to make transmission measurements of an individual repeater or any combination of E1 or E2 and E3 repeaters. Insertion gain and loss measurements are performed with the repeaters working between their normally connected line impedances.

In making transmission and stability measurements, it is sometimes necessary to set up trial connections of the repeater networks during the initial test period or for unusual line conditions. If the actual repeater networks were used, it would require a large number of soldered connections to be made for each condition of the tests. Equivalent jack-ended E2 and E3 networks have been included in the test set, so that with small patch cords, a rapid interconnection of the network components can be made.

As gain and stability of the E-type repeaters are both directly dependent upon impedance variations of the lines, it is sometimes necessary to measure line impedance to determine the causes for low return loss and instability. The last four positions of the function switch are arranged to make positive impedance measurements of lines, negative impedance measurements of the repeaters and return loss measurements between any two lines or impedances. A decade resistance standard has been built into the test set to furnish a direct indication of the magnitude of the unknown impedance. The phase angle of the impedance is determined by a return loss measurement and the angular degrees are read from a chart supplied with the equipment.

Although this test set was designed primarily for tests on E type repeaters, it is possible to connect other types of four-terminal networks into the test set and measure impedances, return loss against known impedances, and insertion gains or losses.

THEORY OF TRANSMISSION MEASUREMENTS

One method of measuring the insertion gain of a negative impedance repeater, without affecting the transmission or stability of the circuit, is to introduce the test voltage, through a low impedance source, in series with the input line and measure the resultant current picked off

through a similar low impedance connection in series with the output line. A comparison of the received currents, with and without a repeater, will give an indication of the insertion gain or loss.

The principles involved in making this type of transmission measurement are shown in Fig. 24. The voltage source and the current measuring detector are assumed to have negligible impedances compared to the impedances of the lines Z_1 and Z_2.

In the reference condition of Fig. 24, the driving voltage E_0 and the current measuring device are in series with the two line impedances Z_1 and Z_2. The resultant current will be determined by the source voltage E_0 divided by the vector sum of impedances Z_1 and Z_2:

$$I_0 = \frac{E_0}{Z_1 + Z_2}$$

where $Z_1 + Z_2$ indicates a vector addition of the two impedances.

In the "measure" condition of Fig. 24 the repeater, represented by the network N, is inserted into the circuit between the voltage source and the measuring device, and, although the voltage E_0 is assumed to remain constant, the addition of network N into the circuit will change

REFERENCE CONDITION

$$I_0 = \frac{E_0}{Z_1 + Z_2}$$

OSCILLATOR   DETECTOR

MEASURE CONDITION

I_1 REPRESENTS A CHANGE FROM I_0 DUE TO INSERTION OF N

OSCILLATOR   DETECTOR

INSERTION TRANSMISSION = $20 \, LOG_{10} \frac{I_1}{I_0}$
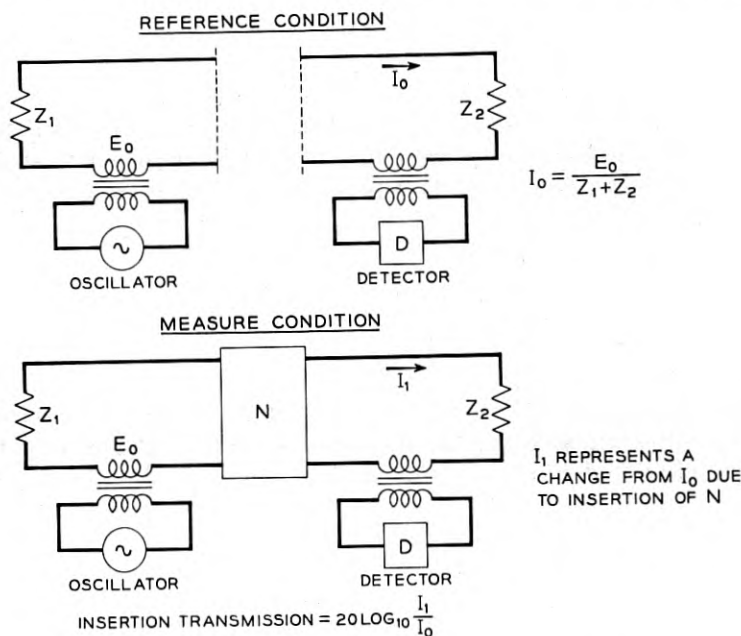
Fig. 24 — Principles of insertion measurements.

Fig. 25 — Test set showing repeaters and test cords.

the current to a new value I_1. The ratio of the currents I_1/I_0 is a direct measure of insertion gain or loss between Z_1 and Z_2 due to inserting the network. The db change in transmission caused by the insertion of N is

$$\text{Insertion transmission in db} = 20 \log_{10} \frac{I_1}{I_0}.$$

When I_1 is less than I_0, the addition of N has caused an insertion loss, and when I_1 is greater than I_0 the addition of N has caused an insertion gain. In the test set the current indicating device has a db scale so that the change in transmission can be read directly in db.

TRANSMISSION MEASUREMENTS

In setting up to make repeater tests, the E2 and E3 units are removed from their shelf positions and plugged into adapters in the test set, as shown in Fig. 25. A test plug, fashioned to simulate the male connector
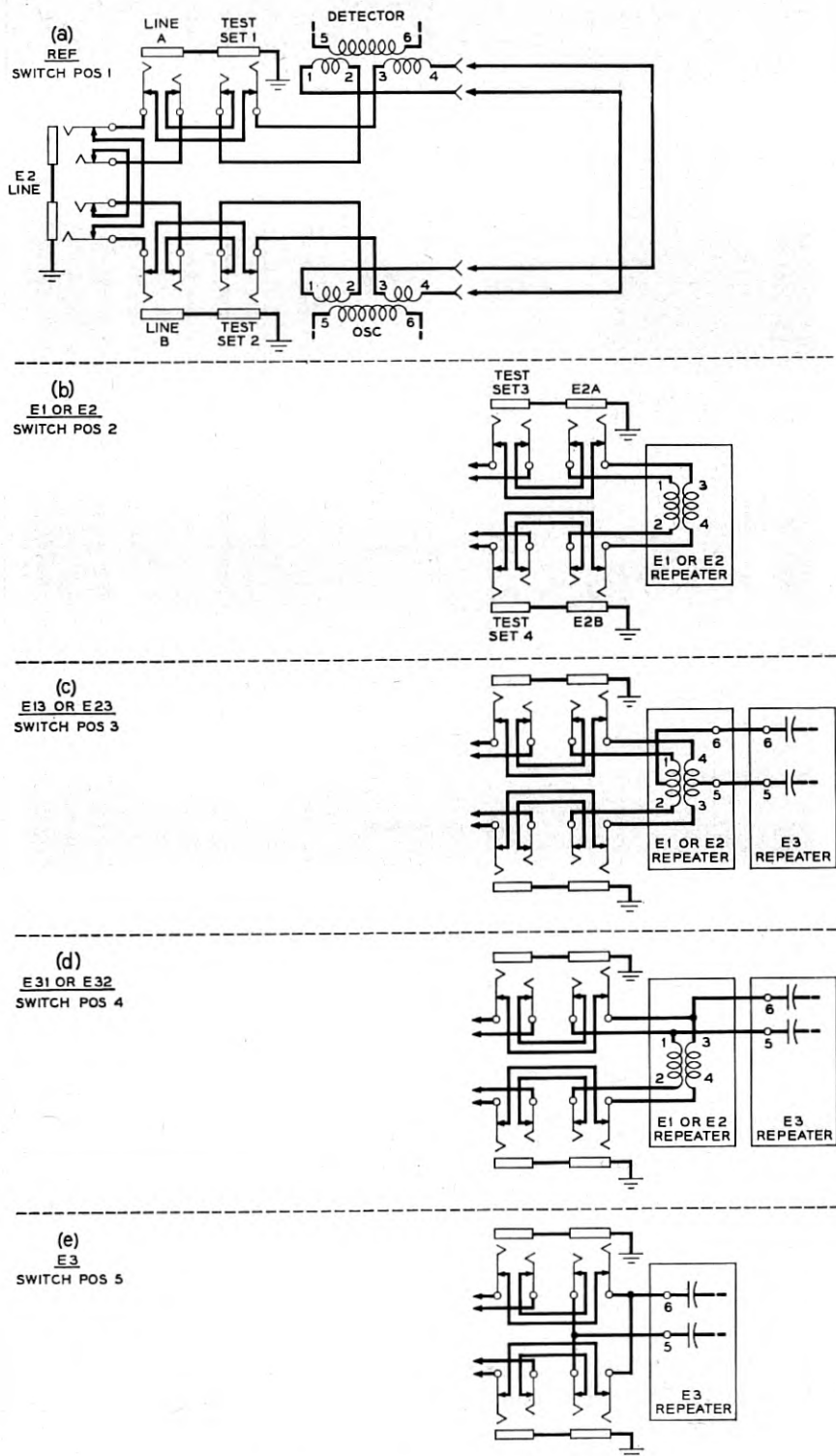
Fig. 26 — Sequence of transmission measurements.

of the repeater, is inserted into the vacant E2 repeater position for picking up the connections to the incoming and outgoing lines. A jack ended cord, connected to the test plug is patched into the test set for applying the line connections to the repeaters under test.

The first position of the rotary function switch arranges the test set for the reference condition. The incoming and outgoing E2 repeater lines provide the terminations, as shown in Fig. 26(a). The low impedance voltage source is obtained by means of an oscillator working through a step-down transformer having an impedance ratio of 600:2 ohms. The low impedance side consists of two equal well balanced windings, one winding being inserted into each side of the line, to form a balanced-to-ground voltage source. The received current is measured by means of a detector working through an identical transformer having one of the 2-ohm windings connected into each side of the line for maintaining the balanced-to-ground circuit.

Switch position 2 connects the E1 or E2 repeater into the test circuit between the sending and receiving impedances as shown in Fig. 26(b). The change in detector reading will indicate the insertion gain or loss of the connected repeater.

The third and fourth switch positions change the arrangements of E1, E2 and E3 repeaters for the insertion measurements of the various repeater combinations, as shown in Figs. 26(c) and (d). Fig. 26(e) indicates the connections for testing the E3 repeater alone on switch position 5.

IMPEDANCE MEASUREMENTS

The second section of the type-E repeater test set has been arranged to measure the impedance of two-terminal networks and the return loss between any two impedances or between an unknown impedance and a specified network. The impedance measuring circuit consists of a hybrid coil arranged in the form of a balanced bridge for measuring return loss. The driving voltage and detecting device are connected across conjugate arms of the bridge and the unknown impedance and a resistance standard are applied across the opposite conjugate arms of the bridge circuit.

Simple transmission measurements made across the hybrid coil, between the oscillator and detector sides of the bridge, are the only determinations required to find the return loss between any two impedances or the magnitude and phase angle of an unknown impedance. Such a device has several advantages over other types of impedance bridges in that no critical balances are required, no calibrations are

Fig. 27 — Sequence of impedance measurements.

necessary, the critical elements are stable passive networks and changes in the sensitivity of the measuring device, which includes variations in oscillator output and sensitivity of the detector circuit, will not affect the accuracy of measurement.

An impedance reference is established, as shown in Fig. 27(a), when the transmission through the hybrid network is measured with connection to the resistance standard. A second transmission measurement is made through the hybrid coil network with the standard impedance connected instead of the unknown. After replacing the unknown with the resistance standard, the transmission through the hybrid coil is adjusted by varying the resistance standard to obtain the same value of loss, as measured with the unknown impedance. When the two transmissions are equal, the resistance in ohms, as read on the resistance standard, will be the same as the magnitude of the unknown impedance. With the magnitude of the resistance standard and unknown impedance the same, the phase angle of the unknown is readily determined by comparing the transmission through the hybrid coil for two polings of one of the hybrid windings. The first poling, Fig. 27(c), which is used as a reference, provides a measure of the transmission through the hybrid network when the current in the unknown branch and the current in the resistance branch are added vectorially in the detector winding. The reverse poling of one of the coil windings, Fig. 27(d), provides a measure of the transmission through the hybrid when the currents in the resistance and unknown branches are subtracted vectorially in the detector circuit. In addition to being a method of measuring the phase angle of an impedance, this comparison of two measurements with different poling is a return loss measurement of an unknown against a known impedance of equal magnitude. A curve of phase versus return loss may be used for convenient interpretation of the return loss measurement in terms of phase angle. After the phase angle has been ascertained it is necessary to determine the sense of the angle, that is, whether the unknown impedance contains positive or negative reactance. A reference condition is established, Fig. 27(e), by shunting a small value of capacitance first across the unknown impedance and then across the resistance standard and noting the change in transmission through the hybrid network. An increase in the transmission, in going from the reference to measure conditions, indicates a positive reactance and a decrease in transmission indicates a negative phase angle. The reference condition is established to minimize indicational errors at small phase angles of the unknown impedance.

Two additional pieces of information are revealed in the return loss

measurement. When the return loss is positive, the unknown impedance contains positive resistance and the phase angle must lie between 0 and ±90 degrees. For negative return losses the unknown impedance contains negative resistance and the phase angle must lie between ±90 degrees and 180 degrees.

ACKNOWLEDGMENTS

REFERENCES

1. J. L. Merrill, Jr., A Negative Impedance Repeater, A. I. E. E. Trans., **69**, Part 2, pp. 1461–1466; 1950.
2. J. J. Pilliod, Fundamental Plans for Toll Telephone Plant, A. I. E. E. Trans. **71**, pp. 248–256.
3. O. B. Blackwell, Time Factor in Telephone Transmission, A. I. E. E. Trans., **51**, pp. 141–7.
4. G. Crisson, Negative Impedance and The Twin 21-Type Repeater, B. S. T. J., **31**, pp. 485–513, July, 1931.
5. J. L. Merrill, Jr., Theory of The Negative Impedance Converter, B. S. T. J., **51**, pp. 88–109, Jan., 1951.
6. W. E. Kahl and L. Pedersen, Some Design Features of the N-1 Carrier Telephone System, B. S. T. J., **51**, pp. 418–446, April, 1951.

Stress Systems in the Solderless Wrapped Connection and Their Permanence

By W. P. MASON and O. L. ANDERSON

(Manuscript received December 16, 1953)

The solderless wrapped connection is initially held together by the hoop stress in the wire which enters the connection as a result of the tension put on the wire by the wrapping tool. Measurements made out to a time of 1.5 years at room temperature show that the tension has decreased to 70 per cent of the one day value (8000 lbs per square inch) in this period. Two methods of extrapolation are discussed, both of which indicate that at least half of the initial one day value will remain at the end of forty years at room temperature.

Another set of stresses enters the connection as a function of time, namely the diffusion forces produced by diffusion of the tin plating into the brass terminal and copper wire. A number of experiments are discussed which show that the activation energy of diffusion is materially reduced by the shearing stresses in the connection. Measurements at two temperatures, which allow extrapolation to room temperature, indicate that at the end of two years the force required to strip the wire from the terminal has increased by 5 per cent over the initial value and that at the end of forty years the increase will be 20 per cent. Support for these conclusions is furnished by tests on actual connections that have been in the field for one year and ten months, which show an increase of 5 per cent in the stripping force even though the relaxed hoop stress is only 68 per cent of the initial value. The increase, which is due to diffusion forces, can be made higher by using zinc, cadmium or aluminum plating, and the fusion occurs in a shorter time.

INTRODUCTION

As discussed in a series of papers,[1] the solderless wrapped connection is an efficient and inexpensive method of connecting a wire to a terminal. All the tests made so far indicate that it is mechanically sound and sufficiently free from the effects of corrosion to have a trouble free life of at least forty years. Photoelastic and stress studies show that the

---

[1] The Solderless Wrapped Connection, B. S. T. J., **32**, May 1953.

connection is initially held together by the hoop stress in the wire which enters the joint as a result of the tension put on the wire by the wrapping tool. As time goes on, another system of stresses are generated, namely, the diffusion stresses caused by the diffusion of one part of the connection into the other which eventually eliminate the surface between the wire and the terminal and in effect join the two together.

It is the principal purpose of this paper to describe a number of experiments which show how these stresses develop, how large they are and how they can be increased by substitution of a different type of plating between the terminal and the wire. A comparison of the strength of a joint formed by a tin plated copper wire and a bare copper wire both wound on nickel silver or brass terminals shows that the diffusion forces develop more quickly when the wire is tin plated than when it is bare. Measurements made at different temperatures show that the activation energy of diffusion is decreased in proportion to the hoop stress in the wire indicating that the shearing stress at the contact surfaces aids diffusion. This activation energy is considerably less for tin than for copper. The diffusion joint has a strength per unit area equal to the limiting shearing stress of the tin plating. This is in the order of 3,000 pounds per square inch for tin but is considerably higher for other types of plating such as zinc, aluminum or cadmium. Measurements of the stripping force of connections made with bare and tinned copper wire on zinc, aluminum or cadmium plated terminals show that the stripping force increases by a factor of two as a function of time, and the time required for the diffusion forces to operate is considerably less with these types of plating.

The combination of relaxation and diffusion stresses that are discussed later show that as the mechanical strength due to the hoop stress decreases, the strength due to diffusion increases and at the end of forty years the standard tin plated wire on nickel silver or brass terminals will be at least 20 per cent stronger than it is initially. The extensive corrosion tests described in Footnote 1, taken together with the mechanical strength tests described here, show that the standard connection should not fail in the forty year period under consideration.

RELAXATION OF HOOP STRESS AS A FUNCTION OF TIME

The rate of relaxation of the hoop stress in the wrapping wire is an important quantity for the stability of the connections. This has been studied by wrapping 24 gauge wire with a constant tension of three pounds around a spring steel terminal 0.0124 inches thick and 0.062 inches wide. As shown by Figure 11 of Mallina's paper,[2] this causes the

terminal to twist through an angle of about 25° when 100 turns are wrapped around the terminal. This twist is the result of a torque which is caused by the fact that the wire has a hoop stress and the wire does not come back on itself but advances by the thickness of the wire for each turn. As shown previously,[2] the total torque is equal to

$$\text{Torque} = (\text{W.F.}) \left(\frac{2ab}{a+b} \right) L \tag{1}$$

where (W.F.) is the wrapping force, $2a$ and $2b$ the thickness and width of the terminal and L the total length of the wrapped section. Hence, by calibrating the spring constant, the average hoop stress can be evaluated. In this manner, Mallina[2] has found that after transient creep (defined
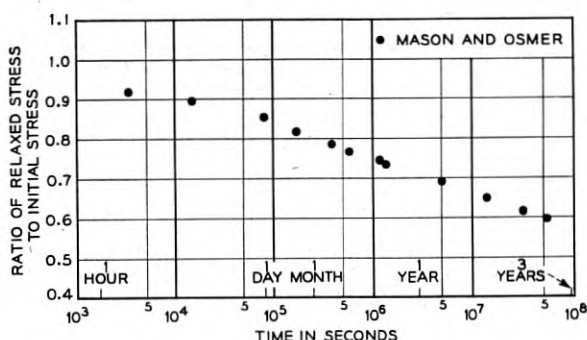
Fig. 1 — Relaxation of stress in copper solderless wrapped connection at room temperature.

in this paper as the loss in stress during one day) has occurred, the stress level for the standard 24 gauge connection is about 8,000 pounds per square inch.

This same technique can be used to measure the loss in hoop stress as a function of time for all one has to do is to put a pointer on the spring and observe the rate the angle decreases. It will be noted that this system reproduces all of the stress systems and strain hardening that occur in the wrapped solderless connection, and hence a measurement of the relaxed angle is the most representative measurement of the relaxation of the solderless wrapped connection. Fig. 1 shows an average of the results of four such springs from the time of their intial formation out to a period of one year and one month. The rate of relaxation is quite rapid during the first day (transient creep) but at the end of one

[2] R. F. Mallina, Solderless Wrapped Connections, Part I — Structure and Tools, B. S. T. J., pp. 525–555, **32**, May 1953.

year and one month the average hoop stress is 5,900 pounds per square inch and it is decreasing at the rate of 240 pounds per square inch between the first and second year. In the previous paper,[3] since the transient creep occurring during the first day is somewhat variable, the angle of twist reached 24 hours after the connection had been made, was taken as the initial 100 per cent value and the relaxation has been plotted with respect to this. Fig. 2 shows this plot with data from Mason and Osmer and a set of eight relaxing springs measured by Mallina and McKettrick all plotted on the curve. At the end of 1.5 years, the observed stress is 70 per cent of 8,000 pounds per square inch or 5,600 pounds per square inch on the average.

The measurements out to 1.5 years by this method appear to be the longest measurements of stress relaxation in annealed copper wire in the
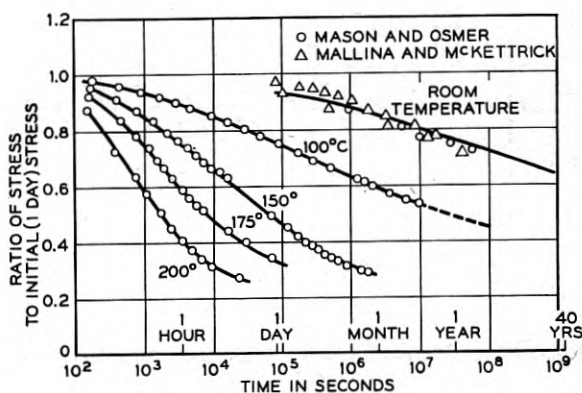
Fig. 2 — Relaxation of stress in tinned copper wire as a function of time and temperature.

literature. Since the wrapped solderless connection is expected to last at least forty years, it is desirable to be able to extrapolate the stress value out to forty years time. Several methods are possible. According to theoretical treatment,[4] stress relaxation proceeds as follows:

$$\sigma_0 - \sigma = \frac{kT}{\beta} \log_e (1 + t/t_0) \qquad (2)$$

[3] W. P. Mason and T. F. Osmer, Solderless Wrapped Connection, Part II — Necessary Conditions for Obtaining a Permanent Connection, B. S. T. J., **32**, pp. 557–590, May 1953.

[4] See *Progress in Metal Physics*, Volume IV, Pergamon Press, Limited, 1953; Chapter V, Theory of Dislocations by A. H. Cottrell, pp. 233 and 251 to 260; Kuhlmann, D. and Z. Physik, **24**, p. 43, 1952; and Proc. Phys. Soc., **64**, p. 64, 1951; and A. H. Cottrell and V. J. Ayetekin, Inst. Metals, **77**, p. 389, 1952. The last reference gives data for stress relaxation in zinc which shows that it obeys equations (2), (3) and (4).

where σ_0 is the initial stress, σ the final stress, k Boltzmann's constant, T the absolute temperature, t_0 a time determined from the equation

$$\sigma_0 = -\frac{kT}{\beta} \log\left(\frac{\beta A t_0}{kT}\right) \tag{3}$$

and A and β are constants in the fundamental equation

$$\frac{d\sigma}{dt} = -A e^{-(H-\beta\sigma)/kT} \tag{4}$$

where H is the activation energy in the absence of any stress.

The result of (2) is that for times large compared to t_0, the stress difference $\sigma_0 - \sigma$, plotted on logarithmic paper will be a straight line relation. Hence, in Fig. 2, for times in the order of forty years, the indicated stress level is 60 per cent of 8,000 pounds per square inch or 4,800 pounds per square inch.

Another method of extrapolation which essentially makes use of (4) is to measure the rates of relaxation at different temperatures and determine an activation energy for each stress level by comparing the logarithms of the times for the same stress levels as a function of temperature. The constant A in (4) is usually considered to have a temperature factor T in it and is usually written as $A'T$. With this relation, (4) can be written

$$-\frac{d\sigma}{A'T e^{-(H-\beta\sigma)/kT}} = \frac{-e^{-(H-\beta\sigma)/kT}}{A'T}\, d\sigma = dt \tag{5}$$

Integrating this equation between the limits σ_0 and σ, we have

$$t = \frac{k}{\beta A'}\, e^{H/kT}[e^{-(\beta\sigma/kT)} - e^{-(\beta\sigma_0/kT)}] = \frac{k}{\beta A'}\, e^{(H-\beta\sigma)/kT}[1 - e^{-\beta(\sigma_0-\sigma)/kT}] \tag{6}$$

Hence, if the quantity

$$e^{-\beta(\sigma_0-\sigma)/kT}$$

is small compared to unity, we have

$$(H - \beta\sigma) = k \log_e (t_1/t_2)\, \bigg/ \left[\frac{1}{T_1} - \frac{1}{T_2}\right] \tag{7}$$

As shown by Fig. 3, the value of β is about 6 calories per pound per square inch and hence if $\sigma_0 - \sigma$ is at least 800 pounds/square inch (i.e., for all values of relaxation of 0.9 or less) this factor will be less than 1 per cent for all temperatures used and hence we can use (7) to evaluate values of the activation energy H-$\beta\sigma$.
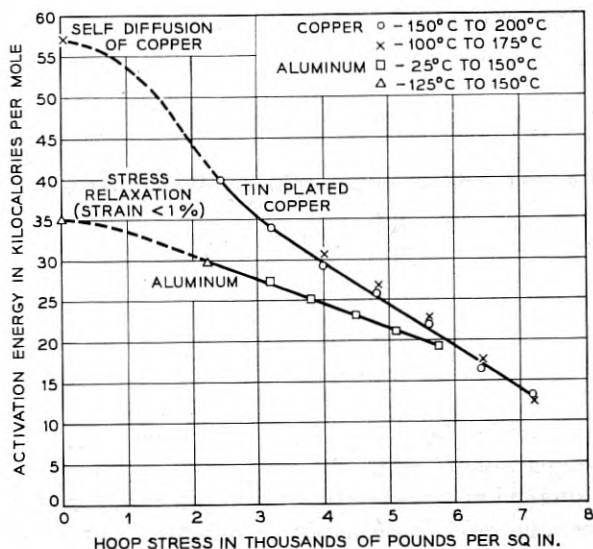
Fig. 3 — Activation energy for stress relaxation as a function of hoop stress.

Measurements of the rate of stress relaxation for tinned copper wire at 200°C, 175°C, 150°C, and 100°C are shown by Fig. 2, and the activation energies plotted against average hoop stress are shown by Fig. 3. Values are given using 150°C to 200°C as the temperature range and 100° to 175° also. Both ranges give the same activation energies within the experimental errors and show that down to about 0.4 relaxation the activation energies satisfy an equation of the type

$$H' = H - \beta\sigma \tag{8}$$

The curvature exhibited by the relaxation versus log t shown for all temperatures indicates that the activation energy must increase faster than (8) for low values of relaxation and the dotted line shows a hypothetical curve ending up at the self diffusion activation energy for copper, 57 kilocalories per mole.

To apply this method in general, one has to take account of any transformation such as recrystallization in the temperature range of measurement. For example, Fig. 4, shows similar curves for aluminum wire. Recrystallization in aluminum is known to occur at temperatures above 150°C and this change is shown in the relaxation measurements by the lower values of relaxation that occur for long times. If one takes values of time above and below the recrystallization temperature, the activa-

tion energy will appear higher for this range than for a temperature range below the recrystallization temperature. The agreement of the activation energy for copper for the two temperature ranges shown by Fig. 3, shows that no transformation occurs from 25°C to 200°C and hence we can extrapolate the relaxation to room temperature taken as 25°C, with the result shown by the solid line labelled 25°C. This agrees well with the measured values and indicates a stress at the end of forty years equal to 5,200 pounds per square in.

DIFFUSION STRESSES IN SOLDERLESS WRAPPED CONNECTIONS

In addition to the hoop stresses, another set of stresses develops as a function of time, namely, the diffusion stresses caused by the diffusion of one part of the connection into the other. The first experiment that showed the presence of these stresses was the stripping force tests of Fig. 23 of the previous paper referred to in Footnote 3. These measurements were carried out on connections which had been held at 175°C for lengths of time up to ten days and it was found that the stripping forces did not decrease with time. A more careful set with twenty connections for each point have recently been run with the results shown by Fig. 5, solid line labelled 175°C. From this curve, it is seen that the stripping force decreases to 88 per cent of its initial value of 15.5 pounds average for six turns of 24 gauge tinned wire and then increases to 120 per cent of the initial value at the end of ten days. Similar increases are shown at 100°C over a longer period of time and recent tests of solderless wrapped connections that have been in the field for one year and ten months show that the stripping force is about 5 per cent higher on the average than it was when the connection was formed.
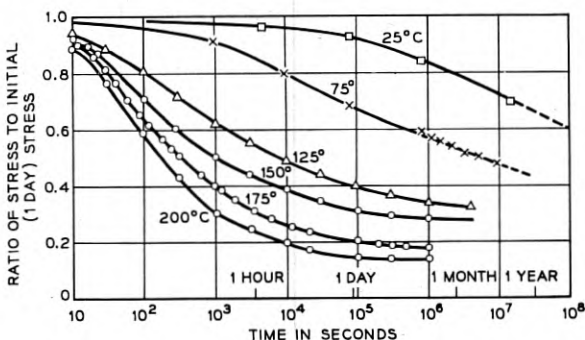
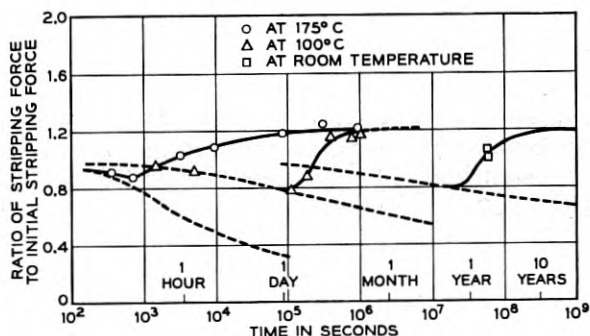Fig. 4 — Relaxation curves for aluminum wire in solderless wrapped connections.

Fig. 5 — Ratio of measured stripping force to initial stripping force as a function of time and temperature for tinned copper wire on nickel silver terminals.

The dashed lines show the corresponding hoop stresses as a fraction of the initial hoop stress and hence it is evident that as the hoop stresses go down the stripping forces first decrease and then increase to higher values than were effective originally. We shall presently show that the difference between the measured stripping force and the proportionally relaxed hoop stress is due to a stress caused by diffusion of the tin in the plating into the wire and terminal of the solderless wrapped connection.

One experiment which shows that the initial stripping force is caused by the hoop stress in the wire is the experiment shown by Fig. 6. Here a terminal is made which has a slightly tapered tin plated pin in the middle and is cut back for some distance beyond the pin. The terminal is wound with five turns of No. 14 gauge (0.065 inch diameter) tinned copper wire. The initial stripping force to pull off the winding was determined and it was found to take 72 pounds force on the average to strip the wire off the terminal. A similar set of measurements was made on the force required to pull the pin out of the terminal and this averaged about 50 pounds or 70 per cent of the stripping force for the wire. Since the pin and terminal had the same coefficient of friction as the wire and terminal, and since the pin is required to support all the compressional stress in the terminal due to the hoop stress in the wire, it is evident that at least 70 per cent of the force required to strip the wire off the terminal is plain frictional force between the wire and the terminal. It is thought that the remainder of the force is due to the gouges cut in the terminal by the winding process. When the wire is stripped off the terminal, these cuts gouge out parts of the wire and hence require a higher force. This effect is equivalent to friction for a rough surface, which is higher than that for a smooth surface.

Next the terminal was held at 175°C for various times as shown by Fig. 6, where the stripping forces and the forces to pull the pins are plotted. It is seen that the force required to pull the pin decreases with time while the force required to strip the terminal increases with time. The pin force duplicates the stress relaxation curve initially but departs from this curve more and more as time progresses. This gradual departure appears to be due to some diffusion in the tin which makes partial contact with the terminal. The amount of diffusion between pin and terminal is less than that between wire and terminal for two reasons: (a) the contact area between pin and terminal is not as intimate as the contact area between wire and terminal due to excessive plastic flow in the latter but not the former case, and (b) the contact area between pin and terminal is much greater than between wire and terminal. Nevertheless, the force required to pull the pin is substantially the same as the frictional force holding the wire on the terminal due to the hoop stress in the wire. Hence, we can conclude from this experiment that the initial stripping force is due to the frictional force resulting from the hoop stress plus shearing forces required to gouge the wire.

Several experiments have been undertaken to measure the effect of diffusion separate from friction. The most successful of these was the arrangement shown by Fig. 7. Here a wire was pressed against a double-toothed sharp edged block, and a constant pressure was maintained for various times at various temperatures. An attempt was made to produce an indentation of the same magnitude as that developed in the wrapped solderless connection, although, of course, the area of contact increased slightly with time.

It was found that for aluminum or copper on nickel silver at room
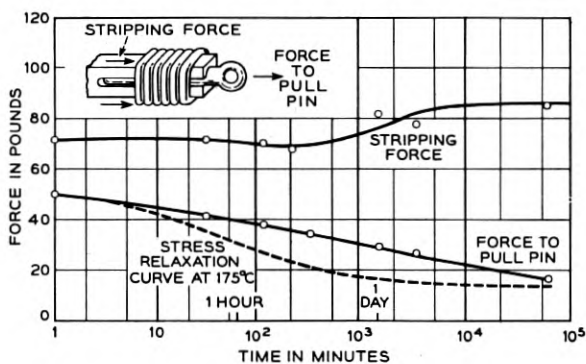

Fig. 6 — Experiment showing difference between stripping force and frictional force due to hoop stress — temperature 175°C.

temperature, no adhesion occurred even when the time of loading was very long. It was also found that if the load was removed, even momentarily, before the sample was placed in the oven, no adhesion occurred. For a given temperature there is an induction period before the wire adheres to the block, and this induction period increased, in general, as the temperature decreased. This induction period was found to be a time of nucleation. This is shown by the fact that the period increases as the square of the contact dimensions. Since diffusion is a function of $x/\sqrt{Dt}$ where x is the distance, D the diffusion constant and t the time, this observation shows that nucleation starts at a given point and proceeds for a certain fraction of the contacting surface before fusion strengths are observed. After the induction period, the fusion force — the force required to pull wire and block apart — increased at a rapid rate for the cases of copper, tinned copper, and zinc wire on a nickel silver block.

In order to account for the effect of fusion due to the increase of contact area, the ratio of the fusion force to the contact area was determined, yielding a shearing stress. The area of contact could be easily measured with a microscope since a bright surface was produced by the shearing process. The shearing stress, Fig. 8, for the case of tinned copper wire on nickel silver is shown to approach a limit of about 3,000 psi which is approximately the limiting shearing stress for tin. Hence, it appears that tin diffuses into the copper wire and the nickel silver base. Further-
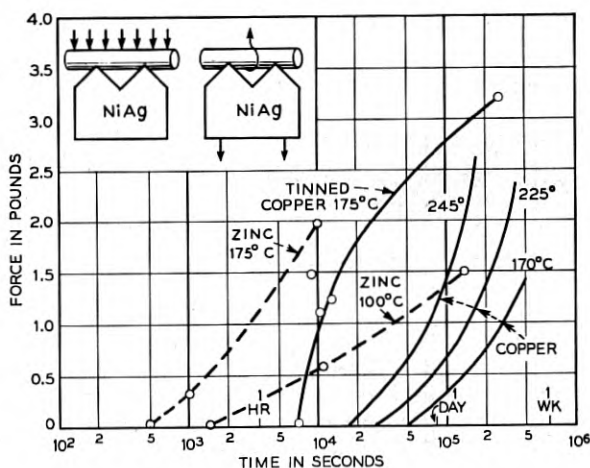
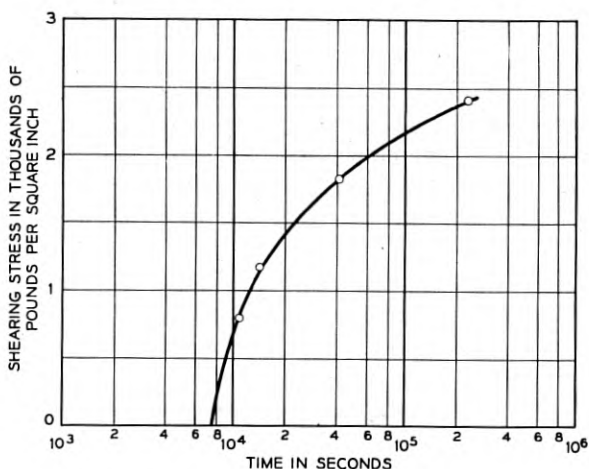Fig. 7 — Diffusion forces for tinned and bare copper and zinc wire on nickel silver base.

Fig. 8 — Diffusion shearing strength for tinned copper wire on nickel silver at 175°C as a function of time.

more, it appears that the fused bond will just withstand a shearing stress equal to the limiting shearing stress of tin. Metallurgical evidence for this diffusion was presented in Fig. 19 of the paper referred to in Footnote 4. In this figure, a tin plate layer between the copper and nickel silver was diffused in the two metals in a time of about 400 hours at 180°C. The new evidence indicates that this layer of tin has the shear strength of bulk tin.

The previously described data constitutes measurements of fusion forces separate from the complications of friction in the solderless wrapped connection. However, the same measurements of the effect of fusion are obtained if one subtracts from the stripping force the product of the relaxed force times the initial stripping force (about 15.5 pounds) of the actual wrapped connections. As shown by Fig. 6, the fusion force so computed divided by the area of contact of a six turn connection (about 0.0045 sq in) yields the shearing stress, previously defined. In Fig. 9, the shearing stress is given for a tinned copper wire on a nickel silver terminal as a function of time for 175°C and 100°C. By way of comparison, the constant stress diffusion process of Fig. 8, is shown plotted by the dashed line on this plot. It is evident that there is a larger induction period in the case of the 14 gauge (0.065 inch wire) than in the case of the smaller 24 gauge (0.020 inch) wire and the ratio of the times is proportional to the square of the wire diameter ratio. This is an indication that we are dealing with a nucleation process.

The previous results show that the effect of temperature above room temperature on the solderless wrapped connection is to promote fusion which brings an additional set of forces into the picture with regard to the mechanical stability of the connection. In order to determine the effect of fusion at room temperature, it is necessary to evaluate the activation energy of diffusion. This is done by calculating the value H in the simple rate equation

$$\tau = \tau_0 \exp\left(H/kT\right)$$

so that a given change of temperature corresponds to a given change of time on the fusion force curve. If we compare the 175°C curve with the 100°C curve of Fig. 9, an activation energy curve as a function of residual hoop stress is obtained as shown by Fig. 10. The value of stress is determined by the average time values used in the calculation of the activation energy. It is shown that the activation energy for diffusion of tinned copper on nickel silver in the presence of stress is in the order of 20 to 24 kilocalories per mole while that with no stress is in the order of 41 kilocalories per mole. It appears that higher stresses lower the activation energy of diffusion just as they lower the activation energy for creep and stress relaxation. Very high stresses can reduce the activation energy to a value approaching zero which is the case of cold welding. The fusion occurring in the case of the solderless wrapped connection is different from cold welding in that it takes a finite time to develop any fusion forces.

From the activation energy values of Fig. 10, it is possible to predict the rate at which the wrapped wire connection increases its strength at room temperature. Such a calculation applied to the case of tinned copper wire on a nickel silver terminal is given in Fig. 5 where it is shown
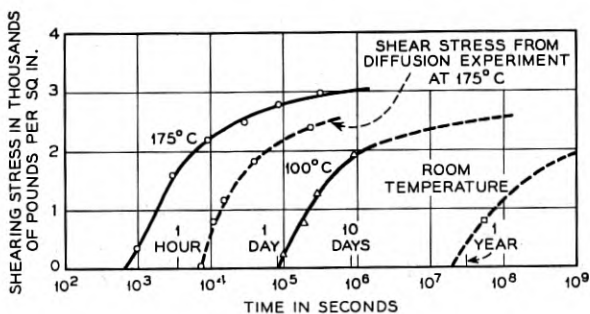

Fig. 9 — Shearing strength of copper-tin-nickel silver connections as a function of time and temperature.
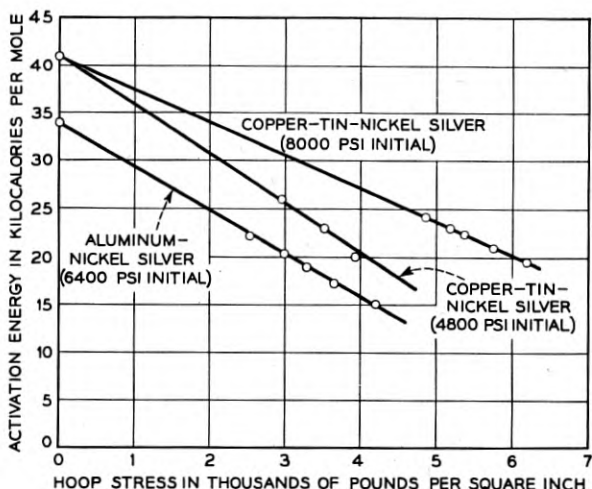
Fig. 10 — Activation energy for diffusion as a function of hoop stress.

that the strength stops decreasing at the end of six months and eventually increases to 20 per cent over the initial value at the end of forty years. Measurements on connections made one year and ten months ago, taken by V. F. Bohman, confirm this calculation.

In all probability, the stress causing the diffusion is the shearing stress applied to the tin layer by the hoop stress of the wire acting on the fixed terminal. For a given initial winding stress, this shear stress will decrease in proportion to the relaxed hoop stress as confirmed by the data of Fig. 10. If we start with a lower winding stress, a smaller indentation is made in the wire and the area of contact is smaller about in proportion to the ratio of the hoop stresses. Hence, although the compressional force on the corners is smaller in proportion to the hoop stress, it is supported by a smaller area and hence the stress on the supporting area is approximately independent of the initial value of the hoop stress. This compressional stress produces shear stresses on the layer of tin since the material of the terminal and the wire have to slide with respect to each other in producing the indentation. Hence, we should expect that the diffusion forces would start at a time independent of the value of the initial hoop stress.

This supposition is confirmed by the data of Fig. 11, obtained by winding tin plated copper wire on a nickel silver terminal with a hoop force half of the usual winding force of 1,300 grams for a 24 gauge wire. The initial strip off force was 60 per cent of that for a 1,300-gram winding

force confirming the data of Fig. 16 of Mallina's paper, referred to in Footnote 2, which shows that the hoop stress decreases less rapidly than the applied tension. Fig. 11 shows the strip off force as a function of time and temperature. If we subtract the relaxed frictional force from the stripping force and divide by the area of 0.0027 square inches (60 per cent of the area of the usual connection) the shear strength curves in pounds per square inch are shown by the lower solid curves. These start sooner than the values on Fig. 9 but require a somewhat longer time to reach their final value. The activation energy obtained from these curves is plotted on Fig. 10 (4800 psi) and shows that the activation energy for the lowest stress is about the same as that for the higher
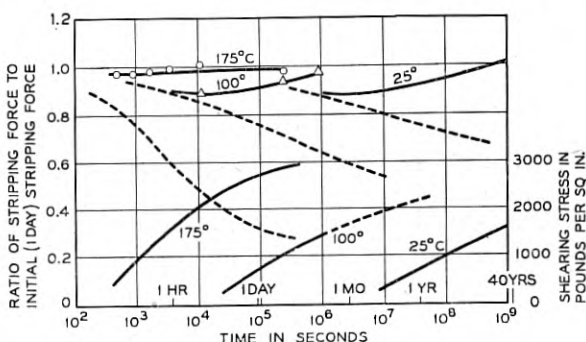
Fig. 11 — Stripping force and shear strength of copper-tin-nickel silver connections as a function of time and temperature. Initial stress is 4,800 pounds per square inch.

stress curve, showing that the shear stress is independent of the wrapping tension. It takes longer to complete the process and as a result, the stripping force at the end of forty years is equal to the initial value rather than 20 per cent higher as in the case for Fig. 5. Corrosion tests for these lower stripping force values[5] show, however, that there is no indication of a loss of electrical contact.

The method for analyzing fusion forces by subtracting relaxation data from stripping force data is verified by measurements on other metal connections. Fig. 12 shows the ratio of stripping force to intial stripping force for aluminum on nickel silver terminals as a function of time and temperature. Subtracting the relaxed force (the original stripping force multiplied by the relaxed stress ratio of Fig. 4) from the stripping force and dividing this difference by the contact area, the shearing

---

[5] R. H. Van Horn, Solderless Wrapped Connections, Part III — Evaluation and Performance Tests, B. S. T. J., **32,** May 1953. See Table II.
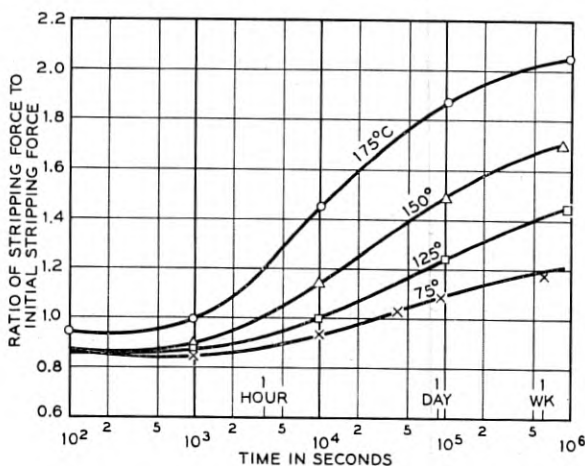
Fig. 12 — Stripping force curves for aluminum on nickel silver as a function of time for four temperatures.

strength is obtained and is shown in Fig. 13. The shearing strength thus obtained approaches 6000 psi for long times at high temperatures. This value agrees approximately with the accepted value for bulk aluminum. Calculating the activation energy of diffusion as previously outlined, one obtains the curve for aluminum in Fig. 10.

The advantage of a diffusion layer such as tin or aluminum as an element in the solderless wrapped connection is shown by the data of Fig. 14 which shows the rate of increase of the stripping force of bare
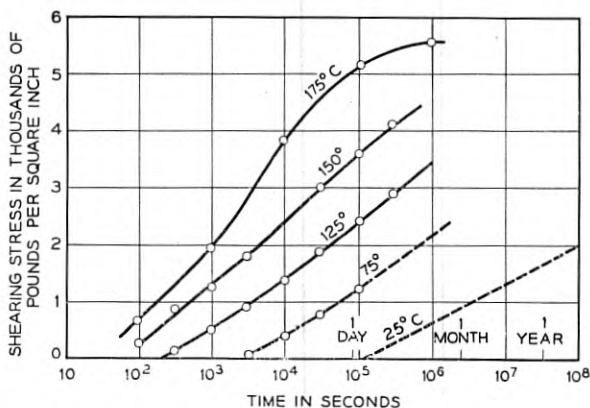
Fig. 13 — Shearing strength of aluminum on nickel silver connections as a function of time.

copper wire on nickel silver terminals at 150°C and 100°C. The increase in strength does not occur as fast as that for tin plated copper, and hence the standard connection with a tin plated copper wire is better than one formed from bare copper wire.

PROPERTIES OF SOLDERLESS WRAPPED CONNECTIONS FOR OTHER TYPES
OF PLATING

A study of the factors governing the diffusion strength of the solderless wrapped connection suggests methods for increasing the rate of diffusion and the strength of the diffusing layer. These methods result
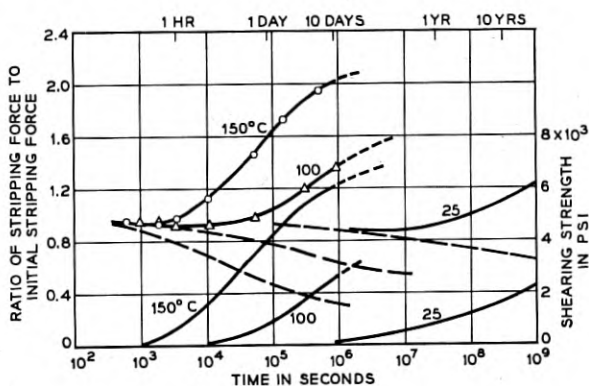
Fig. 14 — Stripping force and shear strength of bare copper on nickel silver connections as a function of time and temperature.

in greater mechanical strength and a faster fusion of the wire and terminal. Experiments show that there are at least four metals which diffuse faster than tin, but due to the economic problems and the brittleness of some of the alloys formed, none of them are being considered for solderless wrapped connection.

The reason the diffusion forces in the tin plated solderless wrapped connection do not cause an increase in strength of more than twenty per cent during the life of the connection is that the limiting shearing stress in tin is only 3,000 pounds per square inch. If now we substitute for tin plating a plating with a larger limiting shear stress, the strength of the connection should increase by a larger factor. To be of use, however, it is necessary that the diffusion forces shall develop rapidly.

The data of Fig. 10 show that if we can produce a higher shearing stress on a layer of aluminum, the activation energy can be lowered and
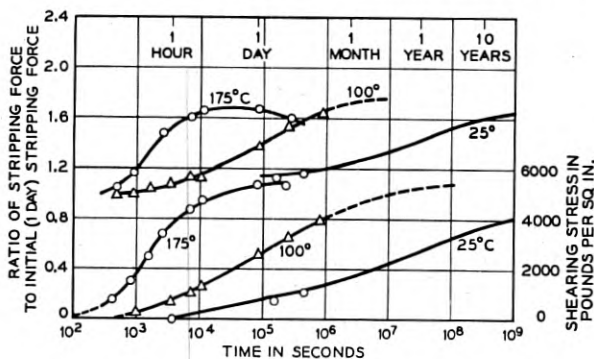
Fig. 15 — Stripping force and shear strength of copper-zinc-brass connections as a function of time and temperature.

be made to approach the cold welding condition. This requires that aluminum be placed on a stronger material such as brass, nickel silver or copper in order that the area of indentation for a given hoop stress will decrease and the shear stress will increase. Hence, the connection should form in a very short time. Furthermore, since the limiting shear stress for aluminum is near 6,000 pounds per square inch, one should except that the strength of the connection will nearly double. Since aluminum is not easily electroplated this suggestion probably is not practical.

Of all the other metals examined, the next most promising are silver, cadmium and zinc. The activation energy for diffusion of zinc into copper
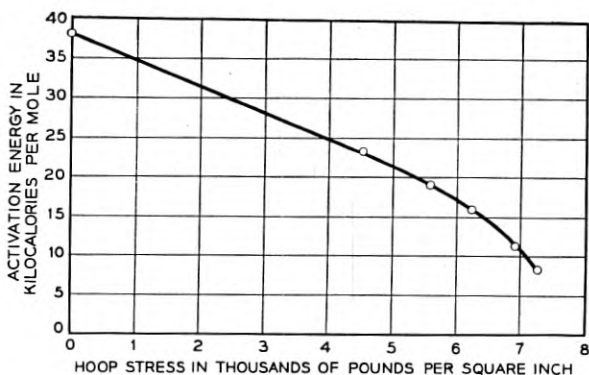
Fig. 16 — Activation energy for a copper-zinc-brass connection as a function of hoop stress.

at no stress is given[6] as 38 kilocalories per mole which is 4 kilocalories higher than that for aluminum and 3 kilocalories under that for tin. The activation energy of silver and cadmium into copper also have low values. Hence, if the effect of stress parallels that for tinned copper, zinc and cadmium should diffuse into copper and nickel silver faster than tin. Furthermore, the limiting shearing 5000 pounds per square inch. Zinc, silver and cadmium are readily plated on the terminals or the wire.

Zinc plating has been tested experimentally by constructing a solderless wrapped connection of bare copper wire on zinc plated nickel silver or brass terminals. The stripping force for a bare copper wire wrapped on a terminal plated with 0.001 inch thickness of zinc has been measured at 175°C and at 100°C as a function of time with the results shown by Fig. 15. The strength increases to 60 per cent over that found initially in a time of less than two hours at 175°C. At 100°C, the time required is a little over a day. If we subtract the relaxed force from the stripping force and divide by the area of the connection, the shear strength of the connection is as shown by Fig. 15, lower curves, for the two temperatures. From these two curves, an activation energy versus hoop stress can be obtained with the results shown by Fig. 16. These values allow one to extend the time variation of the shear stress down to room temperature with the result shown by Fig. 15. Adding these values multiplied by the area of the connection to the relaxed hoop stress, the indicated stripping force at room temperature is shown by Fig. 15, room temperature curve. This force increases at such a fast rate that the strength can be observed to increase at room temperature and corresponding measurements are shown by the circles. Since corrosion cannot occur in a region of fusion, a criterion for the corrodability of a connection is the time required to complete half of the total fusion at room temperature. On this basis, the zinc plated connection has the lowest half fusion time of any of the materials tested.

Although zinc diffuses more readily than other materials examined, it tends to form more brittle alloys and hence its use has not been seriously considered for solderless wrapped connections.

---

[6] R. M. Barrer, *Diffusion In and Through Solids*, Cambridge University Press, 1941, Table 67, p. 275.

A New Multicontact Relay for Telephone Switching Systems

By I. S. RAFUSE

The trend in new telephone switching systems toward faster operation, longer life and lower cost, indicates a need for faster and more capable control circuits. This paper describes a new high speed wire spring multicontact relay designed primarily for these applications. The basic unit contains 30 make-contact pairs. Two variations of the new design provide relays of 60-contact capacity. They are mechanically and electrically interchangeable with all crossbar system multicontact relays.

INTRODUCTION

In a modern dial telephone central office, many thousands of momentary intraoffice control connections are made daily between the various parts of the switching equipment. For example, in the No.5 crossbar system, seven major types of connectors[1] are used to associate markers[2] with other common control circuits, and with the switching frames, for brief intervals, to assist in setting up the talking connection. Connectors are required to simultaneously close a large number of circuit paths, as many as 240 in the trunk link connector. The earlier flat spring type multicontact relays[3] used for this purpose provide large blocks of contacts per relay and provide an economical means for common or multiple wiring.

The trend in new improved switching systems toward longer life, faster operation, lower cost and reduced maintenance, indicates a need for faster and more reliable connector circuits. This paper describes a new multicontact relay, designed primarily for these applications. It is a wire spring relay incorporating the improved manufacturing processes and many of the design features of the new general purpose wire spring relay.[4] The basic unit, Fig. 1, for use in new equipments, is a high speed 30-contact pair relay, with wiring terminals arranged for horizontal multiple connections.
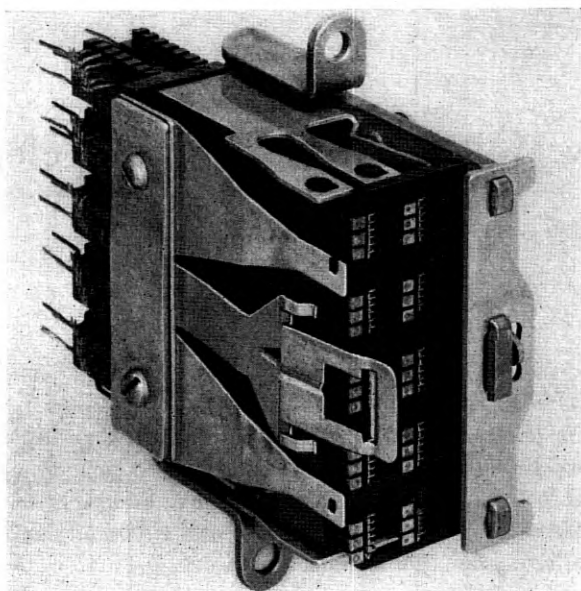
1111

Fig. 1 — New 30-contact relay with contact cover detached.

This development also includes two modifications of the new wire spring relay for replacement use and for additions in existing crossbar equipments. They are 60-contact pair relays, each consisting of two 30-contact units attached to a common mounting bracket. They are completely interchangeable with existing crossbar system multicontact relays. When a new improved relay is developed, it is almost invariably necessary to continue in manufacture and carry in merchandise stock, small demand codes of the old relays for many years. In this case, however, manufacture of the old multicontact relays will be discontinued and all future needs will be supplied by the new product.

OBJECTIVES AND REQUIREMENTS

At the start of the project, all requirements from the standpoint of operating performance, circuit design and equipment use, were prepared in detailed form. The principal design objectives are summarized as follows:

Electrical and Mechanical

1. Operate and release times as fast as economically possible.
2. Forty year life, or 200 million operations, with no adjustment necessary during the first 100 million operations.

3. No contact chatter.

4. No false actuation due to armature rebound.

5. No magnetic or vibrational interference.

6. 120-ohm and 275-ohm coils, to work with equipment already in use.

Equipment

1. Lower manufacturing costs.

2. Reduced mounting space.

3. Terminal arrangement for multiple wiring same as at present, or equivalent from a wiring standpoint.

Maintenance

1. Contact failures due to dirt or insulating films should be substantially equal to and preferably less likely than in the present relay.

2. No contact locking due to contact erosion.

3. Contacts should be replaceable in the field.

4. Coil winding should be replaceable in the field.

5. Field adjustment should be reduced to a minimum.

Replacement Relay

The design objectives also included modification of the new relay, if possible, to replace multicontact relays in existing crossbar equipments.

Design History

During the early stages of this development, considerable effort was directed toward improving the present flat spring multicontact relay. Later, many experimental models were constructed, to investigate other flat spring, and wire spring designs, and several contact actuating methods. The most favorable designs of flat and wire spring multicontact relays were compared, and their differences were resolved by an analysis of manufacturing tolerances and their effect on performance and cost. Preliminary estimates of initial cost were only slightly in favor of the wire spring design. However, the wire spring relay offered significant advantages in (1) higher speed, longer life, less chatter, (2) better manufacturing control of tolerances, (3) less maintenance, and (4) possibilities of future cost reductions as further improvements are made in mechanized methods of manufacture.

DESCRIPTION OF THE NEW RELAY

General

Stationary single wire and moving twin wire spring subassemblies are arranged in alternate layers attached to the core and mounting
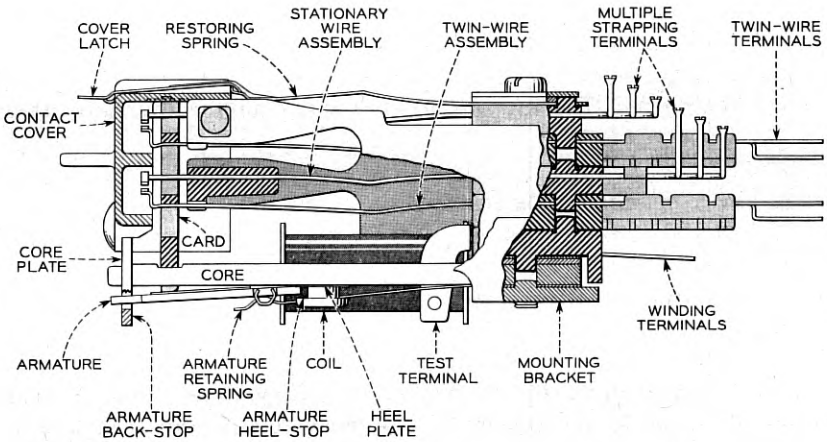
Fig. 2 — Top view of relay showing location of parts.

plate, as shown in Fig. 2. The wire spring assemblies form two rows, each containing 15 make contacts. Each contact pair consists of moving twin contacts on separate twin wires, associated with a single stationary contact. The stationary springs are supported close to the contacts by arms extending from the bracket. A detailed view of all parts and sub-assemblies for a 30-make contact relay is shown in Fig. 3. Moving contacts are pretensioned by relatively large pre-deflections as shown in Fig. 4. The method used in flat spring multicontact relays to obtain contact force is illustrated for comparison. It is apparent that contact force obtained by the "buckle" method depends on operating stud length and therefore is subject to change due to wear. The new pretensioned wire springs are supported and actuated by a single molded phenolic card by the "card release" method as illustrated in Fig. 5. In the unoperated position, the card is held against the core by a restoring spring, which also supplies the force to open all contacts. In the operated position, the armature supplies the force to move the card, releasing the twin wires and closing all contacts. This method of actuation has some important advantages:

1. Contact force is essentially independent of gauging and wear.

2. The effects of wear at points in the relay which affect gauging are compensating to some degree, and therefore tend to minimize changes in gauging.

3. Dimensional variations controlling contact separation and armature travel are reduced, making possible shorter armature travel, faster
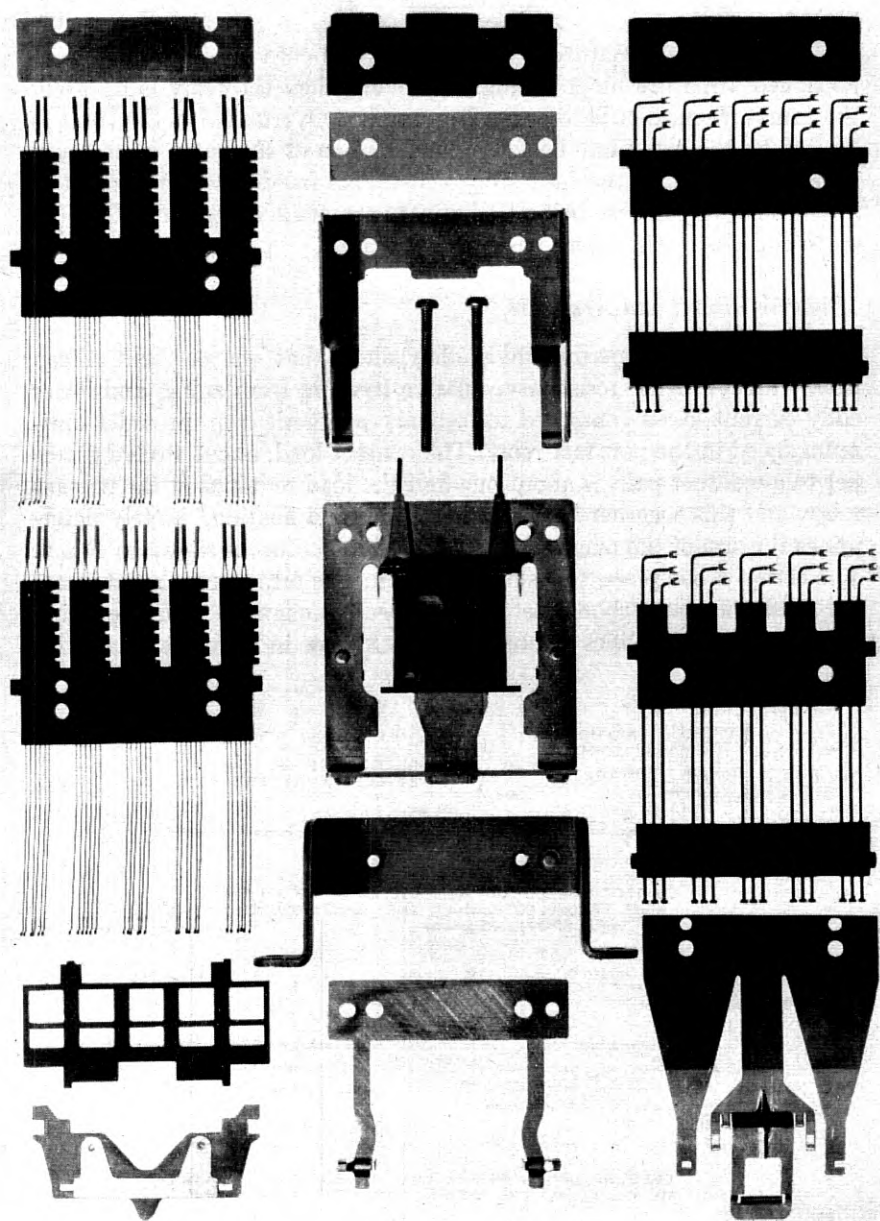
Fig. 3 — Parts of the new 30-contact relay.

operate and release times, less contact chatter and increased mechanical life.

Normally, the armature is held against the card by the lightly pretensioned armature hinge spring. However, when the relay is released, the armature motion becomes quite complex. Overtravel at the front is limited by the core plate backstop, and motion at the back, or heel sections, is limited by the heel stop studs. This freedom of movement is intentional, its purpose being to dissipate armature energy into the core plate and core rather than back into the card.

Magnetic Circuit and Armature

Analytical and experimental studies[5] show that one per cent silicon iron, with its higher resistivity, relative freedom from aging, and lower eddy-current losses compared to ordinary magnetic iron, provides optimum speed in the new fast relay. The contact load, about twelve grams per twin contact pair, is about one-half the load required in the present relay, and this together with winding space and heating,[6] largely determines the size of the magnet. The magnetic structure is shown in Fig. 6. The core is a one piece "E"-shaped section. The armature is a flat member made of low carbon steel having specific magnetic characteristics. This material simplifies manufacture, resulting in a cost saving with
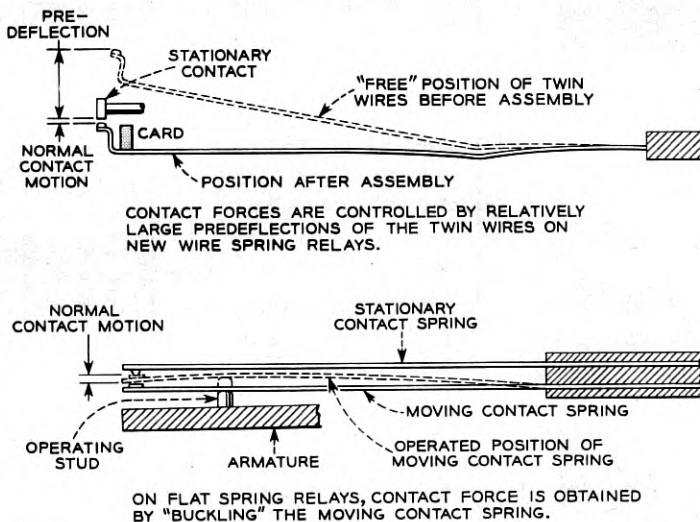

Fig. 4 — Development of contact forces in wire spring and flat spring multi-contact relays.

no appreciable penalty in performance. The armature has adequate sections to carry the flux, optimum poleface area and lowest possible mass. Two small rectangular holes in the armature locate the base of the card in the horizontal direction only. The card is located vertically by the restoring spring as illustrated in Fig. 1. Fast release is obtained by a nonmagnetic separator strip, welded to the face of the armature. This strip also provides a smooth supporting surface for the molded card. Negligible wear at this critical point contributes materially to long life and stable adjustment of this relay.

A cellulose acetate filled coil[7] is assembled to the center leg of the core. A nonmagnetic core plate, illustrated in Fig. 7, is then forced over the three core legs to hold them in alignment. The center hole in the core plate also functions as an armature backstop and permits a certain amount of overtravel of the armature when the relay is released.

Coil Assemblies

For circuit reasons, 120-ohm and 275-ohm coil resistances used in the old relays are required in the new relays. Nominal power savings which ordinarily would result due to an improved magnet and reduced load, are therefore sacrificed in the new relays in favor of increased speed. More than half of the new relays are expected to be used in circuits requiring maximum speed of operation and will, therefore, have 120-ohm
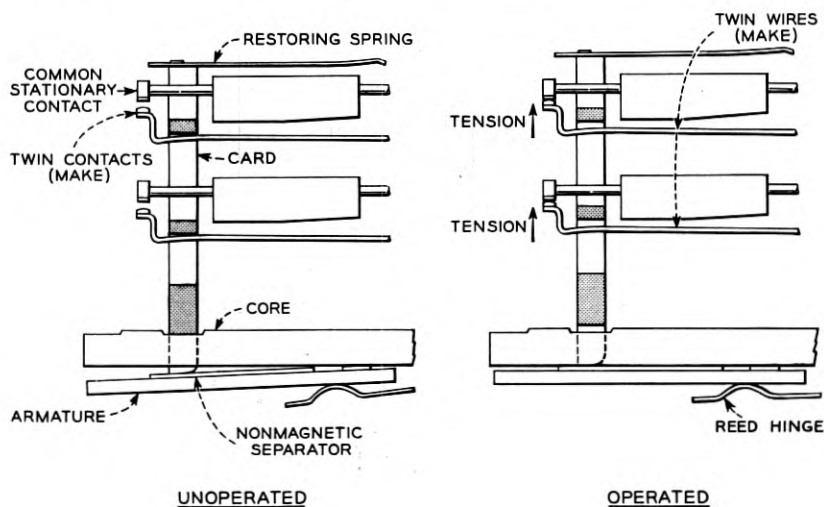

Fig. 5 — Principal of contact operation.

coils. In normal operation, these relays are not energized continuously, but operate only for short intervals while a talking circuit is established. The design provides for replacement of a coil winding in the field, but this is not expected to be necessary except in rare cases.

Molded Wire Spring Subassemblies

Wire spring subassemblies for a 30-contact relay are shown in Fig. 8. The two single wire subassemblies differ only in their terminal arrangement. The twin wire subassemblies are identical. Therefore only three basic molded parts are required which supply all needs for all new production relays. The wire spring sections are molded in continuous ladders[8] as in the general purpose relay. Spring bending, contact welding and coining[9] and terminal forming for solderless wrapped connections,[10] are performed in automatic tools developed by Western Electric Company engineers. A comparison of the wire spring parts used in two new 30 make relays and the corresponding parts of a 60-make flat spring relay, is shown in Fig. 9. This illustrates the reduction in parts and simplicity of wire springs compared with flat springs. Seven types of subassemblies are used in the twelve layers required for an equivalent flat spring relay.

Terminals of the single wire subassemblies are formed for multiple wiring, and therefore differ in length and configuration. An improved
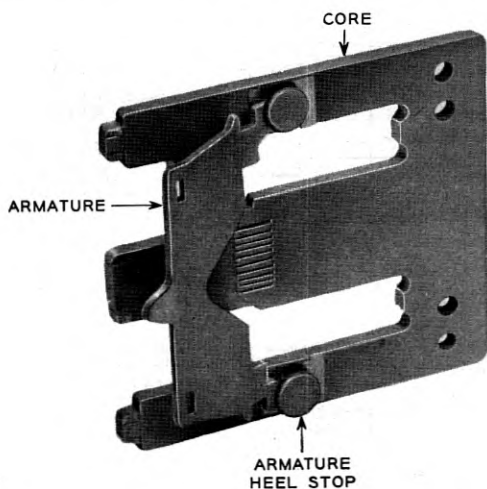

Fig. 6 — Magnetic structure of the new relays.

form of open wire multiple strapping has been developed for use with this terminal arrangement. It consists of bare wires held together in ladder form by means of phenolic plastic blocks molded successively in a continuous process. Fig. 10 shows relays with ladder type horizontal strapping soldered to the single wire terminals. The usual cable with new solderless wrapped connections is used on the twin wire terminals. Fig. 10 also illustrates the accessibility of multiple connections provided by locating them off to one side in the clear area between cable groups.

Contacts

All contacts in the new wire spring relays are palladium having a volume of contact material suitable for forty years life. This is equivalent to about 200 million operations for relays in high usage circuits. Contacts are easily visible, readily cleaned and may be insulated for test purposes.

Contacts may be replaced in the field if necessary using Bell System field welding equipment.[11] Suitable tools and electrodes have been developed to permit use of this equipment on all wire spring relays.

Assembly and Adjustment

The relay pile-up is securely fastened by two high tensile screws and a spring compliance member. Laboratory tests show that a pile-up of
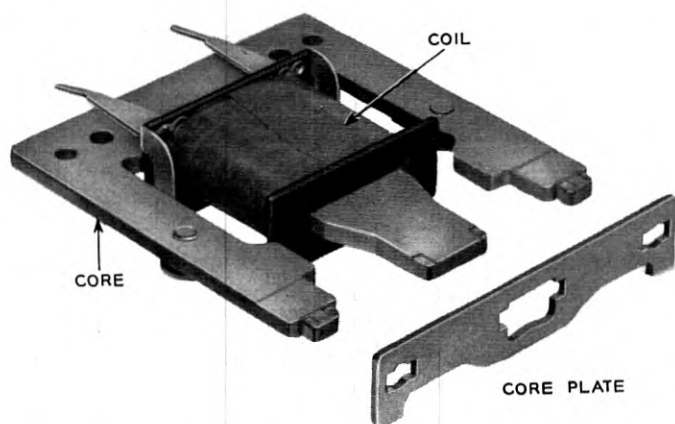

Fig. 7 — Core legs are held in alignment by the core plate, which is forced on the ends after the coil is assembled.
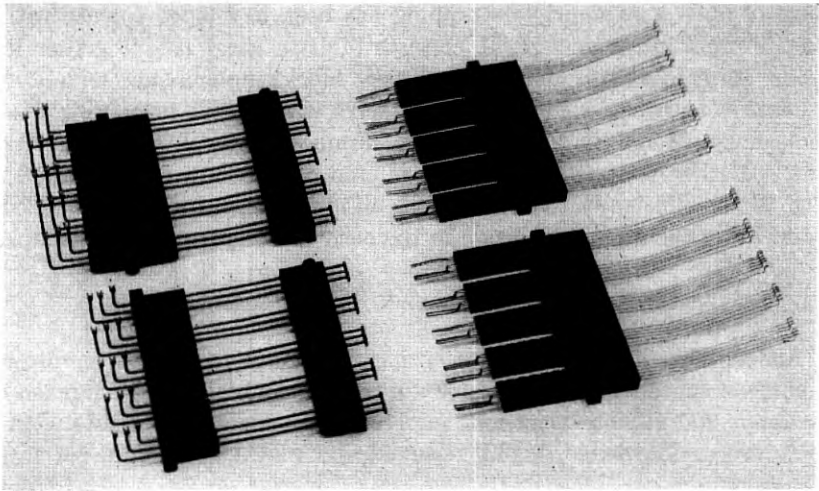
Fig. 8 — Molded wire assemblies for a 30-contact relay.

this design will remain tight under widely varying atmospheric conditions.

In the design of the new relay considerable attention was given to manufacturing control of tolerances, with reduced assembly and adjustment costs as an objective. The molding process provides dowels for aligning the four layers of contact springs, trunnion supports to locate the single wires, and control grooves in the single wire subassemblies to align the twin wires. These features provide accurate registration for mating contacts, for the location of wire subassemblies relative to other relay parts and for the pretensioned restoring spring which in turn locates the actuating card in relation to the operating contacts. The card determines contact separation of all twin moving contacts in relation to their respective single stationary contacts. Due to these controls, and because the pre-deflected twin wire springs require no adjustment of contact force, no factory adjustments are anticipated except on relays which fall outside acceptable limits for back tension or contact gauging (or follow) as assembled. If necessary, therefore, the restoring spring may be adjusted to control the armature back tension. Contact gauging may be controlled if required by independent mass adjustment of the single wire contact rows. Fig. 11 shows this operation being performed by bending the bracket arm using a tool designed for this purpose. The mass adjustment feature is expected to simplify field maintenance practice.
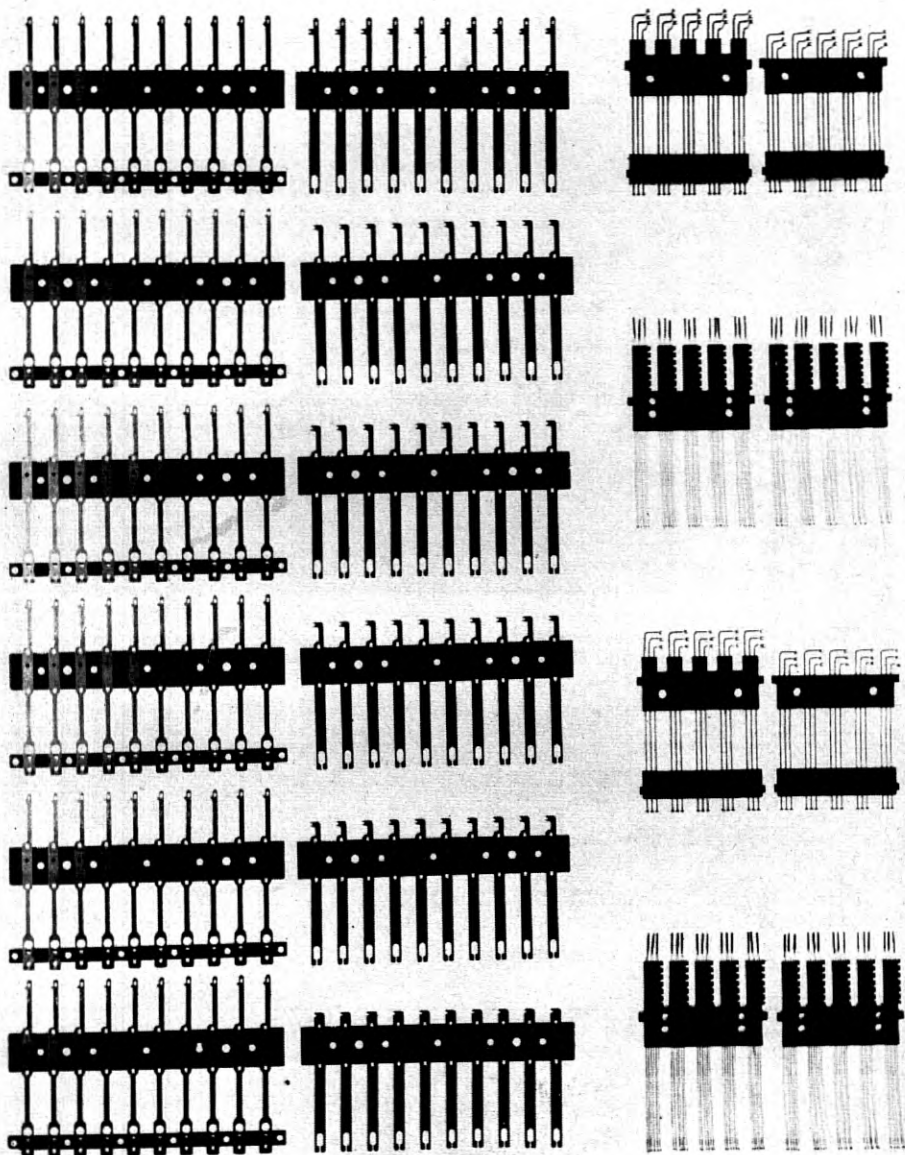
Fig. 9 — A comparison of molded wire assemblies for a 60-contact replacement relay with the corresponding flat spring relay parts.
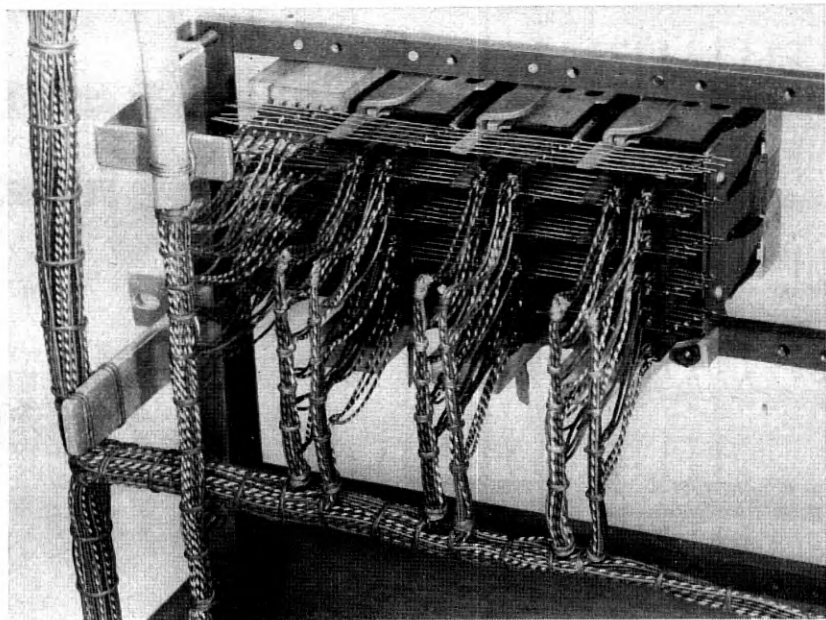
Fig. 10 — New 30-contact relays showing multiple wiring by the new ladder type strapping method, and the new solderless wrapped cable connections.
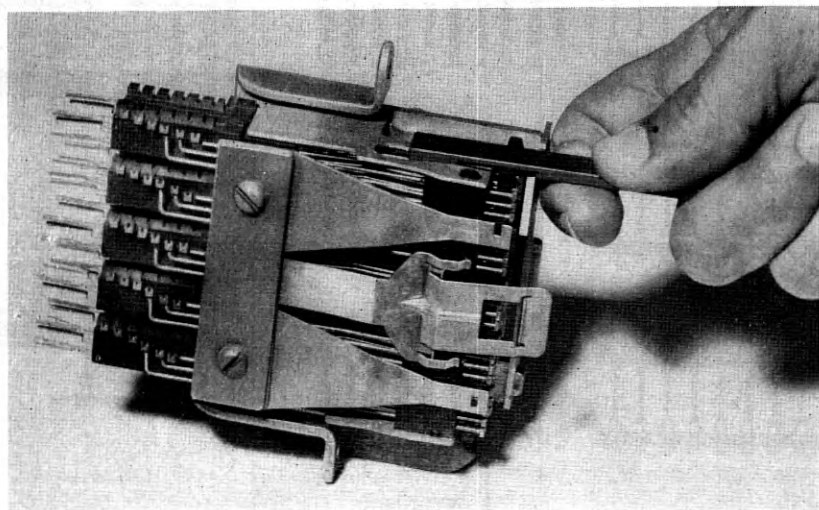

Fig. 11 — New 30-contact relay showing method of mass adjusting stationary contacts.

Replacement Type Relays

Future replacements of flat spring multicontact relays in existing crossbar equipments for maintenance reasons require a slightly modified form of the new relay, capable of complete interchangeability. As these relays are commonly used in connector circuits, operate and release times must be comparable with older type relays in order to avoid circuit interference. This was accomplished in the new wire spring relay with only minor changes in design and in the manufacturing process.

As illustrated by Fig. 12, the interchangeable or replacement relay consists essentially of two 30-contact units assembled on a common mounting bracket having the same vertical mounting centers as the 60-contact flat spring relay. Since horizontal mounting space required by the new relay has been reduced, the 60-contact wire spring unit may also be used to replace 30-, 40- and 50-contact flat spring multicontact relays. The model shown in Fig. 12 has terminals arranged for horizontal multiple wiring. In another variation of the replacement relay all terminals are arranged for cable wiring.

Modifications necessary to slow down the new relays for replacement use are (1) longer armature travel, requiring a different card; (2) an armature of larger mass — although this is a different piece part it has the same contour as the armature for the fast relay and may be punched in the same tool setup; (3) a core of low carbon steel in place of the one per cent silicon iron used in the high speed relay; (4) a leakage reluctance shunt element shown in Fig. 13 to by-pass a portion of the total magnetic flux; and (5) coil windings having resistances of 120 and 275 ohms as required for circuit reasons, but having the number of turns calculated for slower speed consistent with reliable operating capability.[12]

Relay Performance

Measurements have been made on laboratory-built models carefully prepared and adjusted to simulate extreme ranges of manufacturing tolerances, and more recently, on representative samples of pre-production relays. Although some of the performance characteristics studied will be determined accurately only after long-term use in the field, it has been possible by designed experiments and comparative tests, to obtain a fair appraisal of relay capability. These tests and measurements indicate that design objectives stated earlier in this paper have been substantially achieved.
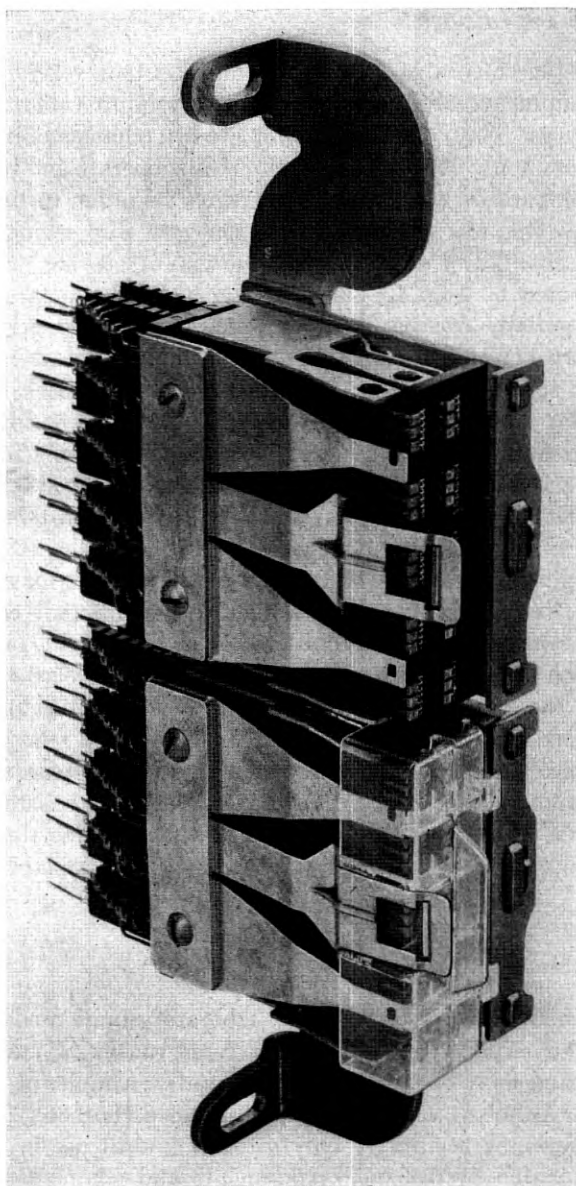
Fig. 12 — A 60-contact replacement relay with one contact cover detached.

Load and Pull Characteristics

Load and pull curves are measured under essentially static conditions. Spring load and armature motion are both observed at the center line of the card. They are measured and simultaneously recorded in chart form in a modification of a tensile testing machine.[13] A typical load and pull chart is shown in Fig. 14. The abscissa shows armature motion, as the armature moves the card and the spring load, through a distance of 0.030 inch to the operated position, and back again. The ordinate shows spring load on the armature on both operate and release, and also the magnetic pull which is developed in the armature for various numbers of ampere turns in the winding.

The load and pull chart provides a comprehensive picture of over-all relay performance. For example, starting from the released position, the force or back tension, holding the card against the core is about 140 grams. Following the upper curve, the spring load increases slowly as the armature moves toward the core, until the first contacts make at a load of about 200 grams. The load increases rapidly as the remaining contacts are closed until the last contacts are closed at about 650 grams. Further travel of the armature to the operated position increases the spring load to a final value of about 700 grams. As the armature is allowed to return to the original position, the lower curve is traced. The area between the two curves is a measure of mechanical hysteresis, or friction, in the relay. This energy loss is a very small fraction of the spring load at all values of armature travel.

The pull curves show ampere turns necessary to assure operation of
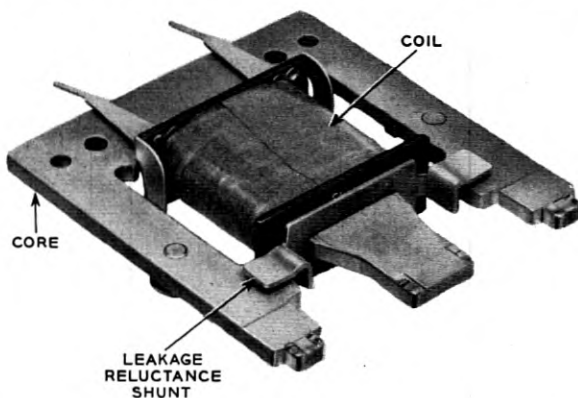

Fig. 13 — Core assembly for replacement type relays showing leakage reluctance shunt.
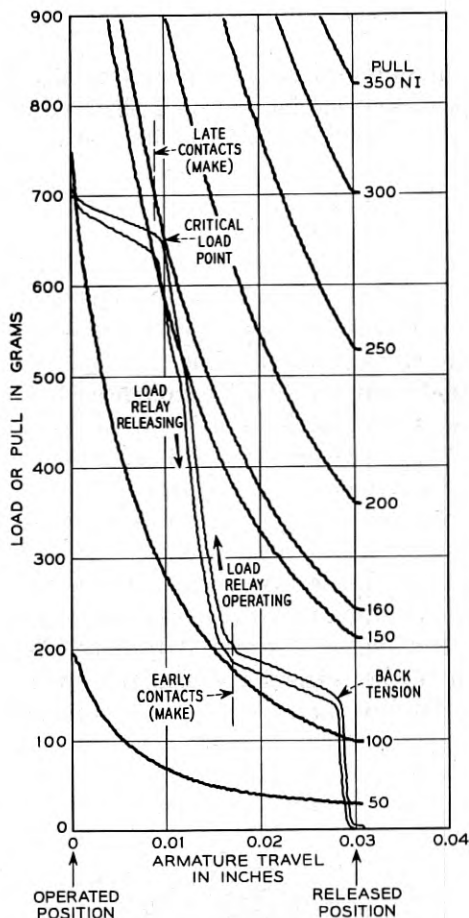
Fig. 14 — Typical load and pull characteristics of a 30-contact fast relay.

the relay. The maximum ampere turns required are determined by the "critical load point." This occurs at 0.010 inch armature travel and about 650 grams. Under static conditions, therefore, 160 ampere turns would be required for complete operation. Circuit uses for these relays do not include nonoperate, hold, or release requirements. This information could however be obtained from the pull curves in a similar manner.

Operate and Release Speed

The new high speed multicontact relay operates two to three times as fast as its predecessor, the flat spring type relay. Operate and release
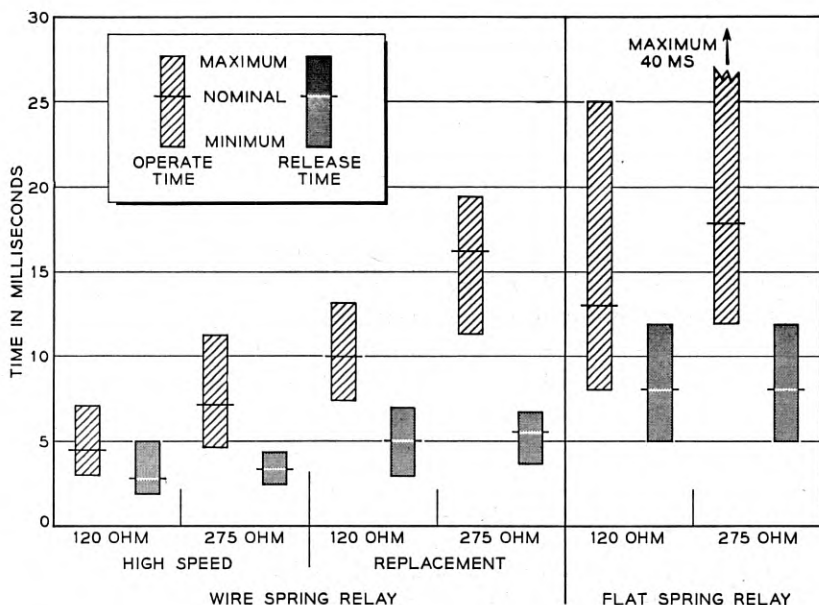
Fig. 15 — Comparison of operate and release times of wire spring versus flat spring multicontact relays.

times are shown in Fig. 15. The improved performance of the new relays is shown by nominal operate and release values, and also by greatly reduced spread, or difference between minimum and maximum values, as compared with corresponding data for flat spring relays.

Minimum operate times of the replacement and existing flat spring relays are comparable. It will be noted however, that operate and release time spreads are much less in the new relay. This generally should improve the operation of existing crossbar circuits as new relays are used for replacements or additions.

Contact Performance

As speed increases, relays and other switching mechanisms become more susceptible to false operation of contacts. It is obvious also that faster operation adds to life requirements and therefore extends the period or increases the number of operations during which trouble-free contact performance must be provided. For these reasons, extensive studies were made of chatter, unprotected erosion, and locked contacts as applied to the new multicontact relay. Additional longer range tests

are planned to study protected contact erosion and susceptibility to open contact failures.

When contacts of the new high speed relay are operated, initial chatter does not normally exceed 0.1 millisecond. There is no shock chatter caused by spring vibration due to impact of the armature with the core or backstop. There is no chatter caused by hesitation of the armature in its travel at the point where it picks up the contact load. This is due largely to the low mass of 0.020 inch diameter twin wires, the low mass and short travel of the actuating mechanism, the type of card operation, and the rigid mounting of the relay structure.

Electrical erosion of contact material is reduced in the new relay, because of the reduction in chatter. For this reason, the contact size provided is expected to be adequate for all normal use for the life of the relay, and contact maintenance should be greatly reduced.

Locked contacts are substantially eliminated in the new relay by the single card release method of operation. Static and dynamic forces associated with the restoring spring and card system are powerful enough to break loose any random pair of locked contacts.

Contact failures due to dirt or the formation of insulating films on the contacts are difficult to check in laboratory tests. Long-term accelerated tests are necessary, with a large test sample, under carefully controlled dust conditions. Many precautions were taken in the design to minimize failures from this source, as follows: (1) a dust cover, Fig. 16, encloses the contacts, but does not enclose the coil; (2) the cover partially segregates the contacts in groups of three pairs of contacts, reducing air movement in the vicinity of the contacts; (3) palladium contact material is used on all relays; (4) twin contacts are coined — the rounded surface reduces the area in contact, effectively restricts the area which may trap lint or other foreign matter, and increases contact pressure; (5) card release actuation and wire springs with large pre-deflections insure that no appreciable loss of contact force will occur due to age or erosion; and (6) twin contacts are attached to completely independent wires.

Rebound chatter is another form of false operation which occurs in the form of contact reclosures caused by rebound of the armature after striking the backstop when the relay is released. Fundamental studies were made of rebound behavior in relay structures[14] and various models were constructed and measured. As a result there is no rebound chatter in the new high-speed wire spring relay within the range of normal adjustment. A comprehensive survey was made to determine the probability of reclosures due to rebound, in relays having limiting adjust-
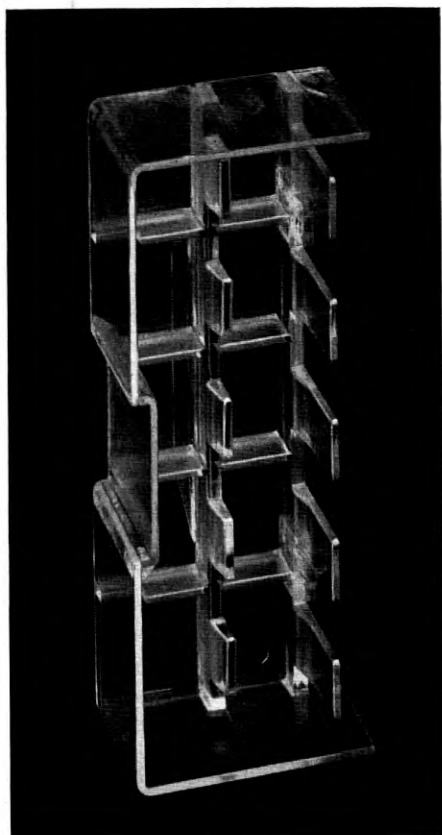
Fig. 16 — Contact cover for the new relays showing compartments in which contacts are grouped.

ments. The probability of reclosures exceeding one millisecond duration is estimated as one in 28,000 relays. This grade of performance is due primarily to: (1) an armature having low travel and the lowest possible mass; (2) an armature suspension designed to dissipate rebound energy into the core plate and core rather than into the actuating card; and (3) a stiff mounting bracket to reduce the natural amplitude of core vibration due to armature impact on operate and on release.

Life

Less than 5 per cent of the new multicontact relays will be required to operate more than 100 million times in crossbar systems during an esti-

mated life term of forty years. Life tests show that no readjustment should be necessary during the first 100 million operations. The tests also indicate that not more than a small percentage of relays will require readjustment prior to an estimated maximum life of 200 million operations. In extreme cases, still greater life may be obtained if required, by replacing the molded card. This is an inexpensive part and replacement is easily accomplished.

Stability

When the new relays are exposed to extreme temperature and humidity cycles, the greatest change in contact separation is, in general, about 0.004 inch, and only a small percentage of relays are likely to be used in this manner. Tests indicate that changes of this magnitude leave adequate margin for 100 million operations before readjustment is necessary.

For economy, most equipment is shop assembled and wired on a frame basis, and shipped complete, ready for installation as equipment units. It is important, therefore, that apparatus units should be capable of withstanding physical shock far in excess of normal usage. Design features in the new relay which provide an adequate margin of safety in this respect are: (1) a rigid mounting bracket; (2) the wire spring pile-up is attached securely to the bracket with two specially heat treated steel screws; (3) the cover is held in place by the bending moment of an embossed section of a spring clip with a force many times greater than the compressive force of a single spring; and (4) guard surfaces molded in the cover prevent twin wires from leaving their respective guide notches in the single wire combs.

Excessive shocks during shipment have, at times, damaged flat spring relays by bending their brackets. The new relays have been subjected to shocks of similar magnitude without damage.

Magnetic Interference

Under certain marginal conditions, a relay may be affected by leakage flux from adjacent relays entering its magnetic circuit, and changing its operate and release values. Tests show that interaction is negligible between the new relays and also between new and old type relays when they are used in adjacent positions.

CONCLUSIONS

The new 30-contact relays provide faster operate and release times, longer life, improved contact performance, reduced maintenance, and

greater adaptability in new circuit and equipment units than previous multicontact relays. The new relays also require less vertical and horizontal space in new equipments. As a result of these improvements, substantial savings are expected when these relays are used. The design includes many features which permit the use of mechanized manufacturing processes, which, in turn provide better control of tolerances. For these reasons, lower initial costs are expected as manufacturing and assembly methods continue to improve.

The new 60-contact relays are completely interchangeable with all codes of flat spring multicontact relays in existing crossbar equipments, and in addition, they provide superior performance, longer life and reduced maintenance. Therefore, manufacture of the flat spring multicontact relays will be discontinued as soon as new relay production becomes adequate for all uses.

REFERENCES

1. G. S. Bishop, Connectors for the No. 5 Crossbar System, Bell Labs. Record, **28,** p. 56, Feb., 1950.
2. A. O. Adam, The No. 5 Crossbar Marker, Bell Labs. Record, **28,** p. 502, Nov. 1950.
3. Bruce Freile, Multicontact Relay, Bell Labs. Record, **17,** p. 301, May, 1939.
4. A. C. Keller, A New General Purpose Relay for Telephone Switching Systems, B. S. T. J., **31,** p. 1023, Nov., 1952.
5. R. L. Peek, Jr. and H. N. Wagar, Magnetic Design of Relays, B. S. T. J., **33,** p. 23, Jan., 1954.
6. R. L. Peek, Jr., Internal Temperatures of Relay Windings, B. S. T. J., **30,** p. 141, Jan., 1951.
7. C. Schneider, Cellulose Acetate Filled Coils, Bell Labs. Record, **29,** p. 514, Nov., 1951.
8. A. J. Brunner, H. E. Cosson and R. W. Strickland, Wire Straightening and Molding for Wire Spring Relays, B. S. T. J., **33,** p. 859, July, 1954.
9. A. L. Quinlan, Automatic Contact Welding in Wire Spring Relay Manufacture, B. S. T. J., **33,** p. 897, July, 1954.

10. Solderless Wrapped Connections, B.S.T.J., **32,** May, 1953. Introduction, J. W. McRae, pp. 523 and 524. Part I — Structure and Tools, R. F. Mallina, pp. 525–556. Part II — Necessary Conditions for Obtaining a Permanent Connection, W. P. Mason and T. F. Osmer, pp. 557–590. Part III — Evaluation and Performance Tests, R. H. Van Horn, pp. 591–610.
11. W. T. Prichard, Relay Contact Welder, Bell Labs. Record, **22,** p. 374, Apr., 1944.
12. M. A.Logan, Design of Optimum Windings, B. S. T. J., **33,** p. 114, Jan., 1954.
13. E. G. Walsh, Continuously Recorded Relay Measurements, Bell Labs. Record, **32,** p. 27, Jan., 1954 and H. N. Wagar, Relay Measuring Equipment, B. S. T. J., **33,** p. 3, Jan., 1954.
14. E. E. Sumner, Relay Armature Rebound Analysis, B. S. T. J., **31,** p. 172, Jan., 1952.

Topics in Guided Wave Propagation Through Gyromagnetic Media

Part III — Perturbation Theory and Miscellaneous Results

By H. SUHL and L. R. WALKER

Some problems, complete discussion of which would be extremely difficult, are treated approximately by means of perturbation theory. Among these are the partially filled cylindrical waveguide, and the problem of multiple internal reflections in a sample of finite length filling the cross section of a cylindrical guide. Propagation in a ferrite between parallel planes, magnetized along the propagation direction is discussed by the methods described in Part I. The paper concludes with an addendum to Part I — a numerical study of field patterns of the TE_{11}-limit and TM_{11}-limit mode for various dc magnetic fields.

INTRODUCTION

Parts I and II of this paper were devoted to a number of specific propagation problems, whose solutions, though frequently quite complicated, could be discussed with a reasonably modest investment of effort. Unfortunately, not all of these problems pertain to situations met with in actual gyromagnetic devices. Actual devices frequently employ structures whose performance could be predicted only as the result of lengthy computing programs. For example, the microwave gyrator using Faraday rotation usually employs a ferrite sample whose cross-section only partly fills that of the cylindrical waveguide. Although it is easy to formulate the corresponding equation for the propagation constant, the classification and survey, let alone the computation of solutions, would be very difficult to carry out.

Thus, one must often be content with approximate results, and the bulk of the present paper is devoted to perturbation methods. These take as starting point a situation whose propagation problem is essentially solved. The small change in propagation constant due to a slight change in the original state of the system is then calculated. The small

1133

change of state may be the weak magnetization of an originally un-magnetized specimen occupying a substantial part of the structure, or the introduction of a very small specimen with arbitrarily large magnetization into the originally empty structure. Under the heading, "Small Magnetization — Arbitrary Sample-Size," we shall discuss the propagation constant for a pencil of ferrite of any radius, coaxial with a cylindrical waveguide, the space between guide wall and pencil being filled with an isotropic medium whose dielectric constant equals that of the ferrite. This is discussed in preparation for the practically more important case of a ferrite pencil of any radius in an air-filled guide. Here the unperturbed state of the system, when the pencil is unmagnetized and therefore isotropic, is already rather complicated and require some preliminary calculations. Under the heading "Small Sample-Size — Arbitrary Magnetization," we consider the case of a thin pencil of ferrite in an originally empty guide.

Another topic, not easily treated except by perturbation methods, is that concerning end effects in samples of finite length. After a preliminary discussion of internal reflections in an extended slab of ferrite (a problem which can be treated rigorously), two cases are considered: a ferrite slug of arbitrary length, closely fitting a cylindrical guide, and a thin disc normal to the guide axis, of arbitrary size. In these cases interest centers around the effect of sample length on Faraday rotation, though for the ferrite slug a subsidiary effect, that of mode conversion, is also mentioned briefly.

It should be emphasized that the perturbation methods employed here are not in themselves novel. They are standard to most linear eigenvalue problems of physics, and have been used in connection with electromagnetic problems by many authors.[1]

The remainder of the paper is devoted to a discussion of a ferrite-filled "cable" in plane parallel form, using the methods of Part I. The treatment is kept in terms of saturation magnetization and magnetizing field, and is based on Polder's equations. The paper concludes with an addendum to Part I, which reports some calculations and graphs of field patterns in a cylindrical waveguide completely filled with ferrite.

1. PERTURBATION METHODS

1.1 General Method

A number of authors have made applications of perturbation theory to the problems of propagation in gyromagnetic media and the exposition which follows is included mainly for completeness. We shall develop the subject in the following fashion: it will be supposed that the unper-

turbed system is a wave guide containing a medium whose permeability and dielectric tensors are diagonal and isotropic, but may vary over the cross section of the guide, although not in the z-direction along the guide. For this system it will be assumed that a complete set of normal modes exists for which appropriate orthogonality relations are known. The perturbation of the system will then consist of changes in the permeability and dielectric tensors of the medium, including the addition of non-diagonal terms. If these changes are to be genuine perturbations, they must be of one of two kinds. Either, the variation in the properties of the medium is confined to a limited region, small in volume in some appropriate sense, in which case its magnitude may be large, or, we may have a small fractional change in the material properties extending over a considerable volume. The fields in the guide may be expanded in the normal modes and a system of equations is developed for the z-dependence of the amplitudes of these modes. These equations are then solved approximately, making use of the smallness of the perturbing terms. The results may then be specialized to the various situations of interest.

Let us suppose that the unperturbed permeability and dielectric constant are $\mu_1(x, y)$ and $\epsilon_1(x, y)$ respectively and that the system is now altered so that it possesses a permeability tensor

$$\begin{Vmatrix} \mu_2(x, y) & -j\kappa(x, y) & 0 \\ j\kappa(x, y) & \mu_2(x, y) & 0 \\ 0 & 0 & \mu_3(x, y) \end{Vmatrix}$$

and a dielectric tensor

$$\begin{Vmatrix} \epsilon_2(x, y) & -j\eta(x, y) & 0 \\ j\eta(x, y) & \epsilon_2(x, y) & 0 \\ 0 & 0 & \epsilon_3(x, y) \end{Vmatrix}.$$

Maxwell's equations for the perturbed system may be written, using the notation of Parts I and II,† in the form:

$$\nabla^* H_z - \frac{\partial H_t^*}{\partial z} - j\omega\epsilon_2 E_t - \omega\eta E_t^* = 0,$$

$$\nabla^* E_z - \frac{\partial E_t^*}{\partial z} + j\omega\mu_2 H_t + \omega\kappa H_t^* = 0, \tag{1}$$

$$\nabla \cdot H_t^* - j\omega\epsilon_3 E_z = 0,$$

$$\nabla \cdot E_t^* + j\omega\mu_3 H_z = 0.$$

----
† We omit the vector signs from all transverse vectors, which are sufficiently labelled by the subscript "t."

These may be rearranged as

$$\nabla^* H_z - \frac{\partial H_t^*}{\partial z} - j\omega\epsilon_1 E_t = j\omega(\epsilon_2 - \epsilon_1)E_t + \omega\eta E_t^* = A_t ,$$

$$\nabla^* E_z - \frac{\partial E_t^*}{\partial z} + j\omega\mu_1 H_t = -j\omega(\mu_2 - \mu_1)H_t - \omega\kappa H_t^* = B_t , \quad (2)$$

$$\nabla \cdot H_t^* - j\omega\epsilon_1 E_z = j\omega(\epsilon_3 - \epsilon_1)E_z = A_z ,$$

$$\nabla \cdot E_t^* + j\omega\mu_1 H_z = -j\omega(\mu_3 - \mu_1)H_z = B_z ,$$

where A_t, B_t, A_z and B_z are introduced as abbreviations for the terms on the right hand side of the equations. E_z and H_z may be eliminated by substituting in the first two equations the expressions

$$E_z = \frac{\nabla \cdot H_t^* - A_z}{j\omega\epsilon_1}$$

and

$$H_z = \frac{-\nabla \cdot E_t^* + B_z}{j\omega\mu_1} .$$

The two equations so obtained are

$$\frac{1}{j\omega} \nabla^* \left(\frac{\nabla \cdot E_t^*}{\mu_1} \right) + \frac{\partial H_t^*}{\partial z} + j\omega\epsilon_1 E_t = -A_t + \frac{1}{j\omega} \nabla^* \frac{B_z}{\mu_1}$$

and

$$\frac{1}{j\omega} \nabla^* \left(\frac{\nabla \cdot H_t^*}{\epsilon_1} \right) - \frac{\partial E_t^*}{\partial z} + j\omega\mu_1 H_t = B_t + \frac{1}{j\omega} \nabla^* \frac{A_z}{\epsilon_1} . \quad (3)$$

We now suppose that E_t and H_t can be expanded in the form

$$E_t = \sum_n a_n(z)E_{tn}(x, y)$$

and

$$H_t = \sum_n b_n(z)H_{tn}(x, y),$$

where

$$E_{tn}e^{-j\beta_n z} \quad \text{and} \quad H_{tn}e^{-j\beta_n z}$$

satisfy the unperturbed form of equations (3) and the boundary condition that tangential E vanishes at the guide wall. These equations have solutions for certain values of β_n only, but, if E_{tn}, H_{tn} are solutions for $\beta_n = c > 0$, then E_{tn}, $-H_{tn}$ are solutions for $\beta_n = -c$. We shall assume

hereafter that E_{tn} and H_{tn} pertain to positive β_n values. For a given unperturbed mode it follows that $\dfrac{b_n(z)}{a_n(z)}$ reverses sign when the direction of propagation reverses. Substituting these series for E_t and H_t in equations (3), one finds

$$\sum_n \left[\frac{db_n}{dz} + j\beta_n a_n \right] H_{tn}{}^* = -A_t + \frac{1}{j\omega}\, \nabla^* \frac{B_z}{\mu_1} \qquad (4a)$$

and

$$\sum_n \left[\frac{da_n}{dz} + j\beta_n b_n \right] E_{tn}{}^* = -B_t - \frac{1}{j\omega}\, \nabla^* \frac{A_z}{\epsilon_1}. \qquad (4b)$$

The orthogonality relation between functions of different n has been given by Adler.[2] It is

$$\int E_{tn}{}^* \cdot \tilde{H}_{tm}\, dS = 0,$$

where $n \neq m$; the tilde denotes the complex conjugate and the integration goes over the cross section of the guide. We consider the fields to be un-normalized and write

$$\int E_{tn}{}^* \cdot \tilde{H}_{tn}\, dS = \triangle_n,$$

Clearly

$$\int H_{tn}{}^* \cdot \tilde{E}_{tn}\, dS = -\tilde{\triangle}_n. \qquad (5)$$

Multiplying equation (4b) by $\tilde{H}_{tn}\cdot$ and equation (4a) by $\tilde{E}_{tn}\cdot$ and integrating each expression over the cross section we have

$$-\tilde{\triangle}_n \left[\frac{db_n}{dz} + j\beta_n a_n \right] = -\int A_t \cdot \tilde{E}_{tn}\, dS + \frac{1}{j\omega} \int \tilde{E}_{tn} \cdot \nabla^* \frac{B_z}{\mu_1}\, dS,$$

$$\triangle_n \left[\frac{da_n}{dz} + j\beta_n b_n \right] = -\int B_t \cdot \tilde{H}_{tn}\, dS - \frac{1}{j\omega} \int \tilde{H}_{tn} \cdot \nabla^* \frac{A_z}{\epsilon_1}\, dS.$$

Now we use the identity

$$\int G_t \cdot \nabla^* F\, dS = -\int F(G_t \cdot ds) + \int F \nabla \cdot G^*\, dS.$$

surface   boundary   surface

This yields

$$\int \tilde{E}_{tn} \cdot \nabla^* \frac{B_z}{\mu_1} \, dS = -\int_{b'dry} \frac{B_z}{\mu_1} (\tilde{E}_{tn} \cdot ds) + \int \frac{B_z}{\mu_1} \nabla \cdot \tilde{E}_{tn}^* \, dS,$$

$$= j\omega \int B_z \tilde{H}_{zn} \, dS,$$

since $E_{tn} \cdot ds = 0$. H_{zn} is the H_z field appropriate to the nth mode. Again, we have

$$\int \tilde{H}_{tn} \cdot \nabla^* \frac{A_z}{\epsilon_1} = -\int_{b'dry} \frac{A_z}{\epsilon_1} (\tilde{H}_{tn} \cdot ds) + \int \frac{A_z}{\epsilon_1} \nabla \cdot \tilde{H}_{tn}^* \, dS,$$

$$= -j\omega \int A_z \tilde{E}_{zn} \, dS.$$

since $A_z = 0$ on the boundary. E_{zn} is now the E_z field of the nth mode. Making use of these results we obtain the equations for the amplitudes in the form:

$$\frac{db_n}{dz} + j\beta_n a_n = \frac{1}{\triangle_n} \left[\int A_t \cdot \tilde{E}_{tn} \, dS - \int B_z \tilde{H}_{zn} \, dS \right],$$

$$\frac{da_n}{dz} + j\beta_n b_n = \frac{1}{\triangle_n} \left[-\int B_t \cdot \tilde{H}_{tn} \, dS + \int A_z \tilde{E}_{zn} \, dS \right].$$

$$(6)$$

Restoring the full expressions for A_t, B_t, A_z and B_z, we have

$$\frac{db_n}{dz} + j\beta_n a_n = \frac{j\omega}{\triangle_n} \left[\int (\epsilon_2 - \epsilon_1) E_t \cdot \tilde{E}_{tn} \, dS - j \int \eta E_t^* \cdot \tilde{E}_{tn} \, dS \right.$$

$$\left. + \int (\mu_3 - \mu_1) H_z \tilde{H}_{zn} \, dS \right], \qquad (7a)$$

$$\frac{da_n}{dz} + j\beta_n b_n = \frac{j\omega}{\triangle_n} \left[\int (\mu_2 - \mu_1) H_t \cdot \tilde{H}_{tn} \, dS - j \int \kappa H_t^* \cdot \tilde{H}_{tn} \, dS \right.$$

$$\left. + \int (\epsilon_3 - \epsilon_1) E_z \tilde{E}_{zn} \, dS \right]. \qquad (7b)$$

Equations (7a) and (7b) are, so far, exact, but they involve, on the right hand side, the functions E_t, H_t, E_z and H_z which are still unknown. We are interested in those cases where the integral terms are small, either as a consequence of the terms $(\epsilon_2 - \epsilon_1)$, η and so forth being small, or of their being finite only over a small region. In the first case the fields E_t, H_t, E_z and H_z may be replaced in the integrals by the values which they would have before the perturbation was made. In the second case this is not possible since a large change in the material constants of a

region alters the field substantially within that region. Here, then, we have a preliminary problem to solve, namely that of determining the field in the perturbed region in a zero order approximation.

Perturbation problems may be divided into two classes by another distinction. The changes in material properties may be independent of the z-coordinate, so that the new problem is to consider propagation in a uniform guide differing slightly from the original one. Typical of such problems is that of a waveguide containing a ferrite rod of infinite length parallel to the z-axis; the perturbation consisting here of the change in the properties of the rod when it is magnetized. Clearly, in such cases, solutions for which all field components vary as $\exp - j\beta z$ are still possible and the perturbation equations (7) become equations to determine β. On the other hand, there is a class of problems for which the perturbation is confined to a limited region in the z-direction, and we are interested, perhaps, in the reflection and transmission coefficients for a wave incident upon the obstacle. Here, for example, we might think of the case of a disc of ferrite across the guide. If we remain in the range for which perturbation theory is valid the changes in the amplitude of reflected and transmitted waves will be small, but the changes in phase may not be, if the perturbed region is sufficiently long. In the latter case, it would be possible, if the perturbation were uniform in z over the region in which it exists, to find solutions going as $\exp j\beta z$, as described above, and to use these to fit the boundary conditions at the ends. It is also possible if the perturbed region is long, with slowly varying properties, to obtain suitable approximate solutions by the WKB method. Some of these cases will arise in the examples which we treat below.

1.2. *Perturbations Uniform in z*

We consider first the general case in which the perturbation is uniform in z. In the absence of the perturbation the mth mode is to be present. For the fields E_t and H_z, in the perturbed region we write $a_m(z)E_{tm0}(x, y)$ and $a_m(z)H_{zm0}(x, y)$, respectively, where $a_m(z)$ is the amplitude function for the mth mode. If the perturbed region is one in which, for no magnetization, the material properties differ only slightly from their unperturbed values, we may justifiably identify E_{tm0} with E_{tm} and H_{zm0} with H_{zm}. If the material properties are appreciably changed even in the absence of a magnetic field, E_{tm0} and H_{zm0} have to be calculated by an independent method. For a_m we put $A_m e^{-j\beta z}$, where $\beta = \beta_m + \delta\beta$ and $\delta\beta$ is small. Similarly for H_t and E_z, we write $b_m H_{tm0}$ and $b_m E_{zm0}$, with $b_m = B_m e^{-j\beta z}$. With such assumptions, the mth set of equations (7)

gives an equation for β, while any other set, with $n \neq m$, gives the excitation of the nth mode. Substituting in (7) we have

$$j\beta_m A_m - j\beta B_m = \frac{j\omega}{\tilde{\triangle}_m}\left(\int \left[(\epsilon_2 - \epsilon_1)E_{tm0}\cdot\tilde{E}_{tm} - j\eta E_{tm0}{}^*\cdot\tilde{E}_{tm}\right.\right.$$
$$\left.\left. + (\mu_3 - \mu_1)H_{zm0}\tilde{H}_{zm}\right]dS\right)A_m \equiv jLA_m \tag{8a}$$

and

$$j\beta_m B_m - j\beta A_m = \frac{j\omega}{\triangle_m}\left(\int (\mu_2 - \mu_1)H_{tm0}\cdot\tilde{H}_{tm} - j\kappa H_{tm0}{}^*\cdot\tilde{H}_{tm}\right.$$
$$\left. + (\epsilon_3 - \epsilon_1)E_{zm0}\tilde{E}_{zm}\right]dS\right)B_m \equiv jMB_m. \tag{8b}$$

Ignoring squares and products of small quantities, one then has

$$\delta\beta = \tfrac{1}{2}(L + M). \tag{9}$$

The first example to be considered is the effect on the propagation in a circularly cylindrical waveguide, when a coaxial, magnetized pencil of ferrite of very small radius is introduced. The guide radius is r_0 and that of the pencil is r_1. Before the ferrite is introduced, $\mu_1 = \mu_0$ and $\epsilon_1 = \epsilon_0$, where μ_0 and ϵ_0 are the free space values. The unperturbed fields are those of the usual TE and TM modes in round guide. It is necessary to calculate first the zero order electric and magnetic fields within the magnetized pencil; it will be sufficient to work out the magnetic case and deduce the electric one by analogy. Since the cross-section of the pencil is very small and transverse propagation effects consequently negligible, the internal field may be calculated by solving a static problem. The transverse magnetic field before the pencil is inserted is H_{tm} and it is assumed that the pencil is so small that over a circle with a few times the radius of the latter, H_{tm} is essentially uniform. We must now solve Laplace's equation for a cylindrical rod immersed in a magnetic field which is to be uniform at large distances. Within the rod, $B_t = \mu H_t - j\kappa H_t{}^*$, and at its surface the usual boundary conditions prevail. Hereafter we write μ for μ_2.

The fields are derivable from potentials Φ_{out}, Φ_{in}, which are of the form

$$\Phi_{\text{in}} = (H_{tm0}\cdot\vec{r}),$$
$$\Phi_{\text{out}} = (H_{tm}\cdot\vec{r}) + \frac{(\vec{a}\cdot\vec{r})}{r^2},$$

where $\vec{r} \equiv (x, y)$, $\vec{a}$ is a constant vector and the coordinate system has its origin at the centre of the rod. Continuity of tangential H at the surface of the rod requires

$$H_{tm0} = H_{tm} + \frac{\vec{a}}{r_1^2}$$

and then

$$\Phi_{\text{out}} = H_{tm} \cdot \vec{r} + \frac{r_1^2}{r^2} (H_{tm0} - H_{tm}) \cdot \vec{r}.$$

The normal derivative at the surface of the rod is

$$\frac{1}{r_1} \left[x \frac{\partial \Phi}{\partial x} + y \frac{\partial \Phi}{\partial y} \right]$$

or, externally,

$$\frac{1}{r_1} [H_{tm} \cdot \vec{r} - (H_{tm0} - H_{tm}) \cdot \vec{r}].$$

Matching the normal B's at the surface then gives

$$\mu_0 [2 H_{tm} - H_{tm0}] = \mu H_{tm0} - j\kappa H_{tm0}{}^*,$$

or

$$H_{tm0} = \frac{2\mu_0 [(\mu + \mu_0)H_{tm} + j\kappa H_{tm}{}^*]}{(\mu + \mu_0)^2 - \kappa^2}. \tag{10a}$$

In a similar manner, one would find if the dielectric constant of the rod were ϵ,

$$E_{tm0} = \frac{2\epsilon_0 E_{tm}}{\epsilon + \epsilon_0}. \tag{10b}$$

The longitudinal fields E_{zm} and H_{zm} are unchanged within the rod.

Turning now to the expression (9) for $\delta\beta$, we have in the present-case,

$$\delta\beta = -\frac{\omega}{2\Delta_m} \int_{\text{pencil}} dS \left[\frac{2\epsilon_0(\epsilon - \epsilon_0)}{\epsilon + \epsilon_0} \mid E_{tm} \mid^2 + (\epsilon - \epsilon_0) \mid E_{zm} \mid^2 \right.$$
$$\left. + 2\mu_0 \frac{\mu^2 - \mu_0{}^2 - \kappa^2}{(\mu + \mu_0)^2 - \kappa^2} \mid H_{tm} \mid^2 - j\kappa \frac{4\mu_0{}^2}{(\mu + \mu_0)^2 - \kappa^2} H_{tm}{}^* \tilde{H}_{tm} \right],$$

where we have anticipated that Δ_m is real, which we verify below. Since the integrand is constant the integral may be replaced by πr_1^2 times the value of the integrand at $r = 0$. We consider now a TE-mode

with variation $e^{jn\varphi}$, $n \neq 0$. We shall have,

$$E_{tm} = -j\omega\mu_0 \nabla^* \Psi_m ,$$

$$H_{tm} = -j\beta_m \nabla \Psi_m ,$$

where

$$\Psi_m = J_n\left(u_{nm} \frac{r}{r_0}\right) e^{jn\varphi}, \qquad J_n'(u_{nm}) = 0$$

and

$$\beta_m{}^2 = \omega^2 \epsilon_0 \mu_0 - \frac{u_{nm}{}^2}{r_0{}^2} .$$

For the fields on the axis, one finds for $n = \pm 1$,

$$nH_r = -jH_\varphi = -jn \frac{\beta_m u_{nm}}{2r_0} e^{jn\varphi}$$

and

$$nE_\Phi = jE_r = j\omega_0 n \frac{u_{nm}}{2r_0} e^{jn\varphi}.$$

If $|n| \neq 1$ there is no first order perturbation. We now have

$$\delta\beta = -\frac{\omega}{2\triangle_m} \pi r_1{}^2 \left[\epsilon_0 \frac{\epsilon - \epsilon_0}{\epsilon + \epsilon_0} \omega^2 \mu_0{}^2 \frac{u_{nm}{}^2}{r_0{}^2} + \frac{\mu_0 \beta_m{}^2 u_{nm}{}^2}{r_0{}^2} \frac{\mu + n\kappa - \mu_0}{\mu + n\kappa + \mu_0} \right].$$

But we have

$$\triangle_m = 2\pi \int_0^{r_0} E_{tm}{}^* \cdot \tilde{H}_{tm} r \, dr,$$

$$= -2\pi \cdot \omega\mu_0\beta_m \int_0^{u_{nm}} \left[J_n'(x)^2 + \frac{J_n(x)^2}{x^2} \right] x \, dx,$$

$$= -2\pi\omega\mu_0\beta_m \frac{J_n(u_{nm})^2}{2} (u_{nm}{}^2 - 1).$$

and then,

$$\delta\beta = \frac{1}{2\beta_m} \cdot \frac{r_1{}^2}{r_0{}^2} \cdot \frac{u_{nm}{}^2}{J_n(u_{nm})^2 (u_{nm}{}^2 - 1)} \cdot$$

$$\left[\beta_m{}^2 \frac{\mu + n\kappa - \mu_0}{\mu + n\kappa + \mu_0} + \beta_0{}^2 \frac{\epsilon_1 - \epsilon_0}{\epsilon_1 + \epsilon_0} \right]. \tag{11}$$

For TM modes we have

$$E_{tm} = -j\beta_m \nabla \chi_m \qquad E_z = \frac{j_{nm}^2}{r_0^2} \chi_m$$

$$H_{tm} = j\omega\epsilon_0 \nabla^* \chi_m$$

where

$$\chi_m = J_n\left(j_{nm}\frac{r}{r_0}\right)e^{jn\varphi}, \qquad J_n(j_{nm}) = 0$$

and

$$\beta_m^2 = \omega^2\epsilon_0\mu_0 - \frac{j_{nm}^2}{r_0^2}.$$

Proceeding as before, we find,

$$\delta\beta = \frac{1}{2\beta_m} \cdot \frac{r_1^2}{r_0^2} \cdot \frac{1}{J_n'(j_{nm})^2}\left[\beta_0^2 \frac{\mu + n\kappa - \mu_0}{\mu + n\kappa + \mu_0} + \beta_m^2 \frac{\epsilon - \epsilon_0}{\epsilon + \epsilon_0}\right]. \quad (12)$$

A problem which is of some interest, although not of immediate practical significance, is that of a ferrite pencil of arbitrary radius and infinite length in a round wave guide, with the remainder of the waveguide filled with a non-magnetic dielectric, whose dielectric constant, ϵ_1, is equal to that of the ferrite. The ferrite is supposed to be only weakly magnetized. For such a problem, we have,

$$\delta\beta = -\frac{\omega}{2\triangle_m} \int_{\text{pencil}} [(\mu - \mu_0)H_{tm} \cdot \tilde{H}_{tm} - j\kappa H_{tm}^* \cdot \tilde{H}_{tm}] \, dS.$$

H_{tm} is the field of an unperturbed TE or TM mode in the dielectric-filled guide. $\mu - \mu_0$ and κ are supposed small, but r_1, the radius of the pencil need no longer be small.

For TE modes, we have as before (again excluding the case $n = 0$),

$$E_{tm} = -j\omega\mu_0 \nabla^* \Psi_m,$$

$$H_{tm} = -j\beta_m \nabla \Psi_m,$$

$$\Psi_m = J_n\left(u_{nm}\frac{r}{r_0}\right)e^{jn\varphi}$$

and

$$\beta_m^2 = \omega^2\epsilon_0\mu_0 - \frac{u_{nm}^2}{r_0^2} = \beta_1^2 - \frac{u_{nm}^2}{r_0^2}.$$

Hence, assuming the pencil coaxial with the guide.

$$-\frac{2\triangle_m}{\omega}\,\delta\beta \;=\; 2\pi \int_0^{r_1} (\mu - \mu_0)\beta_m^{\;2}\left[\frac{u_{nm}^{\;2}}{r_0^{\;2}}\,J_n'^{\;2}\left(u_{nm}\frac{r}{r_0}\right)\right.$$

$$+\left.\frac{n^2}{r^2}\,J_n^{\;2}\left(u_{nm}\frac{r}{r_0}\right)\right]r\,dr$$

$$+\;2\pi\kappa\beta_m^{\;2}\cdot 2\,\frac{u_{nm}}{r_0}\,n\int_0^{r_1}J_n\left(u_{nm}\frac{r}{r_0}\right)J_n'\left(u_{nm}\frac{r}{r_0}\right)dr,$$

$$=\;2\pi\beta_m^{\;2}\left[(\mu - \mu_0)\int_0^{u_{nm}(r_1/r_0)}\left[xJ_n'^{\;2}(x) + \frac{J_n^{\;2}(x)}{x}\right]dx\right.$$

$$+\;2\kappa n\int_0^{u_{nm}(r_1/r_0)}J_n(x)J_n'(x)\,dx\left.\right],$$

$$=\;2\pi\beta_m^{\;2}\left[(\mu - \mu_0)\left(xJ_n(x)J_n'(x) + \frac{x^2}{2}\,J_n'^{\;2}(x)\right.\right.$$

$$+\left.\left.\frac{x^2 - 1}{2}\,J_n^{\;2}(x)\right)_{x=(r_1/r_0)u_{nm}} + \kappa nJ_n^{\;2}\left(u_{nm}\frac{r_1}{r_0}\right)\right].$$

Making use of the value of $\triangle_m$ found in the preceeding paragraphs, we have

$$\delta\beta \;=\; \frac{\beta_m}{(u_{nm}^{\;2} - 1)J_n(u_{nm})^2}\left[\left(\frac{\mu}{\mu_0} - 1\right)\left(xJ_n(x)J_n'(x) + \frac{x^2}{2}\,J_n'^{\;2}x\right)\right.$$

$$+\left.\frac{x^2 - 1}{2}\,J_n^{\;2}(x)\right)_{x=u_{nm}(r_1/r_0)} + n\,\frac{\kappa}{\mu_0}\,J_n^{\;2}\left(u_{nm}\frac{r_1}{r_0}\right)\right]. \qquad (13)$$

For TM modes,

$$E_{tm} \;=\; -j\beta_m\nabla\chi_m\,,$$

$$H_{tm} \;=\; j\omega\epsilon_1\nabla^*\psi_m\,,$$

$$\chi_m \;=\; J_n\left(j_{nm}\frac{r}{r_0}\right)e^{jn\varphi},$$

$$\beta_m^{\;2} \;=\; \omega^2\epsilon_1\mu_0 - \frac{j_{nm}^{\;2}}{r_0^{\;2}} \;=\; \beta_1^{\;2} - \frac{j_{nm}^{\;2}}{r_0^{\;2}}\,.$$

In this case,

$$-\frac{2\triangle_m}{\omega}\,\delta\beta \;=\; 2\pi(\omega\epsilon_1)^2\left((\mu - \mu_0)\int_0^{r_1}\left[\frac{n^2}{r^2}\,J_n^{\;2}\left(j_{nm}\frac{r}{r_0}\right)\right.\right.$$

$$+\left.\left.\frac{j_{nm}^{\;2}}{r_0^{\;2}}\,J_n'^{\;2}\left(j_{nm}\frac{r}{r_0}\right)\right]r\,dr + 2\kappa n\int_0^{r_1}\frac{j_{nm}}{r_0}\,J_n\left(j_{nm}\frac{r}{r_0}\right)J_n'\left(j_{nm}\frac{r}{r_0}\right)dr\right).$$

The value of $\triangle_m$ for this case is

$$\triangle_m = -2\pi\omega\epsilon_1\beta_m \cdot \frac{j_{nm}^2}{2} J_n'^2(j_{nm}).$$

The value of $\delta\beta$ now becomes

$$\delta\beta = \frac{\beta_1^2}{\beta_m j_{nm}^2 J_n^2(j_{nm})}\left[\left(\frac{\mu}{\mu_0} - 1\right)\left(xJ_n(x)J_n'(x) + \frac{x^2}{2} J_n'^2(x)\right. \right. \tag{14}$$
$$\left.\left. + \frac{x^2 - 1}{2} J_n^2(x)\right)_{x=j_{nm}(r_1/r_0)} + n\,\frac{\kappa}{\mu_0} J_n^2\left(j_{nm}\,\frac{r_1}{r_0}\right)\right].$$

We note that for a ferrite filled guide with $r_1 = r_0$, the nonreciprocal part of $\delta\beta$ vanishes which confirms a result found in Part I of this paper for weak magnetization.

The very high dielectric constant of the ferrites (about 10) puts rather severe restrictions on the size of the pencils to which perturbation theory is applicable, even for weak magnetization. This limitation would be substantially relaxed if we possessed exact solutions for rods of high dielectric constant inserted into round guide, which could be used as the basis for magnetic perturbation calculations. Unfortunately, the only extensive published calculations of this kind are for dielectric constants less than 3. However, at the suggestion of M. T. Weiss, a calculation of the propagation constant of the lowest mode varying as $e^{\pm j\varphi}$ in a wave guide containing a coaxial dielectric rod ($\epsilon_1 = 10$) has recently been made in the Mathematics Department, for varying rod diameter, but for a single value of guide radius equal to 0.4 times the free space wavelength. With the aid of this information, which was made available to us, the magnetic perturbation calculation has been carried out.

As before, the radius of the guide is r_0 and that of the rod is r_1. The dielectric constant of the rod is ϵ_1. We consider first the propagation in the unmagnetized case. Since we are considering only one mode, namely, that with an angular variation, $e^{j\varphi}$, and of the lowest order radially, we need not identify the E's and H's by a label. We use a subscript "1" for fields in the dielectric and "0" for fields in the empty part of the guide. In general, we have

$$\alpha^2 E_t = -j[\omega\mu\nabla^* H_z + \beta\nabla E_z],$$
$$\alpha^2 H_t = -j[\beta\nabla H_z - \omega\epsilon\nabla^* E_z],$$

where

$$\alpha^2 = \omega^2\epsilon\mu - \beta^2,$$
$$\nabla^2 H_z = -\alpha^2 H_z,$$
$$\nabla^2 E_z = -\alpha^2 E_z.$$

and ϵ, μ refer, for the time being, to the dielectric constant and permeability of the region considered. It will be convenient to put

$$H_{z,t} = \sqrt{\frac{\epsilon_0}{\mu_0}}\, \bar{H}_{z,t}\;; \qquad \frac{\epsilon}{\epsilon_0} = \bar{\epsilon}; \qquad \frac{\mu}{\mu_0} = \bar{\mu};$$

$$\frac{\beta}{\omega\sqrt{\epsilon_0\mu_0}} = \bar{\beta}; \qquad \frac{\alpha}{\omega\sqrt{\epsilon_0\mu_0}} = \bar{\alpha},$$

and to measure lengths in terms of $\dfrac{1}{\omega\sqrt{\mu_0\epsilon_0}}$. We shall continue to use ∇ and ∇^* with the understanding that they refer to the scaled units.

We now have

$$j\bar{\alpha}^2 E_t = \bar{\mu}\nabla^*\bar{H}_z + \bar{\beta}\nabla E_z\,,$$

$$j\bar{\alpha}^2 \bar{H}_t = \bar{\beta}\nabla\bar{H}_z - \bar{\epsilon}\nabla^*E_z\,,$$

$$\bar{\alpha}^2 = \bar{\epsilon}\bar{\mu} - \bar{\beta}^2,$$

$$\nabla^2\bar{H}_z = -\bar{\alpha}^2\bar{H}_z\,,$$

$$\nabla^2 E_z = -\bar{\alpha}^2 E_z\,.$$

At the surface of the rod E_z, $\bar{H}_z$, E_φ and $\bar{H}_\varphi$ are continuous. We must have

$$\frac{1}{\bar{\alpha}_0^2}\left[\frac{j\bar{\beta}}{r_0}E_z(r_1) - \left(\frac{\partial\bar{H}_z}{\partial r}\right)_0\right] = \frac{1}{\bar{\alpha}_1^2}\left[\frac{j\bar{\beta}}{r_1}E_z(r_1) - \left(\frac{\partial\bar{H}_z}{\partial r}\right)_1\right]$$

and

$$\frac{1}{\bar{\alpha}_0^2}\left[\left(\frac{\partial E_z}{\partial r}\right)_0 + \frac{j\bar{\beta}}{r_1}\bar{H}_z(r_1)\right] = \frac{1}{\bar{\alpha}_1^2}\left[\bar{\epsilon}_1\left(\frac{\partial E_z}{\partial r}\right)_1 + \frac{j\bar{\beta}}{r_1}\bar{H}_z(r_1)\right].$$

where

$$\bar{\epsilon}_1 = \frac{\epsilon_1}{\epsilon_0}, \qquad \bar{\alpha}_0^2 = 1 - \bar{\beta}^2 \qquad \text{and} \qquad \bar{\alpha}_1^2 = \bar{\epsilon}_1 - \bar{\beta}^2.$$

$\bar{\mu} = 1$, everywhere, if the unmagnetized ferrite has the permeability of free space.

These equations may be rearranged in the form:

$$\bar{\beta}\left(\frac{1}{\bar{\alpha}_0^2} - \frac{1}{\bar{\alpha}_1^2}\right)E_z(r_1) = \left\{-\frac{1}{\bar{\alpha}_0^2}\left[r_1\frac{1}{\bar{H}_z(r_1)}\left(\frac{\partial\bar{H}_z}{\partial r}\right)_0\right]\right.$$

$$\left. + \frac{1}{\bar{\alpha}_1^2}\left[r_1\frac{1}{\bar{H}_z(r_1)}\left(\frac{\partial\bar{H}_z}{\partial r}\right)_1\right]\right\}j\bar{H}_z(r_1),$$

$$\bar{\beta}\left(\frac{1}{\bar{\alpha}_0^2} - \frac{1}{\bar{\alpha}_1^2}\right)j\bar{H}_z(r_1) = \left\{-\frac{1}{\bar{\alpha}_0^2}\left[r_1\frac{1}{E_z(r_1)}\left(\frac{\partial E_z}{\partial r}\right)_0\right]\right.$$

$$\left. + \frac{\bar{\epsilon}}{\bar{\alpha}_1^2}\left[r_1\frac{1}{E_z(r_1)}\left(\frac{\partial E_z}{\partial r}\right)_1\right]\right\}E_z(r_1).$$

(15)

Within the dielectric, since all fields are bounded at $r = 0$, both E_z and $\bar{H}_z$ are proportional to $J_1(\bar{\alpha}_1 r)$ and, evidently,

$$-\frac{r_1}{H_z(r_1)}\left(\frac{\partial \bar{H}_z}{\partial r}\right)_1 \equiv \frac{r_1}{E_z(r_1)}\left(\frac{\partial E_z}{\partial r_1}\right)_1 = \frac{\alpha_1 r_1 J_1{}'(\alpha_1 r_1)}{J_1(\alpha_1 r_1)} = F(\alpha_1 r_1),$$

in the notation of Part I. $(E_z)_0$ and $(\bar{H}_z)_0$, similarly, will be those two linear combinations of $J_1(\bar{\alpha}_0 r)$ and $Y_1(\bar{\alpha}_0 r)$, which, respectively, vanish and have zero normal derivative at $r = r_0$, in order to ensure the vanishing of the tangential fields there. The functions

$$\frac{r}{(\bar{H}_z)_0}\frac{\partial(\bar{H}_z)_0}{\partial r} \qquad \text{and} \qquad \frac{r}{(E_z)_0}\frac{\partial(E_z)_0}{\partial r}$$

will be called $H(\bar{\alpha}_0 r)$ and $G(\bar{\alpha}_0 r)$ respectively.

Eliminating $E_z(r_1)$ and $H_z(r_1)$ from equations (15) we obtain the characteristic equation of the problem in the form

$$\bar{\beta}^2\left(\frac{1}{\bar{\alpha}_0^2} - \frac{1}{\bar{\alpha}_1^2}\right)^2 = \left(\frac{F(\alpha_1 r_1)}{\bar{\alpha}_1^2} - \frac{H(\bar{\alpha}_0 r_1)}{\bar{\alpha}_0^2}\right)\left(\bar{\epsilon}_1\frac{F(\bar{\alpha}_1 r_1)}{\bar{\alpha}_1^2} - \frac{G(\bar{\alpha}_0 r_1)}{\bar{\alpha}_0^2}\right).$$

The perturbation in the present problem is that due to a mild magnetization of the rod and referring again to equation (9) we have (in unscaled units)

$$\delta\beta = -\frac{\omega}{2\triangle_n}\int_{\text{rod}}[(\mu - \mu_0)H_t\cdot\bar{H}_t - j\kappa H_t{}^*\cdot\bar{H}_t]\,dS,$$

with

$$\triangle_n = \int_{\text{guide}}E_t{}^*\cdot\bar{H}_t\,dS.$$

Thus, in the scaled system,

$$\delta\bar{\beta} = -\frac{1}{2}\cdot\frac{\int_0^{r_1}\left[\left(\frac{\mu}{\mu_0} - 1\right)|\bar{H}_t|^2 - j\frac{\kappa}{\mu_0}(\bar{H}_t{}^*\cdot{}_t\bar{\tilde{H}})\right]r\,dr}{\int_0^{r_0}E_t{}^*\cdot\bar{H}_t\,r\,dr}. \qquad (16)$$

The evaluation of the normalizing integral in the denominator is an exceedingly tedious business and it seems advisable to avoid it. This may be done in the following manner. The characteristic equation has been solved for numerous values of r_1 and $\bar{\beta}$ may be considered to be a reliably known function of r_1. In particular the slope $\dfrac{d\bar{\beta}}{dr_1}$ is known. But we may also deduce $\dfrac{d\bar{\beta}}{dr_1}$, by a perturbation calculation in which we start with a

rod of radius r_1 and increase the latter to $r_1 + dr_1$ by changing ϵ_0 to ϵ_1 in the shell $r_1 < r < r_1 + dr_1$. For such a perturbation, since E_z and E_φ are continuous at the boundary, they suffer no change when the boundary moves; E_r however is discontinuous and $(E_r)_o = \frac{\epsilon_1}{\epsilon_0}(E_r)_i$ where $(E_r)_c$ and $(E_r)_i$ are the normal fields just outside and just inside the rod. The perturbation formula (unscaled), thus gives

$$\delta\beta = \frac{-\omega}{2\Delta_n}(\epsilon_1 - \epsilon_0)\left(\mid E_z \mid^2 + \mid E_\varphi \mid^2 + \frac{\epsilon_1}{\epsilon_0}\mid (E_r)_i \mid^2\right)\cdot 2\pi r_1\delta r_1,$$

or, scaled, with r and r_1 representing scaled radii,

$$\delta\bar\beta = -\frac{1}{2}\frac{(\bar\epsilon_1 - 1)(\mid E_z \mid^2 + \mid E_\varphi \mid^2 + \epsilon_1\mid (E_r)_i \mid^2)}{\displaystyle\int_0^{r_0} E_t^*\cdot\tilde H_r r\,dr}\cdot r_1\delta r_1.$$

The formula (16) for the magnetic perturbation may now be written

$$\delta\bar\beta = \frac{\dfrac{1}{r_1}\dfrac{d\bar\beta}{dr_1}}{\bar\epsilon_1 - 1}\cdot\frac{\displaystyle\int_0^{r_1}\left[\left(\dfrac{\mu}{\mu_0} - 1\right)\mid \bar H_t \mid^2 - j\dfrac{\kappa}{\mu_0}(\bar H_t^*\cdot\tilde H_t)\right]r\,dr}{\mid E_z(r_1) \mid^2 + \mid E_\varphi(r_1) \mid^2 + \bar\epsilon_1\mid (E_r)_i \mid^2}.$$

Inside the rod, we may write

$$\bar H_z = \frac{\bar H_z(r_1)}{E_z(r_1)} \qquad E_z = jcE_z$$

and then

$$j\bar\alpha_1^{\,2}\bar H_r = jc\bar\beta\frac{\partial E_z}{\partial r} - \bar\epsilon_1\frac{j}{r}E_z,$$

$$j\bar\alpha_1^{\,2}\bar H_\varphi = jc\bar\beta\frac{j}{r}E_z + \bar\epsilon_1\frac{\partial E_z}{\partial r}.$$

The integrals are readily carried out and are as follows:

$$\int_0^{r_1}\mid \bar H_t \mid^2 r\,dr$$

$$= \frac{E_z^2(r_1)}{\bar\alpha_1^{\,4}}\left[(\bar\epsilon_1^{\,2} + c^2\beta^2)\left(F(\bar\alpha_1 r_1) + \frac{F^2(\bar\alpha_1 r_1)}{2} + \frac{\bar\alpha_1^{\,2}r_1^{\,2} - 1}{2}\right) - 2c\bar\beta\bar\epsilon_1\right],$$

$$\int_0^{r_1}(\bar H_t^*\cdot\tilde H_t)r\,dr$$

$$= \frac{jE_z^2(r_1)}{\bar\alpha_1^{\,4}}\left[(\bar\epsilon_1^{\,2} + c^2\bar\beta^2) - 2c\bar\epsilon_1\bar\beta\left(F(\bar\alpha_1 r_1) + \frac{F^2(\bar\alpha_1 r_1)}{2} + \frac{\bar\alpha_1^{\,2}\bar r_1^{\,2} - 1}{2}\right)\right].$$

The term in the denominator may be evaluated by using

$$j\bar{\alpha}_1{}^2 E_r = -\frac{c}{r} E_z + \bar{\beta}\frac{\partial E_z}{\partial r},$$

$$j\bar{\alpha}_1{}^2 E_\varphi = -jc\frac{\partial E_z}{\partial r} + \frac{j\bar{\beta}}{r} E_z.$$

We obtain

$$|E_z(r_1)|^2 + |E_\theta(r_1)|^2 + \bar{\epsilon}_1|(E_r)_1|^2$$
$$= E_z{}^2(r_1)\left[\frac{[\bar{\beta} - cF(\bar{\alpha}_1 r_1)]^2 + \bar{\epsilon}_1[c - \bar{\beta}F(\bar{\alpha}_1 \bar{r}_1)]^2}{r_1{}^2\,\bar{\alpha}_1{}^4}\right].$$

The perturbation may now be written:

$$\delta\bar{\beta} = \frac{r_1\dfrac{\partial\bar{\beta}}{\partial r_1}}{\bar{\epsilon}_1 - 1} \tag{17}$$
$$\cdot\frac{\left(\dfrac{\mu}{\mu_0} - 1\right)[A(\bar{\epsilon}_1{}^2 + c^2\bar{\beta}^2) - 2c\bar{\beta}\bar{\epsilon}_1] + \dfrac{\kappa}{\mu_0}[\bar{\epsilon}_1{}^2 + c^2\bar{\beta}^2 - 2Ac\bar{\epsilon}_1\bar{\beta}]}{r_1{}^2\bar{\alpha}_1{}^4 + [\bar{\beta} - cF(\bar{\alpha}_1 r_1)]^2 + \bar{\epsilon}_1[c - \bar{\beta}F(\bar{\alpha}_1 r_1)]^2},$$

where

$$A = \frac{F^2(\bar{\alpha}_1 r_1)}{2} + F(\bar{\alpha}_1 r_1) + \frac{\bar{\alpha}_1{}^2 r_1{}^2}{2}$$

and c may be obtained from equation 15, and the definition of c

$$c = \frac{\dfrac{G(\bar{\alpha}_0 r_1)}{\bar{\alpha}_0{}^2} - \bar{\epsilon}_1\dfrac{F(\bar{\alpha}_1 r_1)}{\bar{\alpha}_1{}^2}}{\bar{\beta}\left(\dfrac{1}{\bar{\alpha}_0{}^2} - \dfrac{1}{\bar{\alpha}_1{}^2}\right)} = \frac{\bar{\alpha}_1{}^2 G(\bar{\alpha}_0 r_1) - \bar{\epsilon}_1\bar{\alpha}_0{}^2 F(\bar{\alpha}_1 r_1)}{\bar{\beta}(\bar{\epsilon}_1 - 1)}$$

with

$$G(\bar{\alpha}_0 r_1) = \bar{\alpha}_0 r_1\frac{N_1(\bar{\alpha}_0 r_0)J_1{}'(\bar{\alpha}_0 r_1) - J_1(\bar{\alpha}_0 r_0)N_1{}'(\bar{\alpha}_0 r_1)}{N_1(\bar{\alpha}_0 r_0)J_1(\bar{\alpha}_0 r_1) - J_1(\bar{\alpha}_0 r_0)N_1(\bar{\alpha}_0 r_1)}.$$

Fig. 1 shows the propagation constant as a function of the relative diameter, r_1/r_0, of the dielectric rod in the unmagnetized case, with $\bar{\epsilon}_1 = 10$. Fig. 2 shows the derivative $\dfrac{d\bar{\beta}}{d(r_1/r_0)}$ as a function of r_1/r_0. The guide radius is 0.4 times the free space wavelength. From equation (17) $\delta\bar{\beta}$ may be written as
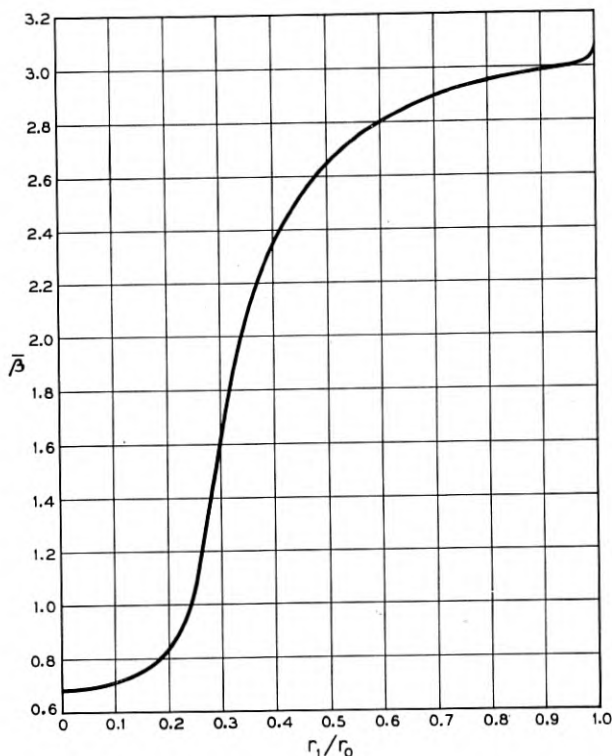
$$\delta\bar{\beta} = P(\mu - \mu_0) + Q\kappa.$$

Fig. 1 — Propagation constant of a circular guide containing an unmagnetized coaxial, dielectric rod ($\epsilon/\epsilon_0 = 10$). r_1 is the radius of the rod and r_0 the radius of the guide. $r_0 = 0.4\lambda_0$, where λ_0 is the free space wavelength.

The computed values of Q and $P - Q$ are shown in Fig. 3 as a function of relative rod radius. $P - Q$ is plotted since P and Q are very nearly equal.*

1.3 *Perturbations Non-Uniform in z*

So far we have been concerned only with structures indefinitely extended in the direction of wave propagation. In practice the non-reciprocal element is, of course, finite, but end effects can frequently be neglected, since the element is matched at its ends (by tapering of the finite

---

* H. Seidel and Miss M. J. Brannon, at the suggestion of M. T. Weiss, have recently calculated the dielectric loss for the guides containing a dielectric rod described above. By combining such information with that obtained here it is possible to discuss figures of merit (degrees of rotation loss in db) for various pencil radii. Such an analysis is being made by M. T. Weiss and will appear in an article, by S. E. Miller, A. G. Fox and M. T. Weiss, in a forthcoming issue of the JOURNAL.

sample, for instance). The matching could be accomplished in such a way that the transition region, whose characteristics would be very difficult to compute, should contribute little to the overall non-reciprocal behavior. Therefore, in many cases, the theory for the indefinitely extended sample is adequate. For some special purposes, however, it is desirable to mismatch the sample deliberately. For instance, Rowen[3] has suggested that the change in Faraday rotation, due to internal reflections in an unmatched specimen, can offset to some extent the frequency dependence of the rotation which is implied by the Polder relations, broadening thereby the useful bandwidth of the device.

Consider an infinite slab of ferrite, magnetized in a direction normal to its two parallel plane bounding surfaces. A circularly polarized wave, normally incident on the slab, will be partially transmitted, and, since for such a wave, the medium behaves as though it had an ordinary scalar permeability, the phase and amplitude of the transmitted portion are readily calculated. It is clear that, as the result of multiple internal reflections, the phase of the emerging wave will differ from the value appropriate to a single trip through the slab (such as would be obtained were the slab perfectly matched). Both amplitude and phase of the transmitted wave will depend on the electrical thickness of the slab and its dielectric constant, and on the effective permeability. The latter
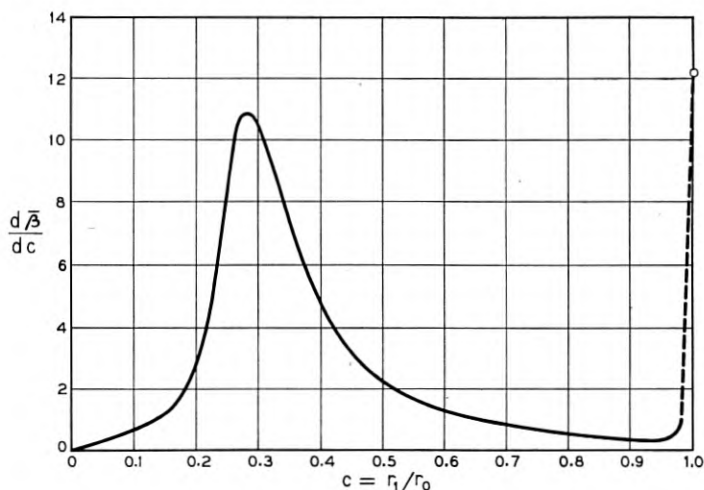
$$\text{Fig. 2} - \frac{d\beta}{d\left(\dfrac{r_1}{r_0}\right)} \text{ versus } \frac{r_1}{r_0}.$$
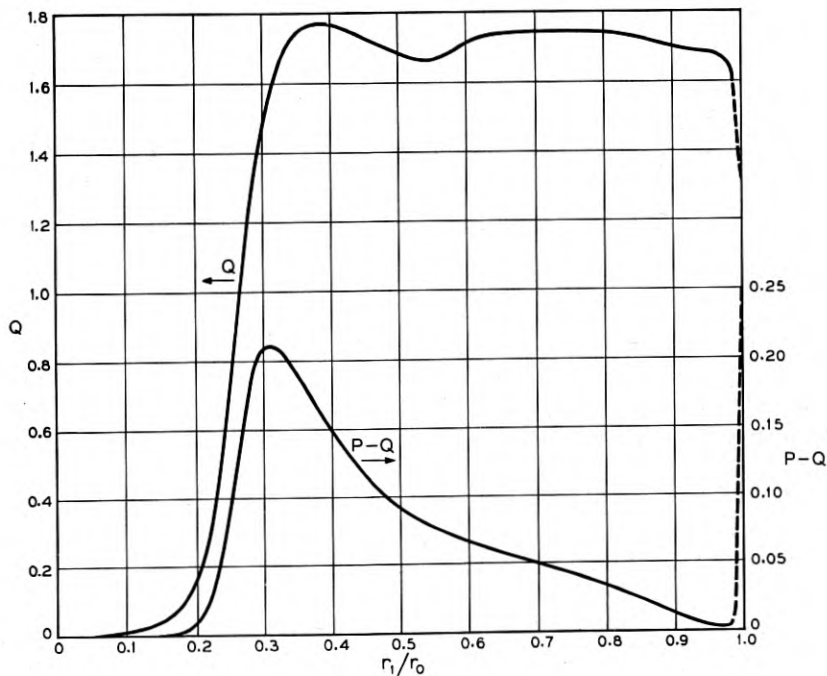
Fig. 3 — Q and $P - Q$ versus r_1/r_0 .

differs for right and left circular waves, so that a plane polarized signal (which is the sum of equal right and left circular components) will emerge, in general, elliptically polarized, with the major axis of the ellipse tilted from the polarization at incidence by an angle which differs from the single trip value as the result of internal reflections. It is clear that this change in rotation can be calculated in a very elementary way.

When the sample is confined to a waveguide a similar effect occurs, but its calculation becomes extremely involved, at least for arbitrarily large magnetizations. The reason, which should be clear from Part I of this paper, is that the circularly polarized modes no longer have the same field configurations inside and outside the sample.* Therefore any incident mode excites *all* of the normal modes of the ferrite; these, in turn, give rise to *all* the mode patterns of the air-filled portion of the guide. Even if all but one of these are cut off, the excitation modifies the phase and amplitude of the reflected and transmitted portions of the propagating mode.

---

* This is due to the fact that there is now no ordinary effective scalar permeability as for infinite geometry.

Thus all modes have to be included in the problem, which consequently takes the form of an infinite system of linear equations for the mode amplitudes. This can be solved only to some approximation whose general validity it would be hard to establish. The problem could also be stated as an integral equation involving a complicated Green's function, with no greater chance of complete solution.

We are therefore forced to restrict the problem to the ranges of magnetization, or of sample size, in which perturbation theory is applicable. However, we begin with a discussion of the infinite, plane, loss-free slab, a problem which can be solved completely, and which has some bearing on the perturbation problem for a slug of ferrite whose cross section completely fills the waveguide.

Let the plane boundaries of the slab be normal to the z-axis, which is also the direction of magnetization and the propagation direction of a circularly polarized wave incident on the boundary $z = 0$ (see Fig. 4). In terms of the parameters p and σ of Section 2.1, Part I, the effective permeability for a circularly polarized wave is

$$\mu \pm \kappa = \mu = \mu_0 \left(1 \pm \frac{p}{1 \pm \sigma} \right),$$

the upper sign referring to right circular polarization. The corresponding propagation constants in the slab are then

$$\beta_\pm = \omega \sqrt{\epsilon \mu_0} \sqrt{1 \pm \frac{p}{1 \pm \sigma}}$$
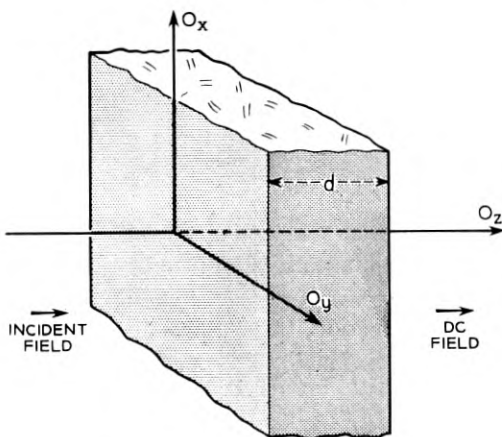
Fig. 4 — Normally magnetized ferrite slab.

where ϵ is the dielectric constant of the ferrite. If d is the thickness of the slab, the electrical thickness is

$$\theta_{\pm} = \beta_{\pm} d = \frac{2\pi d}{\lambda_{\pm}} = \theta_0 \sqrt{1 \pm \frac{p}{1 \pm \sigma}},$$

where $\theta_0 = \omega \sqrt{\mu_0 \epsilon}\, d$ is the electrical thickness of the unmagnetized sample. Let us now confine the discussion to the right circular wave. If the incident electric field is taken to be $e^{-j\beta_0 z}$, where β_0 is the free space propagation constant, $\omega \sqrt{\mu_0 \epsilon_0}$, the incident magnetic field will be

$$-\frac{\beta_0}{\omega \mu_0} e^{-j\beta_0 z},$$

and if the reflected electric field is $\rho e^{j\beta_0 z}$, the reflected magnetic field will be

$$\frac{\beta_0}{\omega \mu_0} \rho e^{j\beta_0 z}$$

since β_0 reverses sign. Inside the slab, the electric field consists of forward and backward travelling parts $\tau_1 e^{-j\beta_+ z}$ and $\tau_2 e^{j\beta_+ z}$, and the corresponding magnetic fields are

$$-\frac{\beta_+}{\omega \mu_+} \tau_1 e^{-j\beta_+ z}$$

and

$$\frac{\beta_+}{\omega \mu_+} \tau_2 e^{j\beta_+ z}.$$

Finally the transmitted electric and magnetic fields will be denoted by

$$\tau_3 e^{-j\beta_0(z-d)}$$

and

$$-\frac{\beta_0}{\omega \mu_0} \tau_3 e^{-j\beta_0(z-d)}$$

respectively. In general ρ, as well as the τ's, will be complex. To obtain τ_3, we write down the equations of continuity of all tangential fields across the boundaries $z = 0$ and $z = d$. Since the fields are confined to a plane normal to the z-direction, these equations are:

$$1 + \rho = \tau_1 + \tau_2,$$

$$\frac{\beta_0}{\omega \mu_0} (1 - \rho) = \frac{\beta_+}{\omega \mu_0} (\tau_1 - \tau_2)$$

and

$$\tau_3 = \tau_1 e^{-j\beta_+ d} + \tau_2 e^{-j\beta_+ d},$$

$$\frac{\beta_0}{\omega\mu_0} \tau_3 = \frac{\beta_+}{\omega\mu_0} (\tau_1 e^{-\beta_+ d} - \tau_2 e^{j\beta_+ d}).$$

These four equations in four unknowns are easily solved for τ_3. Writing

$$x_+ = \sqrt{1 + \frac{p}{1 + \sigma}}$$

and noting that

$$\frac{\beta_+}{\mu_+} \bigg/ \frac{\beta_0}{\mu_0} = \sqrt{\frac{\epsilon}{\epsilon_0}} \bigg/ x_+ ,$$

$$= \frac{a}{x_+}, \qquad \text{say,}$$

where

$$a = \sqrt{\frac{\epsilon}{\epsilon_0}},$$

one finds the solution to be

$$\tau_3 = \frac{1}{\cos \theta_0 x + \frac{j}{2} \left(\frac{a}{x_+} + \frac{x_+}{a} \right) \sin \theta_0 x_+},$$

$$= |\tau_3|_+ e^{-j\Phi_+},$$

where

$$\tan \Phi_+ = \frac{1}{2} \left(\frac{a}{x_+} + \frac{x_+}{a} \right) \tan \theta_0 x_+ \tag{18}$$

and

$$|\tau_3|_+ = \left[\cos^2 \theta_0 x_+ + \frac{1}{4} \left(\frac{a}{x_+} + \frac{x_+}{a} \right)^2 \sin^2 \theta_0 x_+ \right]^{-1/2}. \tag{19}$$

Similar results apply to a left circular wave; it is necessary only to reverse the signs of σ, p in the expression for x_+. Equations (18) and (19) show that equal right and left circular incident waves emerge with different amplitudes and phases; hence an incident plane polarized wave emerges elliptically polarized with its major axis inclined to the polarization direction at incidence. The inclination and the ratio of minor to major axis

are determined as follows: The right and left circular fields, upon emergence, may be written in terms of rectangular components (with the polarization of the total incident field along the x-axis)

$$E_x^+ - jE_y^+ = \tau_+ e^{j\omega t},$$

$$E_x^- + jE_y^- = \tau_- e^{j\omega t},$$

from which the resultant field in the x-direction is seen to be

$$\left. \begin{aligned} E_{xT} &= E_x^+ + E_x^- = |\tau_+| \cos (\omega t - \Phi_+) + |\tau_-| \cos (\omega t - \Phi_-) \\ &\text{and in the } y \text{ direction} \\ E_{yT} &= E_y^+ + E_y^- = |\tau_-| \sin (\omega t - \Phi_-) - |\tau_+| \sin (\omega t - \Phi_+). \end{aligned} \right\} \quad (20)$$

The amplitude at time t, $(E_{xT}^2 + E_{yT}^2)^{1/2}$, is thus given by

$$E_{xT}^2 + E_{yT}^2 = |\tau_+|^2 + |\tau_-|^2$$

$$+ 2|\tau_+| \cdot |\tau_-| \cos [2\omega t - (\Phi_- + \Phi_+)] \quad (21)$$

The major axis of the ellipse is the maximum of $(E_{xT}^2 + E_{yT}^2)^{1/2}$ with respect to ωt. It equals $|\tau_+| + |\tau_-|$ and is attained at

$$\omega t = \tfrac{1}{2}(\Phi_- + \Phi_+).$$

Similarly the minor axis is the minimum and equals $|\tau_+| - |\tau_-|$. The ratio of minor to major axis is therefore

$$\frac{|\tau_+| - |\tau_-|}{|\tau_+| + |\tau_-|}.$$

The angle between the x-axis (the incident polarization direction) and the major axis is found by substituting $\omega t = \tfrac{1}{2}(\Phi_- + \Phi_+)$ in (20). This gives

$$E_{xT} = (|\tau_+| + |\tau_-|) \cos \frac{\Phi_+ - \Phi_-}{2},$$

$$E_{yT} = (|\tau_+| + |\tau_-|) \sin \frac{\Phi_+ - \Phi_-}{2},$$

which shows that the angle is

$$\frac{\Phi_+ - \Phi_-}{2}.$$

$|\tau|$ and Φ are plotted versus x in Fig. 5. τ_+, Φ_+ and τ_-, Φ_- at given
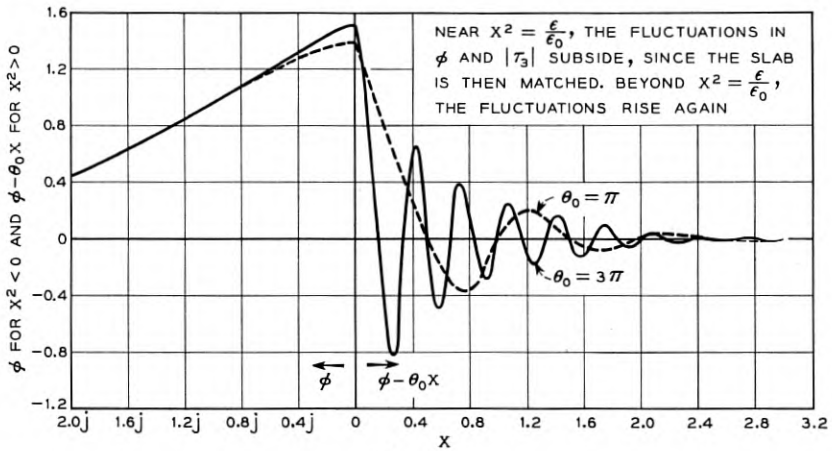
FIG. 5a
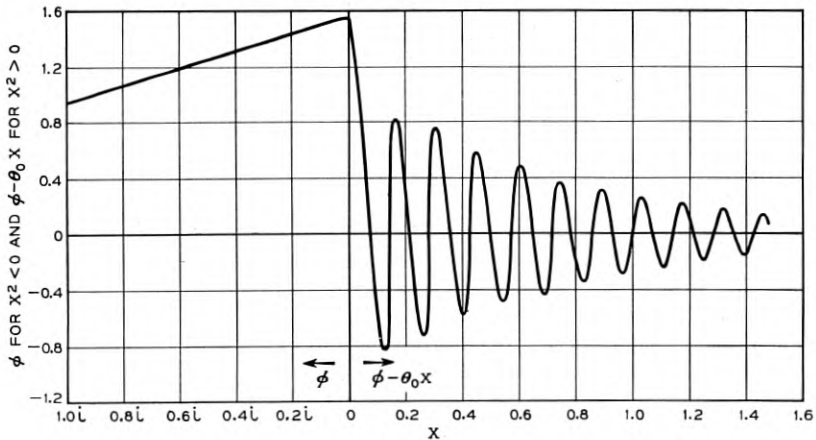
FIG. 5b

Fig. 5 — Phase and amplitude of transmitted circularly polarized wave as a function of $x = \sqrt{1 + \dfrac{p}{1 + \sigma}}$, with $\dfrac{\epsilon}{\epsilon_0} = 10$. (a), top, Φ for $\theta_0 = \pi$ and 3π; (b), bottom, Φ for $\theta_0 = 7\pi$; (c), $|\tau_3|$ for $\theta_0 = \pi$ and 3π; and (d), $|\tau_3|$ for $\theta_0 = 7\pi$.

$|\sigma|$, $|p|$ are found by choosing positive and negative signs for σ and p in

$$x = \sqrt{1 + \frac{p}{1 + \sigma}}.$$

Note that x can be imaginary corresponding to cut-off in the range $-1 < \sigma < -1 - p$ $(p < 0)$.
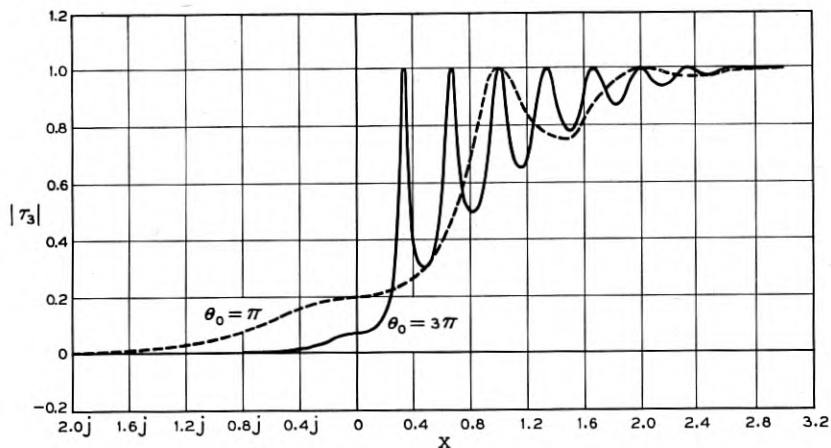
FIG. 5c
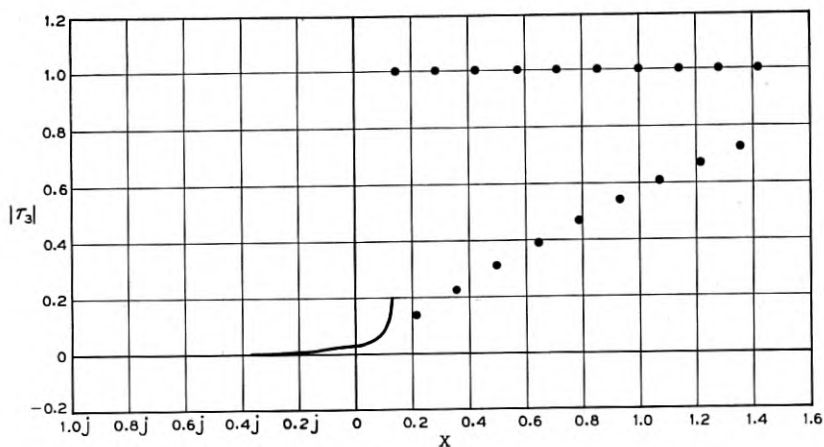
FIG. 5d

Fig. 5(c), top and (d), bottom — See Fig. 5.

Near $x = 1$ (corresponding either to small p or to sufficiently large σ), Φ differs from its value Φ_0 for the isotropic case by a small amount $\delta\Phi$. The rotation, to first order, is then just one half the difference between the $\delta\Phi$ for positive and negative p, σ. Writing

$$x_\pm = 1 + \delta x_\pm = 1 \pm \frac{1}{2}\frac{p}{1 \pm \sigma}$$

and expanding equation (18), we obtain

$$\delta\Phi_{\pm} = \theta_0 \delta x_{\pm} \frac{\cosh \Psi \sec^2 \theta_0 - \dfrac{\tan \theta_0}{\theta_0} \sinh \Psi}{1 + \cosh^2 \Psi \tan^2 \theta_0},$$

where Ψ is defined by

$$a = \sqrt{\frac{\epsilon}{\epsilon_0}} = e^{\Psi}.$$

[This result holds even near $\theta_0 = (n + \frac{1}{2})\pi$ where $\tan \theta_0 = \infty$, as can be seen by expanding the reciprocal of equation (18).] The quantity $\frac{1}{2}\theta_0(\delta x_+ - \delta x_-)$ is the rotation corresponding to a single trip through the sample. The actual rotation is $\frac{1}{2}(\delta\Phi_+ - \delta\Phi_-)$. Hence we may define a *rotation gain* as the ratio

$$g(\theta_0, a) = \frac{\frac{1}{2}(\delta\Phi_+ - \delta\Phi_-)}{\frac{1}{2}\theta_0(\delta x_+ - \delta x_-)},$$

$$= \frac{\cosh \Psi \sec^2 \theta_0 - \dfrac{\tan \theta_0}{\theta_0} \sinh \Psi}{1 + \cosh^2 \Psi \tan^2 \theta_0}. \tag{22}$$

In many cases, $\theta_0 \gg 1$, that is, the thickness of the sample is much greater than a reduced wavelength in the specimen. Then the second term in the numerator of g is always negligible compared with the first. g then simplifies to

$$g_1 = \frac{\cosh \Psi}{\cos^2 \theta_0 + \cosh^2 \Psi \sin^2 \theta_0}.$$

This expression is plotted in Fig. 6 as a function of θ for various $a = e^{\Psi}$. For given Ψ it has minima equal to $\dfrac{1}{\cosh \Psi}$ at $\theta_0 = \left(n + \dfrac{1}{2}\right)\pi$, and maxima equal to $\cosh \Psi$ at $\theta_0 = n\pi (n = 0, 1, 2, \cdots)$. When $a \gg 1$ ($a \sim 3$ for many ferrites), $\cosh \Psi$ is replaced by $\frac{1}{2}e^{\Psi} = \frac{1}{2}a$, and then

$$g_{1\,\text{max}} = \frac{1}{2} a$$

$$g_{1\,\text{min}} = \frac{2}{a}$$

It is to be noted that when $\theta = n\pi$, the condition for maximum g_1, the unperturbed reflected amplitude is zero, and the ellipticity vanishes to first order in δx.
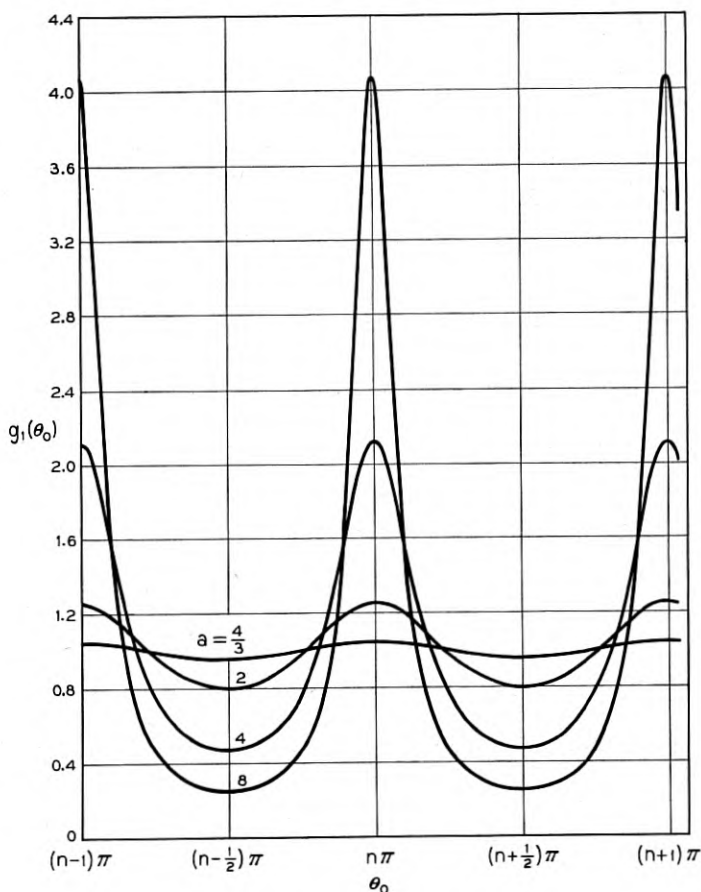
Fig. 6 — Rotation gain, $g_1(\theta_0)$, versus electrical thickness, θ_0, for small magnetization.

Perturbation theory enables us to solve approximately, for weak magnetization, the problem just considered for the case in which a right circular cylinder of ferrite snugly fits a cylindrical waveguide. We will show that, with a suitable reinterpretation of the constants, equation (22) for the rotation gain of the extended slab continues to apply here.

Before magnetization, a particular right circularly polarized mode, say the mth, is present in the sample. The small magnetization distorts the pattern of this mode and changes the propagation constant slightly. The distorted pattern can be expanded in the series of normal modes of the unperturbed material. In these expansions only the coefficient of the

originally present m^{th} mode will be large; all others will at most be of the order of the perturbation. Denoting perturbed quantities by the superfix $+$, we have for the distorted fields

$$E_{tm}^+ = e^{-j\beta_m^+ z} \sum_{n=1}^{\infty} p_{mn} E_{tn} ,$$

$$H_{tm}^+ = e^{-j\beta_m^+ z} \sum_{n=1}^{\infty} q_{mn} H_{tn} ,$$

where p_{mm} and q_{mm} are large compared with the other coefficients. β_m^+ and the p's and q's are determined from equations (7a) and (7b). a_n in these equations is identified with $e^{-j\beta_m^+ z} p_{mn}$, b_n with $e^{-j\beta_m^+ z} q_{mn}$. Since all perturbation integrals involving E_t and H_z, E_z vanish in the present case, we obtain

$$\beta_n q_{mn} - \beta_m^+ p_{mn} = \frac{\omega}{\Delta_n} \left[\int (\mu - \mu_0) H_{tm}^+ \tilde{H}_{tn} \, dS - j \int \kappa H_{tm}^{+*} \tilde{H}_{tn} \, dS \right]$$

and

$$\beta_n p_{mn} - \beta_m^+ q_{mn} = 0.$$

In the first of these equations, H_{tm}^+, the perturbed magnetic field, consists of $q_{mm} H_{tm}$, plus an admixture of other modes with coefficients themselves of order $\mu - \mu_0$, κ. Therefore, to first order, it suffices to write

$$H_{tm}^+ = q_{mm} H_{tm}$$

in the integrand, with the result:

$$\beta_n q_{mn} - \beta_m^+ p_{mn} = I_{mn}^+ q_{mm} ,$$

$$p_{mn} = \frac{\beta_m^+}{\beta_n} q_{mn} ,$$

where

$$I_{mn}^+ = \frac{\omega}{\Delta_n} \int (\mu - \mu_0) H_{tm} \tilde{H}_{tn} - j\kappa H_{tm}^* \tilde{H}_{tn}] \, dS.$$

Elimination of p_{mn} gives

$$(\beta_n^2 - \beta_m^{+2}) q_{mn} = \beta_n I_{mn}^+ q_{mn} .$$

The case $n = m$ determines β_m^{+2}:

$$\beta_m^{+2} = \beta_m^2 (1 - I_{mm}^+/\beta_m). \tag{23}$$

All other cases give, to first order,

$$q_{nm} = \frac{\beta_n I_{mn}^+}{\beta_n^2 - \beta_m^2} q_{mm} ,$$

which, again to first order, equals

$$\frac{\beta_n I_{mn}^+}{\beta_n^2 - \beta_m^2} \, p_{mm} \, . \tag{24}$$

One of the quantities p_{mm}, q_{mm}, is still arbitrary. If it is required that the perturbed field is, to zero order in I_{mn}^+, normalized to the same value as the unperturbed field, it is readily found that one can take

$$p_{mm} = 1, \qquad q_{mm} = \frac{\beta_m}{\beta_m^+} \, .$$

We are now in a position to consider the problem of a right circular mode, say the rth, incident upon the end plane, $z = 0$, of the ferrite cylinder extending to $z = d$. One simplifying feature of this problem is that the unperturbed modes inside, and the modes outside, the sample have the same dependence on radius since the sample fills the whole guide-cross-section. However the modes inside and outside may have different numerical coefficients. Thus, if we distinguish quantities outside the sample by primes, the TE$_{sr}$ mode can be represented outside and inside the sample by

$$E'_{t_{sr}} = E_{t_{sr}} = \nabla^* \psi_{sr} \, ,$$

$$H'_{t_{sr}} = \frac{\beta'_r \, \text{sgn} \, \beta'_r}{\omega \mu_0} \, \nabla \psi_{sr} \, ,$$

$$H_{t_{sr}} = \frac{\beta_r \, \text{sgn} \, \beta_r}{\omega \mu_0} \, \nabla \psi_{sr}$$

Here sgn β means: sign of the propagation direction, $+1$ and -1 for forward and reverse respectively. The function ψ_{sr} is given by

$$\psi_{sr} = J_s \left(u_r \frac{r}{r_0} \right) e^{js\varphi} \, ,$$

where φ is the azimuthal angle, r_0 the guide radius, and u_r the rth zero of $J_s'(x)$. Tor TM modes we have similarly

$$E'_{t_{sr}} = E_{t_{sr}} = \nabla \psi_{sr} \, ,$$

$$H_{t_{sr}} = -\frac{\omega \epsilon_0}{\beta'_r} \left(\triangle^* \psi_{sr} \right) \text{sgn} \, \beta_r \, ,$$

$$H_{t_{sr}} = -\frac{\omega \epsilon_1}{\beta_r} \left(\nabla^* \psi_{sr} \right) \text{sgn} \, \beta_r \, ,$$

where in the definition of the ψ, u_r is replaced by j_r, the rth zero of $J_s(x)$. Since the perturbations considered here do not couple modes with different azimuthal number, s will be considered fixed hereafter, and only the suffix r will be retained.

The field at $z = -0$ (just outside the ferrite) will consist, not only of the incident field and its reflection ρ_r, but also of other modes excited by the perturbation. Taking the incident E_r' to have unit amplitude, we have, from the continuity of tangential electric fields,

$$(1 + \rho_r)E'_{tr} + \sum_{n \neq r} \rho_n E'_{tn} = \sum_n (\tau_{n1} + \tau_{n2}) \sum_\ell p_{n\ell} E_{t\ell},$$
$$= \sum_{n,\ell} (\tau_{n1} + \tau_{n2}) p_{n\ell} E_{t\ell}, \tag{25}$$

where the τ_{n1}, τ_{n2} are respectively the forward and backward traveling amplitudes of the nth perturbed mode. In the same way, we have for the tangential magnetic field:

$$(1 - \rho_r)H'_{tr} - \sum_{n \neq r} \rho_n H'_{tn} = \sum_{n,\ell} (\tau_{n1} - \tau_{n2}) q_{n\ell} H_{t\ell}. \tag{26}$$

The changes in sign of the coefficients of the backward waves have already been explained in Section 1.1. Let us now suppose that the incident mode is the TE_r mode. Multiplying both sides of (25) by $\nabla^*\bar{\psi}_r$ and both sides of (26) by $\nabla\bar{\psi}_r$, and integrating over the cross-section we have, from the orthogonality relations of these functions,

$$1 + \rho_r = \sum_n (\tau_{n1} + \tau_{n2}) p_{nr},$$

$$\beta_r'(1 - \rho_r) = \sum_n \beta_r(\tau_{n1} - \tau_{n2}) q_{nr}.$$

But in these series, all τ except τ_r will be small, as will be all p, q except p_{rr}, q_{rr}. Hence all terms, except those for which $n = r$, will be small of second order, and can be neglected. Further,

$$p_{rr} = 1, \qquad q_{rr} = \frac{\beta_r}{\beta_r^+}.$$

Thus we obtain finally,

$$1 + \rho_r = \tau_{r1} + \tau_{r2},$$

$$1 - \rho_r = (\tau_{r1} - \tau_{r2}) \frac{\beta_r^{2\prime}}{\beta_r'\beta_r^+}.$$

In view of equation (23) for β_r^+, these equations can be written, to

first order in I_{rr}^+,

$$1 + \rho_r = \tau_{r1} + \tau_{r2}$$

$$1 - \rho_r = \frac{\beta_r^+ \mu_0}{\beta_r' \mu_{r+}} (\tau_{r1} - \tau_{r2}) \tag{27}$$

where

$$\mu_{r+} = \mu_0 \left(1 - \frac{I_{rr}^+}{\beta_r} \right).$$

Similarly at the output plane, $z = d$, the transmitted amplitude τ_{r3} satisfies

$$\tau_{r3} = \tau_{r1} e^{-i\theta} + \tau_{r2} e^{i\theta},$$

$$\tau_{r3} = \frac{\beta_r^+ \mu_0}{\beta_r' \mu_{r+}} (\tau_{r1} e^{-i\theta} - \tau_{r2} e^{i\theta}), \tag{28}$$

where $\theta = \beta_r^+ d$. Comparison of equations (27) and (28) with the corresponding equations for the infinite slab shows that they have the same form; however, equations (27) and (28) hold only for small magnetization. Hence only those results for the slab that relate to small magnetization can be generalized to the present case. One such result is that for the rotation gain. If we re-identify variables by

$$\delta x^+ \to \delta x_r^+ = \frac{1}{2} \frac{I_{rr}^+}{\beta_r} = -\frac{1}{2} \frac{I_{rr}^-}{\beta_r},$$

$$\theta_0 \to \theta_r = \beta_r d,$$

$$a \to a_r = \beta_r / \beta_r',$$

we obtain, for the rotation gain,

$$g_r = \frac{\cosh \psi_r \sec^2 \theta_r - \dfrac{\tan \theta_r}{\theta_r} \sinh \psi_r}{1 + \cosh^2 \psi_r \tan^2 \theta_r}, \tag{29}$$

where

$$e^{\psi_r} = a_r = \beta_r / \beta_r'.$$

The formulae and conditions for maximum and minimum rotation gain derived in the previous section, apply here also, in terms of the re-defined variables.

The conversion of part of the incident mode to the sth mode in the transmitted wave can be examined by multiplying the matching equa-

tions by $\nabla^* \tilde{\psi}_s$ or $\nabla \tilde{\psi}_s$ and integrating over the cross-section. It is then found that the transmitted amplitude of the nth mode is

$$\tau_{n3} = 2\gamma_{rn} Z_n \frac{(Z_r + Z_n)(\cos\theta_n - \cos\theta_r) + j(1 + Z_n Z_r)(\sin\theta_n - \sin\theta_r)}{(2Z_n \cos\theta_n + j(Z_n^2 + 1)\sin\theta_n)(2Z_r \cos\theta_r + j(Z_r^2 + 1)\sin\theta_r)},$$

where

$$\theta_r = \beta_r d, \qquad Z_{r,n} = \frac{\beta_r}{\beta_r'}$$

and

$$\gamma_{rn} = \frac{\beta_n I_{rn}^+}{\beta_n^2 - \beta_r^2}.$$

The perturbation theory just outlined assumed a guide closely fitted with a slug of ferrite of finite length, and slightly magnetized. The perturbation consisted in the small changes in permeability. Here we treat another kind of perturbation in which the ferrite does not fill the guide completely, and in which the magnetization can be arbitrarily large, but the sample is a thin lamina, mounted normally to the guide axis which only slightly perturbes the field pattern. Its shape can then be considered arbitrary; its thickness will be assumed uniform and very much smaller than a wavelength in the material.

Under these conditions, the equations for the perturbed amplitudes of the right-circularly polarized n^{th} radial mode are

$$\frac{\partial a_n}{\partial z} + j\beta_n b_n = j\frac{\omega}{\triangle_n}\left[\int (\mu - \mu_0) H_t \tilde{H}_{tn}\, dS - j\int \kappa H_t^* \tilde{H}_{tn}\, dS \right.$$

$$\left. + \int (\epsilon - \epsilon_0) E_z \cdot \tilde{E}_{zn}\, dS\right], \quad (30)$$

$$\frac{\partial b_n}{\partial z} + j\beta_n a_n = j\frac{\omega}{\triangle_n}\left[\int (\epsilon - \epsilon_0) E_t \cdot \tilde{E}_{tn}\, dS\right],$$

in the usual notation. The terms on the right are assumed different from zero only in the range $z, z + \delta z$ occupied by the sample, and the integrals are extended over the cross section of the sample only. E_{tn}, H_{tn} are the mode functions for the empty guide. The fields H_t, E_t, E_z are the actual fields inside the sample. For the first-order calculation E_t and H_t are identical with the incident field and E_z (by continuity of the normal component of D_z) is $\frac{\epsilon_0}{\epsilon}$ times the incident E_z. Now the incident fields may

be taken simply as

$$a_{n0}E_{tn} \; ; \qquad a_{n0}H_{tn} \; , \qquad a_{n0}E_{zn}$$

(since, *in vacuo*, $b_{n0} = a_{n0} \operatorname{sgn} \beta_n$ and $\operatorname{sgn} \beta_n = +1$ for the incident field), and the amplitude a_{n0} may be taken to be unity. Therefore equation (30) may be written

$$\frac{\partial a_n}{\partial z} = j \frac{\omega}{\triangle_n} \left[\int (\mu - \mu_0) H_{tn} \tilde{H}_{tn} \, dS - j \int \kappa H_{tn}{}^* \tilde{H}_{tn} \, dS \right.$$
$$\left. + \int \left(1 - \frac{\epsilon_0}{\epsilon} \right) \epsilon_0 E_{zn} \tilde{E}_{zn} \, dS \right] - j \beta_n b_n \; ,$$

$$\frac{\partial b_n}{\partial z} = j \frac{\omega}{\triangle_n} \int (\epsilon - \epsilon_0) E_{tn} \tilde{E}_{tn} \, dS - j \beta_n a_n \; .$$

We solve these equations by integrating through the small thickness of the sample. Since we are interested only in results of first order in δz, a_n and b_n on the right hand side of these equations may be replaced by a_{n0}, b_{n0}; that is by 1, 1. Writing

$$I_A = \frac{\omega}{\triangle_n} \left[\int (\mu - \mu_0) H_{tn} \tilde{H}_{tn} \, dS - j \int \kappa H_{tn}{}^* \tilde{H}_{tn} \, dS \right.$$
$$\left. + \int \left(1 - \frac{\epsilon_0}{\epsilon} \right) \epsilon_0 E_{zn} \tilde{E}_{zn} \, dS \right],$$

$$I_B = \frac{\omega}{\triangle_n} \int (\epsilon - \epsilon_0) E_{tn} \tilde{E}_{tn} \, dS,$$

we have, upon integration from the incidence plane (1) to the exit plane (2),

$$a_{n2} - a_{n1} = j(I_A - \beta_n) \delta z,$$
$$b_{n2} - b_{n1} = j(I_B - \beta_n) \delta z.$$

a_{n1}, the amplitude at the entrance plane consists of $a_{n0} = 1$, the incident amplitude, plus a small reflected amplitude ρ. Thus $a_{n1} = 1 + \rho$. Similarly b_n consists of $a_{n0} \operatorname{sgn} \beta_n = 1$, and the small reflected amplitude $\rho \operatorname{sgn} \beta_n = -\rho$ (corresponding to a backward wave). b_{n2} is equal to a_{n2} (since the transmitted wave is a forward wave). Hence we have

$$a_{n2} - (1 + \rho) = j(I_A - \beta_n) \, \delta z,$$
$$a_{r2} - (1 - \rho) = j(I_B - \beta_n) \, \delta z.$$

whose solutions for the transmitted and reflected amplitude are

$$a_{n2} = 1 - j\left(\beta_n - \frac{I_A + I_B}{2}\right)\delta z$$

and

$$\rho = j\frac{I_B - I_A}{2}\delta z.$$

Thus, to first order, the transmitted wave only undergoes a phase change, of amount

$$\delta\varphi_+ = \left(\beta_n - \frac{I_A + I_B}{2}\right)\delta z.$$

A similar result applies to a left circular wave; the only difference arises in the contribution

$$-\frac{\omega}{2\triangle_n}\int \kappa H_{tn}{}^* \cdot H_{tn}\, dS$$

to $\frac{I_A}{2}$ which will merely change sign. The remainder of I_A, and also I_B are unchanged. Thus the Faraday rotation of a plane polarized wave, which is one half the difference of the phase change for right and left circular waves, is equal to

$$\frac{\delta\varphi_+ - \delta\varphi_-}{2} = -\frac{\omega}{2\triangle_n}j\int_{\text{area of disc}} \kappa H_{tn}{}^*\tilde{H}_{tn}\, dS\delta z.$$

The integral on the right is real, and, when the disc is circular of radius r_1, is of exactly the type that has already been encountered in the case of the ferrite embedded in a material with the same dielectric constant (Section 1.2). Here, however, κ need not be small, so long as δz is sufficiently small. In using the results of Section 1.2 it must be remembered that the mode functions there related to a dielectric, while here they relate to air-filled guide. When this is taken into account, one obtains for the specific rotation of a TE-mode:

$$\frac{\delta\varphi}{\delta z} = \frac{\beta_m}{(u_{nm}{}^2 - 1)J_n^2(u_{nm})}\left[\frac{n\kappa}{\mu_0}J_n^2\left(u_{nm}\frac{r_1}{r_0}\right)\right], \qquad (31a)$$

a TM-mode:

$$\frac{\delta\varphi}{\delta z} = \frac{\omega^2\mu_0\epsilon_0}{\beta_m j_{nm}{}^2 J_n^{\prime 2}(j_{nm})}\left[\frac{n\kappa}{\mu_0}J_n^2\left(j_{nm}\frac{r_1}{r_0}\right)\right], \qquad (31b)$$

results which show that the rotation in a thin disc is independent of the dielectric constant of the disc.

2. THE PARALLEL PLANE CABLE

Measurements on ferrites are sometimes made by a coaxial cable technique. The ferrite fills a section of the cable, and is magnetized axially. In this section we consider a simplified problem of the same kind: that of wave motion between parallel conducting planes bounding a ferrite slab magnetized in the propagation direction. The characteristic equation for the propagation constant has been established by a number of authors, particularly Van Trier,[1] but as in the case of the cylindrical waveguide, no analysis of the equation in terms of the laboratory variables appears to have been made. We shall make such an analysis by means of the methods already used in Part I for the cylindrical waveguide. The discussion will be limited to the dominant (TEM-limit) mode, and to the principal features of the incipient modes (shape resonances).

The distance between the two conducting boundaries will be denoted by $2a$. The system of axes is as in Fig. 7; the y-axis is perpendicular to the walls (located at $y = \pm a$), the z-axis is the magnetization and propagation direction. The microwave fields are assumed not to vary along the x-axis.

The solution of Maxwell's equation proceeds just as in the case of the cylindrical waveguide (Part I, Section 3), with the simplifying feature that one of the coordinates (x) drops out of the problem. We shall use the reduced notation of Part I. β, the propagation constant will be measured in units of $\omega\sqrt{\mu_0\epsilon}$, the propagation constant of the unmagnetized, unbounded medium. $\bar{a}$ will denote $a\omega\sqrt{\mu_0\epsilon}$, the half-spacing measured in terms of the reduced wavelength $\dfrac{\lambda}{2\pi}$ of the unmagnetized, extended medium.
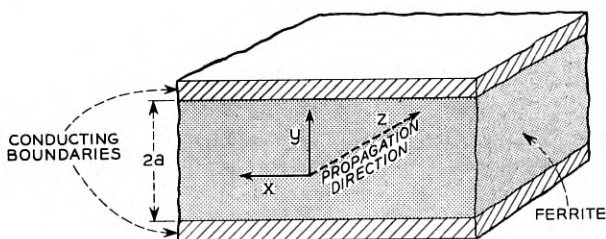
Fig. 7 — Parallel plane cable filled with ferrite magnetized along propagation direction.

It is found that (see Part I, Section 3) the longitudinal electric and magnetic fields are then given by

$$E_z = \frac{\Lambda_2\psi_1 - \Lambda_1\psi_2}{\Lambda_2 - \Lambda_1}; \qquad H_z = j\frac{\psi_1 - \psi_2}{\Lambda_2 - \Lambda_1},$$

where $\psi_{1,2}(y)$ are solutions of

$$\frac{\partial\psi_{1,2}}{\partial y^2} + \chi_{1,2}{}^2\psi_{1,2} = 0, \tag{32}$$

where $\Lambda_{1,2}$ are the roots of the quadratic (16), Part I, and where, finally, the χ's are defined in terms of the Λ by equations (17a) and (17b), Part I. The x-component of E is given by [see equation (22a), Part I]

$$(\Lambda_1 - \Lambda_2)\Omega E_x = \left[\beta\Lambda_1\rho_H - \rho_H^2\nu_H + \nu_H\left(1 - \frac{\beta^2}{\nu_H}\right)\right]\frac{\partial\psi_2}{\partial y},$$

or the same expression with suffixes 1, 2 interchanged. $\bigg($Note that the x component of $\nabla\psi$ is now zero, that of $\nabla^*\psi$ is $\dfrac{\partial\psi}{\partial y}\bigg)$. If the boundary conditions are to be satisfied at both $y = +a$ and $y = -a$, the solutions of equation (32) must be either even or odd functions of y. Since E_z must vanish at $y = \pm a$, we have for the symmetric (or even) case

$$\psi_1{}^s = \Lambda_1\frac{\cos\chi_1 y}{\cos\chi_1 a}; \qquad \psi_2{}^s = \Lambda_2\frac{\cos\chi_2 y}{\cos\chi_2 a},$$

and for the antisymmetric (odd) case

$$\psi_1{}^a = \Lambda_1\frac{\sin\chi_1 y}{\sin\chi_1 a}; \qquad \psi_2{}^a = \Lambda_2\frac{\sin\chi_2 y}{\sin\chi_2 a}.$$

The characteristic equation for these two sets now follows from the fact that $E_x = 0$ at $y = \pm a$. Expressing the Λ's in terms of the χ's by means of equation (17b), Part I, and writing $\beta\Lambda_{2,1} = \lambda_{1,2}$, we obtain

$$\frac{1}{\lambda_1\chi_1{}^2}\chi_1\bar{a}\tan\chi_1\bar{a} = \frac{1}{\lambda_2\chi_2{}^2}\chi_2\bar{a}\tan\chi_2\bar{a}$$

for the symmetric case, and

$$\lambda_1\chi_1{}^2\frac{\tan\chi_1\bar{a}}{\chi_1\bar{a}} = \lambda_2\chi_2{}^2\frac{\tan\chi_2\bar{a}}{\chi_2\bar{a}}$$

for the antisymmetric case. To bring these equations into a form suitable for graphical discussion, we express the χ in terms of λ, σ by means

of the quadratic for λ, and by means of the relations between the tensor components of the permeability (see beginning of Section 4.11, Part I). We then obtain

$$\frac{1}{\lambda_1}\sqrt{\frac{1-\sigma\lambda_1}{1-\lambda_1{}^2}}\,\tan\bar{a}\sqrt{\frac{1-\lambda_1{}^2}{1-\sigma\lambda_1}}$$

$$=\frac{1}{\lambda_2}\sqrt{\frac{1-\sigma\lambda_2}{1-\lambda_2{}^2}}\,\tan\bar{a}\sqrt{\frac{1-\lambda_2{}^2}{1-\sigma\lambda_2}} \qquad (33)$$

for the symmetric modes, and

$$\lambda_1\sqrt{\frac{1-\lambda_1{}^2}{1-\sigma\lambda_1}}\,\tan\bar{a}\sqrt{\frac{1-\lambda_1{}^2}{1-\sigma\lambda_1}} = \lambda_2\sqrt{\frac{1-\lambda_2{}^2}{1-\sigma\lambda_2}}\,\tan\bar{a}\sqrt{\frac{1-\lambda_2{}^2}{1-\sigma\lambda_2}} \qquad (34)$$

for the antisymmetric modes. When λ_1, λ_2 pairs satisfying one of these equations, and the Polder relation

$$\lambda_1 + \lambda_2 - \sigma\lambda_1\lambda_2 = \sigma + p \qquad (35)$$

have been found, β^2 is given by

$$\beta^2 = -\lambda_1\lambda_2 .$$

Appearances to the contrary, equations (33) and (34) describe the ordinary TE and TM modes when $p = 0$, regardless of σ (see the discussion opposite Fig. 3. of Part I). When $\sigma = 0$, the Polder relation transforms $\dfrac{1-\lambda_2{}^2}{1-\sigma\lambda_2}$ into $\dfrac{1-\lambda_1{}^2}{1-\sigma\lambda_1}$, so that either of equations (33) and (34) can be satisfied only by

$$\frac{1-\lambda_1{}^2}{1-\sigma\lambda_1} = \frac{1-\lambda_2{}^2}{1-\sigma\lambda_2} = n^2\,\frac{\pi^2}{\bar{a}^2} \qquad \text{or} \qquad \left(n+\frac{1}{2}\right)^2\frac{\pi^2}{\bar{a}^2}$$

and the two alternatives respectively give

$$-\lambda_1\lambda_2 = \beta^2 = 1 - n^2\,\frac{\pi^2}{\bar{a}^2}$$

or

$$1 - \left(n+\frac{1}{2}\right)^2\frac{\pi^2}{\bar{a}^2} .$$

Since both equations (33) and (34) are satisfied by either the n-, or the $(n + \frac{1}{2})$- dependence, a problem of classification arises: "Which mode, TE or TM, is described, as $p \sim 0$, by the solutions of (33) and (34)?" Leaving aside the question of the TEM mode we note that the following degeneracy exists in the isotropic case:

A TE mode with antisymmetric H_z and a TM mode with symmetric E_z have the same propagation constant

$$\beta^2 = 1 - \frac{\pi^2}{\bar{a}^2}\left(n + \frac{1}{2}\right)^2 \qquad (n = 0, 1, 2 \cdots).$$

A TE mode with symmetric H_z and a TM mode with antisymmetric E_z have the same propagation constant

$$\beta^2 = 1 - \frac{n^2\pi^2}{\bar{a}^2} \qquad (n = 1, 2, \cdots).$$

Since application of a very small magnetization will not destroy the symmetry properties, it follows that the solution of equation (34), and the solution of equation (33), which in the limit $p = 0$ reduce to

$$\beta^2 = 1 - \frac{\pi^2}{\bar{a}^2}\left(n + \frac{1}{2}\right)^2,$$

correspond to a TE-limit and a TM-limit mode respectively. Likewise, the solutions of equation (33) and the solution of equation (34) which in the limit $p = 0$ reduce to

$$\beta^2 = 1 - n^2\frac{\pi^2}{\bar{a}^2}$$

correspond to a TE-limit and a TM-limit mode respectively. When $p \neq 0$, the new β^2 are thus given by different equations, so that the magnetization is seen to have removed the degeneracy of the isotropic case.

In the special case of the TEM limit mode ($\beta^2 = 1$ when $p = 0$) only one of equations (33) and (34) has real roots. For, when $p = 0$, the Polder relation gives

$$\frac{1 - \lambda_1^2}{1 - \sigma\lambda_1} = \frac{1 - \lambda_2^2}{1 - \sigma\lambda_2}, \qquad (36)$$

$$= 0,$$

if β^2 is to equal unity. But equation (36) satisfies equation (34) only [equation (33) would demand $\lambda_1 = \lambda_2$ which is impossible for real β]. Thus the TEM mode exists as the limit of an antisymmetric mode only. In fact it is easily shown that for a value of $\bar{a}$ too small $\left(\text{less than } \frac{\pi}{2}\right)$ to admit any except the TEM mode in the isotropic medium, the only solutions of equation (33) for general σ, p describe incipient modes.

Thus for $\bar{a} < \dfrac{\pi}{2}$ the analysis may be confined to equation (34) which will give the course of the TEM limit mode. The graphical analysis follows closely that of the cylindrical waveguide (Part I, Section 4.1); the part played by the G-function there is now played by the function

$$L = \lambda \sqrt{\frac{1 - \lambda^2}{1 - \sigma \lambda_1}} \tan \bar{a} \sqrt{\frac{1 - \lambda^2}{1 - \sigma \lambda}}.$$

A contour map is drawn of the function L in the upper half of the λ-σ plane. Only the upper half plane need be considered since the L-equation (34) is unchanged by reflection in the origin. This, incidentally, means that the present situation is reciprocal, so that σ, p hereafter can be considered positive. Pairs of values $\lambda_1(>0)$ and $\lambda_2(<0)$ satisfying the L-equation can then immediately be read off, but while they will give $\beta^2 = \lambda_1 \lambda_2$, they do not necessarily, for given σ, p, satisfy the Polder relation, equation (35). To ensure this, the quadrant, $\lambda < 0$, $\sigma > 0$, and the L-contours therein are transformed on to $\lambda > 0$, $\sigma > 0$ by the Polder relation for fixed p:

$$\lambda_2 = \frac{\sigma + p - \lambda_1}{1 - \sigma \lambda_1} = T(\lambda_1).$$

The surfaces $L_1 = L(\lambda_1, \sigma)$ and $L_2 = L(T(\lambda_1), \sigma)$ will intersect in a number of curves, along whose base curves in the λ-σ plane both the Polder equation and the L equation are satisfied, and along which $\beta^2 = -\lambda_1 \lambda_2$ is known as a function of σ, p. The zero and infinity curves of $L(\lambda, \sigma)$ are denoted by 0, I when $\lambda > 0$, and by $0'$, I' when $\lambda < 0$. The transforms of $0'$, I' onto $\lambda > 0$ are denoted by $(0')_T$, $(I')_T$. The suffix n denotes the infinity (zero) curves corresponding to

$$\frac{1 - \lambda^2}{1 - \sigma \lambda} = \left(n + \frac{1}{2}\right)^2 \frac{\pi^2}{\bar{a}^2}; \qquad \left(\frac{1 - \lambda^2}{1 - \sigma \lambda} = n^2 \frac{\pi^2}{\bar{a}^2}\right) \quad n \text{ integral.}$$

The lines $\lambda = 0$, $+1$, -1, are all zero curves denoted by 0_A, 0_B, $0_B'$, respectively. The line $\lambda \sigma = 1$ is a conditional infinity curve, called I_c. It is an I curve when viewed from $\sigma \lambda > 1$ for $\lambda < 1$, and when viewed from $\sigma \lambda < 1$ for $\lambda > 1$. Otherwise (for $\sigma \lambda < 1$, $\lambda < 1$ and $\sigma \lambda > 1$, $\lambda > 1$) it is a limit curve of all possible curves $L = $ const., where the constant takes on any value indefinitely many times. (See Part I, Section 4, where the curve $\sigma \lambda = 1$ is a conditional zero curve, 0_c.) Fig. 8, drawn for $\bar{a} \sim 1$, $p \sim 0.5$, shows the part of the first quadrant allowed by the Polder relation divided into regions of like and unlike sign of $L(\lambda, \sigma)$ and $L(T(\lambda_1, \sigma))$ by the various 0, I and $(0')_T$, $(I')_T$ curves. The un-

shaded regions are regions of like sign, and all these carry solution curves (dotted lines), by the same reasoning as was employed in Part I, Section 4.11. Two branches of the TEM limit mode exist; in the area bounded by $(0_A)_T$, 0_B, $(0_B')_T$ and in the area 0_B, I_1, $(0_B')_T$. The branch in the first region begins at $\sigma = 0$ with λ_1, λ_2 given by

$$\lambda_1 \sqrt{1 - \lambda_1^2} \tan \bar{a} \sqrt{1 - \lambda_1^2} = \lambda_2 \sqrt{1 - \lambda_2^2} \tan \bar{a} \sqrt{1 - \lambda_2^2},$$

$$\lambda_1 + \lambda_2 = p$$

and ends at the intersection of $(0_A)_T$, 0_B with $\sigma = 1 - p$ and $\beta^2 = 0$ (since $\lambda_2 = 0$ on $(0_A)_T$). The branch in the region 0_B, I_1, $(0_B')_T$ begins with $\beta_2 = \infty$, $\sigma = 1$ and proceeds towards $\sigma = \infty$, $\beta^2 = 1$.

The region bounded by I_1, $(0_A)_T$, I_c contains an infinity of solution curves, the incipient modes. The nth of these begins at $\sigma = 1$, $\lambda_1 = 1$, the intersection of I_n and I_c (the line I_c is also the transform of $\lambda_2 = -\infty$,
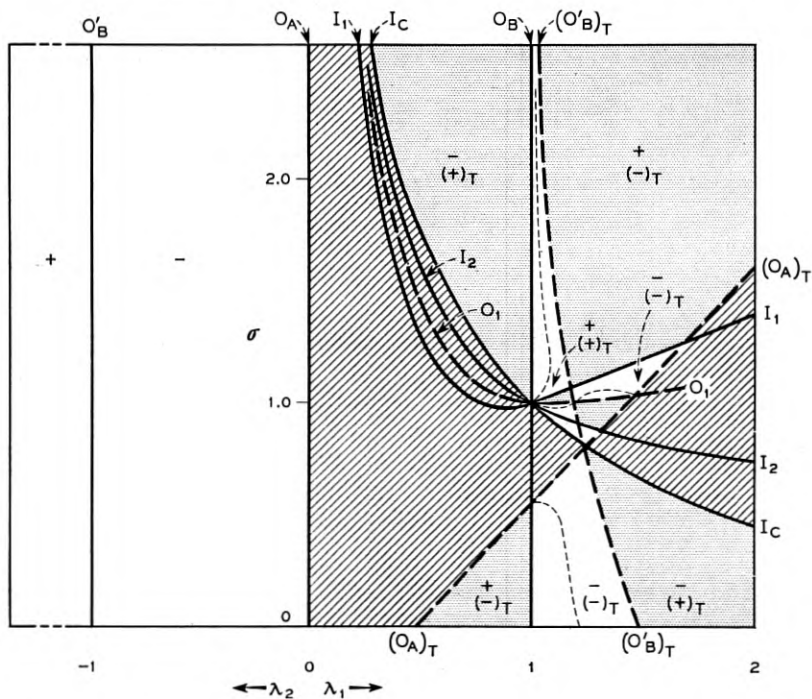
Fig. 8 — Zero and infinity contours of $L(\lambda_1, \sigma)$ and $L(T(\lambda_1), \sigma)$ in the first quadrant of the λ - σ plane. Cross-hatched regions are excluded by the Polder relation; shaded areas are regions of unlike sign of the two functions. Dotted curves are solution curves.

along which $L_2 = \infty$); crosses from one allowed region to the next through the intersection of 0_n with $(0_{B'})_T$ and proceeds to its cut-off point $(0_n - (0_A)_T)$.

Formulae giving β^2 in the neighborhood of special points on the solution curves, or for special values of the parameters, are obtained exactly as in Part I, by expansion of the L-equation. The results are tabulated below. They relate to antisymmetric modes only.

Cut-off of the TEM-limit mode ($\sigma = 1 - p$, $\beta^2 = 0$)

Near cut-off

$$\frac{d\beta^2}{d\sigma} = -\frac{1}{p\left(1 - \dfrac{\tan \bar{a}}{2\bar{a}}\right)} \tag{37}$$

For $p > 1$, the TEM mode has no lower branch.

Behavior near resonance ($\sigma = 1$):

$$\text{TEM mode: } \beta^2 = \frac{\dfrac{\pi^2}{8\bar{a}^2}}{1 - \sigma} p,$$

$$n^{\text{th}} \text{ incipient mode: } \beta^2 = \left(\frac{\left(n + \dfrac{1}{2}\right)^2 \pi^2}{2\bar{a}^2} - 1\right)\frac{p}{1 - \sigma}. \tag{38}$$

$$(n = 1, 2, \cdots)$$

Cut-off of the nth incipient mode (parametric representation):

$$\lambda_1 = e^{\theta}; \qquad \sigma = e^{-\theta}\left(1 - \frac{\bar{a}^2}{n^2\pi^2}\right) + \frac{\bar{a}^2}{n^2\pi^2} e^{\theta}$$

$$p = \sigma - \lambda_1; \qquad \beta^2 = 0 \tag{39}$$

$$\frac{d\beta^2}{d\sigma} = \frac{m^2\pi^2}{\bar{a}^2}\left(\frac{m^2\pi^2}{\bar{a}^2} - 1\right)\coth \theta \Bigg/ \left[\left(\frac{m^2\pi^2}{\bar{a}^2} - 1\right)e^{-\theta} + \frac{2\tan \bar{a}}{\bar{a}} e^{-\theta} - e^{\theta}\right].$$

(The reader may note the similarities of these formulas to those for the cylindrical waveguide).

Spot-point for the nth incipient mode:

$$\sigma = \left[\left(1 - \frac{\bar{a}^2}{n^2\pi^2}\right)\Big/ \beta^2\right] + \frac{\bar{a}^2}{n^2\pi^2} \beta^2,$$

$$p = (1 + \sigma)(\beta^2 - 1). \tag{40}$$

Approximate formulae for all antisymmetric modes at small p, $\sigma \neq 1$:

$$\text{TM modes: } \beta^2 = \beta_{n,1}{}^2 \frac{\sigma p}{1 - \sigma^2}, \tag{41}$$

$$\text{TE modes: } \beta^2 = \beta_{n,2}{}^2 \left(1 - \frac{\sigma p}{1 - \sigma^2} \right), \tag{42}$$

where

$$\beta_{n,1}{}^2 = 1 - \frac{n^2 \pi^2}{\bar{a}^2} \qquad n = 1, 2, \cdots$$

and

$$\beta_{n,2}{}^2 = 1 - \frac{\left(n + \frac{1}{2} \right)^2 \pi^2}{\bar{a}^2} \qquad n = 0, 1, 2, \cdots$$

TEM mode:

$$\beta^2 = 1 - \frac{\sigma p}{1 - \sigma^2}. \tag{43}$$

TEM mode for large σ:

$$\beta^2 = 1 + \frac{p}{\sigma} + O\left(\frac{1}{\sigma^3} \right). \tag{44}$$

TEM mode for very small $\bar{a}$:

for sufficiently small $\bar{a}$, the β^2 for the TEM mode is independent of $\bar{a}$. For general σ, p, except $\sigma = 1$,

$$\beta^2 = \frac{1 - (\sigma + p)^2}{1 - \sigma p - \sigma^2}. \tag{45}$$

Reference to the expression for μ and κ in terms of σ, p will show that the wave progresses as though the medium had a scalar permeability μ_{eff} given by

$$\frac{1}{\mu_{\text{eff}}} = \frac{1}{2}\left(\frac{1}{\mu + \kappa} + \frac{1}{\mu - \kappa} \right).$$

3. FIELD PATTERNS IN THE FILLED CIRCULAR GUIDE

In Part I we discussed propagation in a circular guide filled with ferrite and longitudinally magnetized. Formulae or the field com-

ponents were given there, and it is of some interest to examine numerically or graphically the distribution of E and H. Since all field components vary (in complex notation) as $e^{j(n\theta + \omega t)}$, with $n = 1$ in the present case, it is clear that the field patterns are stationary in a system rotating with angular velocity, $-\omega$. Writing Φ for the angular variable, $\theta + \omega t$, in this system, one finds the following formulas:

$$
\begin{aligned}
E_x &= -E_- \sin 2\Phi, & E_r &= (E_+ - E_-) \sin \Phi, \\
E_y &= E_- \cos 2\Phi + E_+, & E_\theta &= (E_+ + E_-) \cos \Phi, \\
E_z &= E_0 \cos \Phi, & & \hspace{2cm} (46) \\
H_x &= H_- \cos 2\Phi + H_+, & H_r &= (H_+ + H_-) \cos \Phi, \\
H_y &= H_- \sin 2\Phi, & H_\theta &= (H_- - H_+) \sin \Phi, \\
H_z &= H_0 \sin \Phi,
\end{aligned}
$$

where

$$
E_-(r) = \frac{\beta\left(\dfrac{1}{\lambda_1} + 1\right)}{2\chi_1 J_1(\chi_1 r_0)} J_2(\chi_1 r) - \begin{bmatrix} \\ \\ \end{bmatrix}_2,
$$

$$
E_+(r) = \frac{\beta\left(1 - \dfrac{1}{\lambda_1}\right)}{2\chi_1 J_1(\chi_1 r_0)} J_0(\chi_1 r) - \begin{bmatrix} \\ \\ \end{bmatrix}_2,
$$

$$
H_-(r) = -\frac{1 + \dfrac{1 - \chi_1^2}{\lambda_1}}{2\chi_1 J_1(\chi_1 r_0)} J_2(\chi_1 r) - \begin{bmatrix} \\ \\ \end{bmatrix}_2, \hspace{1cm} (47)
$$

$$
H_+(r) = \frac{-1 + \dfrac{1 - \chi_1^2}{\chi_1}}{2\chi_1 J_1(\chi_1 r_0)} J_0(\chi_1 r) - \begin{bmatrix} \\ \\ \end{bmatrix}_2,
$$

$$
E_0(r) = \frac{J_1(\chi_1 r)}{J_1(\chi_1 r_0)} - \begin{bmatrix} \\ \\ \end{bmatrix}_2,
$$

$$
H_0(r) = -\frac{1}{\lambda_1} \frac{J_1(\chi_1 r)}{J_1(\chi_1 r_0)} - \begin{bmatrix} \\ \\ \end{bmatrix}_2.
$$

The terms in square brackets are in each case the same as the corresponding unbracketed terms, λ_2 and χ_2 replacing λ_1 and χ_1. The quantities E_+ and E_- are the amplitudes of the left-handed and right-handed components of circular polarization into which the transverse E-field may be resolved at each point. H_+ and H_- have a similar significance

for the transverse H-field. This may be readily verified by examining the vectors $(E_x + jE_y)e^{-j\omega t}$ and $(H_x + jH_y)e^{-j\omega t}$, which represent the transverse field vectors in the laboratory system. The transverse fields are elliptically polarized at any point and the ratio of minor to major axes of the ellipses are

$$\frac{||E_+| - |E_-||}{||E_+| + |E_-||} \quad \text{and} \quad \frac{||H_+| - |H_-||}{||H_+| + |H_-||}.$$

The fields so far are normalized only by the choice of a simple form for the function, $E_0(r)$; all components may, of course, be multiplied by the same arbitrary constant. There is some virtue to a normalization based upon power flow. The power flow is given in unreduced units by

$$\int_{\text{guide}} (E \times H)_z \, dS.$$

Using the scaled units of part I with

$$r_{\text{actual}} = \frac{r}{\omega \sqrt{\mu_0 \epsilon}}$$

and H replaced by $\sqrt{\frac{\mu_0}{\epsilon}} H$ to give it the same dimensions as E (ϵ is the dielectric constant of the ferrite), the power flow becomes in the present variables

$$P = -\sqrt{\frac{\epsilon}{\mu_0}} \frac{\pi}{\omega^2 \mu_0 \epsilon} \int (E_+ H_+ + E_- H_-) \, r \, dr,$$

$$= -\sqrt{\frac{\epsilon}{\mu_0}} \frac{\pi}{\omega^2 \mu_0 \epsilon} I.$$

We shall normalize the E and H fields by dividing the values given by equations (47) by $I^{1/2}$. This makes the power per (isotropic wavelength in the ferrite)^2 a constant. In Fig. 9 we show the normalized fields for the TE_{11}-limit and TM_{11}-limit modes as a function of r for the case $r_0 = 5.75$, $|p| = 0.6$ and several values of σ. The behavior of the modes as a function of σ and p for this radius is shown in Fig. 14 of Part I. We also show the amplitudes for the isotropic cases, $\sigma = p = 0$. It may be recalled from the discussion of cut-off points in Part I that, for the TM mode at this radius, when cut-off is reached at $\sigma = -0.4$, the amplitude of the H^+ field is overwhelmingly greater than that of the others. Even when normalized to the same power flow, the field amplitudes for a given σ are undetermined to a factor of ± 1. This factor has been
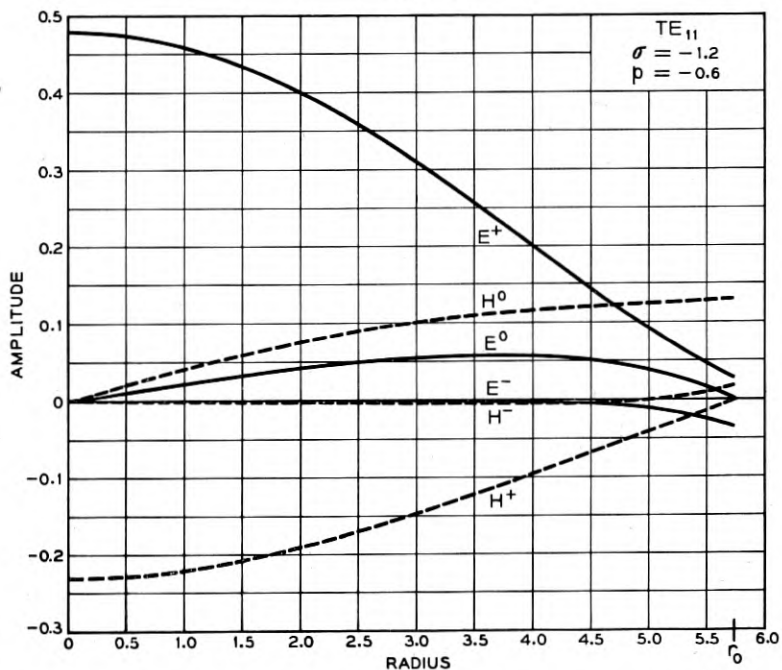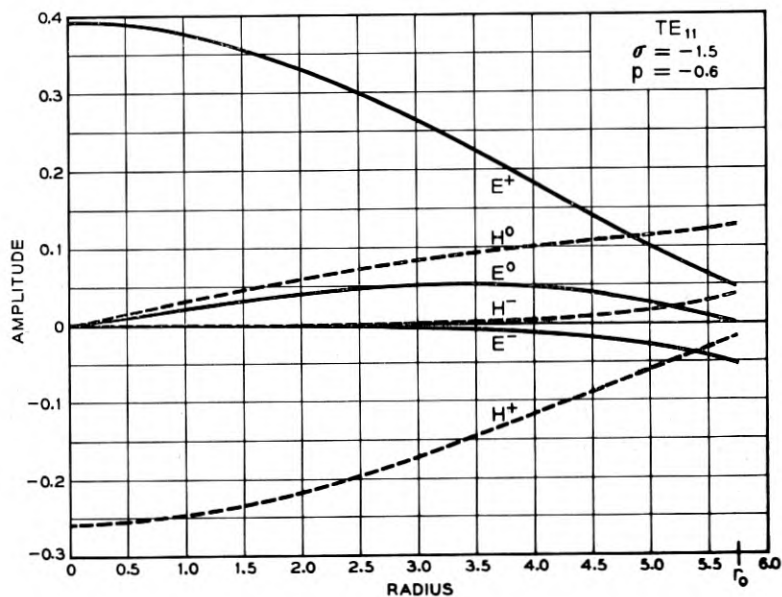
Fig. 9 — Amplitude of the field components in filled cylindrical guide, longitudinally magnetized, as a function of radius, for the TE_{11}-limit and TM_{11}-limit modes at several values of σ. $r_0 = 5.75$. $|p| = 0.6$, except for Figs. 9(f) and (p) which are the isotropic cases, $\sigma = p = 0$. The fields are normalized to a constant power flow per (free space wavelength)². (a), top, (b), bottom.
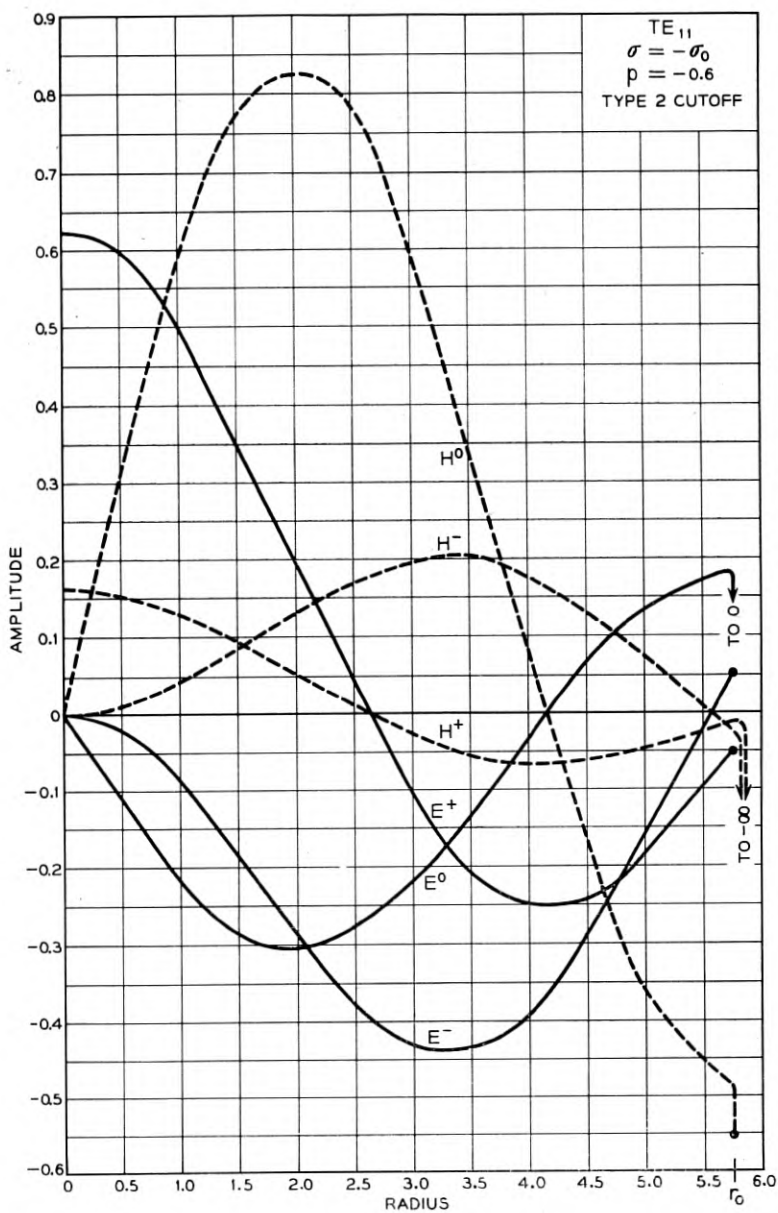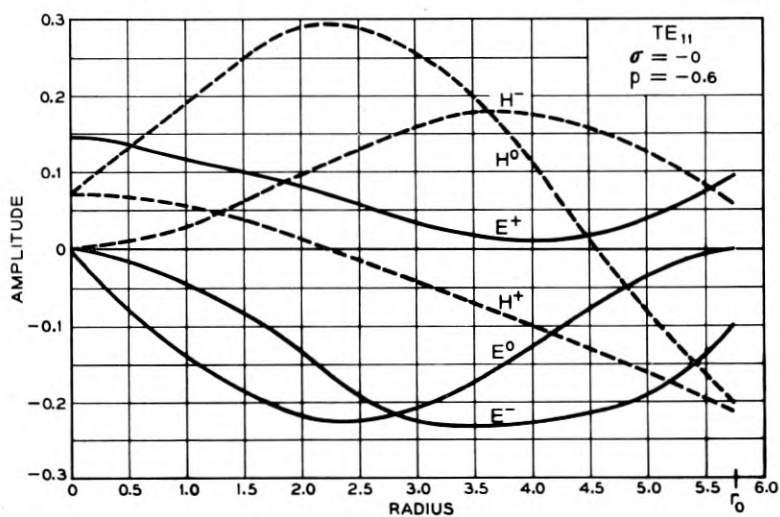
Fig. 9(c) — See Fig. 9.
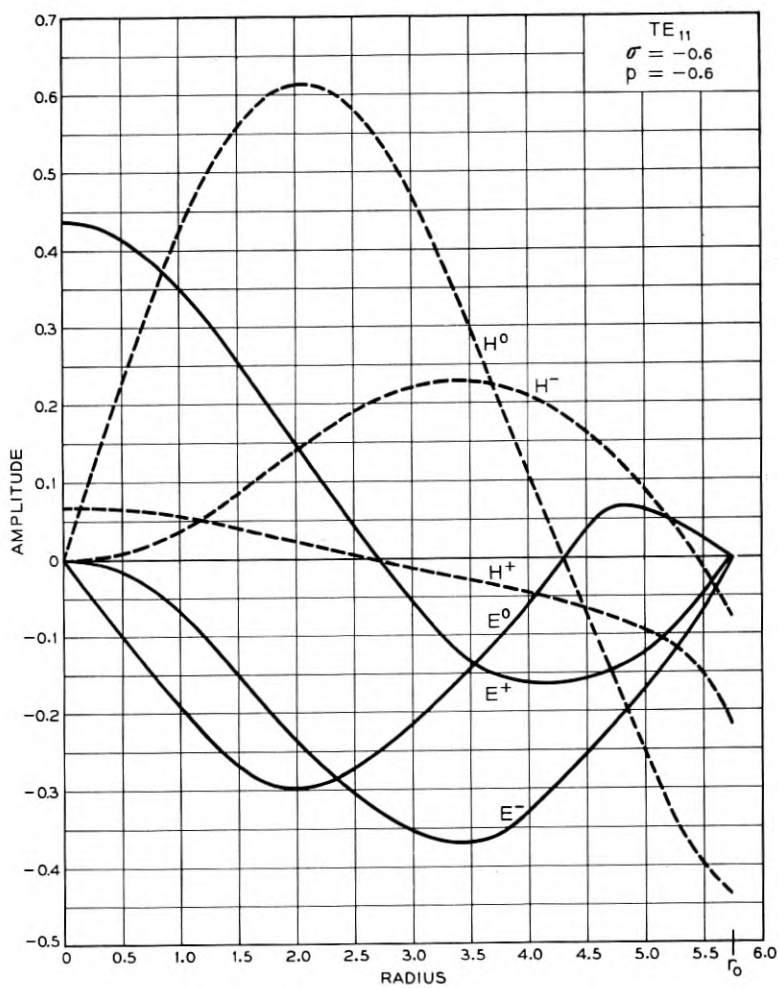
Fig. 9(d) — See Fig. 9.
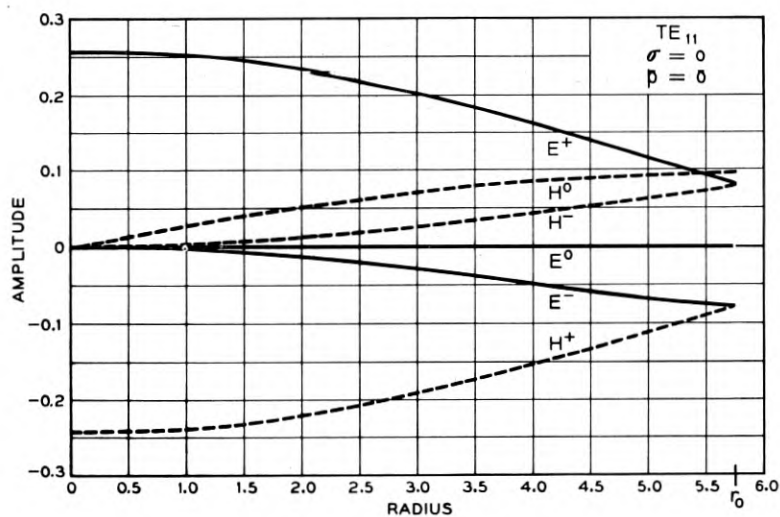
Fig. 9(e), top, and (f), bottom — See Fig. 9.
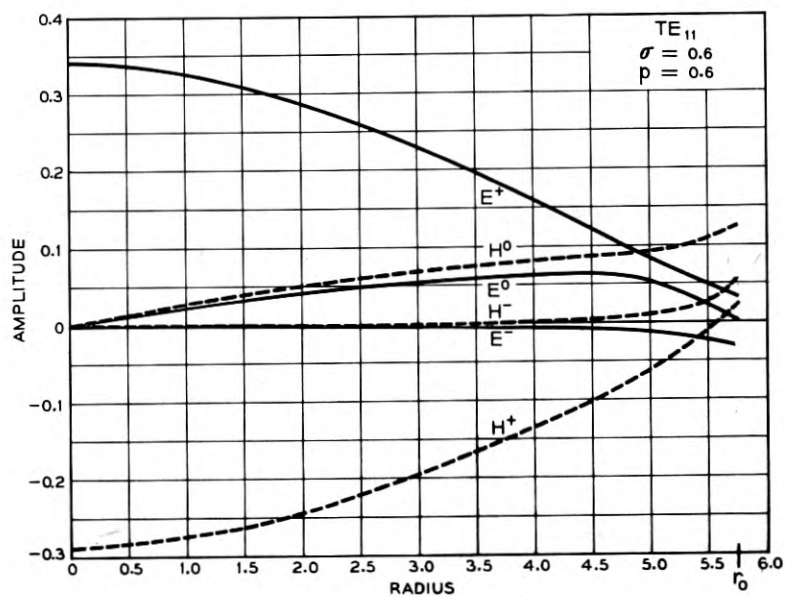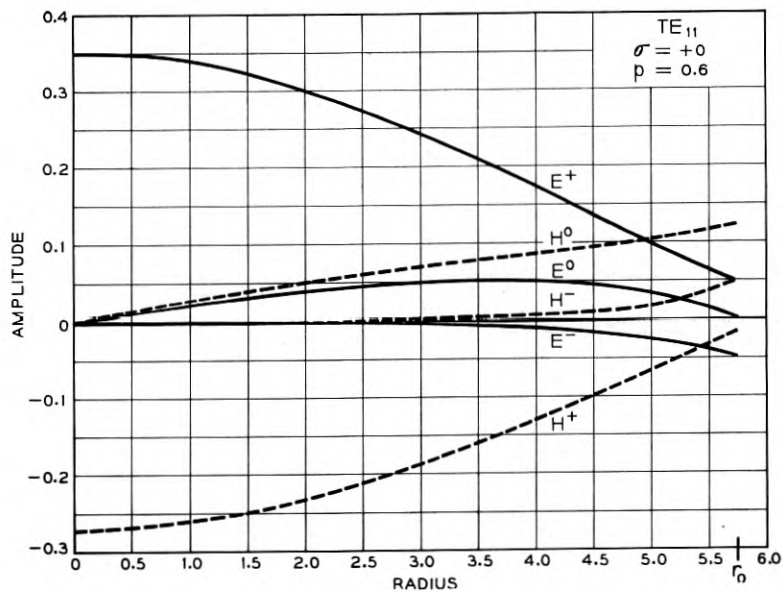
Fig. 9(g), top, and (h), bottom — See Fig. 9.
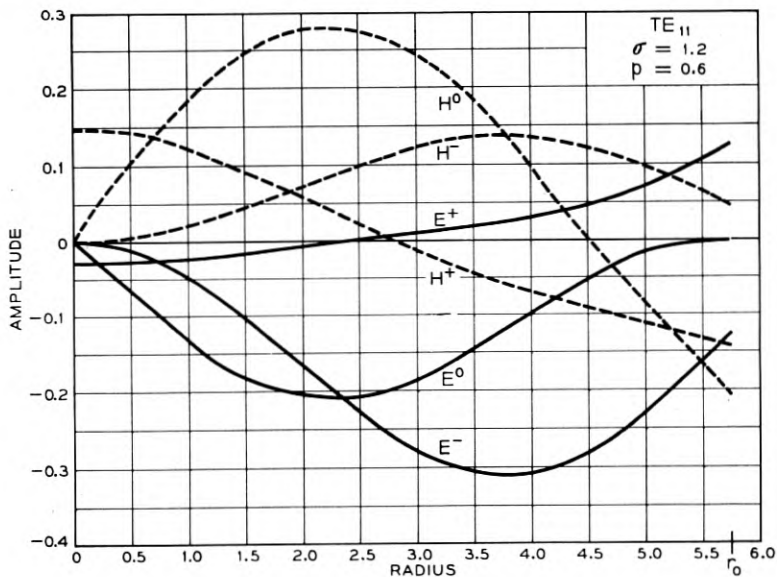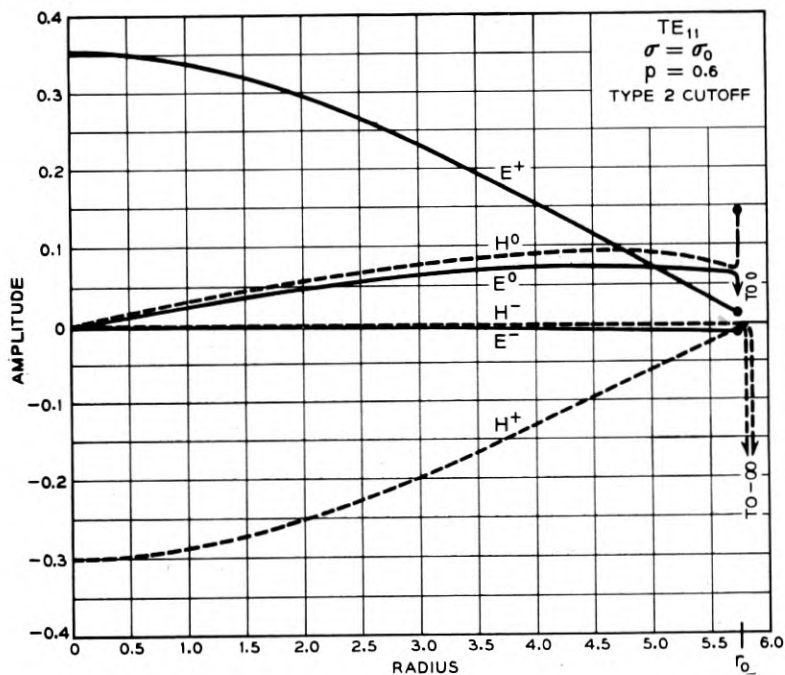
Fig. 9(i), top, and (j), bottom — See Fig. 9.
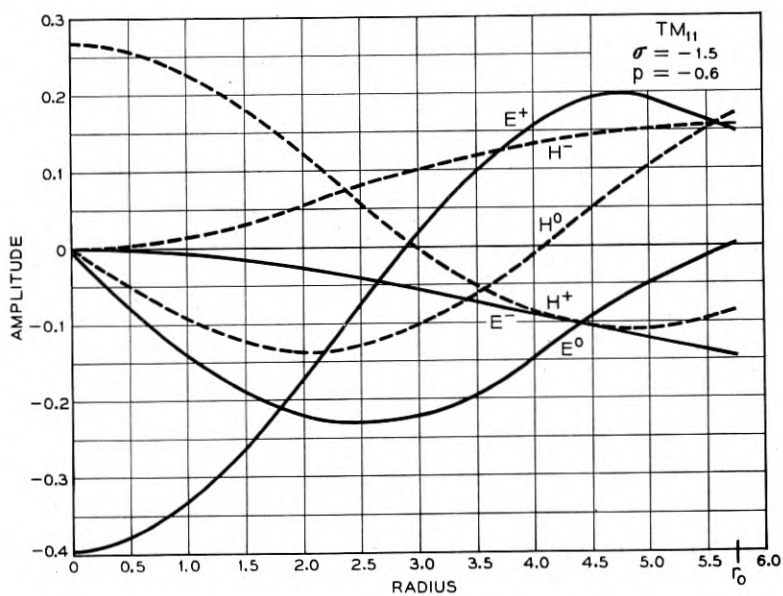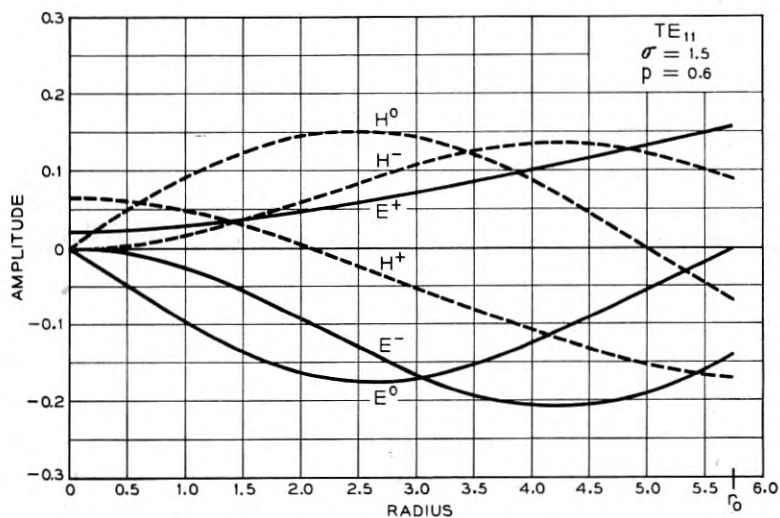
Fig. 9(k), top, and (l), bottom — See Fig. 9.
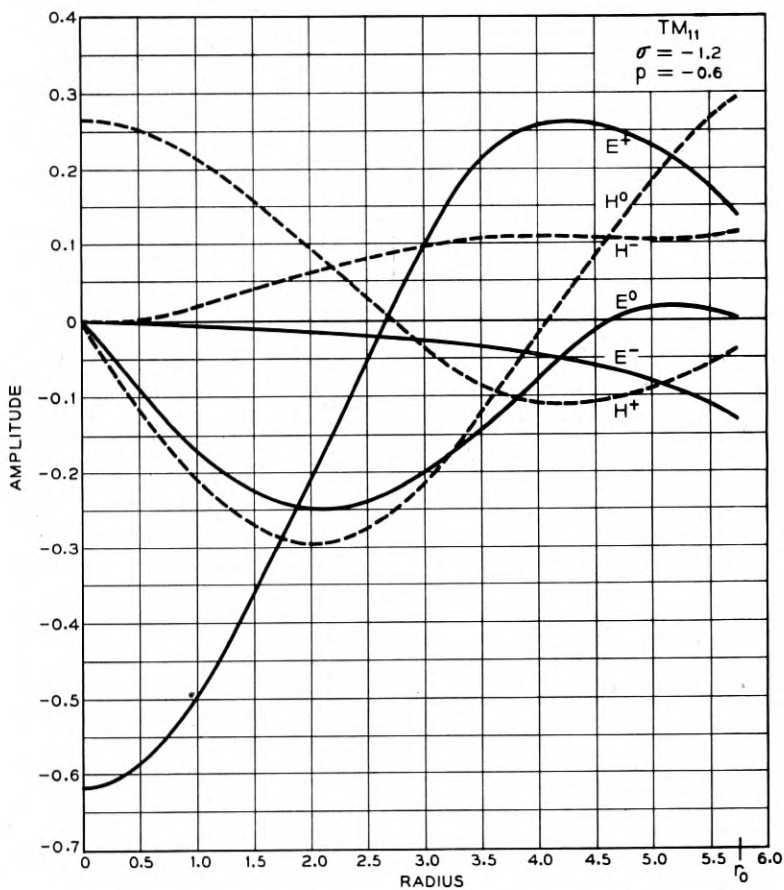
Fig. 9(m) — See Fig. 9.
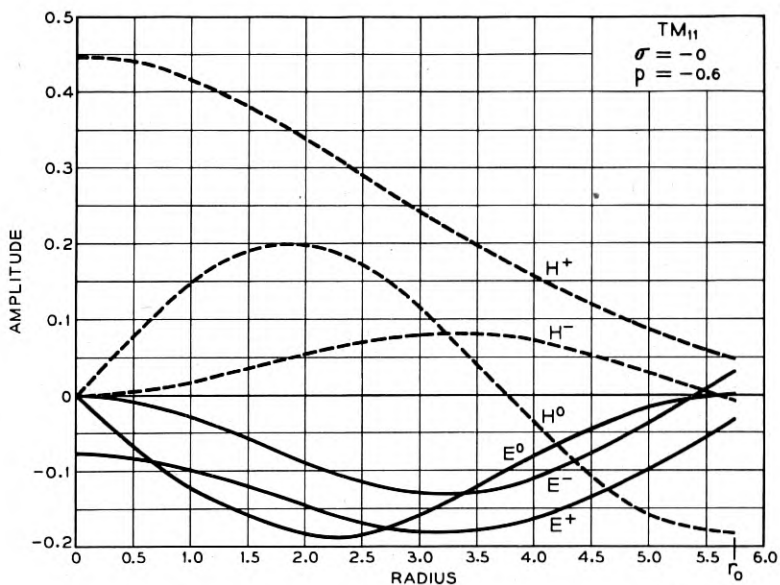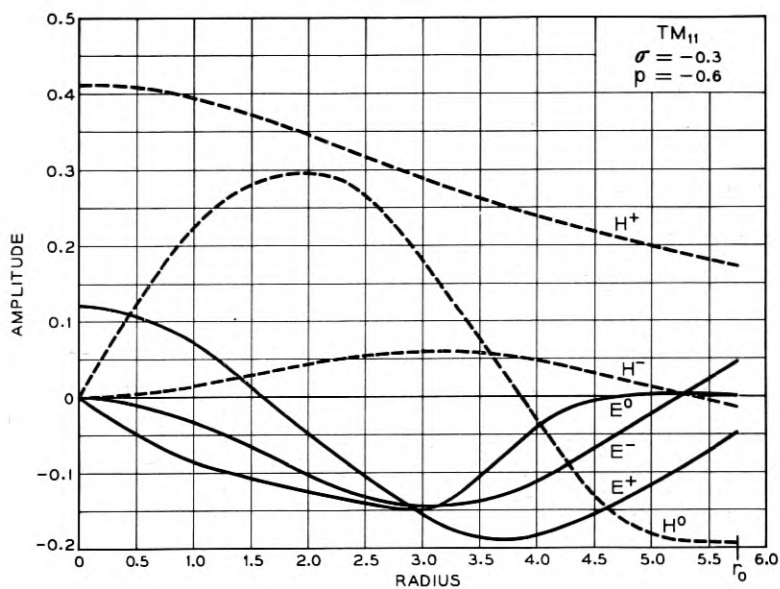
Fig. 9(ᴎ), top, and (o), bottom — See Fig. 9.
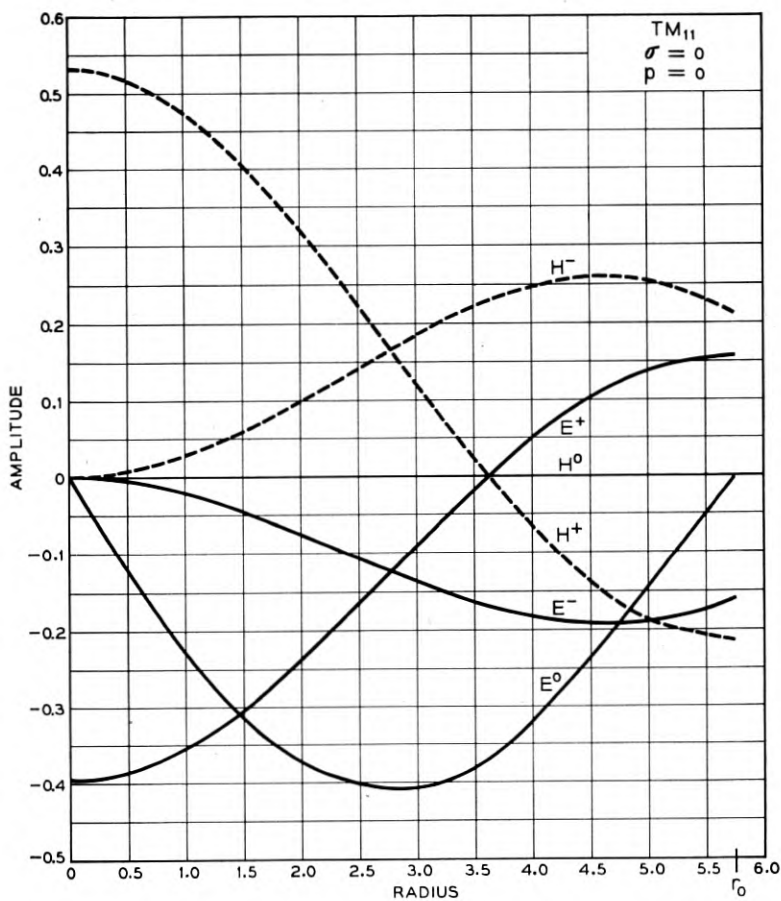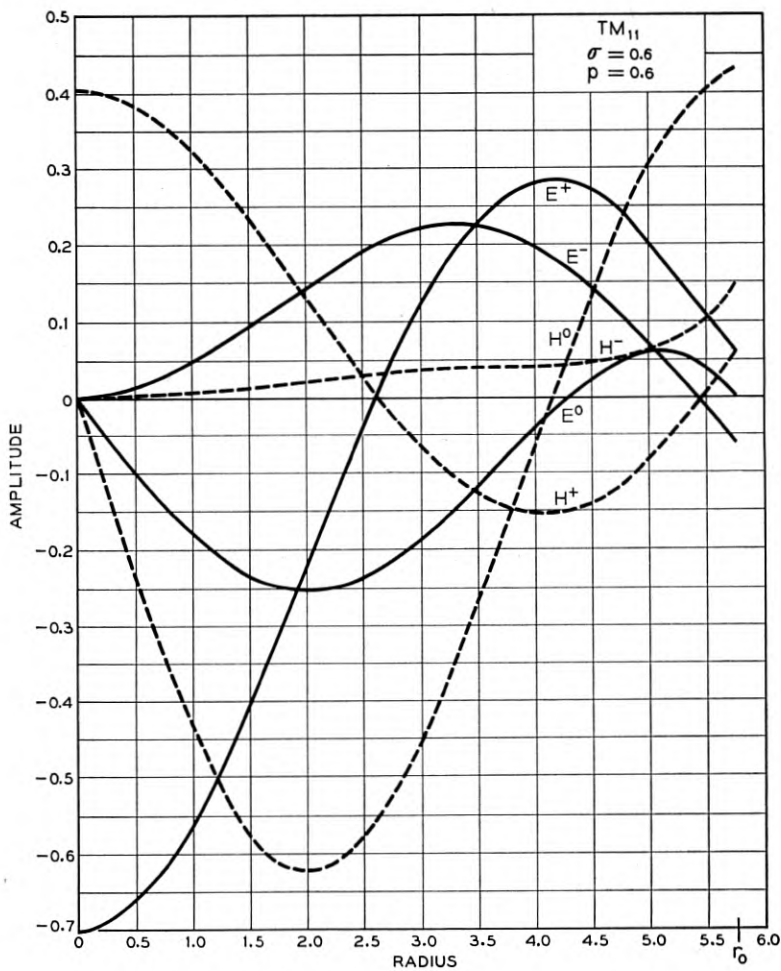
Fig. 9(p) — See Fig. 9.
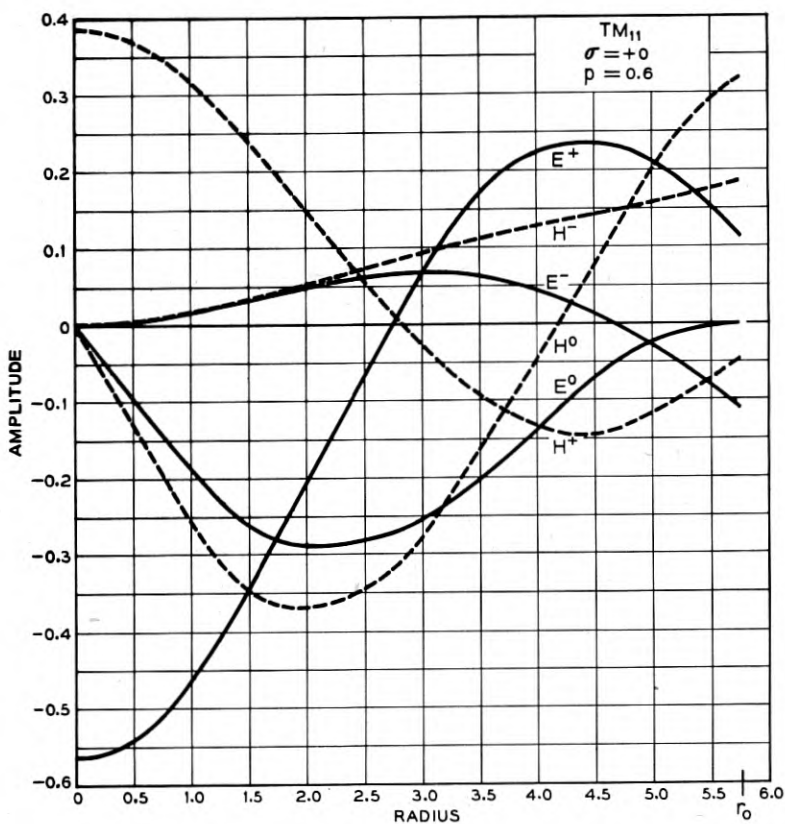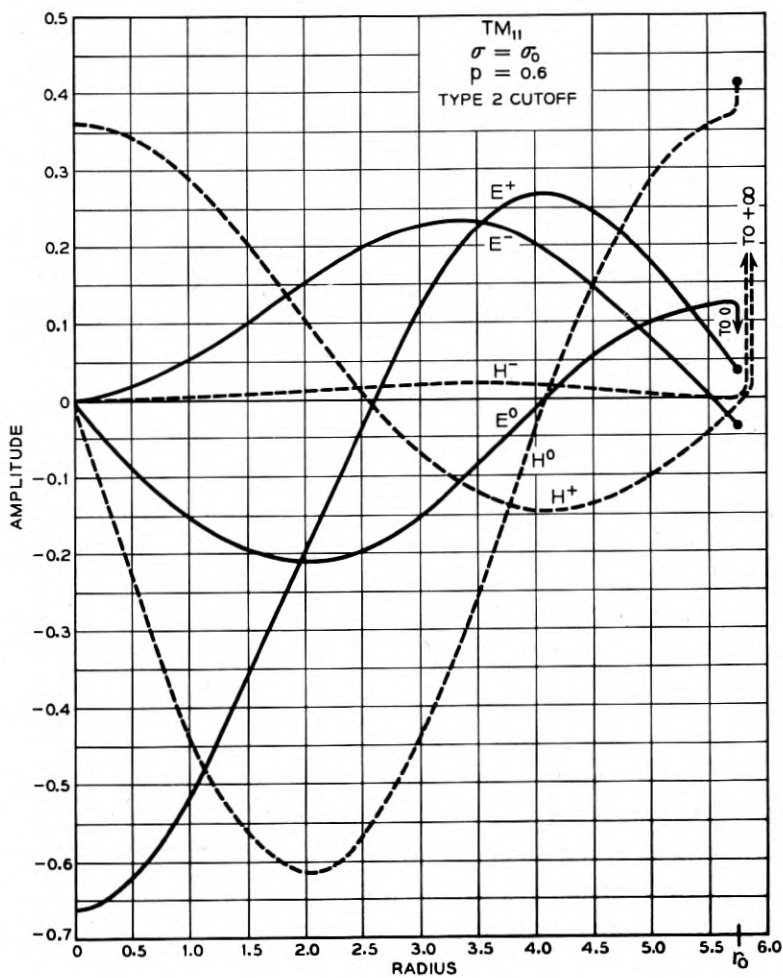
Fig. 9(q) — See Fig. 9.
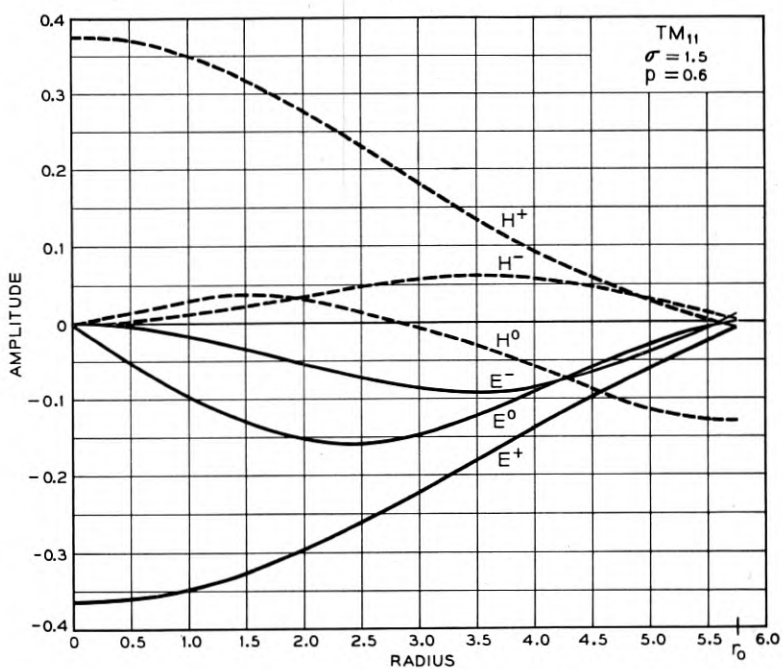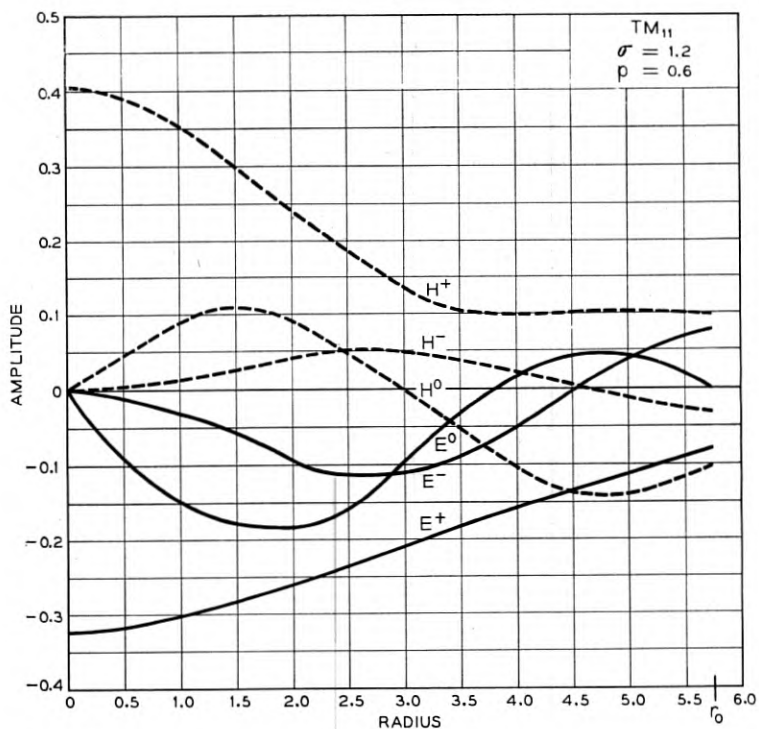
Fig. 9(r) — See Fig. 9.

Fig. 9(s) — See Fig. 9.

Fig. 9(t), top, and (u), bottom — See Fig. 9.

1191

chosen for each pattern according to the following considerations. For large $|\sigma|$ the amplitudes should tend to those of the isotropic case; for $|\sigma| < \sigma_0$ the amplitudes should develop with increasing $|\sigma|$ away from the isotropic amplitudes. Thus, if the phase of the isotropic amplitudes is first fixed, that of all the others may be fixed by the conditions that
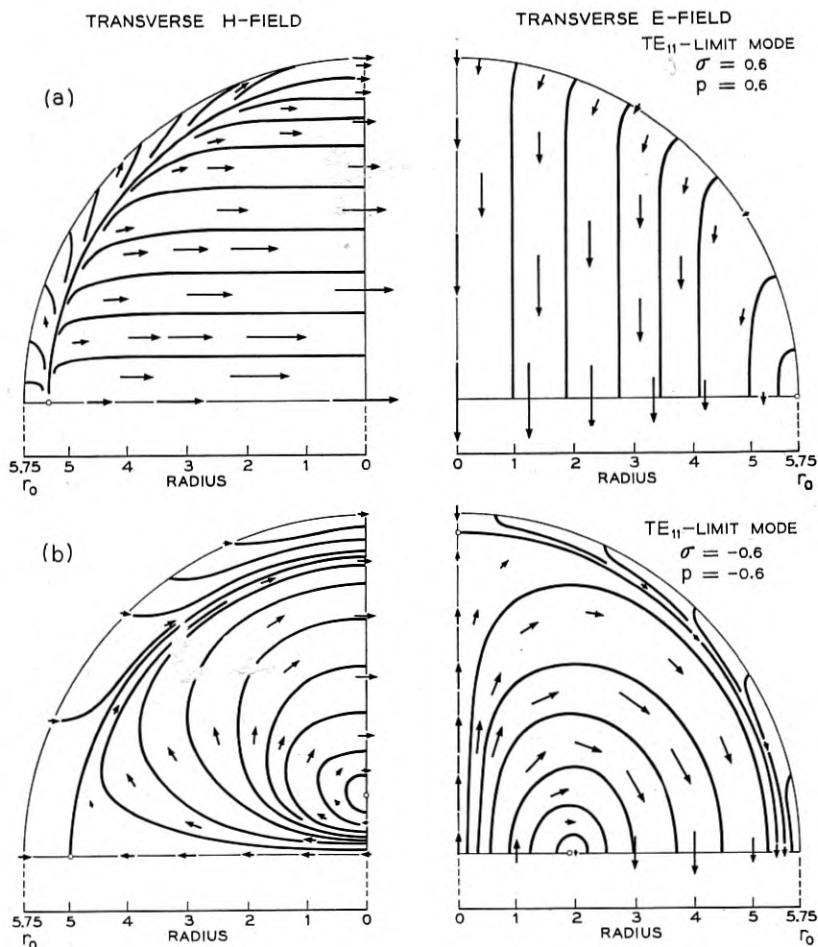

Fig. 10 — Transverse field patterns in a rotating system for four particular cases of Fig. 9. For any pair of E and H patterns the length of the arrows is proportional to field strength, but the patterns for different σ-values have not been given a common normalization. (a), top, TE_{11}-limit mode, $\alpha = 0.6$, $p = 0.6$; (b), bottom, TE_{11}-limit mode, $\sigma = -0.6$, $p = -0.6$; (c), TM_{11}-limit mode, $\sigma = 0.6$, $p = 0.6$; and (d), $\sigma = -0.3$, $p = -0.6$.

they shall fall into an orderly sequence. In Fig. (10) the actual transverse E- and H- field patterns are shown for some representative cases.

It will be noted from Fig. 9 that for both TE- and TM-limit modes, the amplitude patterns for $0 < \sigma < \sigma_0$ resemble those for $\sigma < -1$, while those for $-\sigma_0 < \sigma < 0$ resemble those for $1 < \sigma$. Further, the patterns in the first two ranges of σ are quite similar to the isotropic patterns; those of the latter ranges depart markedly from the isotropic. All of these similarities are more clearly seen for the TE modes than for
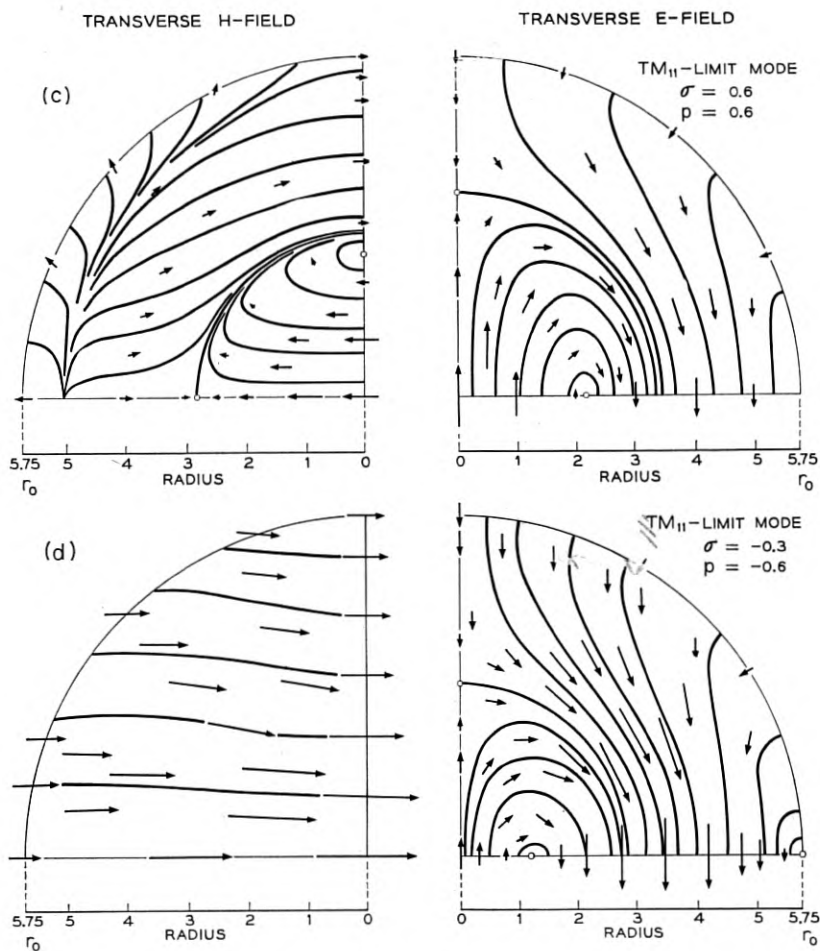

Fig. 10(c), top, and (d), bottom — See Fig. 10.

the TM modes. In Part I where the propagation in guides of very large radius was briefly examined, it may be recalled that in both of the ranges $0 < \sigma < \sigma_0$ and $\sigma < -1$ the field patterns approached those of a plane wave rotating in the same sense as the pattern as a whole. Again, it was found that for $-\sigma_0 < \sigma < 0$ or $\sigma > 1$, the field at most points in the guide was locally rotating in the opposite direction to that of the whole pattern. The points of similarity to the present case are clear and it is also evident that the TE mode more nearly approaches the large guide situation because $r_0 = 5.75$ is much further above the cut-off radius for this mode than it is beyond the cut-off for the TM-mode.

REFERENCES

1. A. A. Th. M. Van Trier, Applied Sci. Res., Sec. B, **3,** p. 305, B. Lax, Private communication.
2. R. B. Adler, Res. Lab. of Electronics, M. I. T., Technical Report No. 102, May, 1949.
3. J. H. Rowen, B. S. T. J., **32,** pp. 1333–1369, Nov., 1953.

Bell System Technical Papers Not Published in this Journal

ALLISON, H. W., see MOORE, G. E.

BANGERT, J. T.[1]

The Transistor as a Network Element, (Abstract), I.R.E. Trans. ED-1, No. 1, p. 7, Feb. 1954.

BECK, A. C.[1]

Microwave Testing with Millimicrosecond Pulses, I.R.E. Trans. MTT-2, No. 1, pp. 93–99, April, 1954.

BICKELHAUPT, C. O.[2]

Long Lines Signal Communication in the Battle of the Bulge, Telephony, **146,** pp. 20–21, 38, May 29, 1954.

BIONDI, F. J.[1]

Corrosion Proofing Electronic Apparatus Parts Exposed to Ozone (Abstract), I.R.E. Trans. ED-1, No. 1, p. 65, Feb. 1954.

BOND, W. L.[1]

Making Crystal Spheres, Rev. Sci. Instr., **25,** No. 4, p. 401, April, 1954.

BRACKETT, G. R.[4]

The Private Branch Exchange, Telephony, **146,** pp. 17–18, 49, April 10, 1954.

---

[1] Bell Telephone Laboratories, Inc.
[2] American Telephone and Telegraph Company.
[4] Northwestern Bell Telephone Company.

CHAPIN, D. M.,[1] FULLER, C. S.,[1] AND PEARSON, G. L.[1]

A New Silicon p-n Junction Photocell for Converting Solar Radiation into Electric Power, J. Appl. Phys., **25,** No. 5, pp. 676–677, May, 1954.

CLARK, M. A.[1]

An Acoustic Lens as a Directional Microphone, I.R.E. Trans. AU-2, No. 1, pp. 5–7, Jan.-Feb. 1954.

CORENZWIT, E., see MATTHAIS, B. T.

CORY, S. I.[1]

A New Portable Telegraph Transmission Measuring Set, A.I.E.E. Commun. and Electronics, No. 11, pp. 59–62, March, 1954.

COWAN, F. A.[2]

Networks for Theater Television, J.S.M.P.T.E., **62,** pp. 306–313, April, 1954.

DEWALD, J. F.[1]

Effects of Space Charge on the Rate of Formation of Anode Films, Letter to the Editor, Acta Metallurgica, **2,** pp. 340–341, Mar., 1954.

DITZENBERGER, J. A., see FULLER, C. S.

FEINSTEIN, J.[1]

Some Stochastic Problems in Wave Propagation—Part II, I.R.E. Trans. AP-2, No. 2, p. 63, April, 1954.

FLETCHER, R. C.,[1] YAGER, W. A.,[1] PEARSON, G. L.,[1] HOLDEN, A. N.,[1] READ, W. T.,[1] AND MERRITT, F. R.[1]

Spin Resonance of Donors in Silicon, Letter to the Editor, Physical Review, **94,** No. 5, pp. 1392–1393, June 1, 1954.

---

[1] Bell Telephone Laboratories, Inc.
[2] American Telephone and Telegraph Company.

FULLER, C. S.,[1] STRUTHERS, J. D.,[1] DITZENBERGER, J. A.,[1] AND WOLF-STIRN, K. B.[1]

Diffusivity and Solubility of Copper in Germanium, Phys. Rev., **93,** pp. 1182–1189, Mar. 15, 1954.

FULLER, C. S., see CHAPIN, D. M.

GEBALLE, T. H.,[1] AND HULL, G. W.[1]

Seebeck Effect in Germanium, Phys. Rev., 94, No. 5, pp. 1134–1140, June, 1, 1954.

GREEN, E. I.[1]

The Decilog — A Unit for Logarithmic Measurements, Elec. Eng., **73,** No. 7, pp. 597–599, July, 1954.

GROSS, A. J., see TANENBAUM, M.

HEFFNER, H.[1]

Analysis of the Backward Wave Traveling Wave Tube, I.R.E. Proc., **42,** No. 6, pp. 930–937, June, 1954.

HOHN, F. E.[1]

The Conference on Training in Applied Mathematics, Am. Math. Monthly, **61,** No. 4, pp. 242–245, April, 1954.

HOLDEN, A. N., see FLETCHER, R. C.

HULL, G. W., see GEBALLE, T. H.

JAFFE, HANS, see MASON, W. P.

LADD, F. E.[1]

50 Mc TVI — Its Causes and Cures, Part I, QST, **38,** No. 6, p. 21, June, 1954. Part II, QST, **38,** No. 7, p. 32, July, 1954.

MASON, W. P., see SHOCKLEY, W.

---

[1] Bell Telephone Laboratories, Inc.

MASON, W. P.,[1] and JAFFE, Hans[5]

Methods for Measuring Piezoelectric, Elastic and Dielectric Co-efficients of Crystals and Ceramics, I.R.E. Proc., 42, No. 6, pp. 921–930, June, 1954.

MATTHIAS, B. T.,[1] CORENZWIT, E.,[1] and MILLER, C. E.[1]

Superconducting Compounds, Letter to the Editor, Phys. Rev., 93, p. 1415, Mar. 15, 1954.

MATTHAIS, B. T.[1] and CORENZWIT, E.[1]

Superconducting Alloys, Letter to the Editor, Phys. Rev., 94, No. 4, p. 1069, May 15, 1954.

MAY, J. E., JR.[1]

Characteristics of Ultrasonic Delay Lines Using Quartz and Barium Titanate, J. Acoust. Soc. Am., 26, No. 3, pp. 347–355, May, 1954.

MCKAY, K. G.[1]

Avalanche Breakdown in Silicon, Phys. Rev., 94, No. 4, pp. 877–884, May 15, 1954.

MENDEL, J. T.,[1] QUATE, C. F.,[1] AND YOCUM, W. H.[1]

Electron Beam Focusing With Periodic Permanent Magnetic Fields. Proc. I.R.E., 42, pp. 800–810, May, 1954.

MERRITT, F. R., see FLETCHER, R. C.

MILLER, C. E., see MATTHIAS, B. T.

MOORE, G. E.,[1] ALLISON, H. W.,[1] AND WOLFSTIRN, K. B.[1]

Reduction of SrO by Methane, J. Chem. Phys, 22, No. 4, p. 726, April, 1954.

MORIN, F. J.[1]

Electrical Properties of NiO, Phys. Rev., 93, pp. 1199–1204, Mar. 15, 1954.

Morin, F. J.[1]

Electrical Properties of α-Fe$_2$O$_3$, Phys. Rev., **93,** pp. 1195–1199, Mar. 15, 1954.

Pearson, G. L., see Chapin, D. M.

Pearson, G. L., see Fletcher, R. C.

Pfann, W. G., see Tanenbaum, M.

Prince, M. B.[1]

Drift Mobilities in Semiconductors: II—Silicon, Phys. Rev., **93,** pp. 1204–1206, Mar. 15, 1954.

Quate, C. F., see Mendel, J. T.

Read, W. T., see Fletcher, R. C.

Shockey, W.,[1] and Mason, W. P.[1]

Dissected Amplifiers Using Negative Resistance, Letter to the Editor, J. Appl. Phys., **25,** No. 5, p. 677, May, 1954.

Slepian, David[1]

Estimation of Signal Parameters in the Presence of Noise, I.R.E. Trans. P.G.I.T.-3, pp. 68–89, Mar. 1954.

Stansel, F. R.[1]

An Improved Method of Measuring the Current Amplification Factor of Junction Transistors, I.R.E. Trans. PG1-3, pp. 41–49, April, 1954.

Struthers, J. D., see Fuller, C. S.

Tanenbaum, M.,[1] Gross, A. J.,[1] and Pfann, W. G.[1]

Purification of Antimony and Tin by a New Method of Zone Refining, J. Metals, **6,** No. 6, pp. 762–763, June, 1954.

Thomas, D. E.[1]

---

[1] Bell Telephone Laboratories, Inc.

A Point Contact Transistor VHF FM Transmitter, I.R.E. Trans. ED-1, No. 1, pp. 43–52, April, 1954.

TURNER, E. C.[6]

Telephone Growth Forecasting. Part I, Telephony, **146,** No. 24, pp. 17–19, 48, June, 12, 1954. Part II, Telephony, **146,** No. 25, pp. 23–25, June 19, 1954.

VANCE, R. L.[1] AND MAGGS, C.[1]

Magnetron Heater Design to Avoid Undesirable Magnetic Effects, (Abstract), I.R.E. Trans. ED-1, No. 1, p. 64, Feb. 1954.

VARNEY, R. N.[1]

Liberation of Electrons by Positive-ion Impact on the Cathode of a Pulsed Townsend Discharge Tube, Phys. Rev., **93,** pp. 1156–1160, Mar. 15, 1954.

WALKER, L. R.[1]

Stored Energy and Power Flow in Electron Beams, Letter to the Editor, J. Appl. Phys., **25,** No. 5, pp. 615–618, May, 1954.

WICK, R. J.[1]

Solution of the Field Problem of the Germanium Gyrator, J. Appl. Phys., **25,** No. 6, pp. 741–750, June, 1954.

WINDELER, A. S.[1]

Polyethylene-Insulated Telephone Cable, A.I.E.E. Commun. and Electronics, No. 12, pp. 106–111, May, 1954.

WOLFSTIRN, K. B., see MOORE, G. E.

WOLFSTIRN, K. B., see FULLER, C. S.

YAGER, W. A., see FLETCHER, R. C.

YOCUM, W. H., see MENDEL, J. T.

Recent Monographs of Bell System Technical Papers Not Published in This Journal*

BENNETT, W.

Telephone-System Applications of Recorded Machine Announcements, Monograph 2213.

BOGERT, B. P.

On the Band Width of Vowel Formants, Monograph 2167.

BROWN, W. L.

N-Type Surface Conductivity on P-Type Germanium, Monograph 2173.

BURTON, J. A., HULL, G. W., MORIN, F. J., and SEVERIENS, J. C.

Effects of Nickel and Copper Impurities on the Recombination of Holes and Electrons in Germanium, Monograph 2193.

BURTON, J. A., PRIM, R. C., SLICHTER, W. P., KOLB, E. D., and STRUTHERS, J. D.

Distribution of Solute in Crystals Grown from the Melt, Monograph 2231.

COY, J. A.

Heat Dissipation from Toll Transmission Equipment, Monograph 2214.

CONWELL, E. M., see DEBYE, P. P.

DEBYE, P. P.

Electrical Properties of n-type Germanium, Monograph 2220.

ELLIS, W. C., and FAGEANT, JACQUELINE.

Orientation Relationships in Cast Germanium, Monograph 2219

FAGEANT, JACQUELINE, see ELLIS, W. C.

FELCH, E. P., see POTTER, J. L.

Preliminary Development of a Magnettor Current Standard, Monograph 2198.

FELKER, J. H.

Arithmetic Processes for Digital Computers, Monograph 2208.

GOERTZ, M., see WILLIAMS, H. J.

GRISDALE, R. O.

The Properties of Carbon Contacts, Monograph 2206.

HAGSTRUM, H. D.

Electron Ejection from Ta by He^+, He^{++}, and He_2^+, Monograph 2148.

HOPKINS, I. L.

The Ferry Reduction and the Activation Energy for Viscous Flow Monograph 2203.

HULL, G. W., see BURTON, J. A.

KARNAUGH, M.

The Map Method for Synthesis of Combinational Logic Circuits, Monograph 2199.

KOLB, E. D., see BURTON, J. A.

LANDER, J. J.

Auger Peaks in the Energy Spectra of Secondary Electrons from Various Materials, Monograph 2215.

LEWIS, W. D

Electronic Computers and Telephone Switching, Monograph 2187.

LINVILL, J. G.

A New RC Filter Employing Active Elements, Monograph 2221.

MAY, J. E.

Characteristics of Ultrasonic Delay Lines Using Quartz and Barium Titanate Ceramic Transducers, Monograph 2223.

McSKIMIN, H. J.

Measurement of Elastic Constants at Low Temperatures by Means of Ultrasonic Waves Data for Silicon and Germanium Single Crystals and for Fused Silica, Monograph 2171.

MORIN, F. J., see BURTON, J. A.

PENNELL, E. S.

A Temperature-Controlled Ultrasonic Solid Delay Line, Monograph 2222.

PFANN, W. G.

Change in Ingot Shape During Zone Melting, Monograph 2218.

PIERCE, J. R.

Spatially Alternating Magnetic Fields for Focusing Low-Voltage Electron Beams, Monograph 2169.

POTTER, J. L., see FELCH, E. P.

PRIM, R. C., see BURTON, J. A.

PRINCE, M. P.

Experimental Confirmation and Relation Between Pulse Drift Mobility and Charge Carrier Drift Mobility in Germanium, Monograph 2168.

READ, W. T., JR.

Dislocations and Plastic Deformations, Monograph 2216.

REISS, H.

Chemical Effects due to the Ionization of Impurities in Semiconductors, Monography 2172.

RYDER, E. J.

Mobility of Holes and Electrons in High Electric Fields, Monograph 2159.

SCHNETTLER, F. J., see WILLIAMS, J. H.

SEVERIENS, J. C., see BURTON, J. A.

SHERWOOD, R. C., see WILLIAMS, J. H.

SHOCKLEY, W.

Transistor Physics, Monograph 2217.

SLICHTER, W. P., see BURTON, J. A.

SNOKE, L. R.

Soil-Block Bioassay of a Creosote Containing Pentachlorophenol Monograph 2212.

STRUTHERS, J. D., see BURTON, J. A.

STRUTHERS, J. D., see THURMOND, C. D.

THURMOND, C. D.

Equilibrium Thermochemistry of Solid and Liquid Alloys of Germanium and of Silicon, Monograph 2189.

TIEN, P. K.

Traveling-Wave Tube Helix Impedance, Monograph 2209.

WILLARD, G. W.

Ultrasonically Induced Cavitation in Water — A Step-by-Step Process, Monograph 2170.

WILLIAMS, H. J., SHERWOOD, R. C., GOERTZ, M., AND SCHNETTLER, F. J.

Stressed Ferrites having Rectangular Hysteresis Loops, Monograph 2200.

Contributors to this Issue

ORSON L. ANDERSON, B.S., M.S. and Ph.D., University of Utah, 1948, 1949 and 1951; Institute of Rate Processes, University of Utah, 1949–1952; Bell Telephone Laboratories, 1952–. Dr. Anderson has been engaged in the investigation of mechanical and electrical properties of solids, with emphasis on glasses, and in studies of the mechanism of plastic flow of amorphous bodies. A member of the mechanics division of the Mathematics Department, he is now studying the strength and flow properties of glasses under high pressure. Member of American Physical Society, American Ceramic Society and Society of Glass Technology.

J. K. GALT, A.B., Reed College, 1941; Ph.D., M.I.T., 1947; O.S.R.D., M.I.T. and Harvard University, 1943–1945; National Research Council Fellow, Bristol, England, 1947–1948; Bell Telephone Laboratories, 1948–. Dr. Galt has been engaged in research on the properties of solids, especially of ferrites, with emphasis on their magnetic properties. Fellow of the American Physical Society and member of Phi Beta Kappa.

W. P. MASON, B.S. in E.E., University of Kansas, 1921; M.A., Ph.D., Columbia, 1928. Bell Telephone Laboratories, 1921–. Dr. Mason has been engaged principally in investigating the properties and applications of piezoelectric crystals, in the study of ultrasonics, and in mechanics. Fellow of the American Physical Society, Acoustical Society of America and Institute of Radio Engineers and member of Sigmi Xi and Tau Beta Pi.

J. L. MERRILL, JR., B.S. and M.S., Pennsylvania State University, 1928 and 1930; Elliot Research Fellow, 1928–1930; American Telephone and Telegraph Company, 1930–1934; Bell Telephone Laboratories, 1934–. Mr. Merrill spent his first years with the Laboratories on transmission features of such projects as the time and weather announcement systems and operator training programs. During World War II, he engaged in planning system operation of air raid warnings as well as work on tactical wire and radio networks for the armed forces. Since the war he has been concerned with the design and application of negative

impedance repeaters for the improvement of exchange transmission. He holds several patents and is the author of numerous technical articles. Member of Theta Alpha Phi.

IRAD S. RAFUSE, B.S. in E.E., Cooper Union, 1927; Columbia University; Western Electric Company, 1920–1925; Bell Telephone Laboratories, 1925–. He worked on the development of high quality vertical disc recording for a number of years before turning to measurements and testing of switching apparatus. During World War II he engaged in the development of sonar equipment in cooperation with the N.D.R.C. and the Bureaus of Ships and Ordnance from which he received a commendation for his work. He was later in charge of a group engaged in the development of a new wire-spring, multi-contact relay and now is in charge of a group developing glass sealed switches.

ARTHUR F. ROSE, B.S. in E.E., Colorado College, 1914; American Telephone and Telegraph Company, 1914–. Mr. Rose immediately joined the General Engineering Department of the A.T.&T. Co. Upon completing the student training course for new employees, he was assigned to the development work then under way on the New York-San Francisco route which culminated in the first transcontinental telephone service in 1915. As a result of this initial acquaintance with telephone repeaters, he continued in transmission work dealing particularly with these devices. In 1919, when the General Engineering Department was divided and the Operating and Engineering Department formed, Mr. Rose was assigned to the group that was concerned primarily with the application of repeaters and carrier systems in toll engineering. In 1939 he was transferred to the Plant Extension Section and in 1953 returned to the Transmission Section as Exchange Transmission Engineer.

J. O. SMETHURST, B.S. in Communications, Tufts College, 1929; Bell Laboratories, 1929–. For many years he was concerned with overseas telephony, concentrating especially on control terminals for radio telephone circuits. During World War II he was associated with various government projects and after the war he worked on NIKE. Since 1953 he has concentrated on E2 and E3 repeaters.

HARRY SUHL, B.Sc., University of Wales, 1943; Ph.D., Oriel College, University of Oxford, 1948. Admiralty Signal Establishment, 1943–46; Bell Telephone Laboratories, 1948–. Dr. Suhl conducted research on the properties of germanium until 1950 when he became concerned with

electron dynamics and solid state physics research. His current work is in the applied physics of solids. Member of the American Institute of Physics and Fellow of the American Physical Society.

LAURENCE R. WALKER, B.Sc. and Ph.D., McGill University, 1935 and 1939; University of California, 1939–41. Radiation Laboratory, Massachusetts Institute of Technology, 1941–1945; Bell Telephone Laboratories, 1945–. Dr. Walker has been primarily engaged in research on microwave oscillators and amplifiers. At present he is a member of the physical research group concerned with the applied physics of solids. Fellow of the American Physical Society.